

INFORMATION TO USERS

While the most advanced technology has been used to photograph and reproduce this manuscript, the quality of the reproduction is heavily dependent upon the quality of the material submitted. For example:

- Manuscript pages may have indistinct print. In such cases, the best available copy has been filmed.
- Manuscripts may not always be complete. In such cases, a note will indicate that it is not possible to obtain missing pages.
- Copyrighted material may have been removed from the manuscript. In such cases, a note will indicate the deletion.

Oversize materials (e.g., maps, drawings, and charts) are photographed by sectioning the original, beginning at the upper left-hand corner and continuing from left to right in equal sections with small overlaps. Each oversize page is also filmed as one exposure and is available, for an additional charge, as a standard 35mm slide or as a 17"x 23" black and white photographic print.

Most photographs reproduce acceptably on positive microfilm or microfiche but lack the clarity on xerographic copies made from the microfilm. For an additional charge, 35mm slides of 6"x 9" black and white photographic prints are available for any photographs or illustrations that cannot be reproduced satisfactorily by xerography.

8704877

Tsay, Si-Chee

NUMERICAL STUDY OF THE ATMOSPHERIC RADIATIVE TRANSFER
PROCESS WITH APPLICATION TO THE ARCTIC ENERGY BALANCE

University of Alaska, Fairbanks

Ph.D. 1986

University
Microfilms
International 300 N. Zeeb Road, Ann Arbor, MI 48106

Copyright 1987

by

Tsay, Si-Chee

All Rights Reserved

NUMERICAL STUDY OF THE ATMOSPHERIC RADIATIVE TRANSFER
PROCESS WITH APPLICATION TO THE ARCTIC ENERGY BALANCE

A
THESIS

Presented to the Faculty of the
University of Alaska in Partial Fulfillment
of the Requirements
for the Degree of

DOCTOR OF PHILOSOPHY

by

Si-Chee TSAY, B.S., M.S.

Fairbanks, Alaska


May, 1986

NUMERICAL STUDY OF THE ATMOSPHERIC RADIATIVE TRANSFER
PROCESS WITH APPLICATION TO THE ARCTIC ENERGY BALANCE

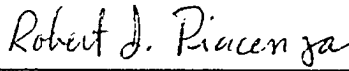
RECOMMENDED:



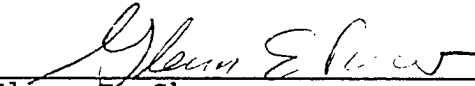
David C. Fritts



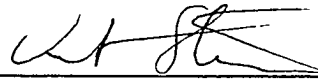
Lou-Chuang Lee



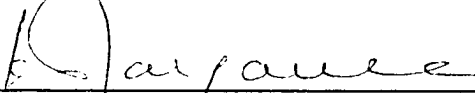
Robert J. Piacenza



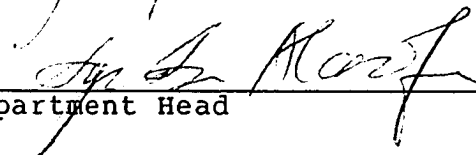
Glenn E. Shaw



Knut H. Stamnes
Co-Chairman, Advisory Committee




Kolf Jayaweera
Co-Chairman, Advisory Committee



Department Head

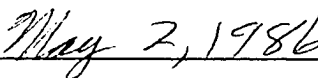
APPROVED:



Dean, College of Natural Sciences



Director of Graduate Programs



Date

© 1987

SI-CHEE TSAY

All Rights Reserved

ABSTRACT

A high-order discrete-ordinate approximation is utilized to solve the radiative transfer equation for both solar and terrestrial spectra. The solutions have been compared with other methods and found to be reliable and efficient. These solutions have been used to construct a complete and comprehensive radiation model for the arctic atmosphere. The bulk radiative properties (e.g. fluxes and heating/cooling rates) as well as the angular distribution of intensity can be computed as functions of wavelength at various levels in vertically inhomogeneous atmospheres.

The radiation model treats Rayleigh scattering, gaseous absorption/emission, scattering and absorption/emission by cloud droplets and haze particles. Snow conditions of the arctic region are simulated by snow grains and soot contamination in the surface layers. A unified treatment of shortwave and longwave radiative transfer is achieved. Use has been made of the five McClatchey atmospheres and of data from the Arctic Stratus Clouds Experiment collected in 1980. Results are compared among broad-band, narrow-band and line-by-line (restricted to gases) computations. We find that at the expense of accuracy by a few watts.m^{-2} for flux or a few tenths $^{\circ}\text{C/day}$ for heating/cooling rate computations, the broad-band models are very fast and suitable for certain types of climate modelling.

During the arctic summer, stratus clouds are a persistent feature and greatly decrease the downward flux at the surface. Arctic haze is important if it is above the cloud layer or in air with low relative humidity, and it decreases the downward flux at the surface. The greenhouse effect of doubling the CO₂ amount can be offset by the haze condition or by an increase in cloudiness of about 4%. In late June, we find that a clear sky condition results in more available downward flux for snow melt than does a cloudy sky condition. This is because the increase of infrared radiation diffused back to the surface by the cloud can not compensate for the reduction of solar radiation. If the snow starts to melt, the decreasing snow albedo further accelerates the melting process.

TABLE OF CONTENTS

| | page |
|----------------------------------------------------------------------|------|
| ABSTRACT | ii |
| TABLE OF CONTENTS | iv |
| LIST OF FIGURES | vi |
| LIST OF TABLES | x |
| ACKNOWLEDGMENTS | xii |
| CHAPTER 1: INTRODUCTION | 1 |
| 1.1 Historical Background | 1 |
| 1.2 Heat Balance Of Arctic Region | 2 |
| 1.3 Summertime Arctic Stratus Clouds | 10 |
| 1.4 Research Emphases | 12 |
| CHAPTER 2: THEORY OF RADIATIVE TRANSFER | 16 |
| 2.1 Discrete Ordinate Method | 25 |
| 2.2 Sensitivity And Accuracy Studies | 41 |
| CHAPTER 3: PARAMETERIZATIONS | 61 |
| 3.1 Absorption/Emission And Scattering Of Gaseous Molecules | 65 |
| 3.2 Extinction Of Arctic Stratus Clouds And Hazes | 74 |
| 3.3 Extinction Of Pure Snow/Ice And Soot Contamination | 99 |
| CHAPTER 4: RESULTS AND DISCUSSION | 108 |
| 4.1 Clear Sky Radiation | 108 |

| | |
|------------------------------------------------------|-----|
| 4.2 Cloudy And/Or Hazy Sky Radiation | 131 |
| 4.3 Summary | 167 |
| APPENDIX A: Principal Symbols | 171 |
| APPENDIX B: Derivation of the Multiple Scattering | |
| Term in Eq.2.26 | 175 |
| APPENDIX C: Derivation of the Analytic Interpolation | |
| Scheme for Intensity at Arbitrary angles .. | 177 |
| APPENDIX D: Delta-M Transformation | 180 |
| APPENDIX E: Derivation of the Expansions of Legendre | |
| Polynomials for Rayleigh and Henyey- | |
| Greenstein Phase Function | 182 |
| APPENDIX F: Computing Code of the Discrete Ordinate | |
| Method a. flow chart | 184 |
| b. program | 185 |
| REFERENCES | 243 |

LIST OF FIGURES

| Figure | Page |
|-----------------------------------------------------------------------------------------------------------------------------------------------------------------------------------|------|
| 1.1 Arctic region | 4 |
| 1.2 Monthly variation of sensible and latent heat fluxes at the surface in the Arctic (a) after Doronin, 1963; (b) after Leavitt <u>et al.</u> , 1978 | 4 |
| 1.3 Monthly variation of (a) infrared radiation, (b) solar radiation, and (c) total radiative energy budget at the surface in the Arctic (after Vowinckel and Orvig, 1964a) | 6 |
| 1.4 Monthly variation of radiative energy (a) loss, (b) gain, and (c) budget in the Arctic troposphere (after Vowinckel and Orvig, 1964b) | 8 |
| 1.5 Monthly variation of sensible and latent heat fluxes in the Arctic atmosphere (after Oort, 1975) | 11 |
| 1.6 Monthly variation of cloud amounts and occurrence frequencies of low clouds (after Huschke, 1969) | 11 |
| 2.1 Geometry for a plane-parallel atmosphere with surface albedo, top and bottom emissivities, and temperatures . | 18 |
| 2.2 Relation of scattering, polar and azimuthal angles ... | 21 |
| 2.3 Angular redistribution patterns for Rayleigh and Mie scattering | 21 |
| 2.4 Interpolations of eigenvectors (after Stamnes, 1982) . | 40 |
| 2.5 Interpolations of azimuthally-averaged intensities (after Stamnes, 1982) | 40 |
| 2.6 Heating/Cooling rates calculation; (a) atmospheric profile of JASIN, 1978; (b) solar heating rate under different orders of approximation; (c) relative errors of (b) | 45 |
| 2.7 Relative errors of fluxes and flux divergences for an inversion cloudy profile | 53 |
| 2.8 Critical errors of upward and downward intensities for an inversion cloudy profile | 54 |
| 3.1 Spectral distribution of solar and terrestrial | |

| | |
|--------------------------------------------------------------------------------------------------------------------------------------------------------------------|----|
| radiation | 64 |
| 3.2 Computed solar elevation angles for the Arctic Stratus Clouds Experiment in 1980 | 64 |
| 3.3 Spectral distribution of gaseous scattering and absorption/emission data gathered during two clear sky observations | 69 |
| 3.4 Spectral distribution for exponential-sum fitting of transmission for gaseous absorption | 69 |
| 3.5 Refractive index of water form wavelength $0.3\mu\text{m}$ to $200\mu\text{m}$, n_r for real and n_i for imaginary parts | 77 |
| 3.6 Scattering efficiency factor as function of size parameter for various size distributions (lower- right, after Hansen and Travis, 1974) | 80 |
| 3.7 Drop size distributions of eight cloud models (after Stephens, 1978) | 80 |
| 3.8 Drop size distributions for model clouds, S-MOD for single-mode and M-MOD for multi-mode | 81 |
| 3.9 Single scattering albedo for seven model clouds from wavelength $0.3\mu\text{m}$ to $200\mu\text{m}$ | 83 |
| 3.10 Asymmetry factor for seven model clouds from wavelength $0.3\mu\text{m}$ to $200\mu\text{m}$ | 84 |
| 3.11 Normalized volume extinction coefficient for seven model clouds from wavelength $0.3\mu\text{m}$ to $200\mu\text{m}$ | 85 |
| 3.12 Least squares fits for single scattering albedo form wavelength $0.3\mu\text{m}$ to $200\mu\text{m}$ | 88 |
| 3.13 Least squares fits for asymmetry factor from wavelength $0.3\mu\text{m}$ to $200\mu\text{m}$ | 89 |
| 3.14 Least squares fits for weighted volume extinction coefficient form wavelength $0.3\mu\text{m}$ to $200\mu\text{m}$ | 90 |
| 3.15 Seasonal trends in aerosol optical depth for 500nm wavelength at Barrow, Alaska (after Shaw, 1982) | 92 |
| 3.16 Vertical profile of aerosol volume extinction coefficient for 500nm wavelength, showing layers of Arctic haze at Barrow, Alaska (after Shaw, 1982) | 92 |
| 3.17 Volume extinction coefficient for five haze models from wavelength $0.2\mu\text{m}$ to $40\mu\text{m}$ | 94 |

| | | |
|------|----------------------------------------------------------------------------------------------------------------------------------------------------------|-----|
| 3.18 | Single scattering albedo for five haze models from wavelength $0.2\mu\text{m}$ to $40\mu\text{m}$ | 95 |
| 3.19 | Asymmetry factor for five haze models from wavelength $0.2\mu\text{m}$ to $40\mu\text{m}$ | 96 |
| 3.20 | Refractive index of ice form wavelength $0.04\mu\text{m}$ to $200\mu\text{m}$, n_r for real and n_i for imaginary parts | 101 |
| 3.21 | Extinction efficiency factor of six snow grains and two soot models for solar spectrum | 103 |
| 3.22 | Single scattering albedo of six snow grains and two soot models for solar spectrum | 104 |
| 3.23 | Asymmetry factor of six snow grains and two soot models for solar spectrum | 105 |
| 4.1 | (a) Temperature, (b) water vapor density (c) Ozone density, (d) air density profiles as function of pressure for five McClatchey atmospheres | 110 |
| 4.2 | Heating/cooling rates of water vapor absorption for tropical and subarctic winter atmospheres | 115 |
| 4.3 | Heating/cooling rates of carbon dioxide absorption for tropical and subarctic winter atmospheres | 116 |
| 4.4 | Heating/cooling rates of carbon dioxide, ozone, water vapor (with and without continuum) absorption for midlatitude summer atmosphere | 119 |
| 4.5 | Heating/cooling rates of carbon dioxide, ozone, water vapor, continuum, and total absorption for subarctic summer atmosphere | 120 |
| 4.6 | Solar heating rates of water vapor absorption for tropical and midlatitude summer atmospheres | 126 |
| 4.7 | Atmospheric profiles for two observed arctic stratus clouds on June 20 and 28, 1980 | 134 |
| 4.8 | Comparison of observed and computed fluxes for stratus clouds on June 28, 1980 | 135 |
| 4.9 | Comparison of observed and computed fluxes for stratus cloud on June 20, 1980 | 136 |
| 4.10 | Comparison of spectral fluxes under different distributions of snow albedo | 138 |
| 4.11 | Surface and system albedos in the solar spectrum for | |

| | |
|-------------------------------------------------------------------------------------------------------|-----|
| clear and cloudy skies, as function of zenith angle . | 142 |
| 4.12 Spectral albedo of snow as function of grain size and density | 144 |
| 4.13 Spectral albedo of snow as function of grain size and impurity | 145 |
| 4.14 Atmospheric heating profiles for various conditions on June 28, 1980 | 148 |
| 4.15 Atmospheric heating profiles for clear and hazy conditions on June 28, 1980 | 149 |
| 4.16 Spectral absorption of cloud and dry haze | 151 |
| 4.17 Spectral absorption of cloud and wet haze | 152 |
| 4.18 Infrared cooling profiles for clear, cloudy and hazy conditions on June 28, 1980 | 157 |
| 4.19 Infrared cooling profiles for clear, cloudy and hazy conditions on June 20, 1980 | 158 |
| 4.20 Daily solar heating and infrared cooling profiles for cloudy condition on June 28, 1980 | 162 |
| 4.21 Daily solar heating and infrared cooling profiles for cloudy condition on June 20, 1980 | 163 |
| 4.22 Daily nte heating/cooling profiles clear and hazy conditions on June 20, 1980 | 165 |

LIST OF TABLES

| Table | Page |
|-------------------------------------------------------------------------------------------------------------------------------------------------------------------------------------------------------------------------------------------------------------------------------------------------|------|
| 2.1 Sensitivity and accuracy comparisons of fluxes computation (after Stamnes and Swanson, 1981) | 43 |
| 2.2 Sensitivity and accuracy comparisons of (a) upward flux at top and (b) flux divergence in layer for thermal emission with various τ , $\omega=0.1$, and $g=0.05$ (in parentheses, for $\omega=0.95$ and $g=0.75$) | 49 |
| 2.3 Critical errors of intensity at quadrature angles for thermal emission with various τ , $\omega=0.1$, and $g=0.05$ (a) upward intensity at top and (b) downward intensity at bottom (in parentheses, for $\omega=0.95$ and $g=0.75$) | 51 |
| 2.4 Optical parameters for flux calculations of an inversion case in thermal emission | 52 |
| 2.5 Comparisons of flux and flux divergence computation with the Doubling method for various τ , ω , and g | 57 |
| 2.6 Critical errors of intensities at quadrature angles relative to Doubling method for various τ , ω , and g .. | 60 |
| 4.1 Comparisons of flux computations for water vapor absorption ($0-580\text{cm}^{-1}$ and $1220-2020\text{cm}^{-1}$) and CO_2 absorption ($540-800\text{cm}^{-1}$) (values in parentheses are for double CO_2 amount) in tropical and subarctic winter atmospheres | 112 |
| 4.2 Comparisons of flux computations for CO_2 , O_3 , and H_2O (without continuum) absorption ($0-2600\text{cm}^{-1}$) in midlatitude summer atmosphere | 124 |
| 4.3 Comparisons of flux and heating/cooling rate computations for water vapor absorption with 60° zenith angle and zero surface albedo in tropical and midlatitude winter atmospheres | 124 |
| 4.4 Comparisons of flux computations for O_3 absorption with 30° zenith angle and zero surface albedo in subarctic summer atmosphere | 128 |

| | | |
|------|---------------------------------------------------------------------------------------------------------------------------------------------------------|-----|
| 4.5 | Comparisons of flux computations for Rayleigh scattering with various zenith angles and surface albedo in subarctic summer atmosphere | 130 |
| 4.6 | Comparisons of flux computations for gaseous absorption with 30° zenith angle and 0.8 surface albedo in subarctic summer atmosphere | 132 |
| 4.7 | Model computations of fluxes for solar and near-infrared (in parentheses) radiation with various components in the atmospheric profile of June 28 | 154 |
| 4.8 | Model computations of fluxes for solar and near-infrared (in parentheses) radiation with various components in the atmospheric profile of June 20 | 155 |
| 4.9 | Model computations of fluxes for infrared radiation with various components in atmospheric profiles of June 20 and 28, 1980 | 160 |
| 4.10 | Model computations of fluxes in daily radiation with various components in atmospheric profiles of June 20 and 28, 1980 | 166 |

ACKNOWLEDGMENTS

The research described in this thesis is the second aspect of a long-run project, spanning the five years and eight months since I came to Alaska. The former, an experimental study, led to my master degree in December, 1982. When we climb a spiral staircase and go in a circle, we think we have come far, but actually we have climbed only to the next step. During this time, I have been extremely fortunate in receiving unflagging support in many ways from many people.

It is not possible to express all my thanks to Professor Kolf Jayaweera, Chairman of my graduate committee, in simple language for his excellent guidance and active help throughout this study.

I sincerely thank Professor Knut H. Stamnes, Co-Chairman of my graduate committee, for his constant help and advice in every way. He was not only a fine academic advisor, but he was also a gracious host on the two occasions when I was doing research in his native Norway.

Thanks are also extended to Professors David C. Fritts, Lou-Chuang Lee, Robert J. Piacenza and Glenn E. Shaw for their extremely valuable insights into the physics, mathematics and philosophy during the course of my graduate education.

Special acknowledgment is due to Dr. Kathryn de la Fuente for editing an extremely difficult manuscript.

I am especially grateful to my dear wife, May-Fong, for her care and encouragement. Even with our second child on the way, she somehow managed to maintain a happy home while pursuing her own career as an artist and getting me through graduate school.

This study was supported by the National Science Foundation through Grant DPP 84-06093.

CHAPTER 1. INTRODUCTION

Energy is transported between the earth-atmosphere system and space by radiation. Radiant energy from the sun is the fundamental energy source for driving the atmospheric and oceanic motions. Because of the astronomical structure of the sun-earth system, there is a radiation surplus in the equatorial region and radiation deficit in both polar areas. Therefore, the Arctic stands for a very important role in the energy exchange process.

1.1 Historical Background

The Arctic region, 23.5 degrees southward from the north pole (Figure 1.1), cover about 8.3% of the northern hemispheric surface. Because of this relatively small area, little attention has been paid to research in polar meteorology. During World War II, the Norwegian Bjerknes and Solberg's Polar Front concept attracted some attention to polar research. However, in the meantime, their Wave Cyclone theory also widely expanded the field of dynamical meteorology, concentrated on mid-latitude and tropical research (Goody, 1980; Haurwitz, 1985), which is now the so-called "Dynamical Paradigm" (Wiscombe and Ramanathan, 1985).

Not until the last decade has it been well recognized that the polar regions are crucial to theories of climate change and also to climate model sensitivity (Kellogg, 1975; Goody, 1980; Warren, 1982). This is simply because the equator-to-pole temperature gradient, in terms of which the polar regions are often referred as "a major heat sink," is the basic driving mechanism for the general circulation of the global atmosphere. However, having rigorous environmental conditions, the Arctic region contain few observational facilities and few well-trained observers; as a result satellite observation has become a powerful and economical technique during the last two decades. The inversion method applied to satellite observation is simply solving radiative transfer problem with complicated boundary-layer phenomena. Therefore, extensive theoretical studies and corresponding observational efforts are urgently required.

1.2 Heat Balance Of Arctic Region

To understand the weather evolution and the climatology of all climatic regions, a study of the heat balance is essential. The heat balance of the Arctic region is determined by three primary components: (a) the transport of sensible and latent heat by the atmospheric and oceanic circulations; (b) the infrared emission to space from the atmosphere and

surface; and (c) the solar radiation absorbed by the atmosphere and surface (Polar Group, 1980). The transport of energy in component (a) is via nonradiative processes, while in components (b) and (c) it is via radiative processes. It is of prime importance to compare the magnitude of the components to determine the dominant factors. For this reason, the heat balance should be discussed both at the surface and in the atmosphere.

1.2.1 Heat balance at the surface

Maykut (1983) summarized the available observational data on the turbulent transport of sensible and latent heat at the surface. The values show large difference. Two commonly cited climatological data sets of the monthly variation of sensible and latent heat fluxes at the surface for the Arctic, as given by Doronin (1963) and Leavitt et al. (1978), are reproduced as Figures 1.2a and 1.2b, respectively. Doronin's data (1963) are gathered from a large amount of results computed by many Russian authors, while Leavitt et al. (1978) use the more sophisticated Monin-Obukhov similarity theory to calculate the sensible and latent heat fluxes. However, Figures 1.2a and 1.2b do not agree with each other either in the dominant flux or in the sign of annual net amount. This disagreement indicates the difficulties and uncertainties inherent in relying on these data for the surface turbulent heat flux specification.

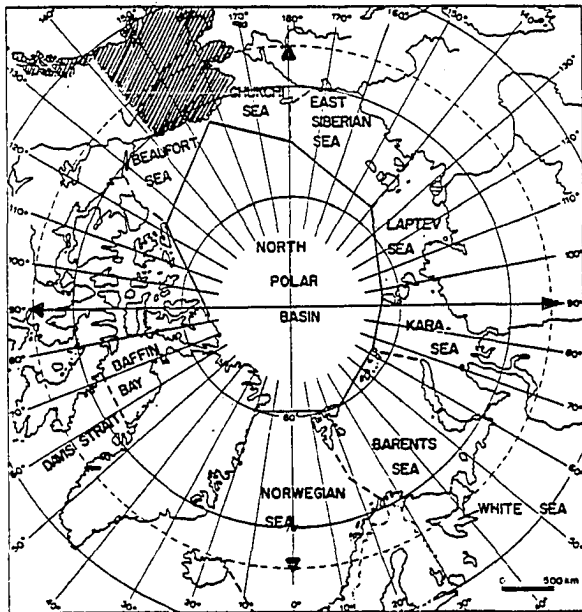


Figure 1.1 Arctic region

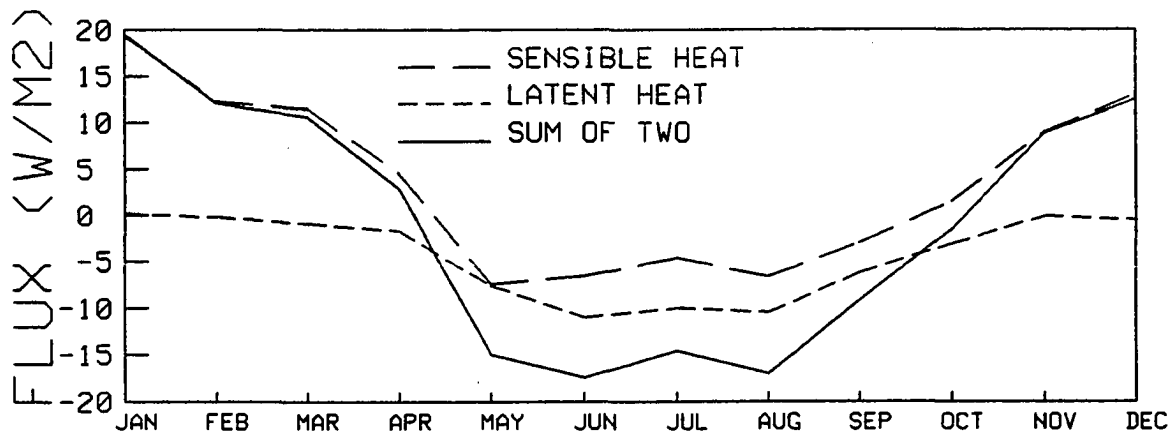


Figure 1.2a Monthly variation of sensible and latent heat fluxes at the surface in the Arctic (after Doronin, 1963)

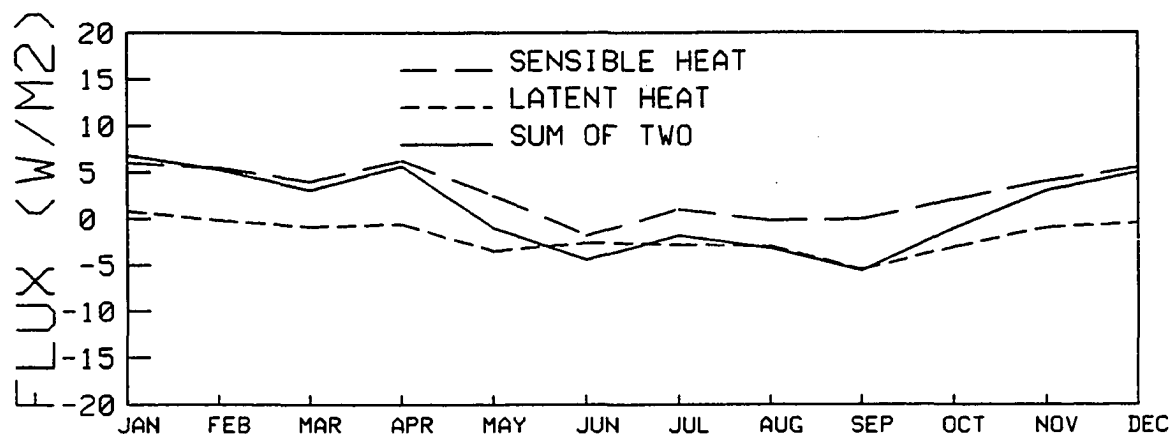


Figure 1.2b Same as 1.2a (after Leavitt et al., 1978)

Obtaining the oceanic heat flux for the Arctic is even more difficult. A conventional value of 2 W.m^{-2} is used in most of the thermodynamic sea ice models of the Arctic (e.g. Maykut and Untersteiner, 1971; Semtner, 1976; Shine and Henderson-Sellers, 1985). A recent computation by McPhee and Untersteiner (1982) showed that the sensible heat flux from the Arctic Ocean to its ice cover was less than 2 W.m^{-2} .

Herman (1980) computed the average monthly radiation fluxes at the surface in the arctic region from the results of Vowinckel and Orvig (1964a). The infrared radiation loss at the surface under "Actual Cloudiness" and "No Clouds" conditions is reproduced as Figure 1.3a. Clearly, the presence of clouds reduces the outgoing infrared radiation from the surface and prevents further cooling of the surface. But clouds also reduce the incoming solar radiation absorbed at the surface, as shown in Figure 1.3b. Figure 1.3c shows the total radiative energy budget at the surface for both clear and cloudy conditions. Except in the month of July, clouds tend to increase the radiative energy budget at the surface.

Comparing the magnitude of energy transported by the non-radiative and radiative processes (Figures 1.2 to 1.3), it is clear that radiative energy is the dominant factor in the surface heat balance because of the large variation between winter and summer months.

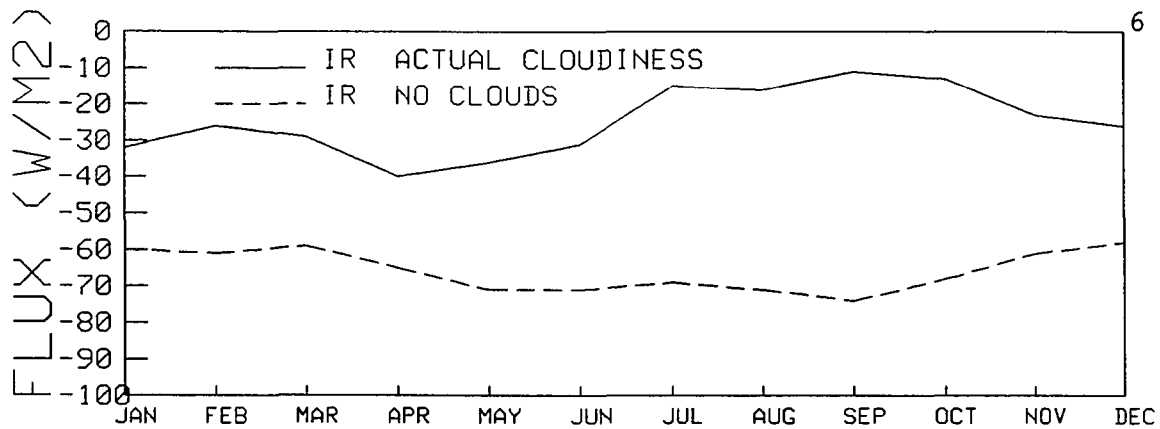


Figure 1.3a Monthly variation of infrared radiation fluxes at the surface in the Arctic (after Vowinckel and Orvig, 1964a)

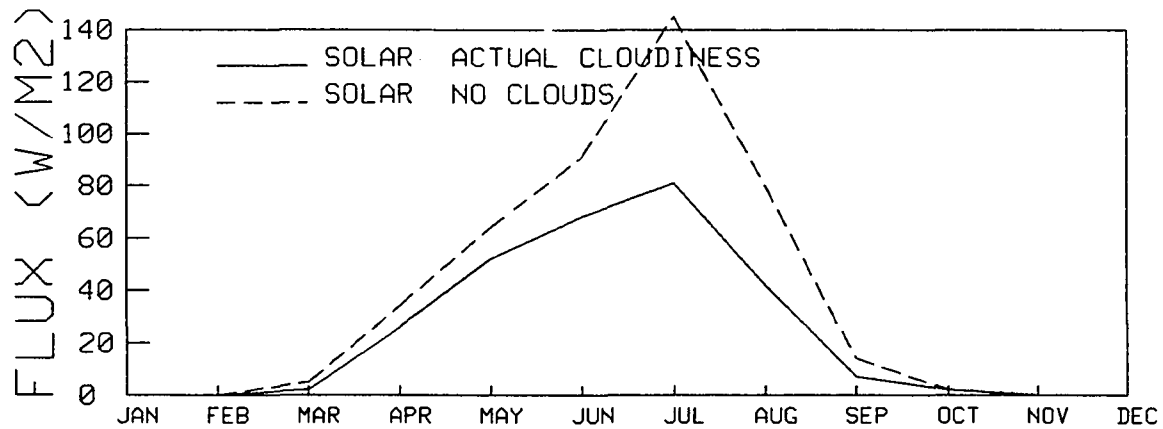


Figure 1.3b Monthly variation of solar radiation fluxes at the surface in the Arctic (after Vowinckel and Orvig, 1964a)

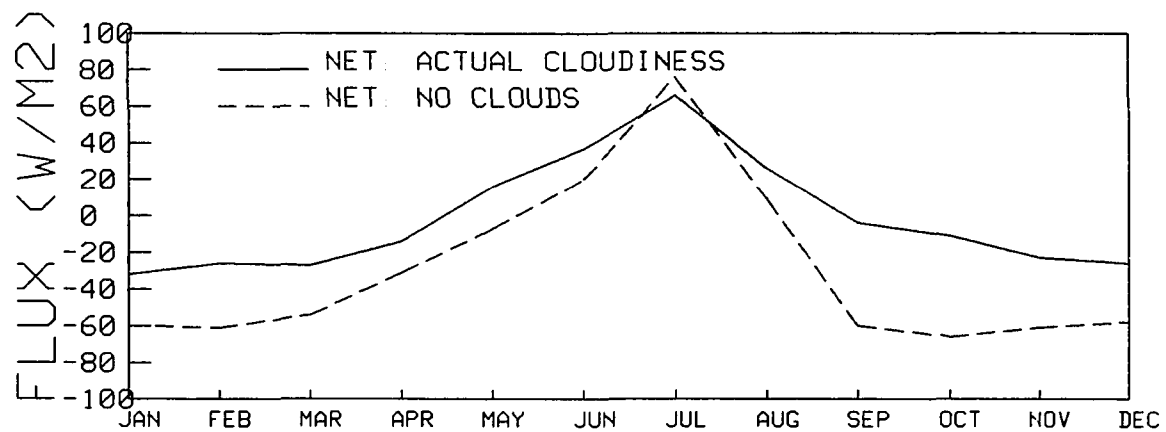


Figure 1.3c Monthly variation of total radiative energy budget at the surface in the Arctic (after Vowinckel and Orvig, 1964a)

1.2.2 Heat balance in the atmosphere

The monthly variation of radiative energy in the Arctic troposphere under both "Actual Cloudiness" and "No Clouds" conditions, inferred from the results of Vowinckel and Orvig (1964b), is reproduced as Figure 1.4a to 1.4c. Figure 1.4a shows the total loss of infrared radiation (to space and surface); 1.4b the total absorption of solar and infrared radiation (from space and surface); 1.4c the total radiative energy budget in the troposphere. The monthly radiative energy budget for the troposphere is negative all year round, as expected to act as "a major heat sink." When clouds form in the lower atmosphere, the infrared radiation loss to space is slightly diminished, due to the lower temperature (on average) at the cloud-top than at the surface. However, Vowinckel and Orvig (1970) indicated that the sharp increase of radiation loss from clouds to surface (downward infrared radiation) results in a larger loss of the infrared radiation (Figure 1.4a). This is not compensated by the slight increase (Figure 1.4b) of the absorption of solar (in summer) and infrared (year round) radiation. Thus, the radiation balance is more negative under "Actual Cloudiness" than under "No Clouds" conditions.

The total amount of radiative energy loss is regained by the troposphere via non-radiative processes, assuming a balanced net energy budget (Vowinckel and Orvig, 1970). The

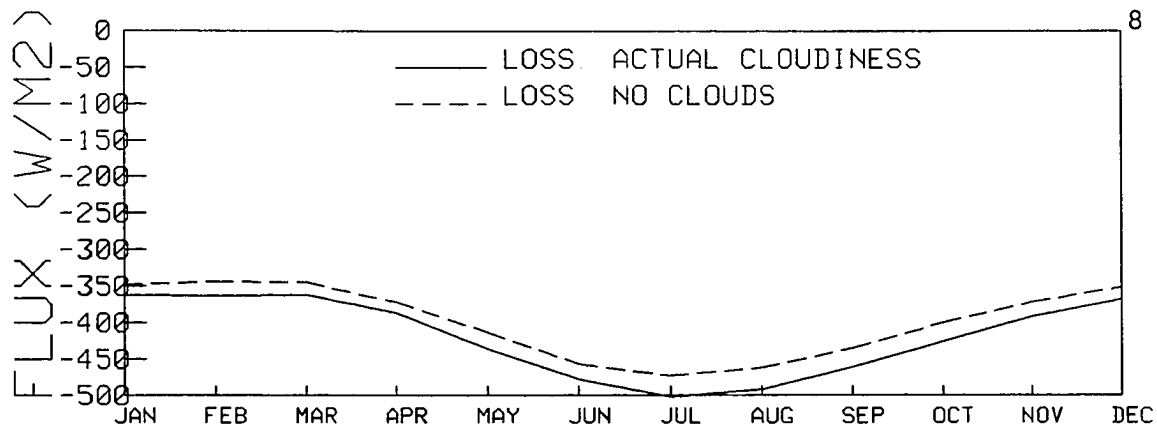


Figure 1.4a Monthly variation of radiative energy loss in the Arctic troposphere (surface to 300mb) (after Vowinckel and Orvig, 1964b)

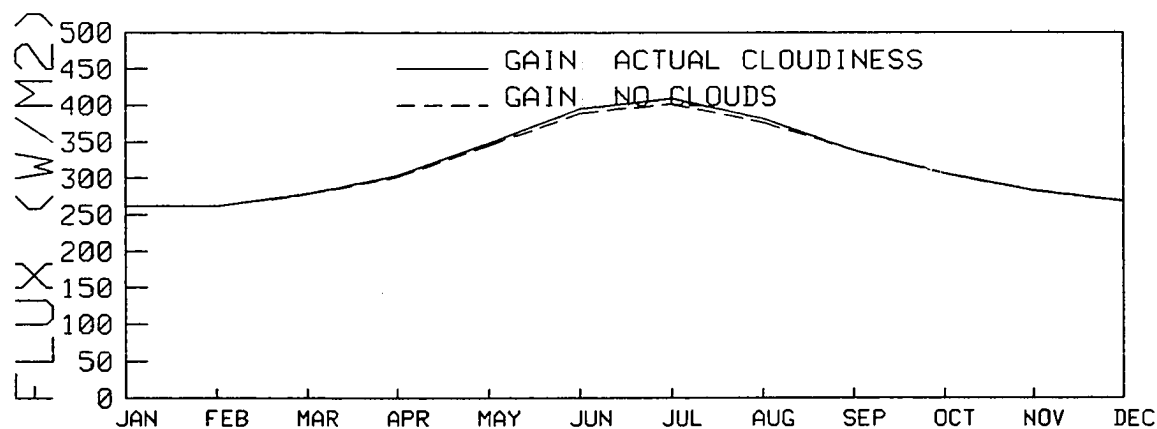


Figure 1.4b Monthly variation of radiative energy gain in the Arctic troposphere (surface to 300mb) (after Vowinckel and Orvig, 1964b)

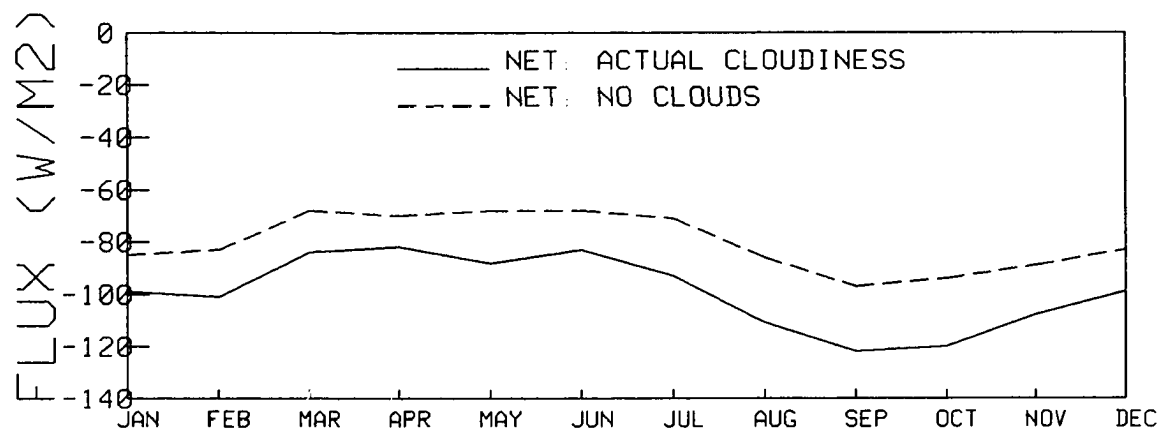


Figure 1.4c Monthly variation of total radiative energy budget in the Arctic troposphere (surface to 300mb) (after Vowinckel and Orvig, 1964b)

commonly cited direct computation of energy transported by non-radiative processes, not a residue of radiative energy, is the result of Oort's study (1975). The monthly variation of sensible heat (plus a small percentage of potential energy) and latent heat fluxes across the subarctic wall (north of 60°N and up to 75mb; Table 1 of Oort, 1975) is reproduced as Figure 1.5. The air masses will get colder and dryer as they move further north to the Arctic regions. Oort (1975) indicated that changes in energy content are dominated by changes in temperature, but that changes in humidity account for about 10-20% of that change.

Figures 1.4c and 1.5 (keeping in mind the effects of temperature and humidity) show that a general agreement could be made about the relative magnitudes of transported energy. These figures indicate that in the Arctic winter without solar radiation the non-radiative processes (Figure 1.5) contribute only about 30% of the infrared radiation loss (Figure 1.4a). In the summer the value becomes even less than 20%. These figures also show the maximum values for radiation balance in summer.

Now it is clear that the radiative components tend to dominate the Arctic heat-balance both at the surface and in the atmosphere because of their relatively large magnitude. Also, cloud conditions exercise a powerful influence on the radiative regime. Therefore, careful examinations of cloud radiative properties are needed.

1.3 Summertime Arctic Stratus Clouds

During the long polar summer, low-level stratiform clouds are a prevalent feature (Figure 1.6) in the Arctic (Huschke, 1969; Vowinckel and Orvig, 1970). These clouds tend to occur in the boundary layer (within 2 Km of height) and are frequently observed to be laminated or comprised of two or more separate, well-defined layers (Jayaweera and Ohtake, 1973; Herman, 1977). A more detailed description of the physical characteristics of the Arctic stratus clouds is given by Tsay and Jayaweera (1984).

The morphology of the Arctic stratus makes it the best candidate for the theoretical study of radiative transfer in a plane-parallel atmosphere with multiple scattering. Many such theoretical studies have been done for radiative transfer through the Arctic stratus. Feigel'son (1964) conducted the first theoretical study of the radiation problem of the Arctic stratus, by using crude approximations of gaseous absorption and droplet scattering, without surface reflection. Wiscombe (1975) presented a fine computational scheme for solar radiation under the Arctic summer stratus conditions. Herman and Goody (1976) constructed a radiative-diffusive model to simulate the formation of the summertime Arctic stratus. However, the dependence of the radiative properties of these clouds on their microphysics, as pointed

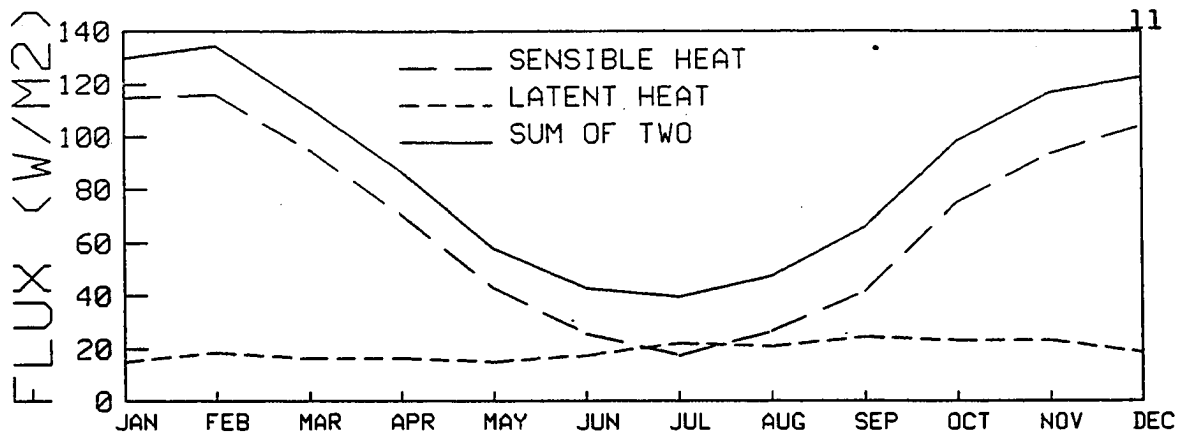


Figure 1.5 Monthly variation of sensible and latent heat fluxes in the Arctic atmosphere (see text) (after Oort, 1975)

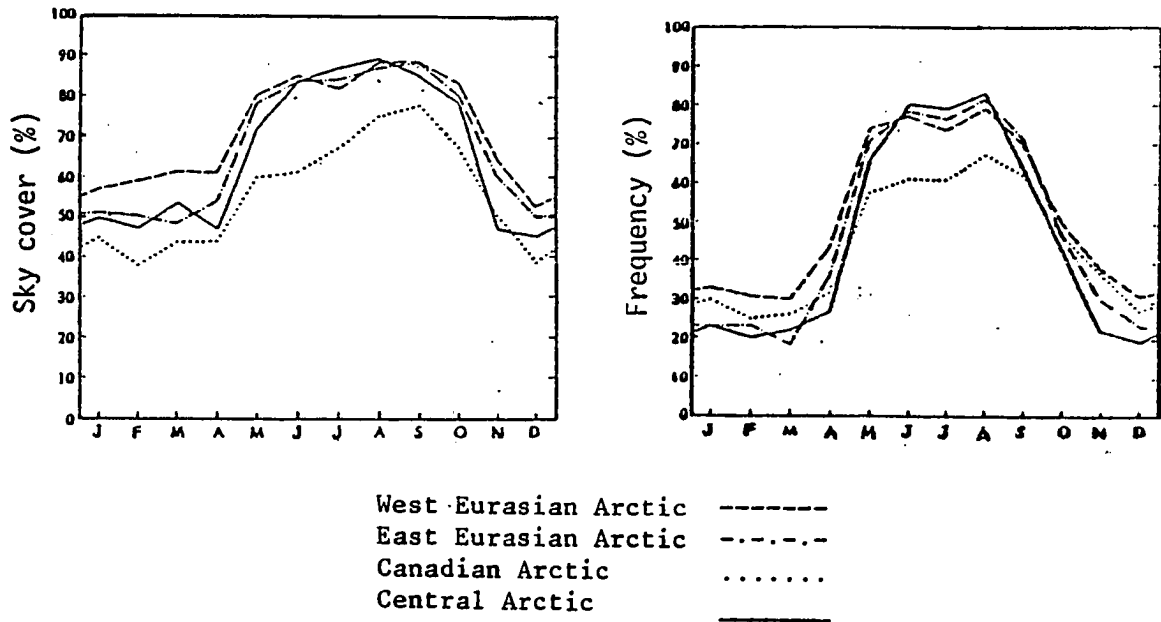


Figure 1.6 Monthly variation of cloud amounts and occurrence frequencies of low clouds (after Huschke, 1969)

out by Tsay et al. (1983) and Herman and Curry (1984), was not considered in the previous two models.

During AIDJEX (Arctic Ice Dynamics Joint Experiment), Herman (1977, 1980) obtained radiation measurements by using the Eppley pyranometers on board the NCAR's (National Center for Atmospheric Research) Electra aircraft. The radiative properties of the summertime Arctic stratus observed by this airborne experiment were the first reported in the western literature. However, not until the summer of 1980 was a complete set of radiative, microphysical, and boundary layer turbulence data for the Arctic stratus collected over the Beaufort Sea, under the auspices of a joint grant by the Universities of Alaska at Fairbanks, Wisconsin at Madison, and North Carolina State at Raleigh. The broadband measurements of radiative fluxes (visible, near-infrared, and infrared) for the surface and atmosphere were presented by Herman and Curry (1984), and Curry and Herman (1985); the corresponding physical and microphysical properties of the Arctic stratus were presented by Tsay and Jayaweera (1984). This comprehensive data set should help in constructing and validating a radiative transfer model of the Arctic atmosphere and the surface under clear and cloudy conditions.

1.4 Research Emphases

Many radiative transfer schemes or models have been developed or proposed. However, in practice, it still remains a demanding task to arrive at an accurate solution and perform efficient computation of fluxes and intensities. To meet this goal, a complete solution for the entire solar and terrestrial spectra using the discrete ordinate method has been established. The discrete ordinate method is the only one which can give the intensities at arbitrary angles directly from the equation. Most of the other methods either provide the intensities only at quadrature angles, which are the azimuthally averaged quantities or infer them by means of some standard interpolation scheme (e.g., linear, quadratic, cubic splines etc.).

Intensity computation at arbitrary (or user specified) angles is important for satellite applications and for radiative transfer model validation. The direct measurements from the satellite sensors are indicators of radiance (intensity). The determination of cloud type and cover by means of multiple channels on a satellite needs a good and reliable interpretation of these intensity measurements. This is because different compositions of the surface and atmospheric conditions within a pixel (the surface area within a satellite sensor's conical viewing field) could

give the same intensity measurements, hence additional information is necessary to distinguish various surface and atmospheric conditions.

The ICRCM group (Inter-Comparison of Radiation Codes in Climate Models, 1984) indicated that without incisive validation in the real atmosphere, radiation models may lead to dangerous errors in the estimation of climatic impacts. To rectify this, intensity measurement is essential. There are two reasons for this: first, intensity instruments are more sturdy and much easier to calibrate than flux instruments; second, intensity measurements can now be made to within 1% accuracy, much better than that of flux measurements (5% and more). In the near future as suggested by the ICRCM group (1984), spectrally-detailed intensity measurements must be undertaken. At that time, model study will have to provide the intensity computation for validating itself against the intensity measurement.

The research emphases for this study are fourfold. The first is to implement and utilize the discrete ordinate method developed by Stamnes and Swanson (1981) for monochromatic radiative transfer throughout the entire solar and terrestrial spectra. The second is to use this model to compute fluxes as well as intensities and perform accuracy tests. The third is to construct a complete radiation model for the Arctic atmosphere and surface. The fourth is to

apply this model to examine closely the Arctic radiative energy budget in the atmosphere and at the surface and thereby contribute to a better understanding of the role of radiation in the Arctic.

The development and extension of the discrete ordinate method for solving the radiative transfer equation in the entire solar and terrestrial spectra will be given in Chapter 2. Also, sensitivity testing of parameters to the solution will be conducted and a brief comparison with other leading methods for computing fluxes, intensities, and other bulk radiation quantities will be presented. Detailed derivation of the equations and a well-documented computer code will be presented in the Appendices. Chapter 3 will describe the construction of a complete radiation model of the Arctic summer atmosphere, including the atmospheric constituents of gaseous absorption/emission, Rayleigh scattering, and particulate scattering/absorption, under the summertime Arctic boundary conditions of long solar insolation and high surface albedo. Chapter 4 will first test the model performance against the existing results of theoretical studies as well as the measured fluxes and bulk radiation quantities. Then, a detailed examination of the effects of each constituent on the radiative energy budget of the atmosphere and of the surface will be conducted. A summary of this study is also given.

CHAPTER 2. THEORY OF RADIATIVE TRANSFER

The theory of radiative transfer becomes complicated in the earth-atmosphere system, because the theory has to deal in the general case, with the transport of radiant energy through scattering, absorbing and emitting media. The complexity of the theory for radiative transfer stems mainly from the mathematical difficulty of solving the multiple scattering of radiation (from internal or external sources) within the medium itself.

The plane-parallel approximation of a planetary atmosphere is adequate to study most of the radiative transfer problems in meteorology. Consideration of the sphericity of an atmosphere (e.g. the curvature of the atmospheric layers) is needed only in dealing with problems involving twilight on low sun phenomena. It proves convenient to describe the vertical inhomogeneity of a plane-parallel atmosphere (e.g., containing finite thicknesses of clouds, aerosols, etc.) as a series of horizontally homogeneous layers, in which the scattering, absorbing and emitting properties are constant. These variables can then vary from layer to layer (Liou, 1975; Stamnes and Conklin, 1984).

Generally, the most difficult problem for radiative transfer is to account for horizontal inhomogeneity of the

atmosphere (e.g., patchy cloud or aerosol fields) and variation of the underlying surface (e.g., reflectivity, texture, etc.). To solve such problems a three-dimensional radiative transfer theory is required. However, in a review paper, Wiscombe (1983) indicated that making adjustments (e.g., in the fraction of cloudiness) in the results of plane-parallel approximation may agree better with actual measurements than does the 3-D approach. Besides we will never know, or want to know, the detailed horizontal inhomogeneity (e.g., the shape, size and composition of every single cloud) on the earth. Furthermore, since the Arctic atmosphere is a highly stratified system, the plane-parallel approximation is adequate for this study.

The conventional coordinates used in radiative transfer for a plane-parallel geometry (Figure 2.1) are λ , θ , ϕ , and τ . λ is the monochromatic wavelength frequently expressed (in μm). θ is the polar angle (in degrees) measured from the local zenith. ϕ is the azimuthal angle (in degrees). τ is the optical depth (or thickness, dimensionless) defined as:

$$\begin{aligned} d\tau &= -\cos\theta K_{\text{ext}} \rho ds \\ &\text{or} \\ \int_{\tau_N}^0 d\tau &= \int_0^{\infty} K_{\text{ext}} \rho dz \end{aligned} \tag{2.1}$$

where s is the actual path-length (in meters) in the medium; K_{ext} is the mass-extinction coefficient (in $\text{m}^2 \cdot \text{Kg}^{-1}$) of the medium; and ρ is the density (in $\text{Kg} \cdot \text{m}^{-3}$) of the medium.

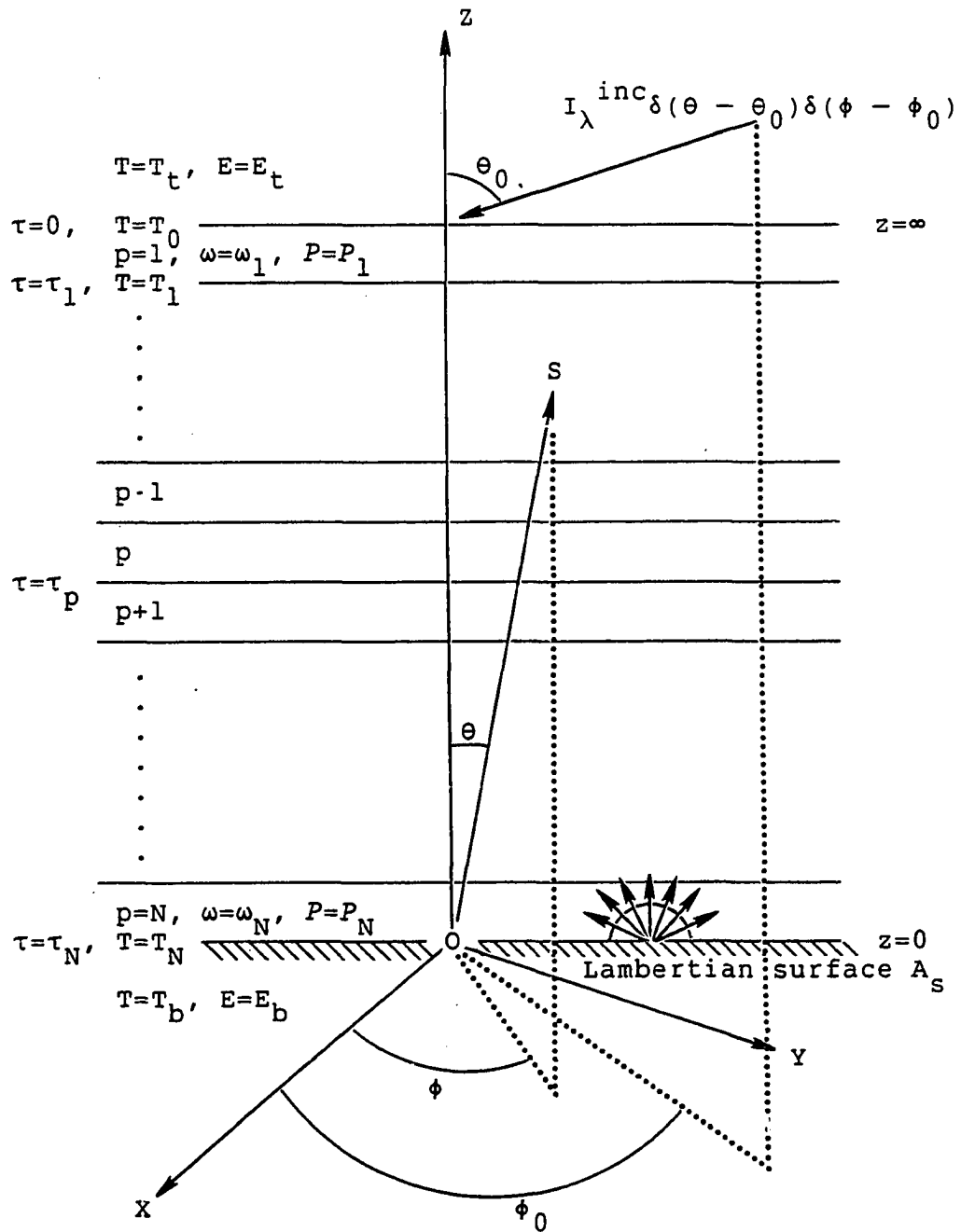


Figure 2.1 Geometry for a plane-parallel atmosphere with surface albedo (A_s), top & bottom emissivities (E_t & E_b), and temperatures (T 's)

Now the general form of the radiative transfer equation in a plane-parallel atmosphere for incoherent scattering and thermal emission can be written as follows:

$$\begin{aligned} \cos\theta \frac{dI(\tau, \theta, \phi, \lambda)}{d\tau} - I(\tau, \theta, \phi, \lambda) = & - [1 - \omega(\tau, \lambda)]B(T, \lambda) \\ & - \frac{\omega(\tau, \lambda)}{4\pi} \int_0^{2\pi} \int_0^\pi P(\tau, \theta, \phi; \theta', \phi', \lambda) I(\tau, \theta', \phi', \lambda) \sin\theta' d\theta' d\phi' \end{aligned} \quad (2.2)$$

where I denotes the intensity (radiance, $\text{W.m}^{-2}.\text{sr}^{-1}.\mu\text{m}^{-1}$); ω , the single-scattering albedo (dimensionless); B , the black body radiance (Planck function, $\text{W.m}^{-2}.\text{sr}^{-1}.\mu\text{m}^{-1}$); and P , the phase function (dimensionless). Before explaining the physics in Eq.(2.2), clear definitions of the terminology are needed.

The single-scattering albedo is defined as the ratio of

$$\begin{aligned} \omega = \frac{K_{\text{sca}}}{K_{\text{ext}}} \quad \text{and} \\ K_{\text{ext}} = K_{\text{sca}} + K_{\text{abs}} \end{aligned} \quad (2.3)$$

where K_{sca} is the mass-scattering coefficient and K_{abs} is the mass-absorption coefficient. For a perfect scatterer (or absorber) ω is equal to unity (or zero). The term $(1-\omega)$ denotes the absorption of the medium. By Kirchhoff's law, under conditions of thermodynamic equilibrium, the emission is identical to the absorption and is a function of temperature and absorbing wavelength only.

The monochromatic black body radiance is given as:

$$B(T, \lambda) = \frac{2hc^2}{\lambda^5 (e^{hc/\lambda kT} - 1)} \quad (2.4)$$

where Planck's and Boltzmann's constants are given by $h = 6.6262 \times 10^{-34}$ J.sec and $k = 1.3806 \times 10^{-23}$ J. $^{\circ}$ K $^{-1}$, respectively; c is the speed of light (3×10^8 m.sec $^{-1}$); T denotes the temperature in degrees Kelvin. Detailed derivation of the Planck function can be found in Liou (1980, Appendix C).

The relationship between the scattering angle (Ξ) and the polar and azimuthal angles, as shown in Figure 2.2, is

$$\cos \Xi = \cos \theta \cos \theta' + \sin \theta \sin \theta' \cos(\phi - \phi') \quad (2.5)$$

and can also be found in most of the textbooks (e.g., Liou [1980], Appendix F). The phase function (P) describes the angular redistribution of scattered intensity by the medium and is normalized to unity.

$$\frac{1}{4\pi} \int_0^{2\pi} \int_0^{\pi} P(\theta, \phi; \theta', \phi') \sin \theta' d\theta' d\phi' = 1 \quad (2.6)$$

Figure 2.3 shows the Rayleigh and Mie phase functions (scattering patterns), which are often encountered in atmospheric radiation. When the size of the scatterer is smaller than the wavelength of the incident radiation, such as for air molecules and visible radiation, the Rayleigh scattering pattern is found. On the other hand, particles larger than the wavelength of incident radiation, such as cloud droplets and shortwave radiation, cause the Mie scattering pattern.

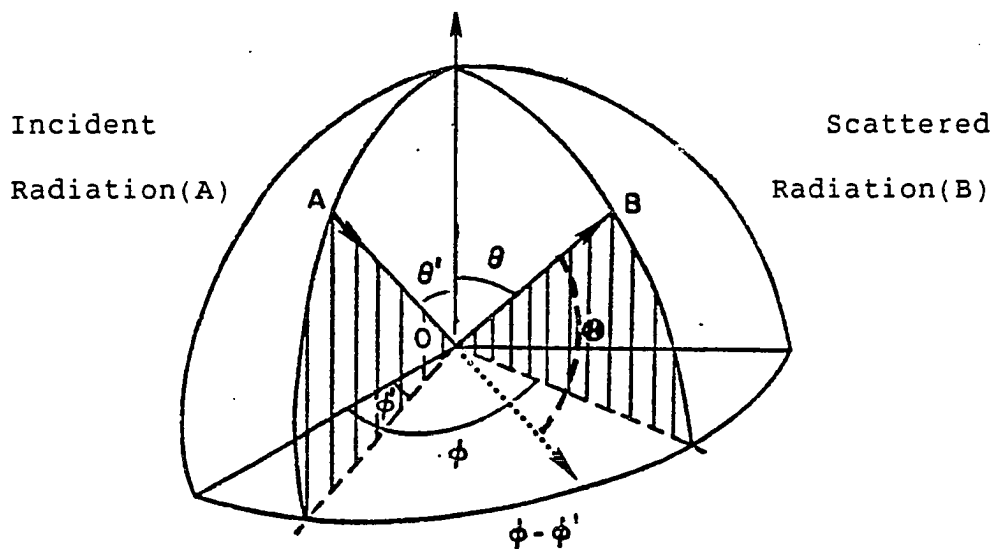


Figure 2.2 Relation of scattering (θ), polar (θ), and azimuthal (ϕ) angles

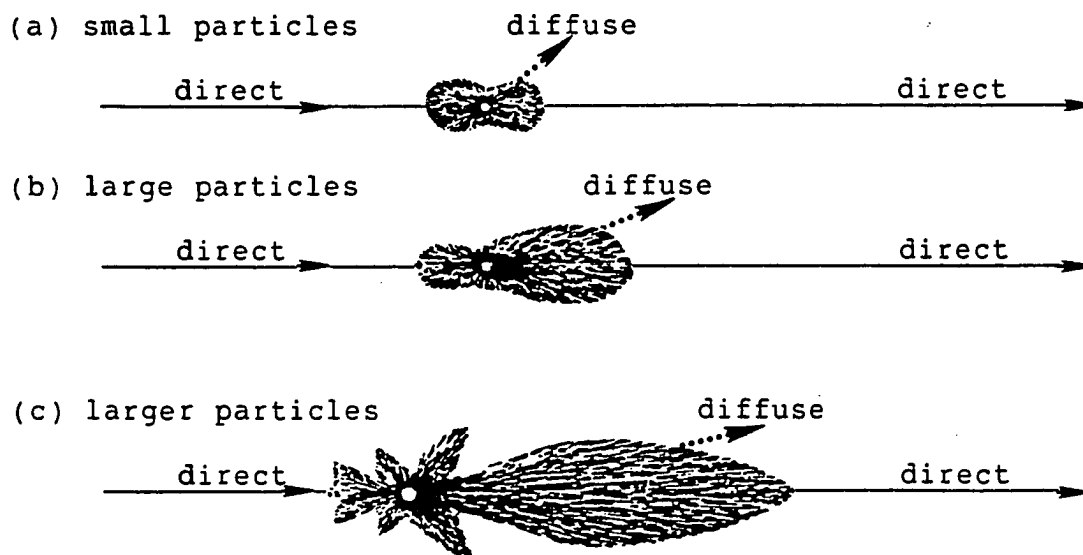


Figure 2.3 Angular redistribution patterns for Rayleigh (a) and Mie (b,c) scattering

Having defined the terms, the physics of Eq. (2.2) can be described as follows:

The terms on the left-hand side are the usual Beer's law, which describes the radiance attenuated by the medium. The first term on the right-hand side is due to the contribution of thermal emission by the medium. The last term on the right-hand side can be interpreted as the contribution of integrated radiance for all directions (from θ' and ϕ' to θ and ϕ) due to the multiple scattering by the medium. The terms on the right-hand side are often defined as the source function (J). Equation 2.2 is completely general for a plane parallel geometry, but very difficult to solve.

Seeking the formal solution of Eq. (2.2) bounded in two layers ($\tau = 0$ and τ_N as in Figure 2.1), it is convenient to express the solution in upward ($\mu = \cos\theta > 0$) and downward ($\mu < 0$) components. Eq. (2.2) is rewritten as:

$$\mu \frac{dI(\tau, \mu, \phi)}{d\tau} - I(\tau, \mu, \phi) = -J(\tau, \mu, \phi) \quad (2.7)$$

For downward intensity, μ in Eq. (2.7) is replaced by $-\mu$ and Eq. (2.7) is multiplied by the integrating factor $e^{\tau/\mu}$.

$$-\mu \frac{d[I(\tau, -\mu, \phi)e^{\tau/\mu}]}{d\tau} = -J(\tau, -\mu, \phi)e^{\tau/\mu} \quad (1 \geq \mu > 0) \quad (2.8)$$

Then, Eq. (2.8) is integrated from $\tau = 0$ to τ . The downward intensity is obtained as follows:

$$I(\tau, -\mu, \phi) = I(0, -\mu, \phi)e^{-\tau/\mu} + \int_0^{\tau} J(t, -\mu, \phi)e^{-(\tau-t)/\mu} \frac{dt}{\mu} \quad (1 \geq \mu > 0) \quad (2.9)$$

Likewise, for upward intensity, Eq. (2.7) is multiplied by the factor $e^{-\tau/\mu}$ and integrated from $\tau = \tau_N$ to τ . Then, the upward intensity is obtained as follows:

$$I(\tau, \mu, \phi) = I(\tau_N, \mu, \phi)e^{-(\tau_N - \tau)/\mu} + \int_{\tau}^{\tau_N} J(t, \mu, \phi)e^{-(t-\tau)/\mu} \frac{dt}{\mu} \quad (1 \geq \mu > 0) \quad (2.10)$$

The solutions (Eqs. 2.9-10) of radiative transfer give the intensity at arbitrary levels and angles. The monochromatic vertical fluxes (or irradiance, $\text{W.m}^{-2}.\mu\text{m}^{-1}$) are defined as the normal component of intensity integrated over the hemispheric solid angle:

$$F^+(\tau, \lambda) = \int_0^{2\pi} \int_0^{\pi/2} I(\tau, \theta, \phi) \cos\theta \sin\theta d\theta d\phi \quad (2.11)$$

$$F^-(\tau, \lambda) = \int_0^{2\pi} \int_{\pi/2}^{\pi} I(\tau, \theta, \phi) \cos\theta \sin\theta d\theta d\phi \quad (2.12)$$

$$F^{\text{net}}(\tau, \lambda) = F^+(\tau, \lambda) + F^-(\tau, \lambda) \quad (2.13)$$

where F^+ , F^- , and F^{net} are upward, downward, and net fluxes, respectively. Then, the bulk radiative properties can be defined (directions unspecified) as follows:

$$\text{Ref} = F_r / F_{\text{inc}} \quad (2.14)$$

$$\text{Trn} = F_t / F_{\text{inc}} \quad (2.15)$$

$$\text{Abs} = 1 - \text{Ref} - \text{Trn} = \text{Emt} \quad (2.16)$$

where Ref, Trn, Abs, and Emt (dimensionless) represent the reflectivity, transmissivity, absorptivity, and emissivity of the medium, respectively; and F_r , F_t , and F_{inc} denote the reflected, transmitted, and incident fluxes, respectively.

The heating/cooling rate (in $^{\circ}\text{C}\cdot\text{day}^{-1}$) of the layers by radiative energy exchange can be defined as follows:

$$\frac{\Delta T}{\Delta t} = - \frac{1}{C_p \rho} \frac{\Delta F^{\text{net}}}{\Delta z} \quad (2.17)$$

where Δt is the period of time (in seconds); Δz , the thickness of the layer (m); $\Delta F^{\text{net}}/\Delta z$, the divergence of net flux across the layer Δz ; and C_p , the specific heat at constant pressure ($\text{J}\cdot^{\circ}\text{K}^{-1}\cdot\text{Kg}^{-1}$). Applying the hydrostatic equation:

$$\Delta p = - \rho g_a \Delta z \quad (2.18)$$

the heating/cooling rate can be expressed as follows:

$$\frac{\Delta T}{\Delta t} = \frac{g_a}{C_p} \frac{\Delta F^{\text{net}}}{\Delta p} \quad (2.19)$$

where Δp is the differential pressure; g_a , the gravitational acceleration ($\approx 9.8 \text{ m}\cdot\text{sec}^{-2}$); and g_a/C_p , the adiabatic lapse rate for air.

The above-mentioned applications are made possible only if the integrals in the formal solutions of Eqs. 2.9-10 can be carried out explicitly. If the source function (J) is neglected completely, the solution is readily obtained, and turn out to be the Beer-Bouguer-Lambert law of extinction. For all other cases, computational methods for solving the integro-differential equation (i.e., Eq.2.2) must be applied

to get solutions and preferably these methods should be capable of achieving the solutions at any desired accuracy.

Comprehensive reviews of several existing and proposed computational methods for radiative transfer problems can be found in the reports of the Radiation Commission of IAMAP (International Association of Meteorology and Atmospheric Physics, 1977 and 1980). However, the present study will concentrate on the discrete ordinate method, which, as will be demonstrated in the following section, has many favorable computational properties.

2.1 Discrete Ordinate Method

The Discrete Ordinate Method (DOM) has been utilized to investigate radiative transfer problems in planetary atmospheres for more than four decades since its introduction by Chandrasekhar in the 1940's. The principle of the discrete ordinate method is to reduce the integro-differential equation (i.e., Eq.2.2) to a system of ordinary differential equations by means of the Gaussian formula, the Legendre polynomials, and the Fourier expansions. However, the numerical difficulties of finding the eigensolutions inherent in the previous computational implementations of DOM's have been reported and discussed by many investigators (e.g., Liou, 1973; Asano, 1975). Not until the contributions of

Stamnes and his colleagues has an unconditionally stable solution been found (Stamnes and Swanson, 1981; Stamnes and Dale, 1981; Stamnes and Conklin, 1984). The key elements for the earlier development and recent extension of the DOM will be presented and a well-documented computing code can be found in Appendix F.

Following the notations of Stamnes and Swanson (1981), the monochromatic radiative transfer equation (Eq. 2.2) is rewritten as follows:

$$\mu \frac{dI(\tau, \mu, \phi)}{d\tau} = I(\tau, \mu, \phi) - \frac{\omega}{4\pi} \int_0^{2\pi} \int_{-1}^1 P(\mu, \phi; \mu', \phi') I(\tau, \mu', \phi') d\mu' d\phi' - Q(\tau, \mu, \phi) \quad (2.20)$$

where Q is the internal source term. If $I(\tau, \mu, \phi)$ represents the diffuse instead of the total intensity (diffuse plus direct), then for a parallel beam of sunlight incident on a thermal emitting atmosphere, the internal source term (Q) can be defined as follows:

$$Q(\tau, \mu, \phi) = \frac{\omega I^{\text{inc}}}{4\pi} P(\mu, \phi; -\mu_0, \phi_0) e^{-\tau/\mu_0} + (1-\omega)B(T) \quad (2.21)$$

where μ_0 is the cosine of the solar zenith angle and $\mu_0 I^{\text{inc}}$ is the incident solar flux. The first term in the right-hand side of Eq. 2.11 is the so-called "pseudo-source" (Wiscombe, 1976), due to single scattering of the direct solar flux.

The diffuse intensity (I) and internal source term (Q) can be expanded as a Fourier cosine series of $2n-1$ terms:

$$I(\tau, \mu, \phi) = \sum_{m=0}^{2n-1} I^m(\tau, \mu) \cos m(\phi_0 - \phi) \quad (2.22)$$

and

$$Q(\tau, \mu, \phi) = \sum_{m=0}^{2n-1} Q^m(\tau, \mu) \cos m(\phi_0 - \phi) \quad (2.23)$$

Also, the phase function (P) can be expanded in a series of $2n-1$ Legendre polynomials by using the addition theorem for spherical harmonics (e.g., Liou [1980], Appendix G):

$$P(\mu, \phi; \mu', \phi') = \sum_{m=0}^{2n-1} (2-\delta_{0,m}) \sum_{l=m}^{2n-1} (2l+1) g_l^m P_l^m(\mu) P_l^m(\mu') \cos m(\phi' - \phi) \quad (2.24)$$

with $g_l^m = g_l (l-m)! / (l+m)!$ and $\delta_{0,m} = 1$ (or 0) for $m = 0$ (otherwise). The coefficients g_l are the moments of the phase function (P) with respect to the Legendre polynomials.

Substituting Eqs. (2.22-24) into the transfer equation (2.20) and noting that $\cos m(\phi_0 - \phi)$ cancels on both sides, a system of $2n$ independent equations is obtained as follows:

$$\begin{aligned} \mu \frac{dI^m(\tau, \mu)}{d\tau} &= I^m(\tau, \mu) - Q^m(\tau, \mu) \\ - \frac{\omega}{2} \sum_{l=m}^{2n-1} (2l+1) g_l^m P_l^m(\mu) \int_{-1}^1 P_l^m(\mu') I(\tau, \mu') d\mu' & \\ (m = 0, 1, \dots, 2n-1) & \end{aligned} \quad (2.25)$$

A detailed derivation of the last term on the right-hand side can be found in Appendix B. Then, applying the double-Gaussian formula to replace the integral by summation over a finite number of quadrature points, Eq.2.25 can be expressed as follows:

$$\begin{aligned} \mu_i \frac{dI^m(\tau, \mu_i)}{d\tau} &= I^m(\tau, \mu_i) - Q^m(\tau, \mu_i) \\ - \frac{\omega}{2} \sum_{l=m}^{2n-1} (2l+1) g_l^m P_l^m(\mu_i) \sum_{j=-n}^n a_j P_l^m(\mu_j) I(\tau, \mu_j) \\ &\quad (i = \pm 1, \pm 2, \dots, \pm n) \end{aligned} \quad (2.26)$$

where the quadrature weights (a 's) and points (μ 's) satisfy $a_{-j} = a_j$ and $\mu_{-j} = -\mu_j$; and the quadrature points of $2n$ are the usual terms of N -stream approximations.

If flux calculations are desired only, they correspond to the azimuth-independent case ($m=0$). The definition of fluxes (Eqs.2.11-12) shows that integration of the intensity over azimuthal components (Eq. 2.22) leads to

$$\int_0^{2\pi} \cos m(\phi_0 - \phi) d\phi = 0, \text{ for } m \neq 0 \quad (2.27)$$

such that only the $m=0$ term remains. Moreover, for intensity calculation (Eq. 2.22) the $m=0$ case is also needed. For simplicity, the following procedures for solving Eq.2.26 should be presented for the azimuth-independent case ($m=0$), though they apply equally well to the higher-order Fourier components (Stamnes and Dale, 1981).

2.1.1 Homogeneous solution

The discrete ordinate approximation to the zero-order Fourier component of Eq. 2.26 is obtained as follows:

$$\mu_i \frac{dI(\tau, \mu_i)}{d\tau} = I(\tau, \mu_i) - \sum_{j=-n}^n C_{i,j} I(\tau, \mu_j) - Q(\tau, \mu_i) \quad (2.28)$$

and

$$C_{i,j} = \frac{\omega}{2} \sum_{l=0}^{2n-1} a_j^{(2l+1)} g_l P_l(\mu_i) P_l(\mu_j), \quad (i, j = \pm 1, \pm 2, \dots, \pm n)$$

Seeking the homogeneous solution of Eq. 2.28, a direct matrix method is developed (Stamnes and Swanson, 1981) to solve this system of $2n$ coupled differential equations:

$$\begin{bmatrix} \frac{d\mathbf{I}^+}{d\tau} \\ \frac{d\mathbf{I}^-}{d\tau} \end{bmatrix} = \begin{bmatrix} -\alpha & -\beta \\ \beta & \alpha \end{bmatrix} \begin{bmatrix} \mathbf{I}^+ \\ \mathbf{I}^- \end{bmatrix}; \quad \mathbf{I}^\pm = \begin{bmatrix} I(\tau, \pm\mu_1) \\ I(\tau, \pm\mu_2) \\ \vdots \\ I(\tau, \pm\mu_n) \end{bmatrix} \quad (2.29)$$

where α and β are unsymmetrical and noncommutable matrices containing $n \times n$ elements, given by:

$$\alpha_{i,j} \equiv \mu_i^{-1} (C_{i,j} - \delta_{i,j}) = \mu_i^{-1} (C_{-i,-j} - \delta_{i,j}),$$

$$\beta_{i,j} \equiv \mu_i^{-1} C_{-i,j} = \mu_i^{-1} C_{i,-j}, \quad (i, j = 1, 2, \dots, n)$$

$$\delta_{i,j} = 1 \text{ (or } 0) \text{ for } i = j \text{ (or } i \neq j)$$

Substituting solutions of the form $\mathbf{I}^\pm = \mathbf{g}^\pm e^{-k\tau}$ into Eq. 2.29, a standard eigenvalue problem is obtained as follows:

$$\begin{bmatrix} \alpha & \beta \\ -\beta & -\alpha \end{bmatrix} \begin{bmatrix} \mathbf{g}^+ \\ \mathbf{g}^- \end{bmatrix} = k \begin{bmatrix} \mathbf{g}^+ \\ \mathbf{g}^- \end{bmatrix} \quad (2.30)$$

where the $2n$ k 's are the eigenvalues of the left-hand side coefficient matrix (of order $2n \times 2n$) and the \mathbf{g}^\pm 's are the corresponding eigenvectors. Equation 2.30 can be written as follows:

$$\begin{cases} \alpha \mathbf{g}^+ + \beta \mathbf{g}^- = k \mathbf{g}^+ \\ -\beta \mathbf{g}^+ - \alpha \mathbf{g}^- = k \mathbf{g}^- \end{cases} \quad (2.31)$$

Then, switching rows and changing signs in Eq. 2.31, a set of new but related equations is obtained as follows:

$$\begin{cases} \alpha \mathbf{g}^- + \beta \mathbf{g}^+ = -k \mathbf{g}^- \\ -\beta \mathbf{g}^- - \alpha \mathbf{g}^+ = -k \mathbf{g}^+ \end{cases} \quad \text{or} \quad \begin{bmatrix} \alpha & \beta \\ -\beta & -\alpha \end{bmatrix} \begin{bmatrix} \mathbf{g}^- \\ \mathbf{g}^+ \end{bmatrix} = -k \begin{bmatrix} \mathbf{g}^- \\ \mathbf{g}^+ \end{bmatrix} \quad (2.32)$$

Eqs. 2.30-32 show that the eigenvalues occur in pairs $(k, -k)$ and also that the corresponding eigenvectors have symmetric forms $([\mathbf{g}^+, \mathbf{g}^-], [\mathbf{g}^-, \mathbf{g}^+])$. Eq. 2.30 can be solved for k^2 rather than k and the order of problems can be reduced by a factor of two. This can be done by adding and subtracting rows of Eq. 2.31 to and from each other.

$$(\alpha - \beta)(\mathbf{g}^+ - \mathbf{g}^-) = k(\mathbf{g}^+ + \mathbf{g}^-) \quad (2.33)$$

$$(\alpha + \beta)(\mathbf{g}^+ + \mathbf{g}^-) = k(\mathbf{g}^+ - \mathbf{g}^-) \quad (2.34)$$

Substituting Eq. 2.34 into 2.33, a reduced system ($n \times n$) of the eigenvalue problem is obtained as follows:

$$(\alpha - \beta)(\alpha + \beta)(\mathbf{g}^+ + \mathbf{g}^-) = k^2(\mathbf{g}^+ + \mathbf{g}^-) \quad (2.35)$$

Eq. 2.35 can be solved by using standard and reliable eigenvalue subroutines such as IMSL (International Mathematical and Statistical Library, 1975), which return k^2 and $(\mathbf{g}^+ + \mathbf{g}^-)$. Substituting k and $(\mathbf{g}^+ + \mathbf{g}^-)$ into Eq. 2.34, $(\mathbf{g}^+ - \mathbf{g}^-)$ is found, in terms of which the complete set of eigenvalues $(k, -k)$ and eigenvectors $([\mathbf{g}^+, \mathbf{g}^-], [\mathbf{g}^-, \mathbf{g}^+])$ are obtained from the reduced system. The homogeneous solution of Eq. 2.28 can be expressed as follows:

$$I(\tau, \mu_i) = \sum_{j=-n}^n L_j \mathbf{g}_j(\mu_i) e^{-k_j \tau} \quad (2.36)$$

where L_j 's are constants of integration and can be found from the boundary conditions.

2.1.2 Particular solution

If the internal source term (Q) contains single scattering of the direct solar flux and thermal emission as in Eq. 2.21, a particular solution consisting of two parts is needed to complete the general solution of Eq. 2.28. The azimuth-independent case ($m=0$) of the single scattering term can be expressed as follows:

$$x(\mu_i) e^{-\tau/\mu_0} = \frac{\omega_1^{inc}}{4\pi} \sum_{l=0}^{2n-1} (-1)^l (2l+1) g_l P_l(\mu_i) P_l(\mu_0) e^{-\tau/\mu_0} \quad (2.37)$$

Seeking a particular solution of $I_s(\tau, \mu_i) = z(\mu_i) e^{-\tau/\mu_0}$ and substituting it into Eq. 2.28, a system of $2n$ linear algebraic equations is obtained as follows:

$$\sum_{j=-n}^n [(1 + \mu_i/\mu_0)\delta_{ij} - C_{ij}] Z(\mu_j) = X(\mu_i) \quad (2.38)$$

Likewise, similar systems of linear algebraic equations can be obtained for the thermal emission term. In general, any continuous functions (i.e., the Planck function) may be approximated by a polynomial form. Since the Planck emission is a function of temperature and temperature is related to height, the thermal emission term can be approximated as a polynomial in optical depth:

$$Q(\tau, \mu) = \sum_{r=0}^M X_r \tau^r \quad (2.39)$$

Substituting a particular solution of $I_t(\tau, \mu_i) = \sum_{r=0}^M Z_r(\mu_i) \tau^r$ into Eq. 2.28 and equating the coefficients, systems of linear algebraic equations are obtained as follows:

$$\sum_{j=-n}^n (\delta_{ij} - C_{ij}) Z_M(\mu_j) = X_M$$

and

$$\sum_{j=-n}^n (\delta_{ij} - C_{ij}) Z_r(\mu_j) = X_r + (r+1)\mu_i Z_{r+1}(\mu_i) \quad (r = M-1, M-2, \dots, 0) \quad (2.40)$$

However, an even simpler approximation of linear dependence has been used to study thermal radiation problems since Schwarzschild (1906). This is because the Planck function is proportional to the exponential of temperature at fixed

wavelength (Eq.2.4) and the temperature lapse rate decreases linearly with height in most convective atmospheres:

$$B(T) \propto e^T \propto e^{-z}$$

Optical depth is proportional to density of species (e.g., Eq. 2.1); and by the barometric law, density decreases exponentially with height for hydrostatic atmospheres:

$$B(\tau) \propto (\text{proposed}) \tau \propto \rho \propto e^{-z}$$

Wiscombe (1976) examined comprehensively the maximum errors in approximating the Planck function as linear in optical depth with respect to temperatures and wavelengths. The averaged error over the layer is quite small if ΔT and $\Delta \tau$ are properly chosen. Then, the thermal emission term is:

$$Q(\tau) = (1-\omega)(X_0 + X_1 \tau)$$

with

$$X_1 = [B(T_N) - B(T_0)] / (\tau_N - \tau_0) \text{ and } X_0 = B(T_0) - X_1 \tau_0$$

where T_0 , τ_0 and T_N , τ_N are temperatures and optical depths at the top and bottom of the layer, respectively. Eq. 2.40 can be reduced as follows:

$$\sum_{j=-n}^n (\delta_{ij} - C_{ij}) Z_1(\mu_j) = (1-\omega) X_1$$

and

$$\sum_{j=-n}^n (\delta_{ij} - C_{ij}) Z_0(\mu_j) = (1-\omega) X_0 + \mu_i Z_1(\mu_i)$$

Since $(1-\omega) X_1$ is a constant and the summation of C_{ij} is identical to ω , Z_1 must be a constant and identical to X_1 .

$$z_1 = X_1 \text{ and } \sum_{j=-n}^n (\delta_{ij} - C_{ij}) z_0(\mu_j) = (1-\omega)X_0 + \mu_i z_1 \quad (2.41)$$

Again, solutions of Eqs. 2.38 and 2.40 (or Eq. 2.41) can be obtained by using the linear equation solvers provided by IMSL or LINPACK (LINEar algebra in PACKage, 1979). The accuracy and efficiency of the linear-in-optical-depth approximation of the Planck function will be examined in the next section.

Now, the complete solution of Eq. 2.28 can be written as follows:

$$I(\tau, \mu_i) = \sum_{j=-n}^n L_j g_j(\mu_i) e^{-k_j \tau} + z(\mu_i) e^{-\tau/\mu_0} + z_0(\mu_i) + z_1 \tau \quad (2.42)$$

which has to satisfy boundary (top & bottom) and continuity (layer interface) conditions so that the constant of integration (L_j) can be determined.

2.1.3 Boundary conditions

We assume that the vertically inhomogeneous atmosphere is divided into a number of N homogeneous layers and bounded by top and bottom boundaries, having temperatures and emissivities of T_t, E_t and T_b, E_b , respectively. The layers are allowed to have different optical properties (i.e., ω and P) and the temperature is allowed to vary linearly across each layer as explained above. The top of the atmosphere is illuminated by known sources, such as isotropic (I_{iso}) and/or

parallel beam ($I_{\text{par}} \delta[\mu-\mu_0] \delta[\phi-\phi_0]$) radiation. The bottom boundary is assumed to be a Lambertian surface of albedo A_s , which is an isotropic reflector. If the usual distinction of direct-diffuse intensity is made, as Eq. 2.20, the diffuse intensity of the parallel beam at the top is eliminated. The boundary and continuity conditions can be expressed as follows:

$$\text{Top:} \quad I_1(0, -\mu_i) = I_{\text{iso}} + E_t B(T_t)$$

$$\text{Bottom:} \quad F_{\text{iso}}^+(\tau_N) = E_b B(T_b) + A_s [(F_{\text{dif}}^-(\tau_N) + F_{\text{dir}}^-(\tau_N))]$$

$$\text{Interface:} \quad I_p(\tau_p, \pm\mu_i) = I_{p+1}(\tau_p, \pm\mu_i)$$

$$\text{with } (i = 1, 2, \dots, n) \text{ and } (p = 1, 2, \dots, N-1) \quad (2.43)$$

where "iso", "dif", and "dir" denote the isotropic, diffuse, and direct conditions, respectively. Substituting the complete solution (Eq. 2.42) and the definition of fluxes (Eqs. 2.11-12) into Eq. 2.43, a system of linear algebraic equations is obtained as follows:

$$\text{Top:} \quad \sum_{j=-n}^n L_{j1} g_{j1}(-\mu_i) = -Z_1(-\mu_i) - Z_{01}(-\mu_i) + I_{\text{iso}} + E_t B(T_t)$$

$$\begin{aligned} \text{Bottom:} \quad \sum_{j=-n}^n L_{jN} \{g_{jN}(\mu_i) - 2A_s \sum_{s=1}^n a_s \mu_s g_{jN}(-\mu_s)\} e^{-k_{jN} \tau_N} = \\ - Z_N(\mu_i) e^{-\tau_N/\mu_0} - [Z_{0N}(\mu_i) + Z_{1N} \tau_N] + E_b B(T_b) \quad + \end{aligned}$$

$$A_s \left[\sum_{s=1}^n 2a_s \mu_s \{Z_N(-\mu_s) e^{-\tau_N/\mu_0} + Z_{0N}(-\mu_s) + Z_{1N} \tau_N\} + \mu_0 I^{\text{inc}} e^{-\tau_N/\mu_0} \right]$$

$$\begin{aligned} \text{Interface: } & \sum_{j=-n}^n \left\{ L_{jp} g_{jp}(\pm\mu_i) e^{-k_{jp}\tau_p} - L_{jp+1} g_{jp+1}(\pm\mu_i) e^{-k_{jp+1}\tau_p} \right\} \\ & = [z_{p+1}(\pm\mu_i) - z_p(\pm\mu_i)] e^{-\tau_p/\mu_0} + \\ & \quad [z_{0p+1}(\pm\mu_i) - z_{0p}(\pm\mu_i)] + [z_{1p+1} - z_{1p}] \tau_p \end{aligned}$$

$$\text{with } (i = 1, 2, \dots, n) \text{ and } (p = 1, 2, \dots, N-1) \quad (2.44)$$

However, in solving Eq. 2.44 for optically thick atmospheres, the exponential factors of positive one become out of the range of computation and lead to numerical ill-conditioning. Many scaling algorithms have been suggested (i.e., Yamamoto et al., 1971; Shettle and Green, 1974), but only the one suggested by Stamnes and Conklin (1984) works unconditionally for multi-layered atmospheres. This scaling scheme is:

$$\begin{aligned} L_{+jp} &= D_{+jp} \exp(k_{jp}\tau_{p-1}) \\ L_{-jp} &= D_{-jp} \exp(-k_{jp}\tau_p) \end{aligned} \quad (2.45)$$

with $(j = 1, 2, \dots, n)$, $(p = 1, 2, \dots, N-1)$, and $k_{jp} \geq 0$

Substituting Eq. 2.45 into Eq. 2.44 and solving for D_{jp} instead of L_{jp} , all exponential terms with positive arguments are removed. Again, this system of linear algebraic equations can be solved by the subroutines of either IMSL or LINPACK. For the lower-order-stream approximations (e.g., 2- or 4-stream), the computational speed is faster by using the IMSL than LINPACK, and vice versa for higher-order-stream.

The procedures described in sections 2.1.1 to 2.1.3 give the complete solution to the zero-order ($m=0$) Fourier

component of the intensities. The same procedures can be applied to the higher-order Fourier components (Stamnes and Dale, 1981).

2.1.4 Interpolation scheme of intensity

The importance of intensity calculations for satellite applications and model validations has been discussed in the previous chapter. Intensities at quadrature angles can be obtained by solving the $2n$ similar but independent equations of radiative transfer (Eqs. 2.22 and 2.26). In many applications, however, the intensity is desired at other angles. For most dynamical systems of measurements, interpretations of intensities at arbitrary angles are essential.

After comprehensive studies of the Radiation Commission (1977), most computational methods (e.g., Matrix Operator, Spherical Harmonics, Successive Orders of Scattering, etc.) provide the intensity at quadrature angles while some others (e.g., Doubling/Adding) provide only the azimuth-independent intensity. Therefore, many schemes (e.g., Lagrange, spline, etc.) have been used to interpolate intensities at arbitrary angles from those at quadrature angles (Fricke, 1979; Karp, 1981). However, an analytic interpolation scheme derived directly from the basic transfer equation, developed by Stamnes and Swanson (1981) and recently extended for thermal emission, provides the most reliable result.

Since the thermal emission term contributes only to the azimuth-independent ($m=0$) intensity, the derivation of this scheme is presented for this case. After the Fourier expansion, Eq. 2.7 is written as follows:

$$\mu \frac{dI(\tau, \mu)}{d\tau} = I(\tau, \mu) - J(\tau, \mu) \quad (2.46)$$

A similar form to Eq. 2.42 can be assumed for the intensity at arbitrary angles, because the intensity is a continuous function over μ , as follows:

$$I(\tau, \mu) = \sum_{j=-n}^n L_j g_j(\mu) e^{-k_j \tau} + z(\mu) e^{-\tau/\mu_0} + z_0(\mu) + z_1 \tau \quad (2.47)$$

Substituting Eq. 2.47 into 2.46, the source function (J) is obtained as follows:

$$J(\tau, \mu) = \sum_{j=-n}^n (1+k_j \mu) L_j g_j(\mu) e^{-k_j \tau} + \left(1 + \frac{\mu}{\mu_0}\right) z(\mu) e^{-\tau/\mu_0} + z_0(\mu) + (\tau - \mu) z_1 \quad (2.48)$$

To obtain intensity at arbitrary angles, the relationships between eigenvectors [$g(\mu)$ and $g(\mu_i)$] and between components of particular solutions [$z(\mu), z_0(\mu)$ and $z(\mu_i), z_0(\mu_i)$] have to be established. The spline interpolation is frequently used and indeed provides reasonable accuracy in some cases. However, Stamnes (1982) presented and discussed erroneous and uncertain results encountered in spline interpolation of either eigenvectors or intensities. Fortunately, from Eq.

2.48 and the principle of expansion for source function, the following relations are obtained:

$$g_i(\mu) = \frac{\omega}{1+k_i\mu} \sum_{l=0}^{2n-1} (2l+1)g_l P_l(\mu) \left(\frac{1}{2} \sum_{j=-n}^n a_j P_l(\mu_j) g_i(\mu_j) \right)$$

$$Z(\mu) = \frac{\omega}{1+\mu/\mu_0} \sum_{l=0}^{2n-1} (2l+1)g_l P_l(\mu) \left(\frac{1}{2} \sum_{j=-n}^n a_j P_l(\mu_j) Z(\mu_j) + \frac{I^{inc}}{4\pi} (-1)^l P_l(\mu_0) \right)$$

$$Z_0(\mu) = \mu Z_1 + (1-\omega)X_0 + \frac{\omega}{2} \sum_{l=0}^{2n-1} (2l+1)g_l P_l(\mu) \sum_{j=-n}^n a_j P_l(\mu_j) Z_0(\mu_j) \quad (2.49)$$

where X_0 is given in Eq. 2.41. (The detailed derivation of this interpolation scheme can be found in Appendix C.) The superiority of this scheme is shown in Figures 2.4 and 2.5, as reproduced from Stamnes (1982), in which the oscillatory behavior is not found by using this scheme. Both figures are results corresponding to those of the test case of the Radiation Commission (1977) of unit intensity with incident angle of 30° on a slab of optical depth $\tau_N=1$, $\omega=0.9$, and Haze-L phase function (Deirmendjian, 1969).

Using the formal solutions (Eqs.2.9-10) with the source function of Eq.2.48, expressions for intensities (upward and downward) at arbitrary angles and depths can be obtained for both solar and thermal radiation.

$$I(\tau, \mu) = \sum_{j=-n}^n L_j g_j(\mu) \left(e^{-k_j \tau} - e^{-[k_j \tau_N + (\tau_N - \tau)/\mu]} \right) +$$

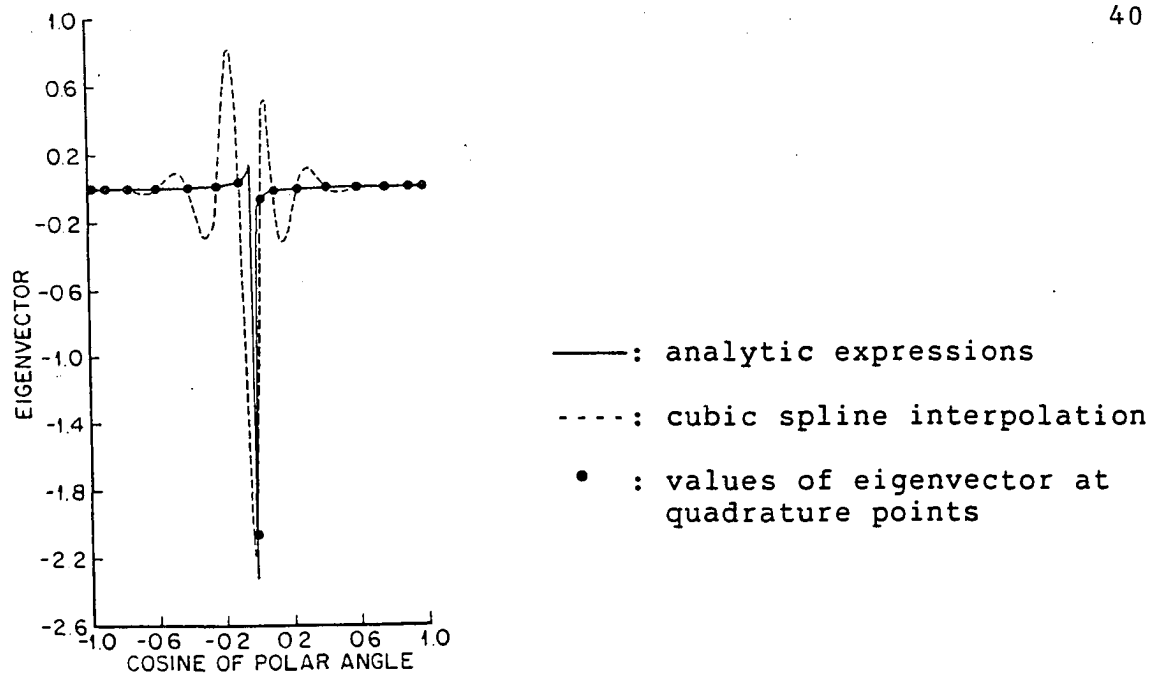


Figure 2.4 Interpolations of eigenvectors (after Stamnes, 1982)

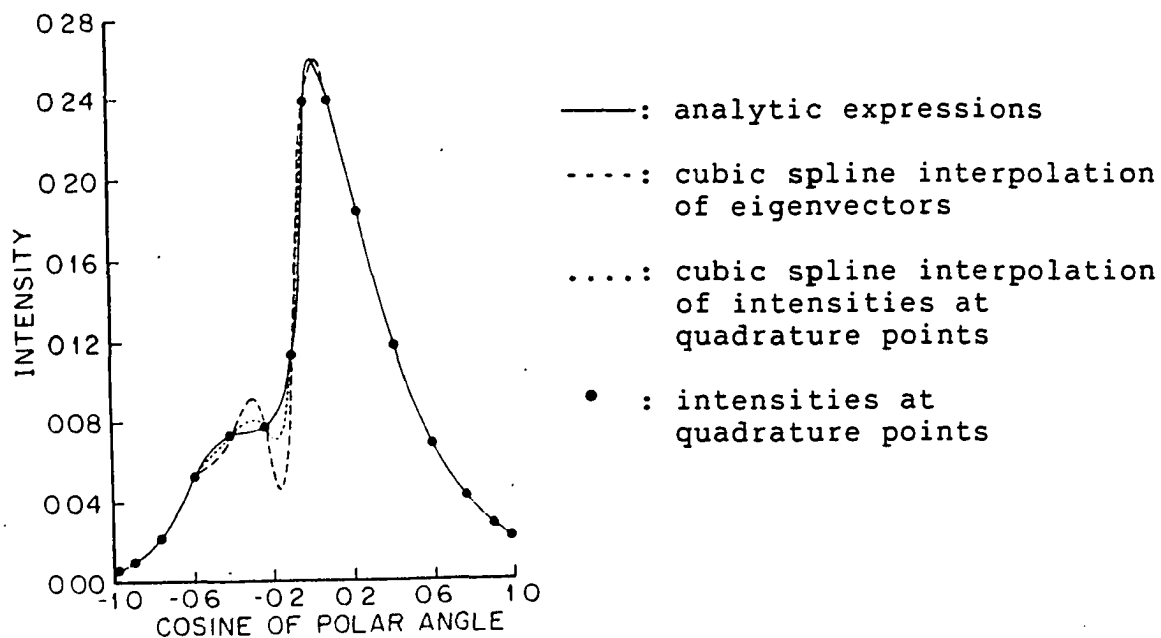


Figure 2.5 Interpolations of azimuthally-averaged intensities (after Stamnes, 1982)

$$\begin{aligned}
& z(\mu) \left(e^{-\tau/\mu} - e^{-[\tau_N/\mu + (\tau_N - \tau)/\mu]} \right) + \\
& z_0(\mu) \left(1 - e^{-(\tau_N - \tau)/\mu} \right) + z_1 \left(\tau - \tau_N e^{-(\tau_N - \tau)/\mu} \right) \\
I(\tau, -\mu) = & \sum_{j=-n}^n L_j g_j(-\mu) \left(e^{-k_j \tau} - e^{-\tau/\mu} \right) + \\
& z(-\mu) \left(e^{-\tau/\mu} - e^{-\tau/\mu} \right) + z_0(-\mu) \left(1 - e^{-\tau/\mu} \right) + z_1 \tau \\
& \qquad \qquad \qquad (1 \geq \mu > 0) \qquad (2.50)
\end{aligned}$$

The historical development and recent extension of the discrete ordinate method for solar and terrestrial radiation has been presented. To emphasize the superiority and soundness of this method, self-sensitivity tests and accuracy comparisons with other leading methods will be conducted in the next section.

2.2 Sensitivity and Accuracy Studies

The degree of sophistication of the radiative transfer solution depends entirely on the degree of accuracy desired. For problems of global energy balance, the spherical albedo, which is a ratio of two integrated quantities (fluxes), is of primary importance. The local heating/cooling rate, which is basically the divergence of fluxes, must be considered in the study of atmospheric dynamics. The investigation of the composition and state of a planetary atmosphere needs the ordinary quantity of intensity. Thus, from a practical point

of view, methods of solving the transfer equation should be made flexible to meet varying needs; and the sensitivity with which the system responds to these modifications and how much accuracy is lost should be studied.

Sensitivity and accuracy studies for the discrete ordinate method are threefold: one should examine the Fourier expansion terms (streams), phase function expansion in the Legendre polynomials, and approximation of thermal emission. However, during the series papers of Stamnes and co-authors (1981, 1982, and 1984), the first two parts have been studied comprehensively. Therefore, their main results will be adopted and discussed; however, an original approximation of thermal emission shall be presented in this thesis.

The following Tables and Figures adopted from the works of Stamnes are test case studies of the Radiation Commission (1977), in which as a parallel beam of incident radiation (intensity normalized to unity or flux being equal to π) on a plane-parallel layer of haze particles (Haze-L phase function) of total optical depth $\tau_N=1$. Table 2.1, as reproduced from Stamnes and Swanson (1981), shows how the integrated fluxes respond to different orders of approximation (i.e., number of streams). $F^+(0)$ and $F^-(\tau_N)$ denote the upward-reflected and downward-transmitted fluxes at top and bottom, respectively. $F^{\text{net}}(0)$ and $F^{\text{net}}(\tau_N)$ denote the downward net fluxes at top and bottom, respectively. Results from Table

Table 2.1 Sensitivity and accuracy comparisons of fluxes computation (after Stamnes and Swanson, 1981)

| (a) non-conservative scattering ($\omega=0.9$) with overhead sun | | | | |
|--------------------------------------------------------------------|----------|---------------|---------------------|--------------------------|
| Method | $F^+(0)$ | $F^-(\tau_N)$ | $F^{\text{net}}(0)$ | $F^{\text{net}}(\tau_N)$ |
| 4-Stream | 0.1207 | 1.5274 | 3.0209 | 2.6831 |
| 8-Stream | 0.1238 | 1.5159 | 3.0178 | 2.6716 |
| 16-Stream | 0.1237 | 1.5155 | 3.0179 | 2.6712 |
| *Spherical harmonics | 0.1236 | 1.5155 | 3.0180 | 2.6712 |
| Matrix operator | 0.1237 | 1.5156 | 3.0179 | 2.6713 |
| Monte Carlo | 0.1230 | 1.516 | 3.019 | 2.672 |
| Discrete ordinates | 0.1237 | 1.5155 | 3.0178 | 2.6714 |
| Doubling* | 0.1237 | 1.5155 | 3.0179 | 2.6713 |

| (b) conservative scattering ($\omega=1.0$) with overhead sun | | | | |
|----------------------------------------------------------------|----------|---------------|---------------------|--------------------------|
| Method | $F^+(0)$ | $F^-(\tau_N)$ | $F^{\text{net}}(0)$ | $F^{\text{net}}(\tau_N)$ |
| 4-Stream | 0.1634 | 1.8225 | 2.9782 | 2.9782 |
| 8-Stream | 0.1733 | 1.8126 | 2.9683 | 2.9683 |
| 16-Stream | 0.1733 | 1.8126 | 2.9683 | 2.9683 |
| *Spherical harmonics | 0.1736 | 1.8124 | 2.9680 | 2.9682 |
| Matrix operator | 0.1734 | 1.7954 | 2.9688 | 2.9512 |
| Monte Carlo | 0.165 | 1.820 | 2.976 | 2.976 |
| Discrete ordinates | 0.1732 | 1.8127 | 2.9644 | 2.9684 |
| Doubling* | 0.1732 | 1.8126 | 2.9684 | 2.9684 |

- methods listed in the report of the Radiation Commission of IAMAP (1977)

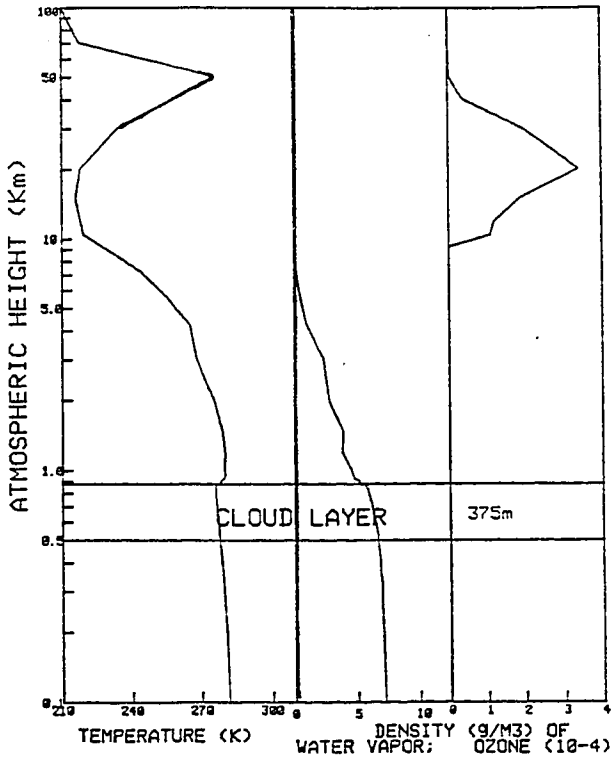
$F^+(0)$, upward flux at top; $F^-(\tau_N)$, downward flux at bottom;

$F^{\text{net}}(0)$, net flux at top; $F^{\text{net}}(\tau_N)$, net flux at bottom;

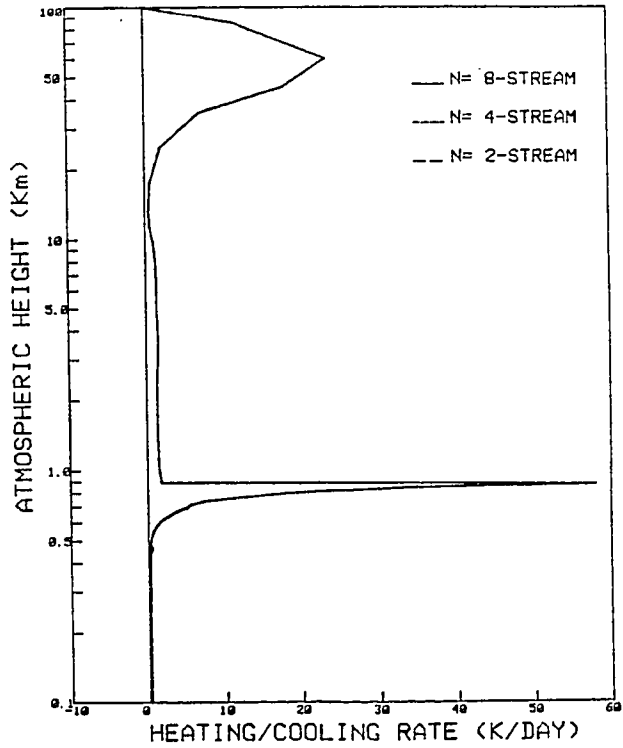
ω , single scattering albedo of haze particles.

2.1 for both cases show insensitivity to the number of streams if the order is higher than 8. The relative variations of results for 4-stream (or lower-order) as compared to those of 8-stream (or higher-order) approximations are about 2 to 5%. Results from spherical harmonics and doubling methods are regarded as benchmark values in the study of the Radiation Commission (1977), in terms of which the 8-stream and higher-order approximations yield very accurate results (better than .1%). However, care should be used in different types of applications. For instance, assuming an overhead sun and a solar constant of 1370 W.m^{-2} , a 2.5% decrease of the upward-reflected flux (4-stream of 0.1207 as opposed to 16-stream of 0.1237, in column 1) corresponds to a decrease of 1.3 W.m^{-2} , which would not alter the global picture. On the other hand, a 0.8% increase of the downward-transmitted flux (1.5274 vs 1.5155, in column 2) permits an increase of 5.2 W.m^{-2} , which would give a local melting rate of snow of about 3cm per month. These arguments are based upon a model of atmospheric profile; a real case study is shown in Figure 2.6. Figure 2.6a shows atmospheric profiles of temperature, water vapor and ozone densities, and a marine stratocumulus cloud taken from JASIN (Joint Air-Sea Interaction) in 1978 (Curry, 1984; private communication). Figure 2.6b shows atmospheric solar heating rates for different streams of approximations. The results agree very well. Figure 2.6c

(a)



(b)



(c)

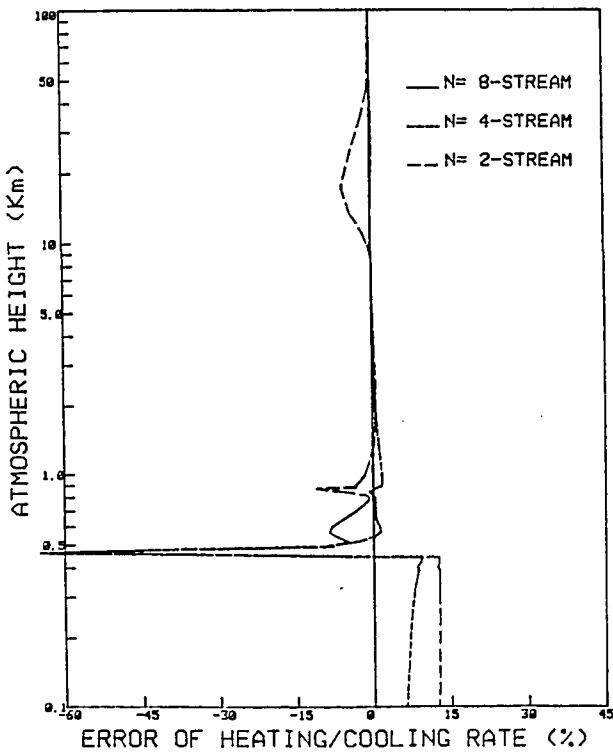


Figure 2.6 Heating/Cooling rates calculation;

- (a) atmospheric profile of JASIN, 1978
- (b) solar heating rate under different orders of approximation
- (c) relative errors of (b) (see text)

shows the relative errors, regarding 8-stream as a standard. Even though a 60% error is shown just beneath the cloud, it corresponds to a 0.1°C variation, which would not be detectable by most conventional instruments. This suggests that 4-stream and 8-stream approximations are adequate for studies of radiative transfer problems when the integrated quantities (e.g., albedo, heating/cooling rate) are concerned.

The speed of diffuse intensity converges as a function of azimuthal components (Eq. 2.22) has been shown by Stamnes and Dale (1981, Figures 2 and 3). For both Figures ($\Delta\phi=0^{\circ}$ and 90°) to meet the desired accuracy, fewer than 10 terms are needed for convergence for angles away from the forward direction ($\mu= -0.1, +0.2, +0.5, \text{ and } +0.8$), whereas about 20 terms are needed for angles close to the forward direction ($\mu= -0.7$ and -0.4). This suggests that 16-stream approximations generally meet the need of intensity computation.

In general, the phase function (P) is assumed to be adequately approximated by a finite series of Legendre polynomials, as in Eq. 2.24. However, low degree polynomials can not approximate the highly asymmetric phase functions which are often found in atmospheric haze particles and droplets, and which have the strong forward peak as shown in Figure 2.3. Furthermore, Wiscombe (1977) indicated that even high order Legendre polynomials are difficult to use to approximate these strongly asymmetric phase functions because of

the numerical ill-conditioning inherent in computational methods and the growth of computer round-off error. To overcome this problem, Wiscombe (1977) introduced a new phase function representation named the "Delta-M method," simply separating the forward peak of phase function from the residual. The forward peak of phase function is represented by a Dirac delta function (f) and the residual ($1-f$) is expanded into a series of Legendre polynomials. This new representation of phase function does not alter the form of the radiative transfer equation (see Appendix D).

Stamnes and Dale (1981, Table 1) also presented the sensitivity and accuracy of net fluxes in different orders of approximation for Haze-L phase function with and without delta-M method. Only for the lower-order approximation (less than 8) are the results improved by the presence of delta-M method for Haze-L. However, when phase functions become extremely asymmetric, results become far better and converge more rapidly with the delta-M than without using the delta-M method. This was shown by Stamnes and Swanson (1981, Table 7), which presented the plane albedo for an atmosphere of $\tau_N=1$, $\omega=0.8$, and various asymmetry factors. The asymmetry factor (g) is defined as the first moment of phase function, where the values of g for 1, 0, and -1 represent the phase function in complete forward, isotropic, and complete backward scattering, respectively. When the values of g approach

unity, as shown by Stamnes and Swanson (1981, Table 7), negative plane albedos appear, which are totally unacceptable. Therefore, using the delta-M method for solving radiative transfer problems involving highly asymmetric scattering is necessary, especially for low-order-stream approximations.

The sensitivity and accuracy studies of thermal emission proceed in three steps: (1) studying extreme cases through model profile, (2) conducting a real cloudy profile, and (3) validating results by comparing them with those from other leading methods. A layer, having a linear temperature profile of 270°K at the top and 280°K at the bottom, emits in the wavenumber interval of 300 to 800 cm^{-1} , corresponding to the peak of these temperatures' emissions. At the bottom of the layer a black-body boundary, having a temperature of 280°K and an emissivity of 1, is assumed. The optical depths of layers range from 0.1 to 100, covering transparent and opaque conditions; and the single scattering albedos vary from 0.1 to 0.95, and the corresponding asymmetry factors from 0.05 to 0.75, representing the absorption/emission and scattering dominant, respectively. A 100-layer isothermal model is considered to be standard because of results converging and the temperature difference across the sublayer being small enough.

Table 2.2 shows sensitivity and accuracy comparisons for flux and flux divergence calculations. When the optical

Table 2.2 Sensitivity and accuracy comparisons of flux computation for thermal emission with various τ , $\omega=0.1$, and $g=0.05$ (in parentheses, for $\omega=0.95$ and $g=0.75$)

| (a) Upward Fluxes at Top | | | | |
|--------------------------|--------------------------|--------------------------|--------------------------|--------------------------|
| τ | Linear Approximation | | Isothermal Approximation | |
| | 4-Stream | 16-Stream | 16-Stream | 16-Stream |
| | only | 1-layer | 100-layer | |
| 0.1 | 176.94458 (173.89310) | 177.08130 (174.65261) | 177.13814 (174.65407) | 177.05495 (174.65090) |
| 1.0 | 167.04579 (148.15121) | 167.16580 (149.63816) | 169.10465 (149.71403) | 167.04295 (149.62221) |
| 10.0 | 158.74234 (107.54546) | 158.80280 (107.58572) | 166.71194 (109.29712) | 158.71082 (107.50042) |
| 100.0 | 157.57259 (101.96455) | 157.63305 (102.01918) | 166.71185 (107.35707) | 157.64155 (101.96778) |

| (b) Flux Divergences in Layer | | | | |
|-------------------------------|----------------------------|----------------------------|----------------------------|----------------------------|
| τ | Linear Approximation | | Isothermal Approximation | |
| | 4-Stream | 16-Stream | 16-Stream | 16-Stream |
| | only | 1-layer | 100-layer | |
| 0.1 | -25.45913 (-1.59585) | -24.62246 (-1.59166) | -24.58588 (-1.58930) | -24.56961 (-1.58824) |
| 1.0 | -119.53798 (-14.88863) | -120.23331 (-14.91903) | -120.05469 (-14.89686) | -119.98355 (-14.88698) |
| 10.0 | -157.44203 (-84.00174) | -157.50162 (-84.06272) | -157.26764 (-83.93784) | -157.28399 (-83.88862) |
| 100.0 | -157.44262 (-101.37064) | -157.50307 (-101.42691) | -157.26908 (-101.27623) | -157.38746 (-101.29851) |

Note: Wavenumber interval, 300 to 800 cm^{-1} ;

Temperature at top, 270 °K; at bottom, 280 °K;

Thermal flux at top, 160.81 $\text{W}\cdot\text{m}^{-2}$; at bottom, 179.85 $\text{W}\cdot\text{m}^{-2}$;

depth is small (transparent), the upward flux is essentially produced by the radiation emitted from the lower boundary. As the optical depth becomes larger, the absorption of the layer approaches saturation (for a small ω it is reached faster) and quasi-black body behavior is observed. Similar results are found for the downward flux. In general, the linear approximation of a 16-stream 1-layer model yields an accuracy of 0.1 W.m^{-2} , and of 0.5 W.m^{-2} for a 4-stream 1-layer model. However, an isothermal approximation of a 16-stream 1-layer model systematically overestimates the upward flux at the top and underestimates the downward flux at the bottom, especially for a large optical depth (quasi-black body radiation). This is because isothermal approximations have the characteristics of overestimating temperature at the top and of underestimating temperature at the bottom ($T_i = 0.5[T_t + T_b]$ and $T_t < T_b$). For flux divergence (Table 2.2b), somewhat better results are obtained for 1-layer isothermal approximation because of compensating errors in upward and downward flux computations. As the optical depth increases, the net loss of the layer increases because of large losses to the bottom boundary. This explains why the surface stays warm when a cloudy (optically thick) layer is above it.

Table 2.3 shows the critical errors of upward and downward intensity at the top and bottom, respectively. Again, the isothermal approximation of a 16-stream 100-layer model

Table 2.3 Critical errors of intensity at quadrature angles for thermal emission with various τ , $\omega=0.1$, and $g=0.05$ (in parentheses, for $\omega=0.95$ and $g=0.75$)

| (a) Upward intensity at top | | |
|-----------------------------|---------------------------------|--------------------------------|
| τ | Linear 16-stream | Isothermal 16-stream |
| 0.1 | 0.01 ~ 0.08% (0.00 ~ 0.01%) | 0.01 ~ 3.36% (0.00 ~ 0.35%) |
| 1.0 | 0.03 ~ 0.09% (0.01 ~ 0.02%) | 0.57 ~ 5.42% (0.01 ~ 0.99%) |
| 10.0 | -0.03 ~ 0.07% (0.06 ~ 0.08%) | 4.67 ~ 5.76% (1.18 ~ 2.87%) |
| 100.0 | -0.05 ~ 0.01% (0.02 ~ 0.06%) | 5.73 ~ 5.78% (5.20 ~ 5.44%) |

| (b) Downward intensity at bottom | | |
|----------------------------------|--------------------------------|------------------------------------|
| τ | Linear 16-stream | Isothermal 16-stream |
| 0.1 | 0.08 ~ 0.10% (0.01 ~ 0.04%) | -0.05 ~ -3.11% (0.01 ~ -0.31%) |
| 1.0 | 0.06 ~ 0.10% (0.01 ~ 0.05%) | -0.84 ~ -4.74% (-0.01 ~ -0.51%) |
| 10.0 | 0.06 ~ 0.08% (0.02 ~ 0.06%) | -4.20 ~ -4.98% (-0.85 ~ -1.24%) |
| 100.0 | 0.06 ~ 0.10% (0.02 ~ 0.05%) | -5.01 ~ -5.12% (-1.51 ~ -3.39%) |

Note: Wavenumber interval, 300 to 800 cm^{-1} ;

Temperature at top, 270 $^{\circ}\text{K}$; and 280 $^{\circ}\text{K}$ at bottom;

Planck function at top, 51.19 $\text{W}\cdot\text{m}^{-2}\cdot\text{sr}^{-1}$;

Planck function at bottom, 57.25 $\text{W}\cdot\text{m}^{-2}\cdot\text{sr}^{-1}$

Table 2.4 Optical parameters for flux calculations of an inversion case in thermal emission

| ν | 0 | 100 | 200 | 300 | 400 | 500 | 600 | 700 | 800 | 900 | 1000 | 1100 | 1200 | 1300 | ∞ |
|-----------|---|------|------|------|------|------|------|------|------|------|------|------|------|------|----------|
| λ | | 66.0 | 40.0 | 28.5 | 22.2 | 18.0 | 15.4 | 13.3 | 11.8 | 10.5 | 9.5 | 8.7 | 8.0 | | |
| τ | | 0.6 | 0.9 | 1.4 | 2.0 | 2.4 | 2.4 | 2.1 | 1.2 | 1.1 | 1.4 | 2.0 | 2.4 | | |
| ω | | 0.05 | 0.13 | 0.25 | 0.29 | 0.31 | 0.29 | 0.26 | 0.23 | 0.43 | 0.65 | 0.75 | 0.79 | | |
| g | | 0.03 | 0.07 | 0.14 | 0.23 | 0.34 | 0.41 | 0.48 | 0.55 | 0.60 | 0.64 | 0.69 | 0.72 | | |
| I(%) | 1 | 3 | 7 | 10 | 11 | 12 | 11 | 10 | 8 | 7 | 5 | 4 | 3 | 8 | |

Note: Temperature at top: 279.2 degree K; $B(T_t) = 109.678 \text{ W.m}^{-2} \text{ .sr}^{-1}$

at bottom: 271.2 degree K; $B(T_b) = 97.637 \text{ W.m}^{-2} \text{ .sr}^{-1}$

ν (cm^{-1}), wavenumber; λ (microm), wavelength at center of interval;

ω , single scattering albedo of droplet; g , asymmetry factor;

I(%), percentage of intensity over entire spectrum.

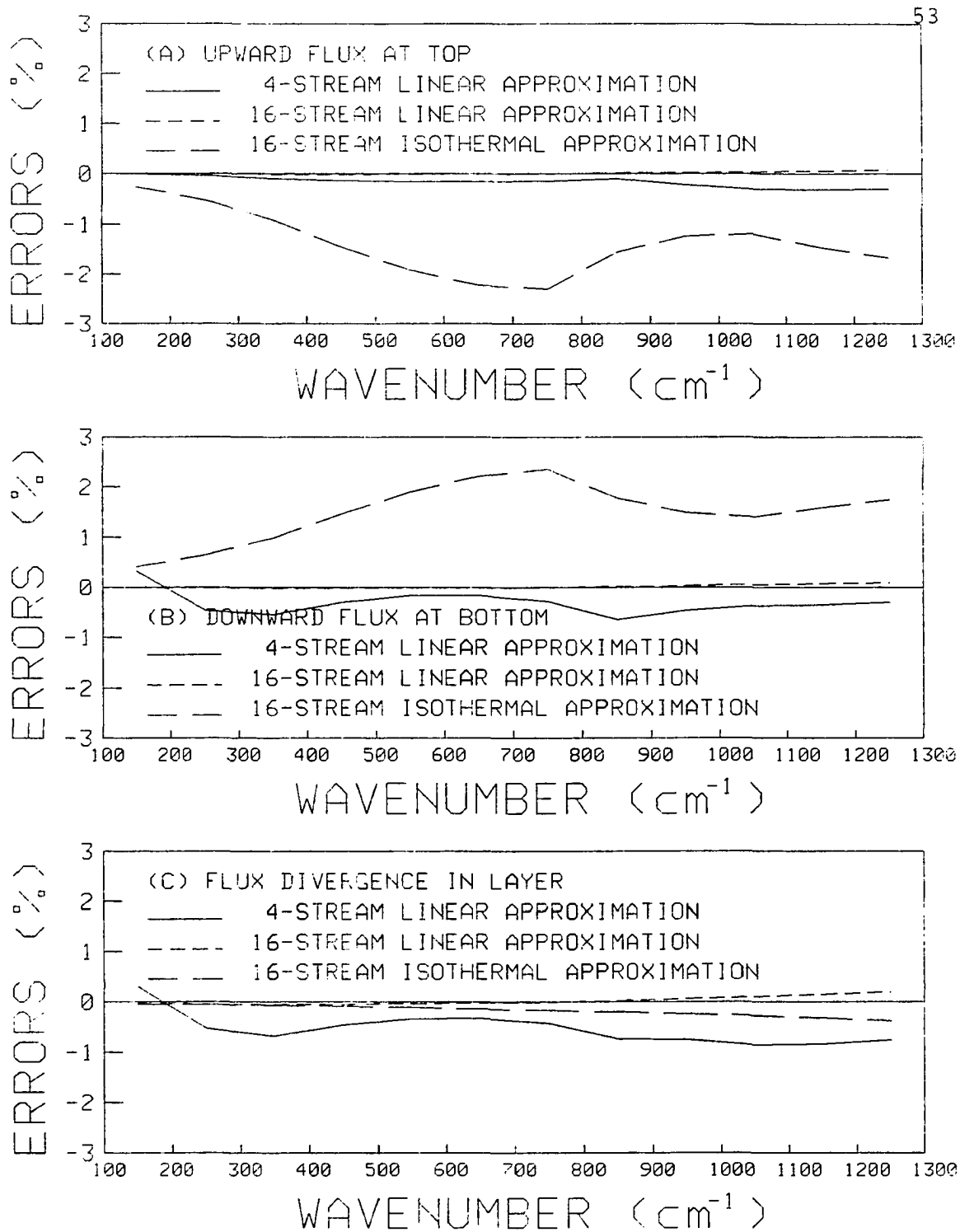


Figure 2.7 Relative errors of fluxes and flux divergences for an inversion cloudy profile (see text)

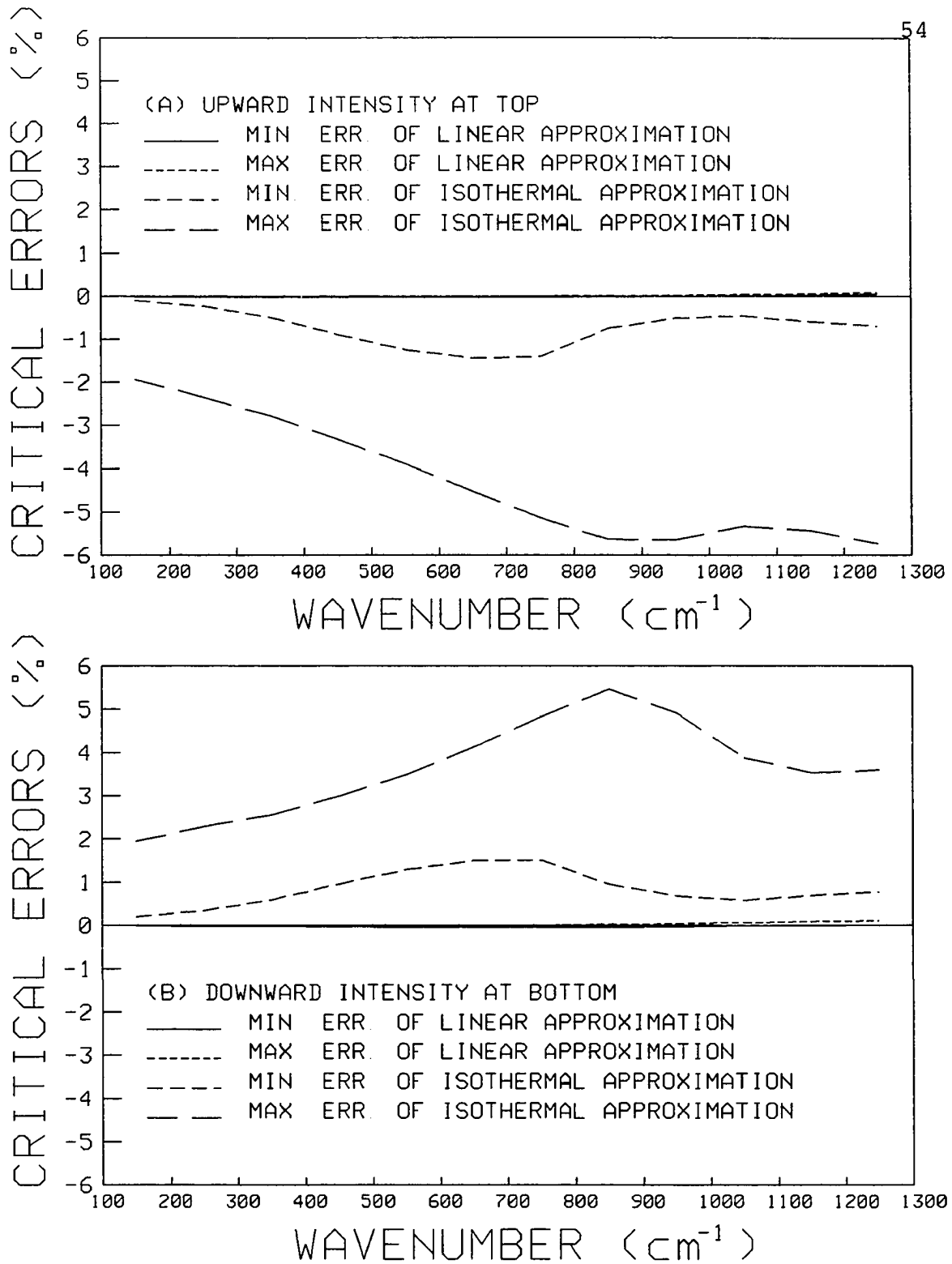


Figure 2.8 Critical errors of upward and downward intensities for an inversion cloudy profile

is considered to be standard. The positive critical errors represent overestimation with respect to standard values; and the negative errors, for underestimation. Clearly, the linear approximation performs far better than the isothermal approximation does. In general, intensities of the linear approximation agree with standard values in 2 to 3 digits.

During the Arctic stratus cloud experiment (Tsay and Jayaweera, 1984), a frequently observed phenomenon was the low level stratus cloud in the surface inversion layer. An atmospheric profile is assumed as the inversion layer starts from the sea surface (about -1.8°C or 271.2°K) to about 200m high with a temperature of about 279.2°K . The St-II drop size distribution (Stephens, 1979) is assumed to infer the optical properties shown in Table 2.4. Figure 2.7 shows the relative errors of fluxes and flux divergences for three 1-layer approximations, regarding the isothermal approximation of 16-stream 100-layer as standard. Similar results to those shown in Table 2.2 are obtained, while the overestimation of the isothermal approximation becomes an underestimation for upward flux (and vice versa for downward flux) because of the inversion structure. Figure 2.8 shows the critical errors of intensities at quadrature angles, which are also consistent with those shown in Table 2.3.

The average computer CPU time, in VAX-785, for linear approximation of 4-stream 1-layer models is about 0.1

seconds; about 0.4 seconds for 16-stream 1-layer models; and about 40 seconds for 16-stream 100-layer isothermal models. Clearly, the computer CPU times increase linearly with the number of layers. To study climatic problems the process of calculating radiative terms, often taking up to 90% of total computing time, has to be performed many times over the time and space domains. Thus, the linear approximation in optical depth for thermal emission can improve computing efficiency and still maintain accuracy.

The Doubling method is considered one of the most accurate methods in flux and azimuth-independent intensity computation (Wiscombe, 1976; Radiation Commission, 1977); the computing code for this study has been supplied by Dr. Wiscombe (1985, private communication). Results for thermal emission will be tested against those produced by the Doubling method, which generally has an accuracy of 3 to 4 digits (Wiscombe, 1977). A similar profile as for Table 2.2 is assumed, except for the Planck function being integrated for the entire spectrum.

Table 2.5 shows the comparisons of flux and flux divergence computation for various τ , w , and g . In general, the results of linear approximation for 16 streams yield very good agreement (within 3 to 4 digits) with those from the Doubling method. Results from 4-stream models have an accuracy of a few $W.m^{-2}$. For intensities at quadrature

Table 2.5 Comparisons of flux and flux divergence computation with Doubling method for various τ , ω , and g

| (a) Upward Flux at top | | | | | |
|------------------------|----------|------|----------------------|-----------|-----------|
| τ | ω | g | Linear Approximation | | Doubling |
| | | | 4-Stream | 16-Stream | |
| 0.1 | 0.05 | 0.05 | 343.15221 | 343.36550 | 343.36742 |
| | 0.50 | 0.50 | 337.76812 | 338.60296 | 338.60286 |
| | 0.95 | 0.75 | 336.93579 | 338.40760 | 338.40745 |
| | 1.00 | 0.80 | 337.87899 | 339.54780 | 339.54938 |
| 1.0 | 0.05 | 0.05 | 321.71745 | 321.92726 | 321.92764 |
| | 0.50 | 0.50 | 305.52117 | 306.49134 | 306.49146 |
| | 0.95 | 0.75 | 286.57414 | 289.46036 | 289.46029 |
| | 1.00 | 0.80 | 287.25486 | 291.15461 | 291.15486 |
| 10.0 | 0.05 | 0.05 | 301.46970 | 301.52745 | 301.52743 |
| | 0.50 | 0.50 | 280.30720 | 280.99086 | 280.99084 |
| | 0.95 | 0.75 | 204.77987 | 204.84524 | 204.84527 |
| | 1.00 | 0.80 | 136.45177 | 135.59093 | 135.59099 |
| 100.0 | 0.05 | 0.05 | 298.60583 | 298.66359 | 298.66357 |
| | 0.50 | 0.50 | 276.26904 | 276.95128 | 276.95126 |
| | 0.95 | 0.75 | 191.43607 | 191.53746 | 191.53748 |
| | 1.00 | 0.80 | 21.93605 | 21.68752 | 21.68752 |

Note: Wavenumber interval, 1 to 100000 cm^{-1} ;

Temperature at top, 270 $^{\circ}\text{K}$; and 280 $^{\circ}\text{K}$ at bottom;

Thermal flux at top, 301.345 $\text{W}\cdot\text{m}^{-2}$;

Thermal flux at bottom, 348.528 $\text{W}\cdot\text{m}^{-2}$

| (b) Flux Divergences in Layer | | | | | |
|-------------------------------|----------|------|----------------------|------------|------------|
| τ | ω | g | Linear Approximation | | Doubling |
| | | | 4-Stream | 16-Stream | |
| 0.1 | 0.05 | 0.05 | -50.02499 | -48.30426 | -48.31028 |
| | 0.50 | 0.50 | -28.00336 | -27.43646 | -27.43837 |
| | 0.95 | 0.75 | -2.99055 | -2.98271 | -2.98273 |
| | 1.00 | 0.80 | 0.00000 | 0.00000 | 0.00000 |
| 1.0 | 0.05 | 0.05 | -229.10460 | -230.42474 | -230.42912 |
| | 0.50 | 0.50 | -168.98433 | -170.11709 | -170.11942 |
| | 0.95 | 0.75 | -27.90069 | -27.95764 | -27.95769 |
| | 1.00 | 0.80 | 0.00000 | 0.00000 | 0.00000 |
| 10.0 | 0.05 | 0.05 | -298.28673 | -298.34298 | -298.34296 |
| | 0.50 | 0.50 | -275.78033 | -276.45025 | -276.45024 |
| | 0.95 | 0.75 | -157.41582 | -157.53010 | -157.53020 |
| | 1.00 | 0.80 | 0.00000 | 0.00000 | 0.00000 |
| 100.0 | 0.05 | 0.05 | -298.28762 | -298.34538 | -298.34536 |
| | 0.50 | 0.50 | -275.82029 | -276.50234 | -276.50231 |
| | 0.95 | 0.75 | -189.96443 | -190.06987 | -190.06990 |
| | 1.00 | 0.80 | 0.00000 | 0.00000 | 0.00000 |

Note: Wavenumber interval, 1 to 100000 cm^{-1} ;

Temperature at top, 270 $^{\circ}\text{K}$; and 280 $^{\circ}\text{K}$ at bottom;

Thermal flux at top, 301.345 $\text{W}\cdot\text{m}^{-2}$;

Thermal flux at bottom, 348.528 $\text{W}\cdot\text{m}^{-2}$

angles the results agree in 3 to 4 digits for both methods. But as the τ and ω increase, agreements are reduced to within 2 or 3 digits. The critical errors of intensities relative to those from the Doubling method are shown in Table 2.6.

However, the Doubling method requires large significant digit in computation to achieve the desired accuracy because of heavy matrix manipulation. For instance, the VAX mini-computer has 7 significant digits for single precision and 16 for double precision. Running conservative scattering ($\omega=1$) and optically thick cases ($\tau>1$) with single precision on the VAX, results of the flux divergence from the Doubling method become unstable with spurious absorption/emission. Refining on the initial-layer size (Wiscombe, 1976) does not improve this situation. The only explanation for this is the computer round-off errors. These spurious results are not observed in the discrete ordinate method with single precision. The computer CPU times for the Doubling method and the discrete ordinate method are generally compatible for double precision. But as optical depth increases, the Doubling method requires more time than usual, while the speed of the discrete ordinate method remains about the same.

Table 2.6 Critical errors of intensities at quadrature angles relative to Doubling method for various τ , ω , and g

| τ | ω | g | Upward intensity | Downward intensity |
|--------|----------|------|------------------|--------------------|
| 0.1 | 0.05 | 0.05 | -0.001 ~ -0.006% | -0.091 ~ 0.001% |
| | 0.50 | 0.50 | -0.000 ~ 0.000% | -0.000 ~ -0.002% |
| | 0.95 | 0.75 | 0.000 ~ 0.000% | 0.000 ~ 0.000% |
| | 1.00 | 0.80 | 0.000 ~ 0.000% | 0.000 ~ 0.000% |
| 1.0 | 0.05 | 0.05 | -0.000 ~ 0.026% | -0.092 ~ 0.003% |
| | 0.50 | 0.50 | -0.000 ~ 0.000% | -0.000 ~ -0.002% |
| | 0.95 | 0.75 | -0.000 ~ 0.000% | -0.000 ~ 0.000% |
| | 1.00 | 0.80 | -0.000 ~ 0.000% | 0.000 ~ 0.000% |
| 10.0 | 0.05 | 0.05 | -0.037 ~ 0.010% | -0.114 ~ 0.087% |
| | 0.50 | 0.50 | -0.204 ~ 0.006% | -0.005 ~ 0.074% |
| | 0.95 | 0.75 | -0.206 ~ 0.006% | -0.000 ~ 0.009% |
| | 1.00 | 0.80 | -0.206 ~ 0.006% | -0.000 ~ 0.000% |
| 100.0 | 0.05 | 0.05 | -0.230 ~ 0.032% | -0.794 ~ 0.582% |
| | 0.50 | 0.50 | -0.585 ~ 0.012% | -0.035 ~ 0.280% |
| | 0.95 | 0.75 | -0.586 ~ 0.014% | -0.005 ~ 0.095% |
| | 1.00 | 0.80 | -0.586 ~ 0.014% | -0.001 ~ 0.013% |

Note: Wavenumber interval, 1 to 100000 cm^{-1} ;

Temperature at top, 270 $^{\circ}\text{K}$; and 280 $^{\circ}\text{K}$ at bottom;

Planck function at top, 51.19 $\text{W}\cdot\text{m}^{-2}\cdot\text{sr}^{-1}$;

Planck function at bottom, 57.25 $\text{W}\cdot\text{m}^{-2}\cdot\text{sr}^{-1}$

CHAPTER 3. PARAMETERIZATIONS

Solutions of monochromatic radiative transfer problems can be obtained (Eq. 2.42) if the optical properties (i.e., optical depth, single scattering albedo, phase function, etc.) of the media are known. These optical properties are generally determined by the mixture of physical characteristics of all constituents (i.e., gaseous species, particles, etc.) in the media and in terms of wavelength. Before discussing the parameterization of atmospheric constituents, this thesis will present the characteristics of the forcing term for the transfer equation, which are the spectral distribution of energy and the associated incident angle of shortwave radiation from the sun.

Figure 3.1 shows schematically the energy spectrum of solar and terrestrial radiation. It is convenient and conventional to separate solar and terrestrial radiation at $4\mu\text{m}$ because of the negligible amounts of energy existing beyond $4\mu\text{m}$ for each relative to the other. Thus, the forcing term of the transfer equation signifies only either solar or terrestrial radiation, which simplifies the problem. However, for the special problem of night-time remote sensing (e.g., channel 3 [$3.55\mu\text{m}$ - $3.95\mu\text{m}$] of TIROS-N/NOAA Advanced Very High Resolution Radiometer), a high noise level will be found in

the day-time sensing because of this separation at $4 \mu\text{m}$. For example, terrestrial radiation at 300°K for the wavelength range of channel 3 is about 0.5 W.m^{-2} and solar radiation is about 4.5 W.m^{-2} for the overhead sun. Reflectivity of the earth-atmosphere system at this wavelength region is roughly about 0.1, implying that the reflected solar flux received by the AVHRR sensor is comparable to the terrestrial thermal emission. Neglecting either one will definitely lead to an erroneous interpretation of this special application. Except for special cases like this, it is adequate to separate the two distinct radiations at $4 \mu\text{m}$.

The polar (zenith) angle of the sun, which determines the factor of energy spread, is an important variable for solar radiation studies such as computations of photo-dissociation and ionization rates in the mesosphere and thermosphere, thermal stability of the troposphere, and surface heating. This effect is most pronounced during the arctic summer because of the long illumination period. While tables of zenith angles and sunrise/sunset times at earth's surface are available (i.e. US Naval Observatory, 1945; List, 1968), more precise computation of the solar elevation angle ($\xi = 90^\circ - \theta_0$) can be obtained as follows (Woolf, 1968):

$$\sin\xi = \sin\psi \sin\eta + \cos\psi \cos\eta \cos\zeta \quad (3.1)$$

where ψ is the latitude; η is the solar declination; and ζ is the solar hour angle (all notations are in dimension of

degrees). The solar declination, depending on the angular fraction of a year for a particular date ($d = 360^\circ[\text{date} - 1]/365.242$), can be obtained as follows:

$$\sin\eta = (\sin 23^\circ 26' 37.8'') \sin\epsilon \quad (3.2)$$

where $\epsilon = 279.9348 + d + 1.914827\sin(d) - 0.079525\cos(d) + 0.019938\sin(2d) - 0.00162\cos(2d)$

The solar hour angle is a function of time (GMT, Greenwich Mean Time), true solar noon (M), and longitude (ϕ , counted positive west of Greenwich) of the desired location.

$$\sin\eta = \sin[360^\circ(\text{GMT}-M)/24 - \phi] \quad (3.3)$$

where $M = 12 + 0.123570\sin(d) - 0.004289\cos(d) + 0.153809\sin(2d) + 0.060783\cos(2d)$

Figure 3.2 shows three curves computed from Eq. 3.1 of solar elevation angles for the Arctic Stratus Clouds Experiment in 1980. Mean zenith angles averaged over a few minutes flight were reported by Herman and Curry (1984, column 3 of Table 1), which agree very well with the calculated values (i.e., 53.6° vs 53.50° for June 20 and 53.8° vs 53.83° for June 28). The effect of refraction by the atmosphere is not considered in the computation of solar elevation. A maximum increase of about $36'$ (0.6°) near the horizon is found (i.e. McClatchey *et al.*, 1972; Iqbal, 1983), depending on the atmospheric temperature and pressure profiles. However, when the sun is near the horizon, the plane-parallel approximation is not appropriate for this study and also the energy amount

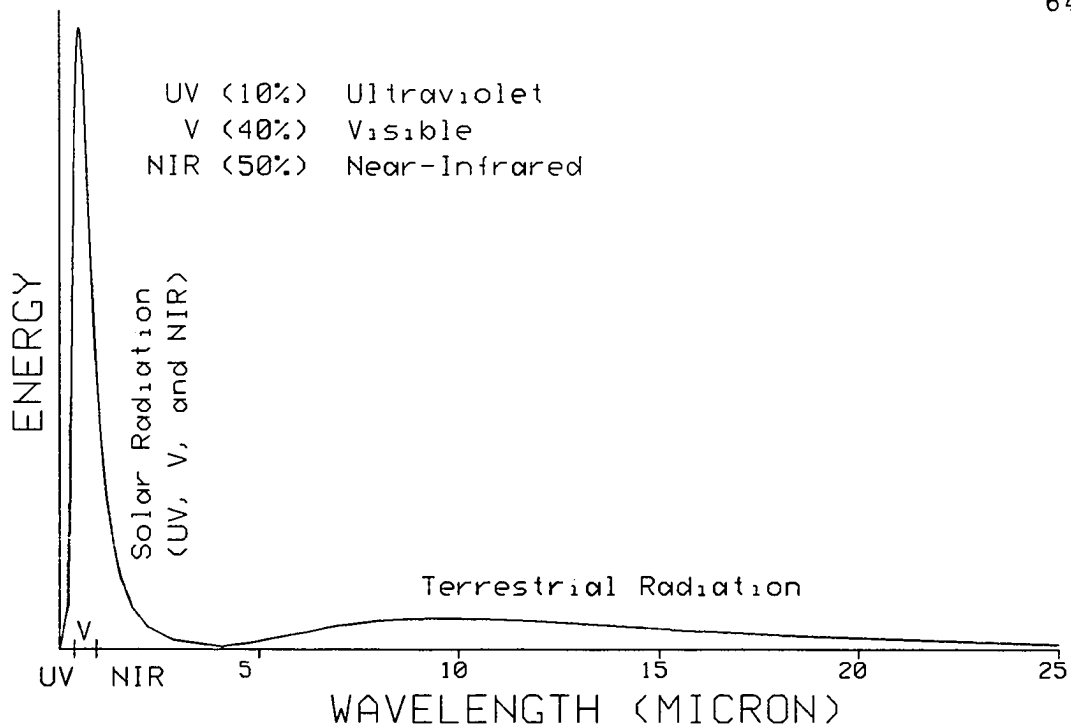


Figure 3.1 Spectral distribution of solar and terrestrial radiation

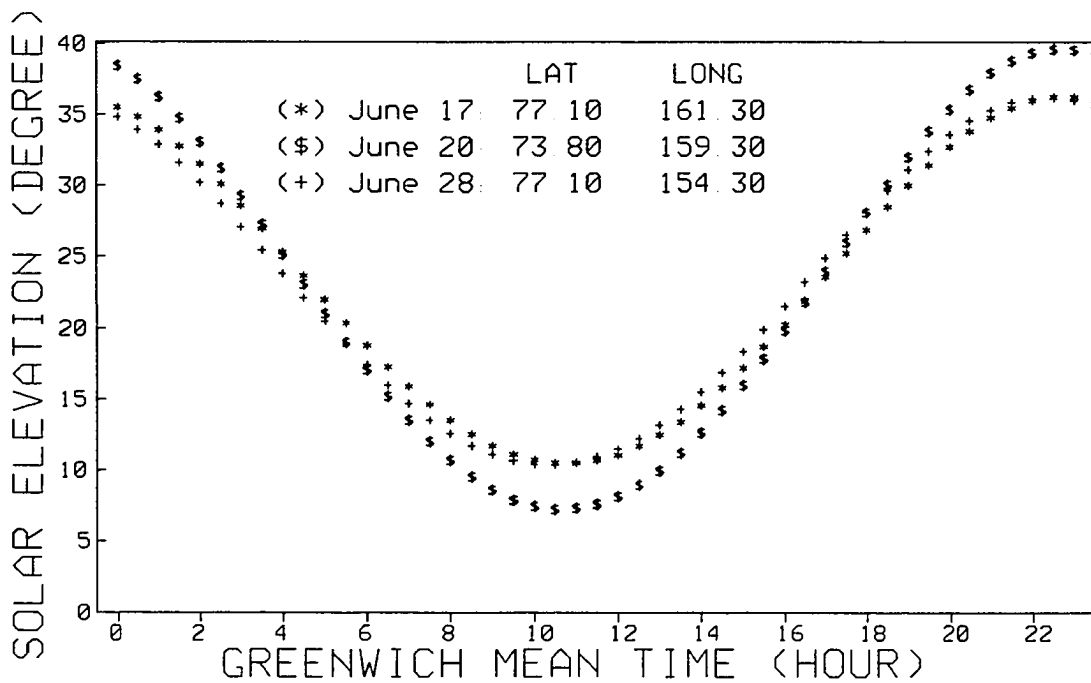


Figure 3.2 Computed solar elevation angles for the Arctic Stratus Clouds Experiment in 1980

associated with the error is quite small. Furthermore, the arctic atmosphere is relatively thin; therefore, the effect of refraction is even smaller. Thus, Eq. 3.1 is considered accurate enough for this study.

Parameterization of constituents for the Arctic atmosphere and surface will be concentrated to the following: (a) three main trace gases -- water vapor, carbon dioxide, and ozone; (b) low-level stratus clouds and haze particles; and (c) pure snow/ice and soot contamination.

3.1 Absorption/Emission And Scattering Of Gaseous Molecules

More than 99% of the earth's atmosphere is composed of nitrogen (N_2) and oxygen (O_2) gases. Because of their molecular structures, these two gases do not absorb radiant energy of wavelengths beyond the ultraviolet portion (about 90% of solar radiation, Figure 3.1), except for an absorption band around $0.76\mu m$ for oxygen. Rayleigh scattering is dominant for them and will be discussed later. The atmospheric (or greenhouse) effect which provides a liveable environment for life on the earth is due to the absorption/emission of trace gases (less than 1% of the air): mainly water vapor (H_2O), carbon dioxide (CO_2), and ozone (O_3).

Figure 3.3 shows radiation data gathered in two clear-sky observations. For solar radiation, the outer curve was

observed at top of the atmosphere while the inner curve was observed at sea level. The shaded area is due to the absorption of gases (H_2O , CO_2 , and O_3) and the area between the outer curve and the shaded area is caused by scattering. For terrestrial radiation (noting that the vertical scale is changed), the emission spectrum was observed by satellite interferometer from space on a clear day. The surface was emitting at temperature of about 300°K . The two dips in the emission spectrum were caused by the re-emission of CO_2 and O_3 at their stratospheric temperatures (about 220 and 260°K , respectively), and surface emission was completely absorbed at those two bands. Water vapor and continuum absorption/emission are dominant in the moist atmosphere of middle and lower troposphere and cover large portions of the spectrum.

The gaseous absorption spectroscopy appears essentially in fine line structures, due to the energy transition from one quantum state to another. The important parameters of spectral lines (e.g., frequency at line center, intensity, half-width, etc.) have been compiled and reported by McClatchey et al. (1972) and continuously updated since then up to some 159,000 lines (Rothman, 1981). However, spectral lines can be broadened as band structures, mainly because of the Doppler effect (molecular movement) in the higher atmosphere ($<6\text{KPa}$) or the pressure effect (molecular collision) in the lower atmosphere ($>30\text{KPa}$) or a combination of both effects for in between (6KPa to 30KPa).

No matter how the gaseous absorption structures look, they pose a difficult problem to solve with great accuracy in radiative transfer computations. At first, the radiative transfer in a multiple scattering atmosphere involving cloud and aerosol particles requires monochromatic parameters such as the absorption coefficient of Eq.2.1. Broad band measurements of gaseous absorption can not be applied directly to the transfer equation. Secondly, even using modern computers for line-by-line computation of radiative transfer, which requires the increment of spectral intervals about 10^{-2}cm^{-1} (owing to the rapid variation of absorption lines), the price is far too high to repeat the calculation frequently over time and space domains. Therefore, parameterization of gaseous absorption over a spectral region containing many lines has to be done. For this purpose, two methods, named exponential-sum fitting of transmissions (ESFT) and photon path-length distributions (PPLD), have been established.

The concept for both ESFT and PPLD methods began with the Beer-Bouguer-Lambert law, in which the monochromatic transmittance is expressed as $\text{Trn}(u) = e^{-xY}$, where x denotes the volume absorption coefficient (m^{-1}) and y is the path-length. Band transmission functions are generally not exponential functions. Then, the ESFT method approximates the transmission function of a given spectral region by a finite sum of M exponential terms (Hunt and Grant, 1969; Yamamoto et al., 1971; Wiscombe and Evans, 1977), as follows:

$$\text{Trn}_B(u) \equiv \sum_{i=1}^M w_i e^{-b_i u} \quad \text{and} \quad \sum_{i=1}^M w_i = 1 \quad (3.4)$$

Here, b_i 's are the equivalent absorption coefficients; w_i 's are associated weights ($b_i \geq 0$, $w_i > 0$); and u is the equivalent absorber amount. On the other hand, the PPLD method introduces a function $\varepsilon(y)$, the photon path-length distribution which can be solved by the Monte Carlo method, into transfer equation (Irvine, 1964; Bakan and Quenzel, 1976). Although these two methods have been shown to be equivalent by Bakan *et al.* (1978), the ESFT method provides three advantages: (1) $b_i u$'s behave like monochromatic optical depths which can be incorporated easily into the multiple scattering scheme; (2) considering the observed multiplication property of transmission (Goody, 1964) the overlap of absorbing gases can be treated easily; (3) a unified treatment of shortwave and longwave radiation can be made. Therefore, the ESFT method is adopted for the present study.

Figure 3.4 shows the spectral distribution of ESFT for gaseous absorption. Water vapor absorption is dominant for almost the entire spectrum except for wavelengths shorter than $0.7\mu\text{m}$. Carbon dioxide has a weak absorption band in the near-infrared (around 1.4 to $5\mu\text{m}$) and a strong band in the infrared (centered at $15\mu\text{m}$). Two ozone absorption bands are centered at wavelengths shorter than $0.7\mu\text{m}$ and at $9.6\mu\text{m}$. A narrow absorption band of oxygen molecules is located at

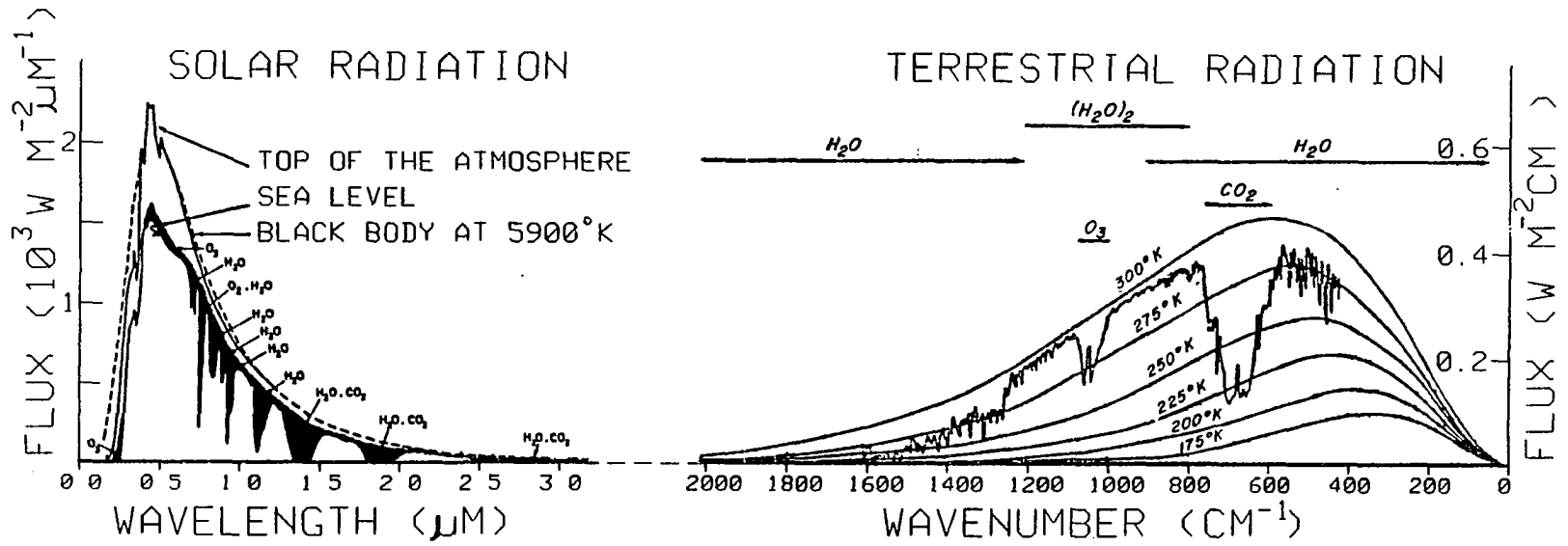


Figure 3.3 Spectral distribution of gaseous scattering and absorption/emission data gathered during two clear-sky observations

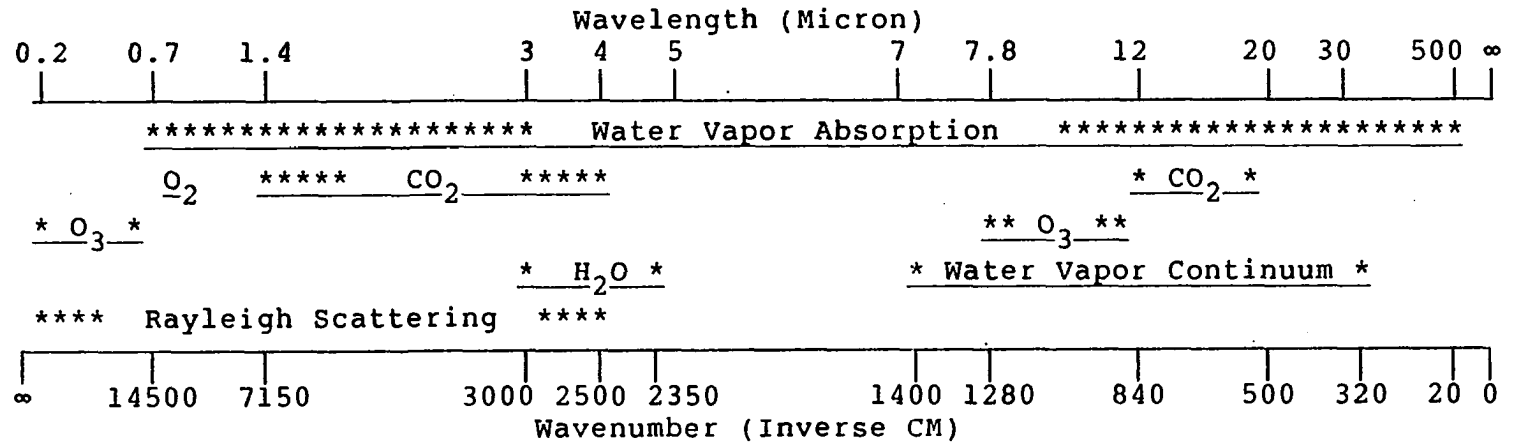


Figure 3.4 Spectral distribution for exponential-sum fitting of transmission for gaseous absorption

0.76 μm . Since solar radiation of wavelengths shorter than 0.2 μm is absorbed completely by O, N, O₂ and N₂ gases before reaching the stratosphere (about 50km high), the spectral region appropriate for present study is from 0.2 μm to 500 μm . Therefore, each set of b_i and w_i for gaseous absorption by H₂O, CO₂, O₃ and O₂ is obtained from fitting the LOWTRAN-5 (LOW-resolution TRANmission, version 5) transmission functions (Kneizys et al., 1980) with 20cm⁻¹ spectral intervals. Because of the low significant digits in the VAX computer, two different ESFT data sets have kindly been provided by Dr. Wiscombe (1985, personal communication) and by Drs. Slingo and Schrecker (1982). The latter treats shortwave radiation for O₃ and H₂O absorption and without overlapping. (A detailed description can be found in their paper.) Their results will be compared with those derived from using ESFT data provided by Dr. Wiscombe.

Empirical scaling of absorber amounts (u_0) is needed to account for the pressure and temperature dependence. Thus, the effective absorber amount (u) is obtained as follows:

$$u(z) = u_0(z) \left\{ \frac{p(z)}{p(0)} \left[\frac{T(0)}{T(z)} \right]^{1/2} \right\}^n \quad (3.5)$$

where $p(0) = 1\text{ATM}$ (1013.25mb); $T(0) = 273.15^\circ\text{K}$; and the constant n is determined empirically to be 0.9 for H₂O, 0.75 for the uniformly mixed gases (i.e., CO₂, O₂), and 0.4 for O₃. For overlapping gases, the combined transmittance (Trn_C)

is obtained by multiplying all individual transmittances (Trn_L , Trn_M , etc.), as follows:

$$\begin{aligned} \text{Trn}_C &= \text{Trn}_L(u_L) \times \dots \times \text{Trn}_M(u_M) \\ &= \sum_{i=1}^L \dots \sum_{j=1}^M w_i \dots w_j e^{-(b_i u_L + \dots + b_j u_M)} \end{aligned} \quad (3.6)$$

This multiplication property of transmissions, together with the behavior of $b_i u$'s as monochromatic optical depths, allows transfer theory to solve problems of multiple scattering involving various gaseous absorption.

Absorptions due to the water vapor continuum is still not well understood theoretically. A possible cause could be the distant wings of H_2O absorption lines being broadened by the collision effect through H_2O molecules themselves or through foreign N_2 molecules. The other possible absorption mechanism could be the presence of dimer molecule $(\text{H}_2\text{O})_2$, which is produced by the reaction of two H_2O molecules which release the binding energy (Carlson, 1981). However, despite the arguments about mechanisms for continuum absorption (Deepak *et al.*, 1980), LOWTRAN-5 accounts for the continuum absorption by a weak band from $3.3\mu\text{m}$ to $4.3\mu\text{m}$ and a strong band from $7\mu\text{m}$ to $31\mu\text{m}$ (as shown in Figure 3.4), based on the far-wing explanation. Therefore, the mass absorption coefficient of water vapor continuum (K_{wvc}) is determined empirically at temperature 296°K , as follows:

$$K_{\text{wvc}}(\nu, 296) = 4.18 + 5578 \exp(-0.00787\nu) \quad (3.7)$$

where ν is the wavenumber (cm^{-1}). Also, the absorber amount has to be scaled to account for temperature and pressure dependence, as follows:

(a) For the infrared region from 7 to $31\mu\text{m}$, in which self-broadening is much more important than foreign-broadening,

$$u(z) = u_0(z) \left\{ p(\text{H}_2\text{O}) \exp \left[6.08 \left(\frac{296}{T(z)} - 1 \right) \right] + 0.002 [p(T) - p(\text{H}_2\text{O})] \right\} \quad (3.8)$$

(b) For the near-infrared region from 3.3 to $4.3\mu\text{m}$, in which foreign-broadening is dominant,

$$u(z) = u_0(z) \left(p(\text{H}_2\text{O}) + 0.12 [p(T) - p(\text{H}_2\text{O})] \right) \times \exp \left(4.56 \left(\frac{296}{T(z)} - 1 \right) \right) \quad (3.9)$$

where $p(T)$ is the ambient pressure (ATM) and $p(\text{H}_2\text{O})$ is the partial pressure (ATM) of water vapor. Other minor gaseous absorptions (e.g., N_2 , N_2O , CH_4 , etc.) are not included in the present study because of their relative unimportance.

Besides the molecular absorption *per se*, the well-known phenomena (i.e., blue sky) caused by air molecules are due to Rayleigh scattering, discovered by Lord Rayleigh in 1871. Rayleigh scattering involves no absorption ($\omega = 1$) and its phase function is symmetric (Figure 2.3a), given as follows (Chandrasekhar, 1960):

$$P_R(\cos E) = 0.75 (1 + \cos^2 E) \quad (3.10)$$

Expanding Rayleigh's phase function in Legendre polynomials (i.e., Eq.2.24) and noting the orthogonality, only two coefficients exist (i.e., $g_0=1$, $g_2=0.1$). A detailed derivation can be found in Appendix E. Because of the dependence of scattered radiation on λ^{-4} , Rayleigh scattering is considered only in the spectral region from $0.2\mu\text{m}$ to $4.0\mu\text{m}$ (Figure 3.4). Penndorf's formula (1957) for Rayleigh's volume extinction coefficient (b_R , m^{-1}) has been widely adopted (Kneizys et al., 1980; Slingo and Schrecker, 1982) and given as follows:

$$b_R(z) = [0.9793(n_a^2 - 1)^2 p(z)] / [\lambda^4 T(z)] \quad (3.11)$$

where n_a denotes the refractive index of air and temperature and pressure dependence is also taken into account. LOWTRAN uses Penndorf's tabulated values of b_R to get the following expression of wavenumber dependence by the least-square fit:

$$b_R = v^4 / (9.26799 \times 10^{18} - 1.07123 \times 10^9 v^2) \quad (3.12)$$

Again, the temperature and pressure dependence is taken into account in the calculation of effective absorber amounts (Eq. 3.5). Moreover, Nicolet (1984) indicated that Rayleigh scattering cross sections (σ_R , cm^2) can be expressed in a simple empirical formula for wavelengths from 0.2 to $1\mu\text{m}$:

$$\sigma_R = 4.02 \times 10^{-28} / \lambda^{4+f} \quad (3.13)$$

where $f = 0.389\lambda + 0.09426/\lambda - 0.3228$ for λ less than $0.55\mu\text{m}$; and $f = 0.04$ for λ greater than $0.55\mu\text{m}$. This will provide a comparison between two different parameterization schemes.

3.2 Extinction Of Arctic Stratus Clouds And Hazes

The extinction of radiation by optically small objects whose radii are far smaller than the incident wavelengths of radiation can be described by the Rayleigh theory. On the other hand, geometrical optics deals with the extinction of radiation by optically very large objects. Not until Gustav Mie's study was a theory propounded to solve the extinction of radiation by objects whose radii are comparable to or larger than wavelengths of incident radiation, the so-called "Mie theory" (Mie, 1908). Although the Mie theory specifically deals with homogeneous isotropic spheres, it is still often the best approximation for nonspherical particles, if they have been turned to "equivalent spheres of equal-volume and/or equal-projected-area" (Van de Hulst, 1957; Mugnai and Wiscombe, 1980; Chylek and Ramaswamy, 1982).

Important parameters for multiple scattering problems (i.e., Eq.2.2) involving particles are the single scattering albedo; the extinction efficiency factor, determining the optical depth; and the asymmetry factor, characterizing the phase function. However, due to the instrumental limitation, the efficiency factors (Q_{ext} , Q_{sca}) are very difficult to measure in the laboratory (e.g., Mugnai and Wiscombe, 1980). Thus, the Mie theory is the most convenient method to obtain these quantities and will be used to establish a parameterization scheme for stratus clouds.

A complete description of the Mie theory can be found in the classical treatise by Van de Hulst. Only a brief description of the Mie computation is attempted here. The heart of the Mie theory is to compute the Mie coefficients a_n and b_n (Van de Hulst [1957], p119), which are determined physically from the complex refractive index of the particle relative to the medium ($n_c = n_r - in_i$) and the size parameter ($\chi = 2\pi r/\lambda$). Therefore, for a single sphere of radius r , the scattering and extinction efficiency factors (Q_{sca} , Q_{ext}) and the asymmetry factor (g) are given as follows (Van de Hulst, 1957; Hansen and Travis, 1974):

$$Q_{sca} = \frac{2}{\chi^2} \sum_{n=1}^{\infty} (2n+1) (a_n a_n^* + b_n b_n^*)$$

$$Q_{ext} = \frac{2}{\chi^2} \sum_{n=1}^{\infty} (2n+1) \operatorname{Re}(a_n + b_n)$$

$$g = \frac{4}{\chi^2 Q_{sca}} \sum_{n=1}^{\infty} \left[\frac{n(n+2)}{n+1} \operatorname{Re}(a_n a_{n+1}^* + b_n b_{n+1}^*) + \frac{2n+1}{n(n+1)} \operatorname{Re}(a_n b_n^*) \right] \quad (3.14)$$

where the "Re" denotes the real part of the complex function; and the asterisk denotes the complex conjugate of the coefficients. If the scattered radiation is represented by an infinite series of the multipole expansion, the coefficients a_n specify the amount of electric multipole radiation (e.g., dipole for $n=1$, quadrupole for $n=2$, octupole for $n=3$, etc.), while the b_n are the coefficients for magnetic multipole radiation. Shortly after n exceeding χ , the series con-

verges, which can be interpreted physically as the incident radiation missing the sphere. Therefore, for polydispersed particles, optical properties can be obtained by the appropriate integrals over all sizes. For example, the extinction optical depth of particles, with a layer thickness of Δz (m) and a size distribution function of $n(r, z)$ ($\text{cm}^{-3} \cdot \mu\text{m}^{-1}$), can be obtained as follows:

$$\tau(\lambda, \Delta z) = \int_z^{z+\Delta z} dz \int_{r_{\min}}^{r_{\max}} \pi r^2 Q_{\text{ext}}(\lambda, r) n(r, z) dr \quad (3.15)$$

Similar integrals for obtaining scattering optical depth and the asymmetry factor can be made (Hansen and Travis, 1974).

To obtain the optical properties of the Arctic stratus as functions of wavelengths, the drop size distributions and the refractive index of water have to be known. Figure 3.5 shows the refractive index of water used in this study. Data sets from 10 to 5000cm^{-1} are taken from Downing and Williams (1975); 5000 - 14500cm^{-1} , from Palmer and Williams (1974); and 14500 - 50000cm^{-1} , from Hale and Querry (1973). The real part of the refractive index for water lies in the range of 1.3 to 2 , while the imaginary part lies in the range of 10^{-10} to 0.6 for the spectral region of interest in this study. The real part of the refractive index characterizes the phase shift of the radiation traveling through medium, while the imaginary part determines the damping (absorption) of the radiation (Feynman et al., 1980, Volume II). Therefore, high

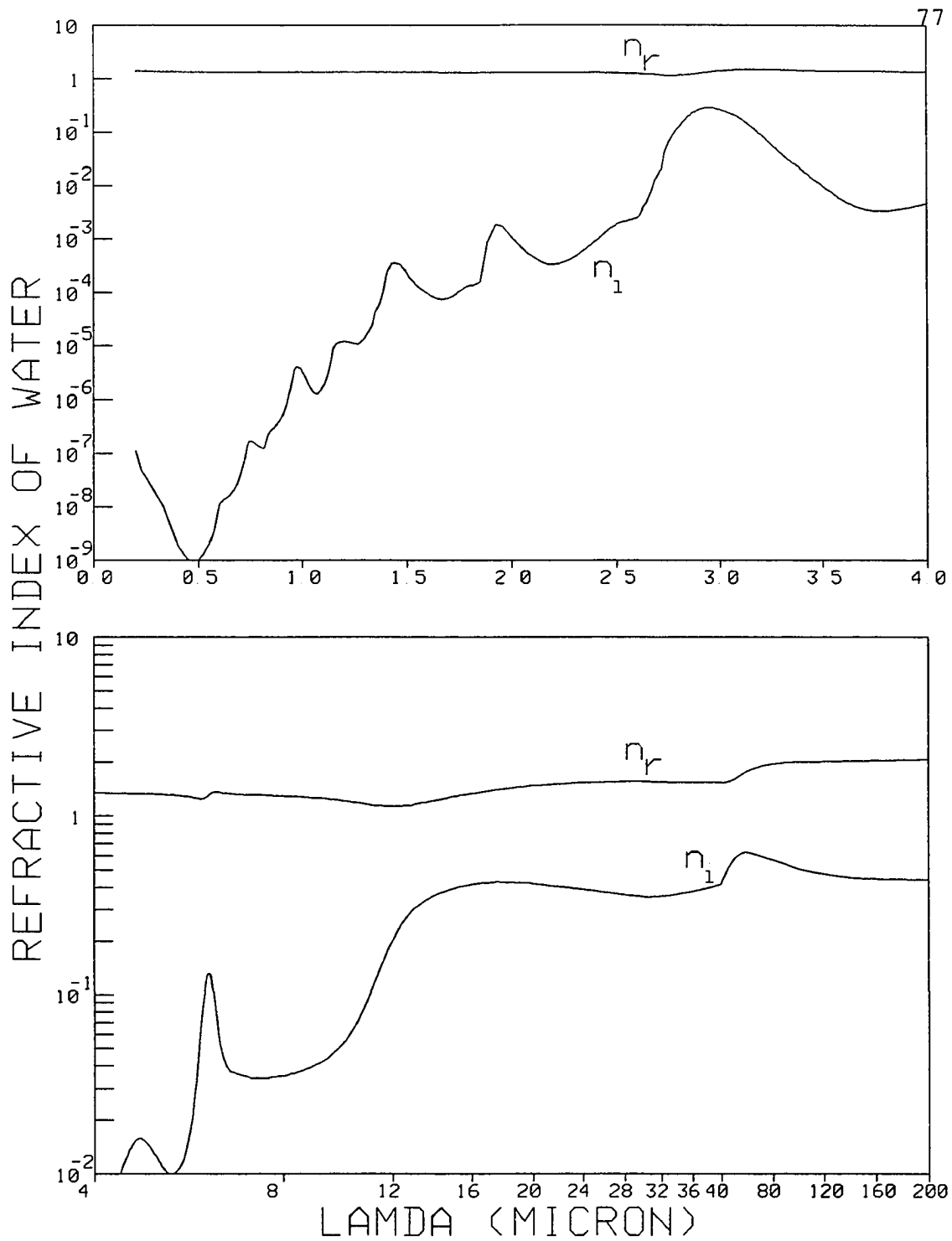


Figure 3.5 Refractive index of water from wavelength $0.3\mu\text{m}$ to $200\mu\text{m}$, n_r for real and n_i for imaginary parts

transparency in the visible and great absorption in the infrared regions will be expected. The near-infrared region has the intermediate extinction property, except for an outstanding band around $3\mu\text{m}$.

Drop size distributions vary from one cloud to another and are determined mainly by complicated cloud regimes. However, even for the stable and stratiform clouds such as the Arctic stratus, different size distributions were observed from cloud base to top. A single-mode size distribution was often found near the cloud base; then, the shape of the size spectrum shifted toward large size at the upper levels and finally a bimodal distribution was observed near the cloud top. Explanation for this change is given by Tsay and Jayaweera (1984). However, such detailed microphysical properties are generally difficult to obtain as functions of cloud heights. Moreover, Mie theory computations are time-consuming. Parameterization schemes of cloud optical properties should be sought with the help of Mie theory.

Figure 3.6, reproduced from Hansen and Travis (1974), shows the Mie computation of the efficiency factor as a function of the size parameter for four size distributions with non-absorption ($n_r = 1.33$ and $n_i = 0$). The ripple on the solid curve for a single particle arises from edge rays grazing the sphere (Hansen and Travis, 1974). As the size spectrum becomes dispersed, smoothed and simplified features

are observed, which suggests that bulk quantities may be adequate to represent microphysics. The microphysics of clouds are commonly described by the liquid water content (LWC, $\text{g}\cdot\text{m}^{-3}$), the equivalent radius (RE, μm), and the number concentration (CON, cm^{-3}). These are defined as follows:

$$\begin{aligned} \text{LWC}(z) &= \frac{4\pi\rho_w}{3} \int_{r_{\min}}^{r_{\max}} r^3 n(r,z) dr; & \text{CON}(z) &= \int_{r_{\min}}^{r_{\max}} n(r,z) dr \\ \text{RE}(z) &= \int_{r_{\min}}^{r_{\max}} r^3 n(r,z) dr / \int_{r_{\min}}^{r_{\max}} r^2 n(r,z) dr \end{aligned} \quad (3.16)$$

where ρ_w ($1.0\text{g}\cdot\text{cm}^{-3}$) is the density of water.

Based on the extensive survey of cloud microphysics by Carrier et al. (1967), Stephens (1978) established eight cloud models to cover a wide range of observed drop size distributions, which are reproduced in Figure 3.7. A tabulation of the optical properties of these eight water clouds was made by Stephens (1979) through Mie computations from $0.2\mu\text{m}$ to $200\mu\text{m}$. However, cumulus (Cu) and cumulonimbus (Cb) are cube-shaped clouds which have very different characteristics from stratiform clouds. The Arctic stratus have equivalent characteristics (RE, LWC and CON), somewhat between ST-II and SC-II (Figure 3.7). Therefore, a multi-mode size distribution (having the same LWC and CON with SC-II) was generated to resemble the distribution at cloud top. Figure 3.8 shows the splined SC-II (S-MOD) and the multi-mode (M-MOD) size distributions. Mie computations were performed for

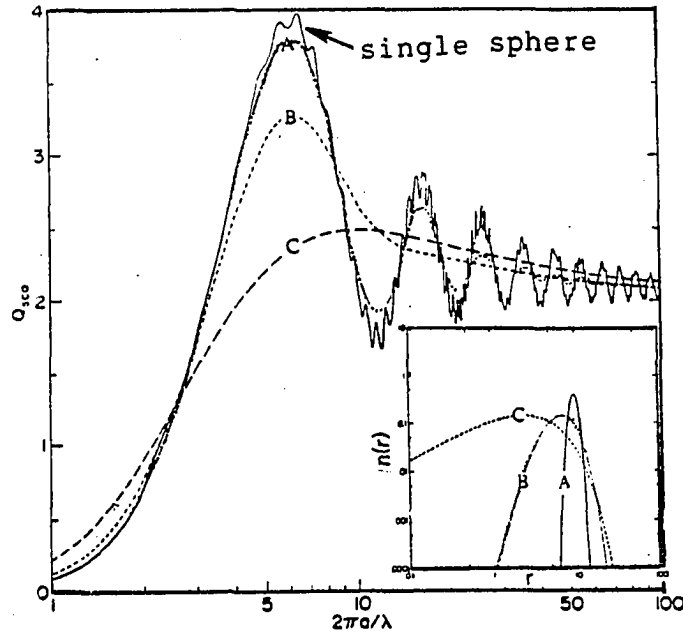


Figure 3.6 Scattering efficiency factor as function of size parameter for various size distributions (lower-right, after Hansen and Travis, 1974)

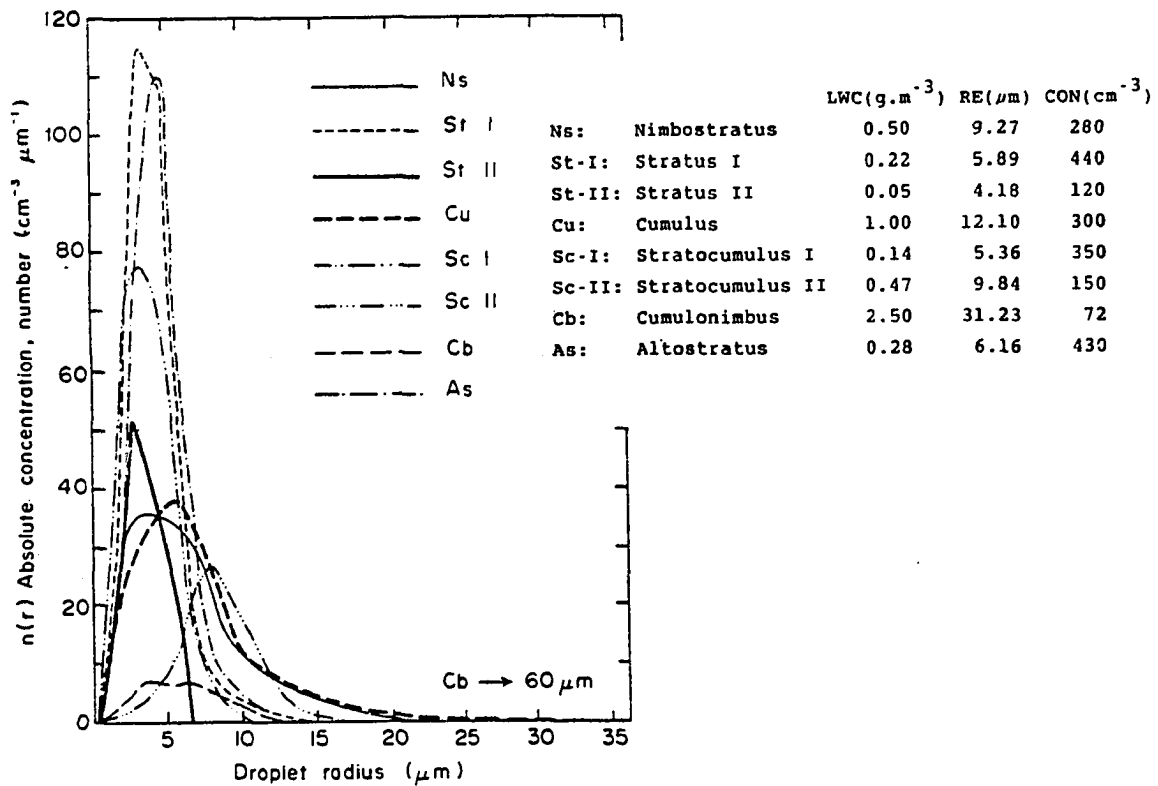


Figure 3.7 Drop size distributions of eight cloud models (after Stephens, 1978)

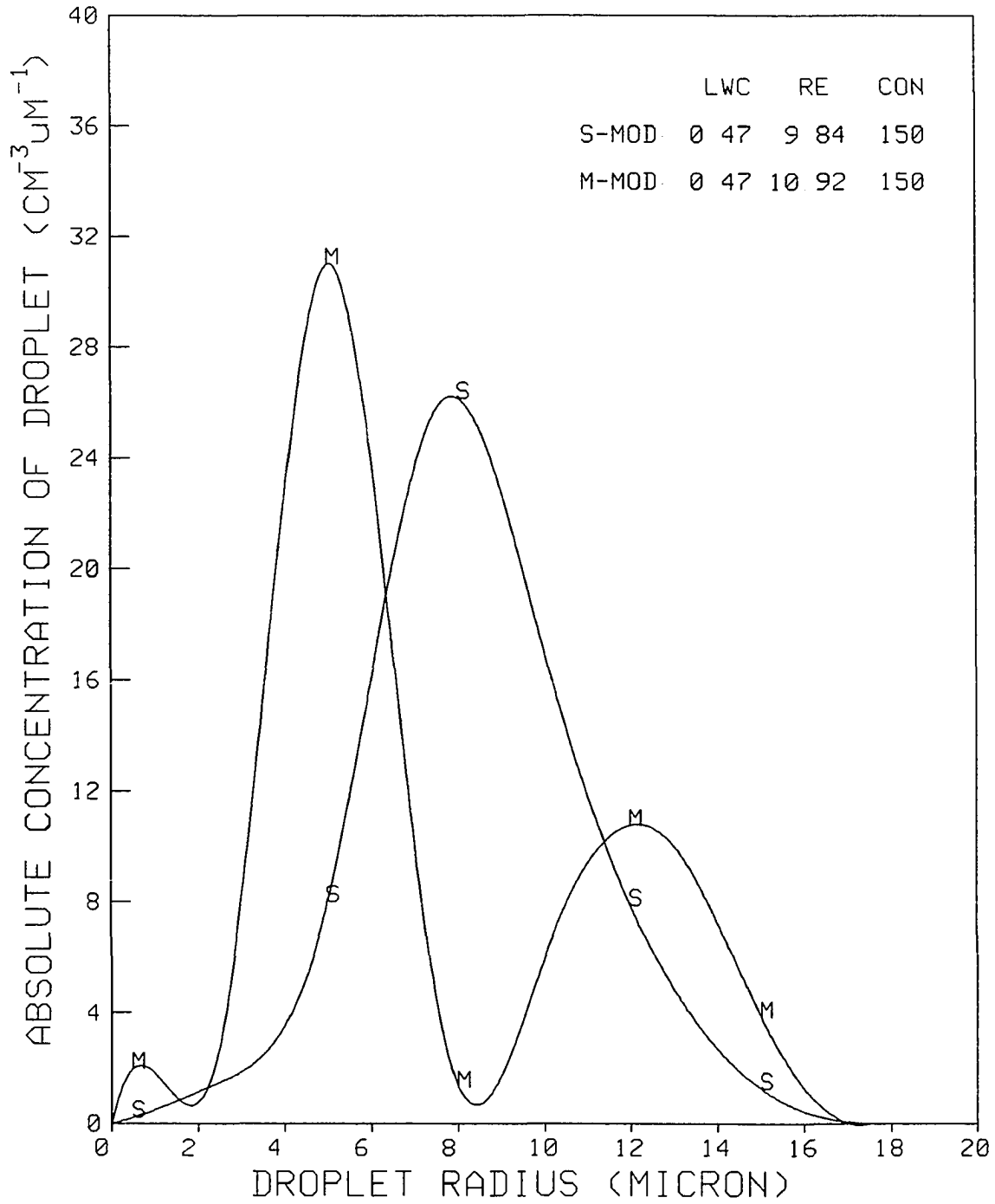


Figure 3.8 Drop size distributions for model clouds, S-MOD for single-mode and M-MOD for multi-mode

these two size distributions, using the same procedures as used by Stephens (1979). A slight difference between the results of SC-II and S-MOD was observed, due to the different refractive indices of water used.

Figures 3.9 to 3.11 show the single scattering albedo, the asymmetry factor and the normalized volume extinction coefficient for solar and terrestrial spectra, respectively. These figures contain seven cloud models and their important physical parameters (RE, LWC and CON) are also shown. If the ST-II and M-MOD clouds serve as the envelope, based on the rank of RE, the rest of the five model clouds are generally bounded inside, except for the case shown in Figure 3.11. It can be understood that ω and g depend closely on RE rather than on other parameters. First, they are ratios between two quantities, which are generally smooth functions. RE denotes a ratio of the third and the second moments of size distribution (Eq.3.16), which has the dominant representativeness. Second, scattering patterns (Figure 2.3) are characterized by g . If RE is large (large drops being dominant), forward scattering prevails, and g is large. ω is characterized by the scattering efficiency factor. In the solar spectrum where absorption is negligible, large drops have small Q_{sca} (the decreasing curve in the right-hand side of Figure 3.6), and ω is small. However, at $3\mu m$ the opposite situation is observed, in which a small RE corresponds to a small ω . When

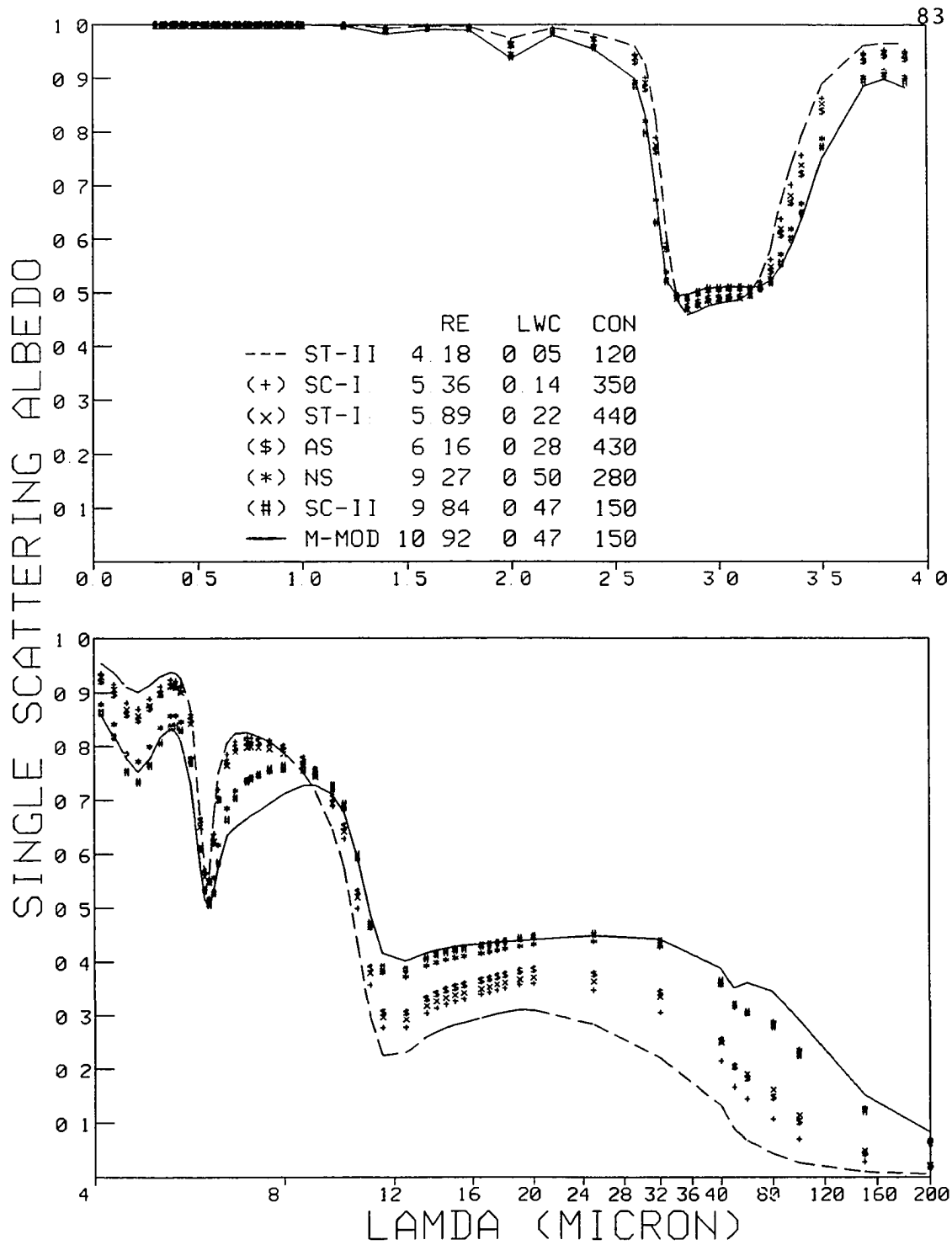


Figure 3.9 Single scattering albedo for seven model clouds from wavelength $0.3\mu\text{m}$ to $200\mu\text{m}$

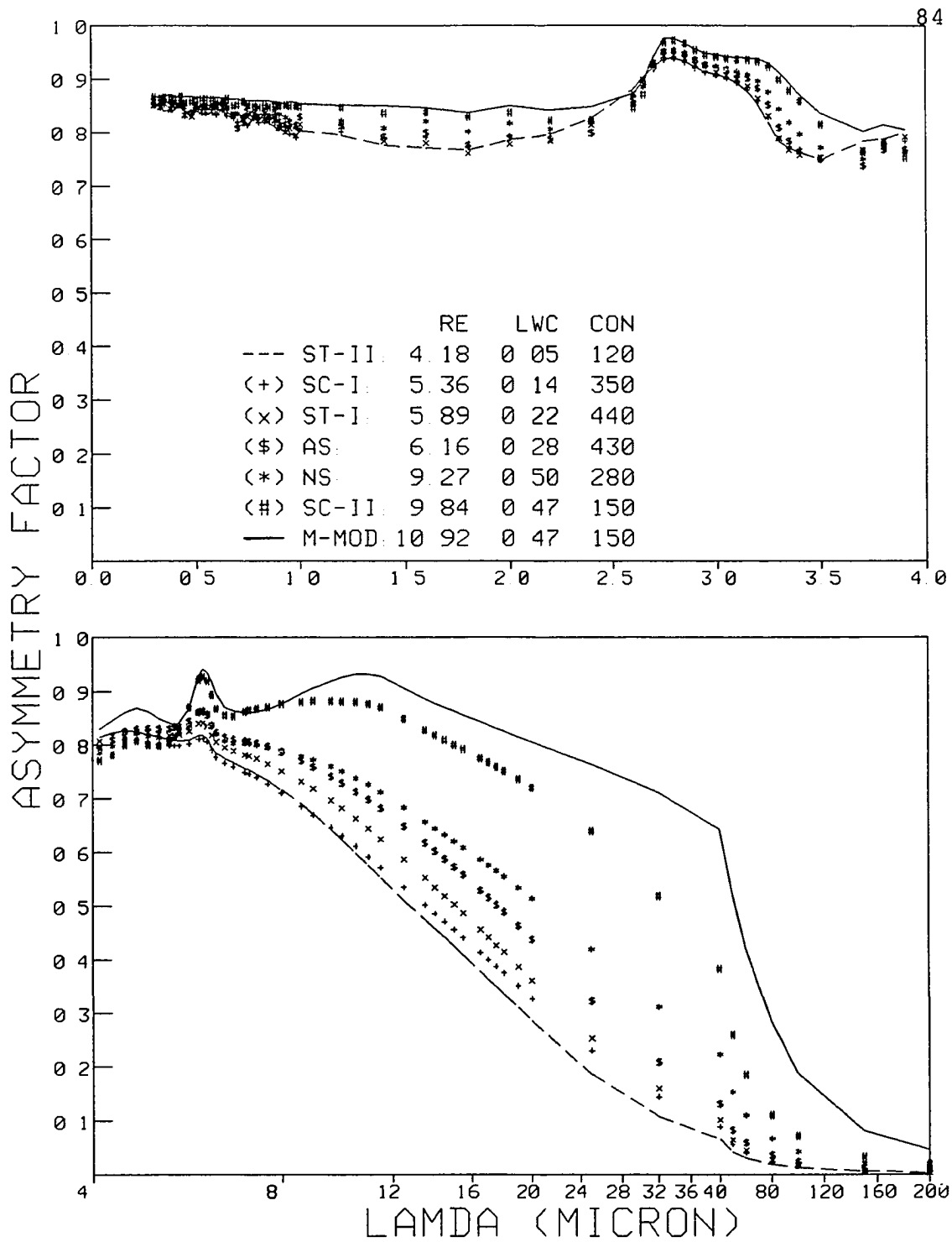


Figure 3.10 Asymmetry factor for seven model clouds from wavelength $0.3\mu\text{m}$ to $200\mu\text{m}$

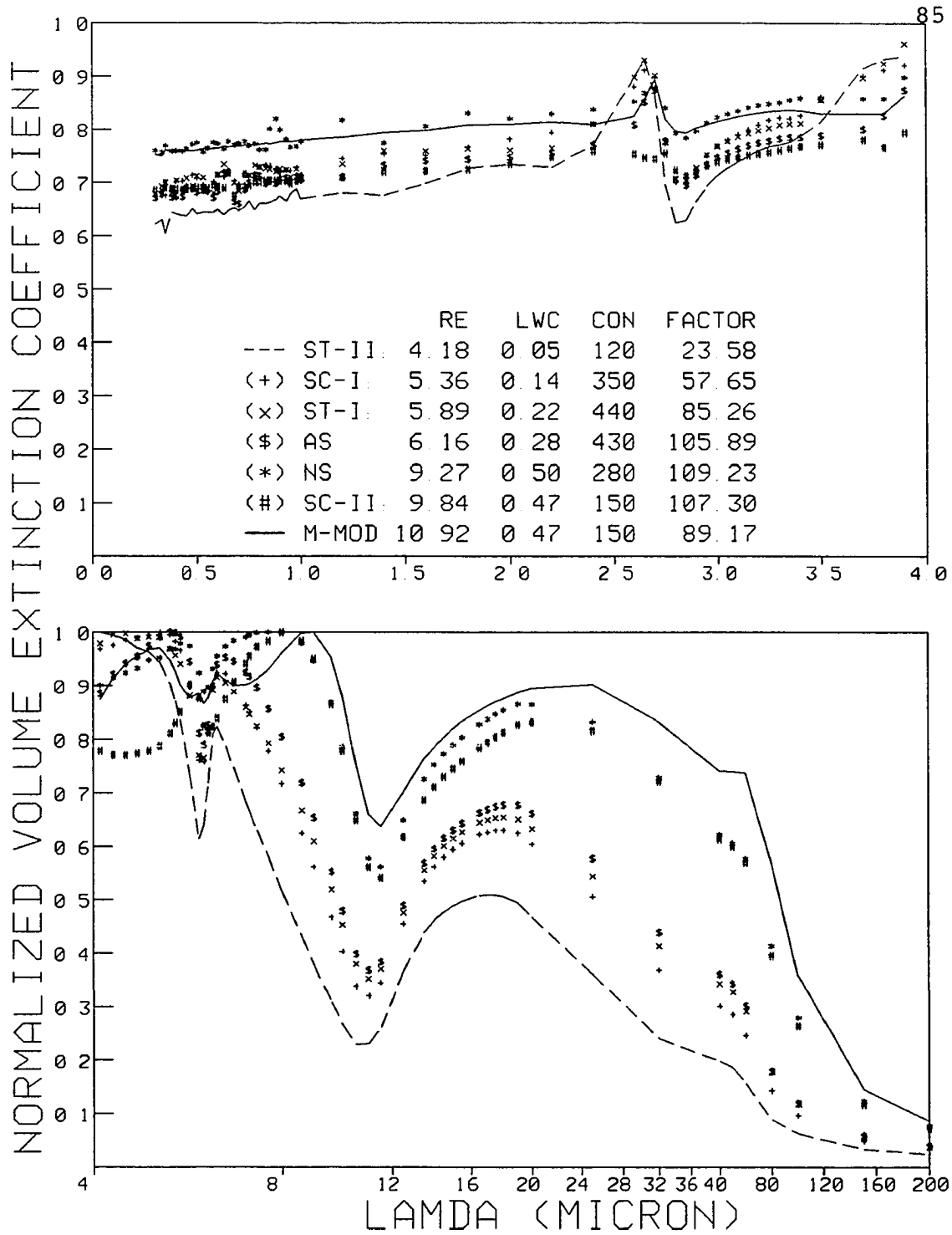


Figure 3.11 Normalized volume extinction coefficient for seven model clouds from wavelength $0.3\mu\text{m}$ to $200\mu\text{m}$

strong absorption takes place, Q_{sca} increases with increasing size parameter and approaches an asymptote of 2. Therefore, a large RE is associated with a large Q_{sca} . This also explains the situation occurring in the infrared region, due to strong absorption (Figure 3.5).

The volume extinction coefficient (b_{ext}) is much more complicated. The usual large-drop approximation ($Q_{sca} = 2$) shows clearly its dependence on more than one parameter. By substituting Eq.3.16 into 3.15 and setting $Q_{sca}(\lambda, r) = 2$, b_{ext} is obtained:

$$\tau(\lambda, \Delta z) = \int_z^{z+\Delta z} b_{ext}(\lambda, z) dz = \frac{3}{2\rho_w} \int_z^{z+\Delta z} \frac{LWC(z)}{RE(z)} dz \quad (3.17)$$

or simply, $b_{ext} = 1.5(LWC/RE)$ if they are all in the right units. The wavelength dependences of b_{ext} disappear because of the large-drop approximation. Indeed, only slight wavelength dependences (Figure 3.11) are observed in the normalized b_{ext} for wavelengths shorter than $2.5\mu m$, where Q_{ext} (or Q_{sca}) is approximately equal to 2. However, when the absorption becomes important or wavelength is increasing, this approximation may not be valid.

Recent studies have attempted to parameterize shortwave optical properties, based on one or two bulk quantities of cloud microphysics (Stephens, 1978; Twomey and Bohren, 1980; Slingo and Schrecker, 1982; Wiscombe et al, 1984). To obtain a unified treatment of both solar and terrestrial radiation,

an extension of Slingo and Schrecker's parameterization scheme is attempted here. Based on the discussions above, it is suggested that ω and g closely depend on RE and weighted b_{ext} (by factor LWC) depends on inverse RE (Figures 3.9-11). Therefore, the least squares fits for the following linear equations were performed for the wavelengths from $0.3\mu\text{m}$ to $200\mu\text{m}$.

$$\omega = a + b\text{RE}$$

$$g = c + d\text{RE}$$

$$b_{\text{ext}}/\text{LWC} = e + f/\text{RE} \quad (3.18)$$

Figures 3.12 to 3.14 show the fits for ω , g and weighted b_{ext} , respectively. It was observed to be a good fit for ω throughout solar and terrestrial spectra. Very high absolute values of correlation coefficients are obtained. This is very important for cloud parameterization, because cloud absorption is very sensitive to the variation of ω . The fits for g are also good, except for the region around $4.5\mu\text{m}$. However, the error may not produce serious problems because of the relatively less amount of radiation energy involved. Good fits of weighted b_{ext} were obtained for shortwave and longerwave regions. Relatively low correlation coefficients were found in the window region ($8 - 12\mu\text{m}$), which may cause some errors for thin clouds. The study of this effect is beyond the scope of this thesis.

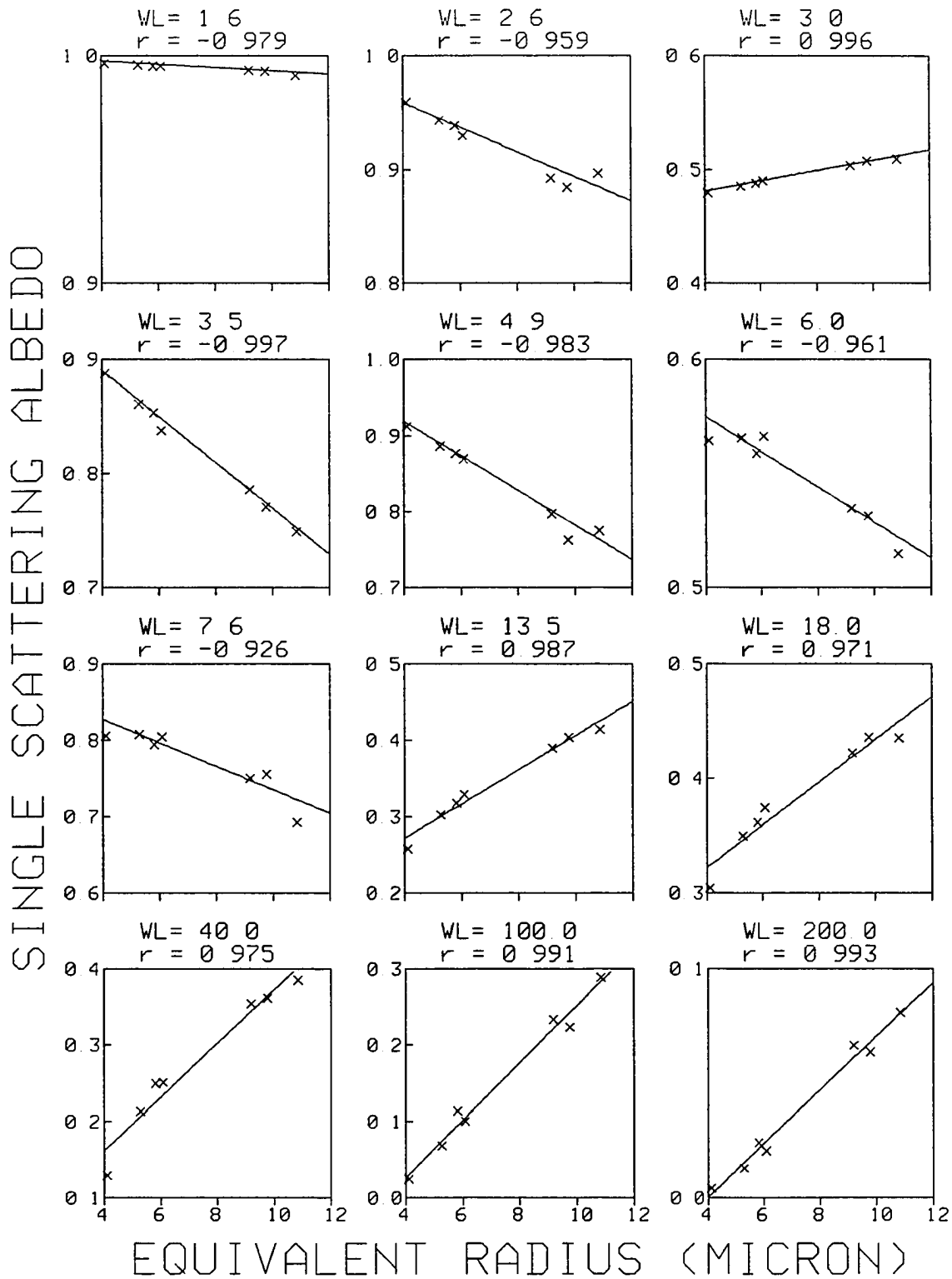


Figure 3.12 Least squares fits for single scattering albedo form wavelength $0.3\mu\text{m}$ to $200\mu\text{m}$, WL for wavelength (μm) and r for correlation coefficient

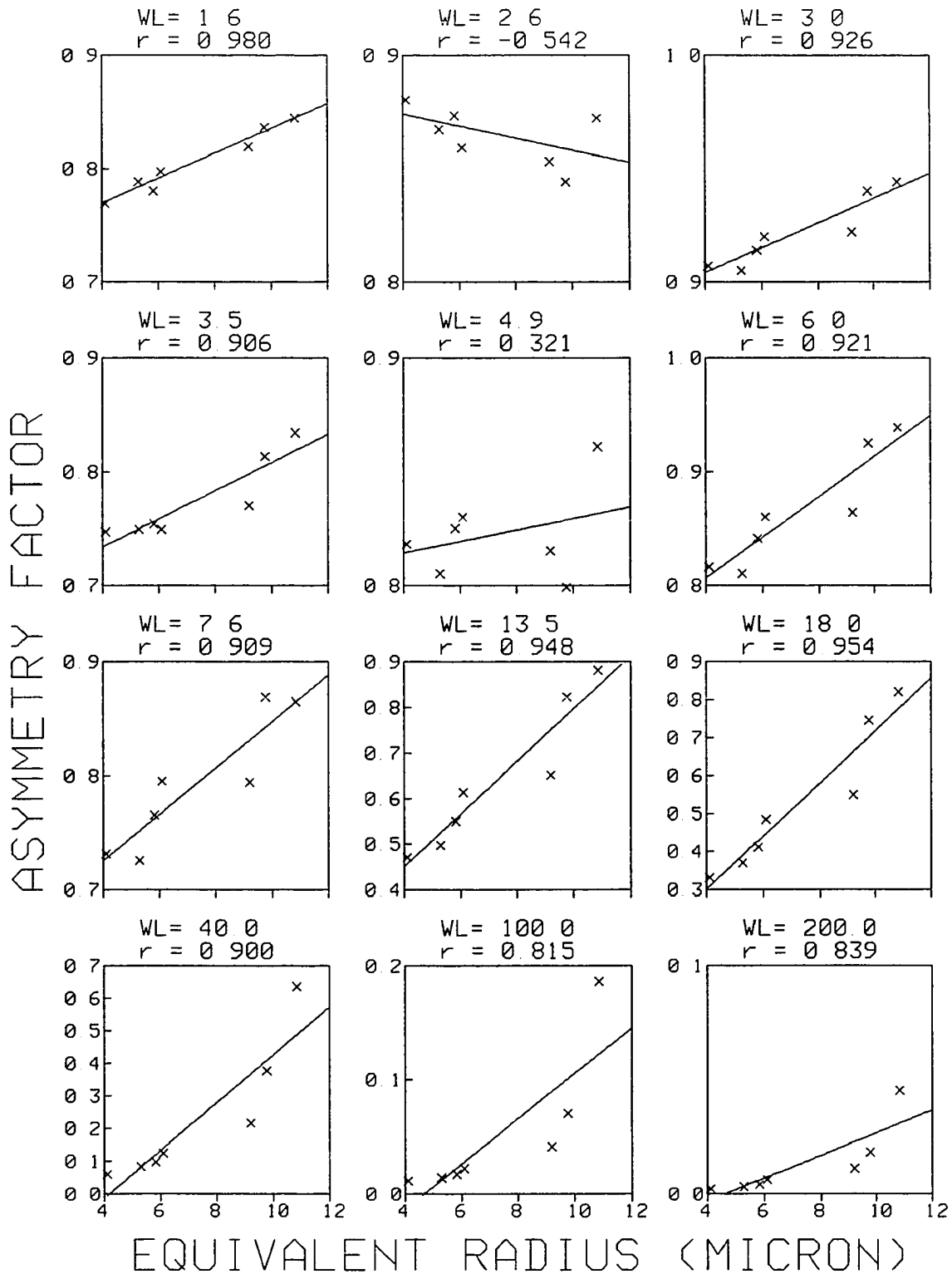


Figure 3.13 Least squares fits for asymmetry factor from wavelength $0.3\mu\text{m}$ to $200\mu\text{m}$, WL for wavelength (μm) and r for correlation coefficient

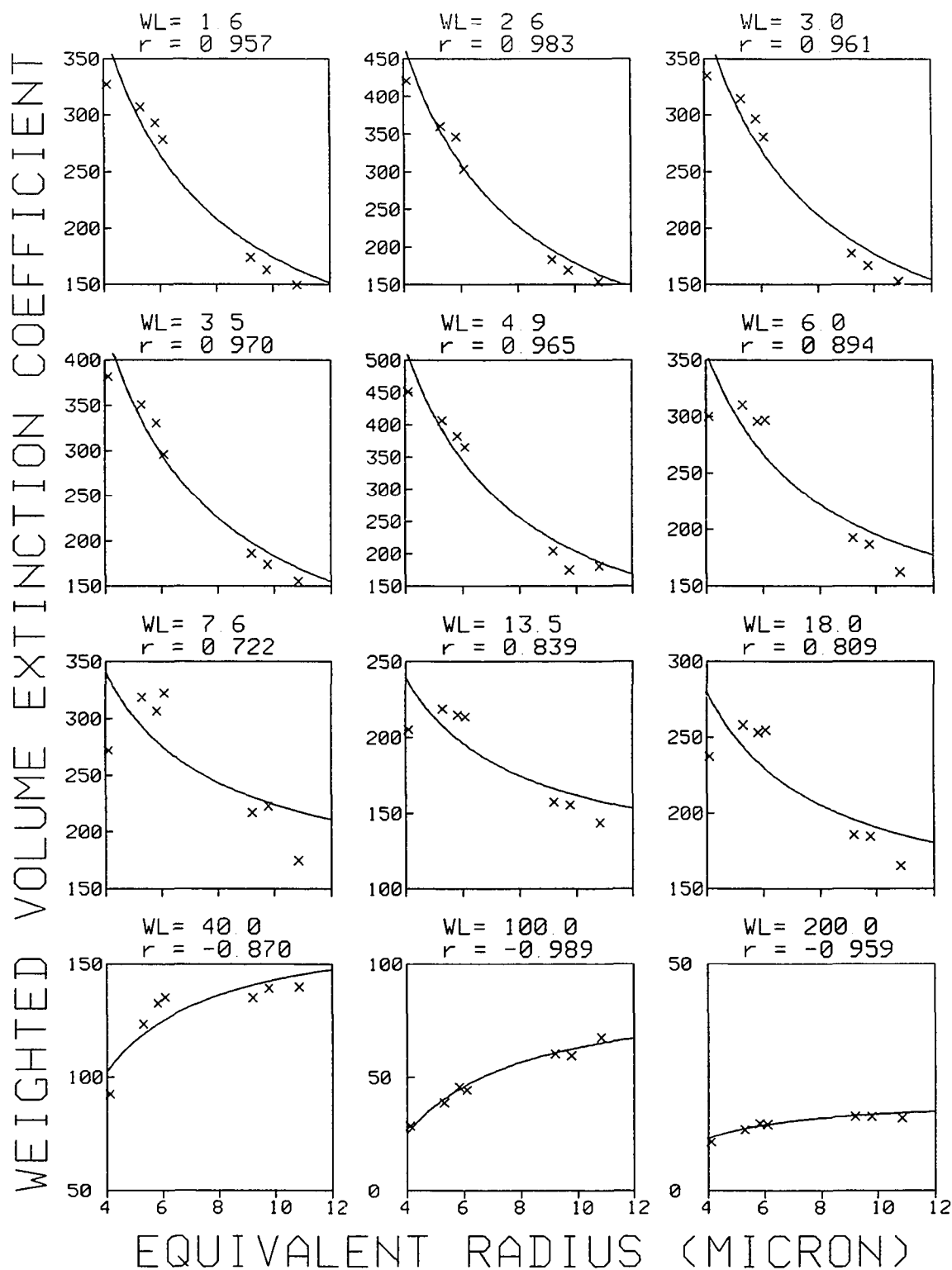


Figure 3.14 Least squares fits for weighted volume extinction coefficient form wavelength $0.3\mu\text{m}$ to $200\mu\text{m}$, WL for wavelength (μm) and r for correlation coefficient

Besides the persistent summertime arctic stratus, the arctic haze has received attention because of possible climatic effects since the last decade. Arctic haze was first reported (Mitchell, 1956) in the Project Ptarmigan weather reconnaissance flights. After that, more studies of arctic haze were carried out in Alaska during the period of 1971-75 (Shaw and Wendler, 1972; Holmgren et al., 1974; Shaw, 1975; Rahn et al., 1977).

Physical properties (e.g., size distribution, chemical composition, etc.) of the arctic haze indicated that it appears to be produced at middle latitudes, moving by means of long range transport to the Arctic (Rahn and McCaffrey, 1980; Rahn, 1981). Sulfates, carbonaceous particles, Vanadium, and other elements were found in the arctic haze, indicating its enrichment from highly polluted sources.

Arctic haze also varies with seasons. Figure 3.15, reproduced from Shaw (1982), shows the seasonal trends of the haze, a maximum in late spring and a minimum in late summer. Similar results were also found by Patterson et al. (1982). Arctic haze tends to occur in multiple layers rather than being well mixed throughout the lower atmosphere (Carlson, 1981; Valero et al., 1983). Figure 3.16 shows a vertical profile of arctic haze measured at Barrow, Alaska (Shaw, 1982). The layering of the haze often occurs within 3 Km above the surface, which is about the upper height limit for

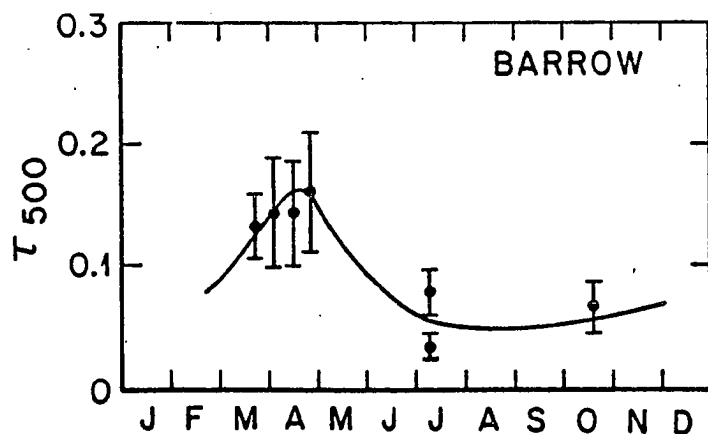


Figure 3.15 Seasonal trends in aerosol optical depth for $\lambda=500\text{nm}$ at Barrow, Alaska (after Shaw, 1982)

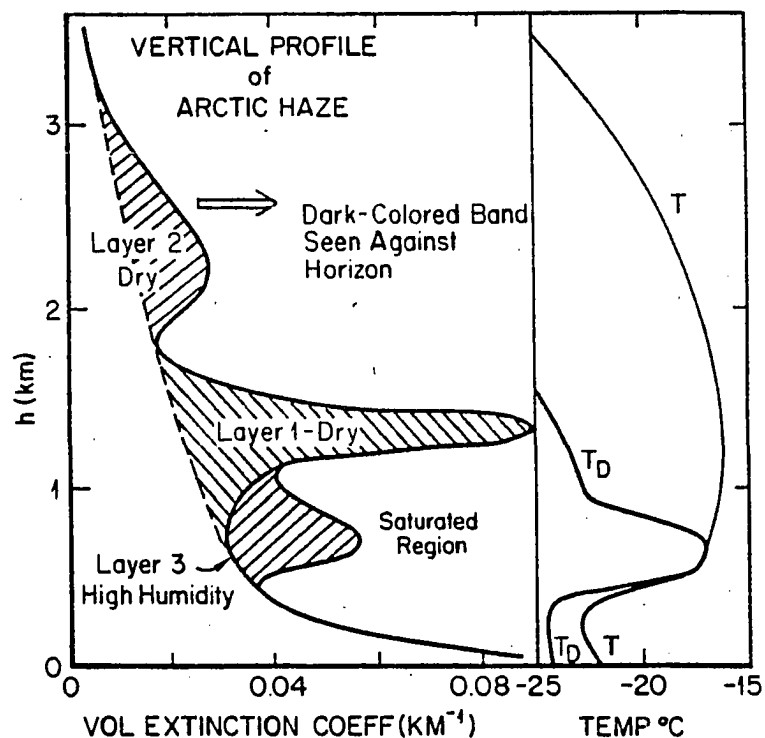


Figure 3.16 Vertical profile of aerosol volume extinction coefficient for $\lambda=500\text{nm}$, showing layers of Arctic haze at Barrow, Alaska (after Shaw, 1982)

the summertime arctic stratus cloud. The low concentration of arctic haze during the summer season may be related to the high occurrence of stratus clouds.

However, the optical properties (b_{ext} , ω , g , etc.) of the arctic haze have not been extensively measured (Shaw, 1985), and only in a few single wavelengths (e.g., 500nm). To estimate the effect of haze on the Arctic radiative energy budget, wavelength dependence of optical properties is essential. Therefore, Mie calculations again may provide the optical properties, based on the measured microphysics of haze. Recent model computations of the optical properties for aerosol particles were made by Shettle and Fenn (Tables 12-43, 1979) and Blanchet and List (Figures 10-12, 1983). The former contains four general models of aerosols; the latter is specified for arctic haze.

Figures 3.17 to 3.19 show b_{ext} , ω , and g for both model calculations. Effects of humidity on aerosol properties are considered in both models, and dry (RH=50%) and wet (RH=99%) conditions are shown here to represent cases of haze located above and inside the clouds, respectively. The microphysics used by Blanchet and List were obtained from measurements of Heintzenberg (1980); and model predictions of b_{ext} agree well with measurements from Rahn (1978). Shettle and Fenn had four models: "RURAL" for mixture of water-soluble and dust-like aerosols; "URBAN" for "RURAL" aerosol mixture with

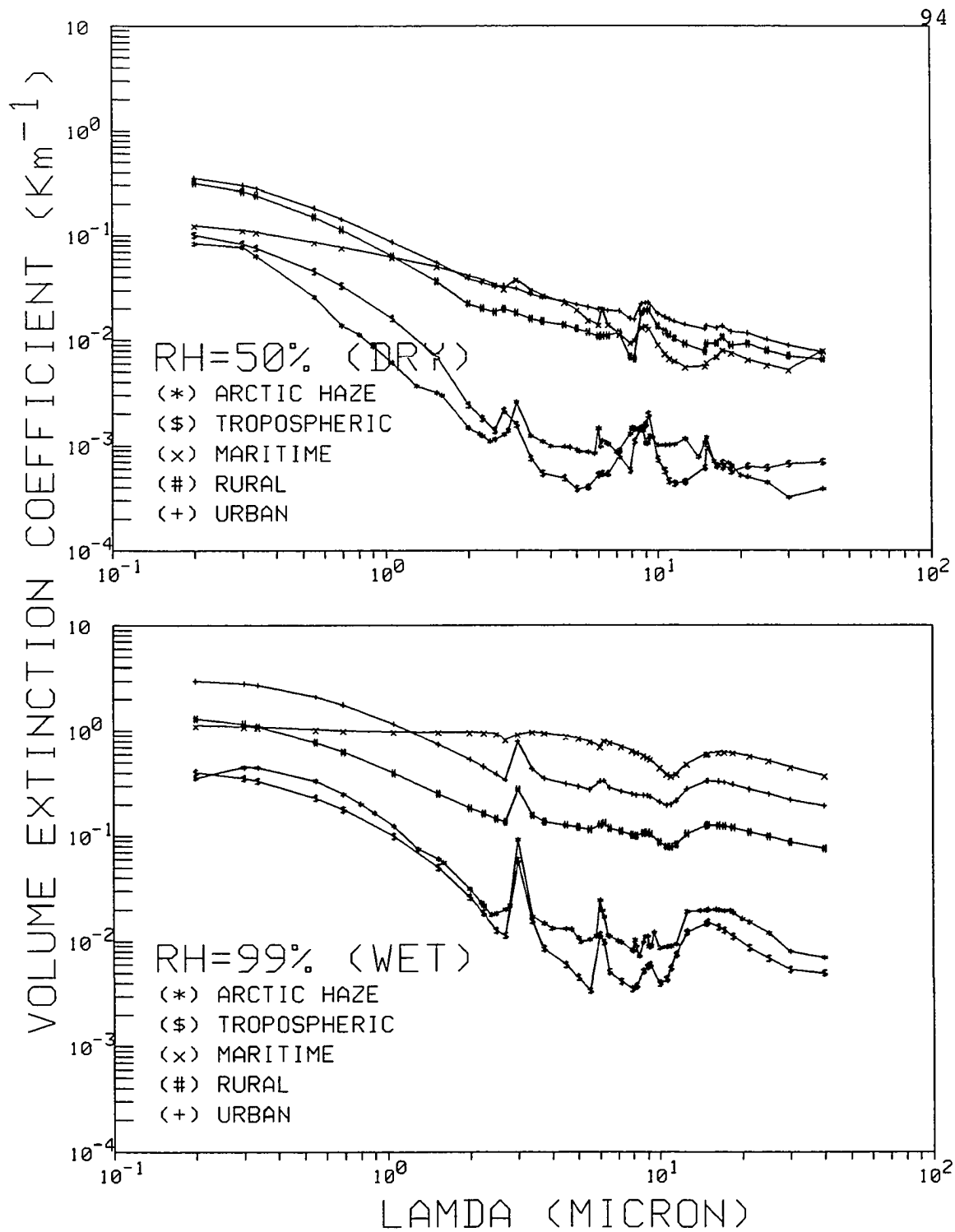


Figure 3.17 Volume extinction coefficient for five haze models from wavelength $0.2\mu\text{m}$ to $40\mu\text{m}$, RH for relative humidity

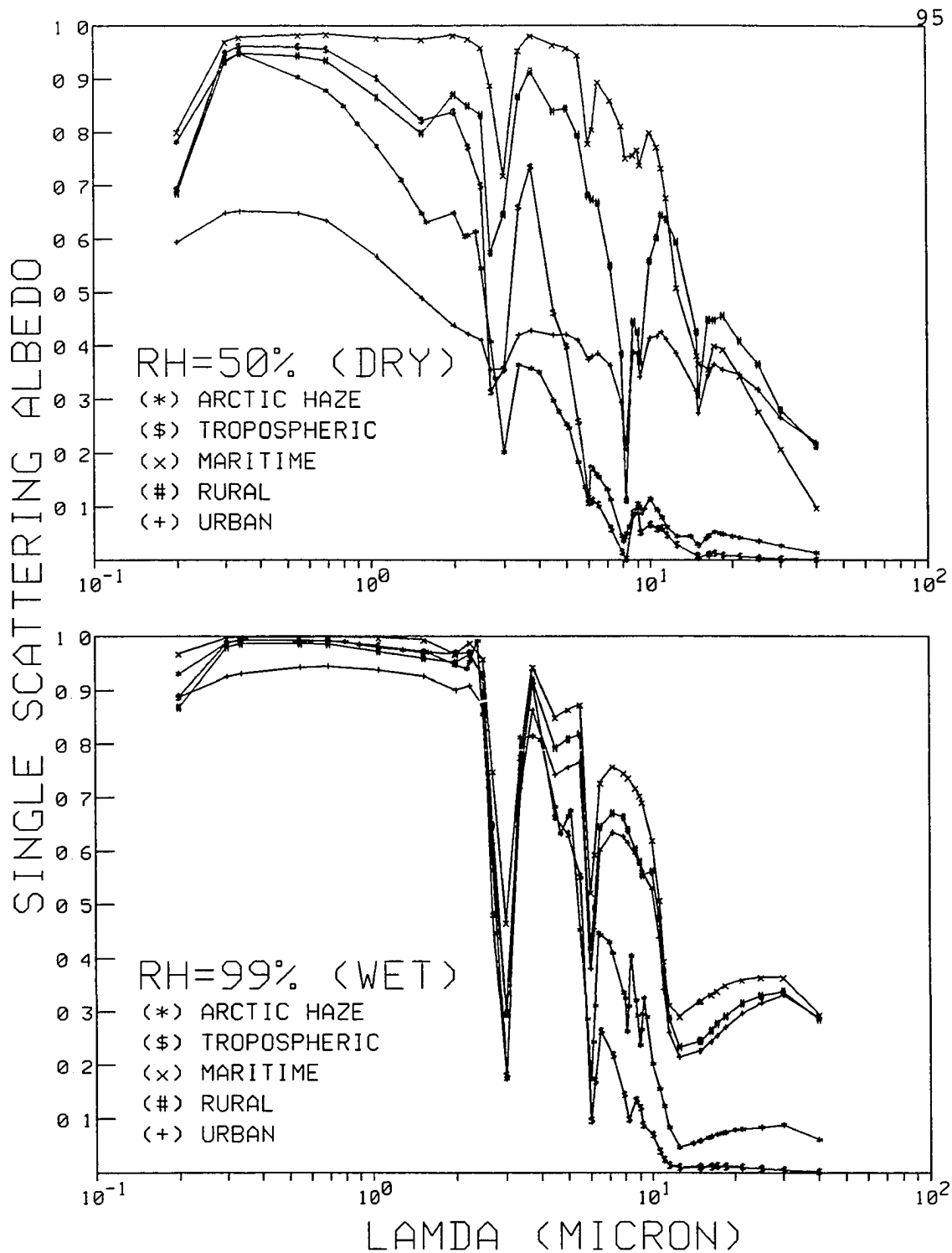


Figure 3.18 Single scattering albedo for five haze models from wavelength 0.2 μ m to 40 μ m, RH for relative humidity

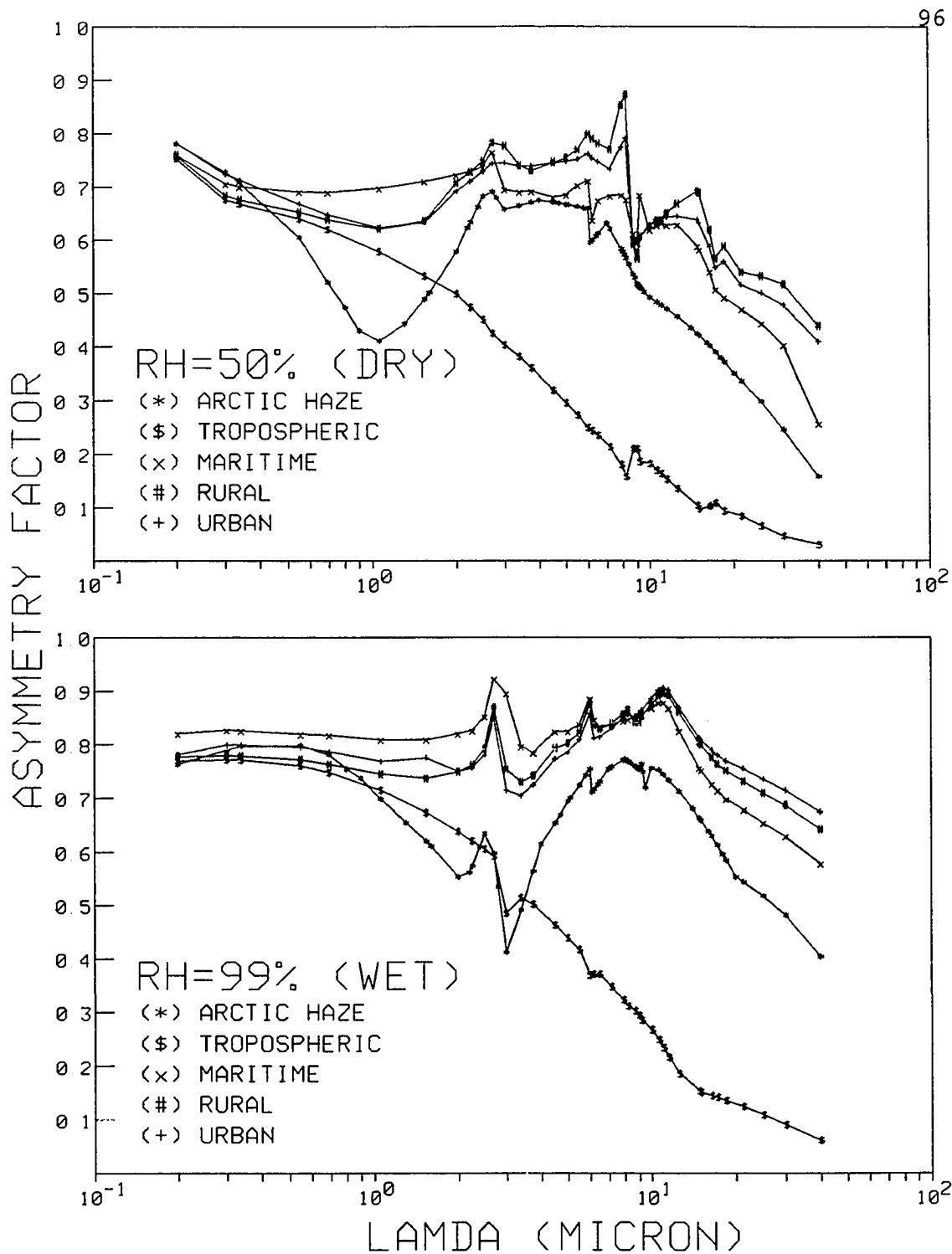


Figure 3.19 Asymmetry factor for five haze models from wavelength $0.2\mu\text{m}$ to $40\mu\text{m}$, RH for relative humidity

soot-like aerosols; "MARITIME" for "RURAL" aerosol mixture with sea salt solution in water; "TROPOSPHERIC" for "RURAL" aerosol mixture with less total number concentration. These four aerosol models are representative for various general types of environments and their corresponding microphysics have been measured in many investigations in the boundary layer for the first three models and above the boundary layer for the last model (Shettle and Fenn, 1979). Unfortunately, validations of the optical properties were not provided.

The volume extinction coefficient of the arctic haze is generally of the same order of magnitude as that of the tropospheric aerosols rather than the maritime aerosols. When the relative humidity is high (99%), sharp increases of b_{ext} are apparent in $3\mu\text{m}$ and $6\mu\text{m}$ regions, due to the strong water absorption. Moreover, in the wet condition (99%), b_{ext} in the infrared regions is roughly steady at the order of 10^{-2} , which is about the same order of magnitude as b_{ext} at $0.5\mu\text{m}$. The first attempt to compute the perturbation of the arctic radiation by haze was made by Shaw and Stamnes (1980). They concluded that the arctic haze heats the atmosphere by about $25\text{W}\cdot\text{m}^{-2}$ and cools the surface by about $5\text{W}\cdot\text{m}^{-2}$. The calculations were based on the following assumptions: (a) $\tau = 0.2$, $\omega = 0.8$, $g = 0.75$ for a monochromatic wavelength centered at $0.5\mu\text{m}$; (b) for multiwavelength radiation by weighting result

of (a) properly; and (c) negligible b_{ext} in the infrared region. Assumption (c) is acceptable only in the dry case. Thus, a reconsideration of the haze effect in the infrared regime is needed for the wet condition.

The single scattering albedo for the wet condition is very similar to that of cloud droplets (Figure 3.9), due to the absorption of water vapor. In the dry condition, characteristics of aerosols are more pronounced and the property of arctic haze is somewhat between that of tropospheric and urban aerosols. The asymmetry factor generally increases with relative humidity, due to the growth of aerosols. Low values of g for the tropospheric aerosol are essentially caused by the low concentration of large particles in the observed size distribution. Both model calculations are made up to $40\mu\text{m}$. However, extrapolation may not lead to serious errors because of the relatively smooth functions beyond about $20\mu\text{m}$.

When the atmosphere contains a mixture of gas molecules and atmospheric particles, the effective optical properties of this mixture can be obtained as follows:

$$\begin{aligned}\tau_{\text{eff}} &= \tau_G + \tau_R + \tau_D + \tau_H \\ \omega_{\text{eff}} &= (\tau_R + \omega_D \tau_D + \omega_H \tau_H) / \tau_{\text{eff}} \\ P_{\text{eff}}(\cos \Xi) &= aP_R(\cos \Xi) + bP_D(\cos \Xi) + cP_H(\cos \Xi) \quad (3.19) \\ a &= \tau_R / d; \quad b = \omega_D \tau_D / d; \quad c = \omega_H \tau_H / d; \quad d = (\tau_R + \omega_D \tau_D + \omega_H \tau_H)\end{aligned}$$

Here, the subscripts "G", "R", "D" and "H" denote the components for gaseous absorption, the Rayleigh scattering, the droplets and the haze particles, respectively. The effective optical depth and single scattering albedo can be obtained straightforwardly. However, the Mie phase function for droplets and haze particles is difficult to obtain. Therefore, Henyey-Greenstein's phase function has been accepted widely for the use of Mie scatters, because of its dependence only on the asymmetry factor (Van de Hulst, 1957; Hansen and Travis, 1974). The Henyey-Greenstein phase function was given by Henyey and Greenstein (1941), as follows:

$$P_{HG}(\cos\Xi) = (1-g^2)/[1 + g^2 - 2g\cos\Xi]^{3/2} \quad (3.20)$$

The expansion of this phase function in Legendre polynomials leads to a very simple form. A detailed derivation of the Henyey-Greenstein phase function, together with the expansion of the Rayleigh phase function in Legendre polynomials, can be found in Appendix E.

3.3 Extinction Of Pure Snow/Ice And Soot Contamination

The striking feature of the arctic surface is its high reflectivity, caused mainly by snow and sea ice. The surface radiative energy budget depends strongly on its albedo. A high snow/ice albedo produces a positive climatic feedback mechanism, which is to lessen the solar input by making the

temperature decrease and inducing further extension of snow/ice (Kellogg, 1975). To obtain a quantitative value for this feedback mechanism, the radiative properties of snow/ice (i.e., Q_{ext} , ω , g) have to be known.

The snow/ice albedo is generally not a constant: it depends on incident wavelengths, snow/ice age, depth, air bubble distribution, sun angle, cloud cover, and impurities (such as dust, ash, soot, salt, etc.). A good discussion of snow/ice optical properties can be found in a review paper by Warren (1982). The optical properties of pure snow/ice and soot contamination for the present study were obtained through Mie computations, which require the refractive index of ice/soot and the mean grain radii of snow/ice and soot particles as input (Wiscombe and Warren, 1980; Warren and Wiscombe, 1980). Their results have been compared extensively with the available field measurements and agree well. These data sets will be used in the present study.

Figure 3.20 shows the refractive index of ice, from the recent compilation by Warren (1984). Absorption for pure snow/ice is negligible in the visible region because of the very small imaginary refraction index. Therefore, to reduce the abnormally high albedo (up to 15% higher than observed) predicted by Mie computations, trace amounts of absorptive impurities are introduced. In the air masses there are indeed large amounts of impurities, which are most likely

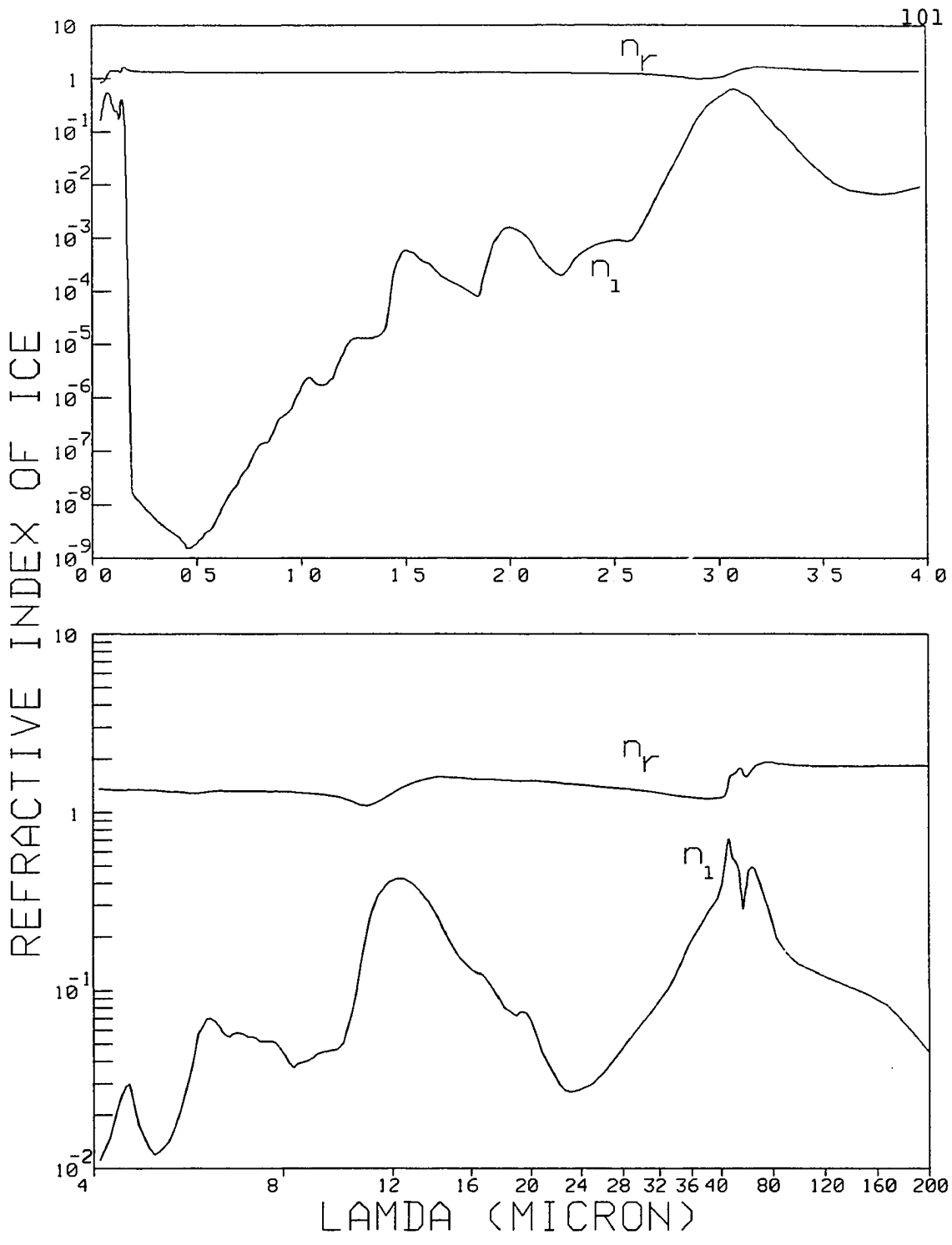


Figure 3.20 Refractive index of ice from wavelength $0.04\mu\text{m}$ to $200\mu\text{m}$, n_r for real and n_i for imaginary parts

graphitic soot, continental dust and volcanic ash. For reducing the pure snow/ice albedo in the visible region, soot is about 50 times more effective than dust, and about 200 times more effective than ash (Warren, 1982). The introduction of trace amounts of graphitic soot alters the snow/ice albedo only in the visible, and changes nothing for the rest of the spectral wavelengths because of the high imaginary refractive index for ice. A constant refractive index ($1.8 - 0.5i$) of soot with monodispersion ($r = 0.1 \mu\text{m}$) is used in the model computation of Warren and Wiscombe (1980), based on the findings of Twitty and Weinman (1971).

The other parameter needed in Mie computations is the mean snow/ice grain size, which is proportional to the ratio of volume to surface. In general, grain radius (R_g) varies with snow/ice depth and age. However, after an examination of a wide variety of references, Wiscombe and Warren (1980) concluded that the average grain radii are in the range 20-100 μm for new snow; 100-300 μm for fine-grained older snow; and 1000-1500 μm for old snow near the melting point.

Figures 3.21 to 3.23 show Q_{ext} , ω , and g of pure snow/ice and graphitic soot for the solar spectrum, respectively. Because of the large imaginary part of the ice refractive index throughout the infrared region and the large grain radius (or in terms of the extinction cross-section), only a very thin layer of snow/ice could behave like a quasi-black

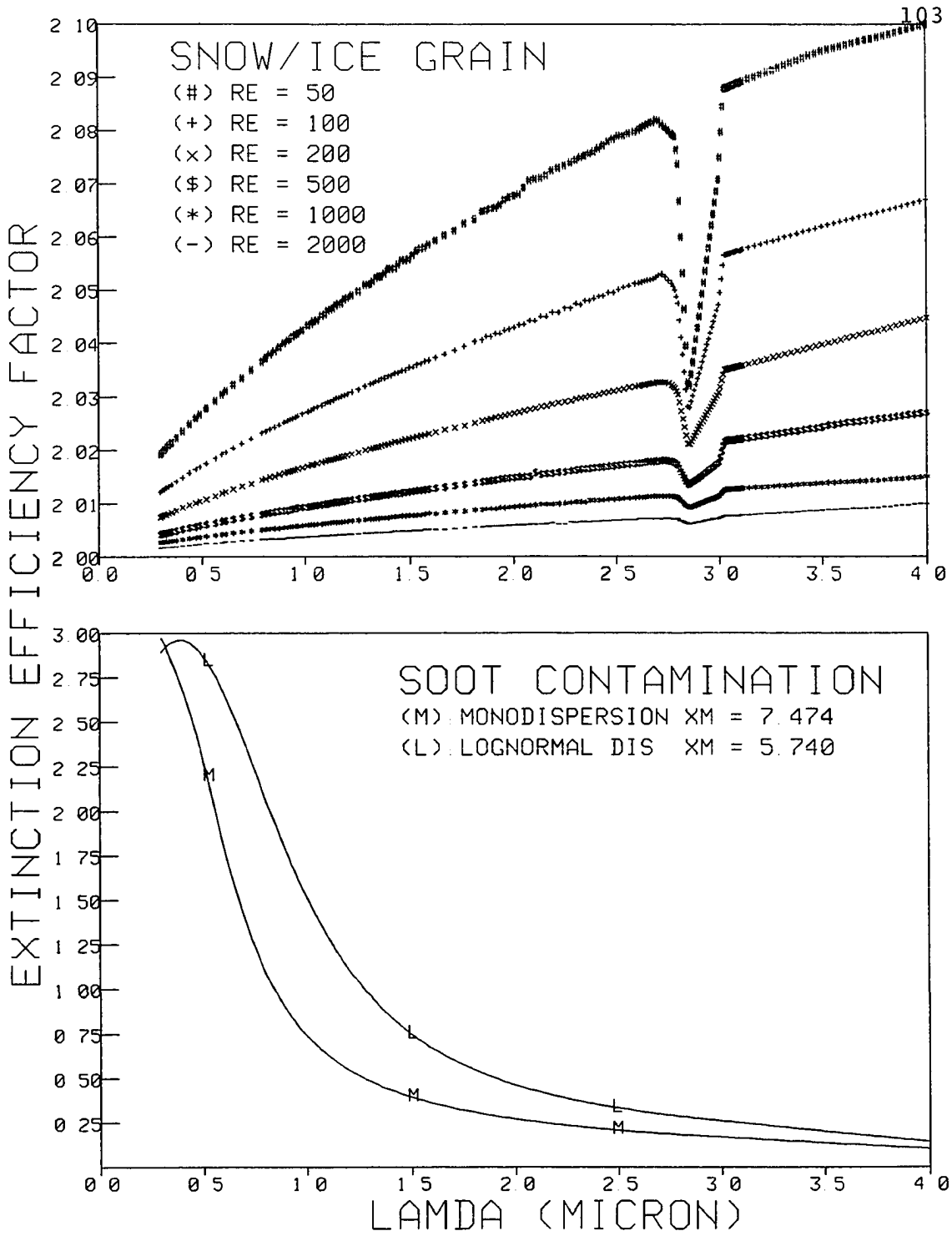


Figure 3.21 Extinction efficiency factor of six snow grains and two soot models for solar spectrum, RE for equivalent radius and XM for cross-section area per unit mass

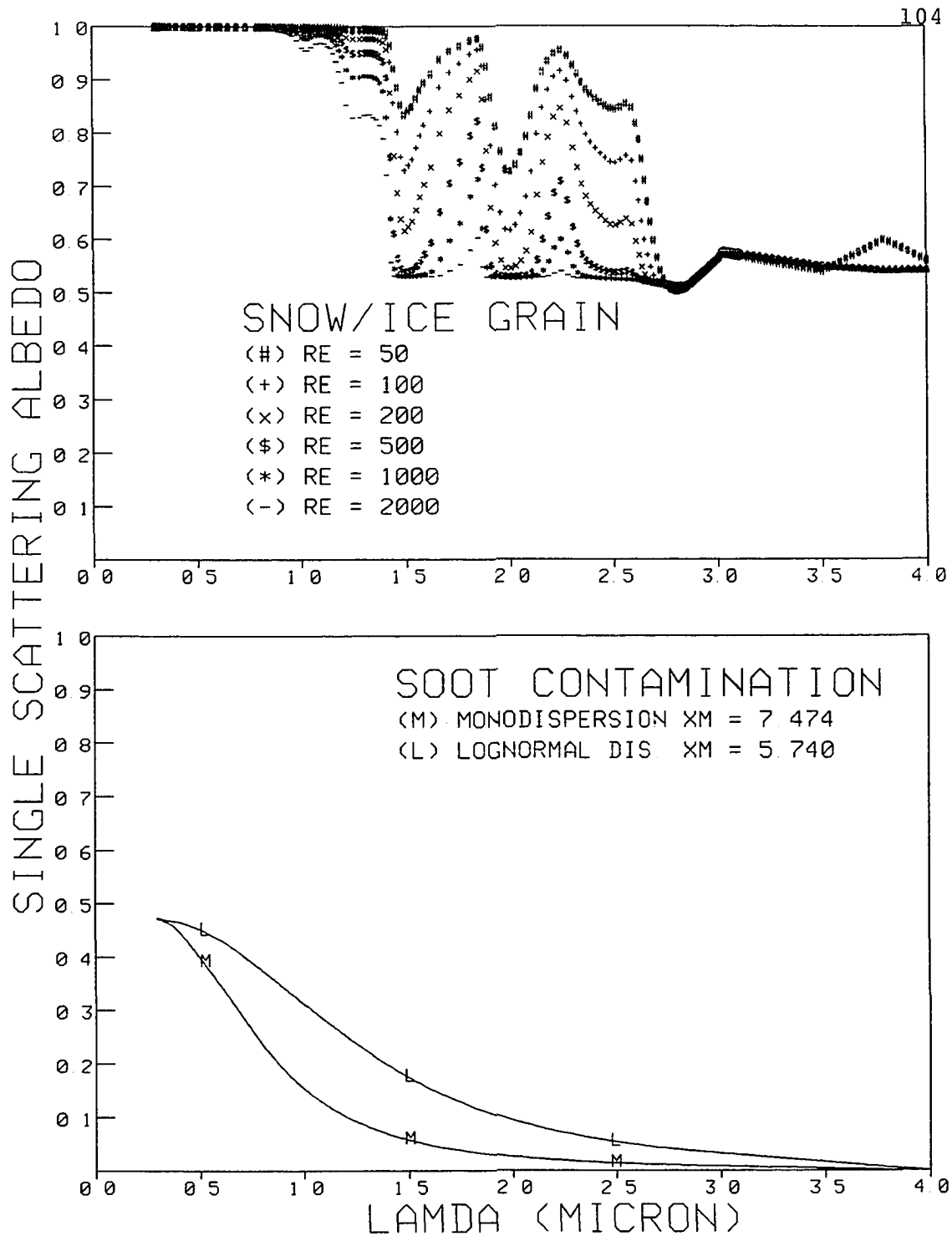


Figure 3.22 Single scattering albedo of six snow grains and two soot models for solar spectrum, RE for equivalent radius and XM for cross-section area per unit mass

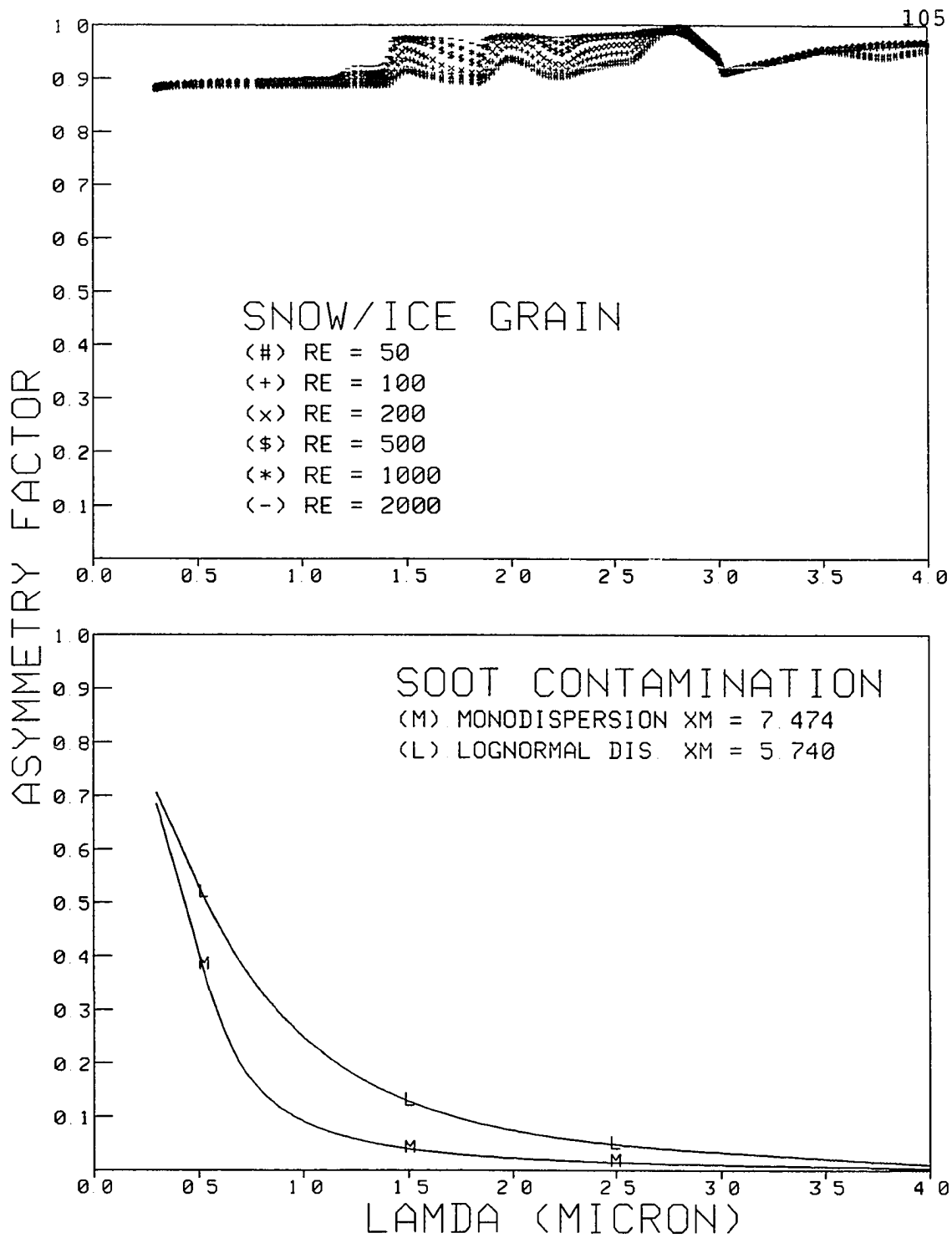


Figure 3.23 Asymmetry factor of six snow grains and two soot models for solar spectrum, RE for equivalent radius and XM for cross-section area per unit mass

body with an emissivity of about 99% and up. Therefore, the optical properties are not shown for the infrared spectrum.

Obviously, the grain radius of snow/ice is optically very large (about 10 to 100 times larger than cloud drops, Figures 3.9-11), and Q_{ext} approaches its geometric-optics limit of 2. The sharp dips at about $3\mu\text{m}$, shown on Figure 3.21, are caused by the vanishing surface reflection due to the real part of the ice refractive index approaching 1. The effective radii for soot are $0.1004\mu\text{m}$ for the monodispersion one and $0.1307\mu\text{m}$ for the lognormal distribution one. Therefore only in the visible region are the optical properties of soot important. The single scattering albedo of pure snow/ice is close to unity in the visible (Figure 3.22), due to the small imaginary part of ice refraction index. In the near-infrared, contributions from diffraction are essential, and ω reaches its lower limit of about 0.5. The asymmetry factor ranges from about 0.9 to 1, due to the strong forward scattering. For the same reason as in Q_{ext} , g approaches unity at $3\mu\text{m}$.

For the mixture of impurities, the optical properties of the mixture are obtained by weighting each component properly. For instance, the mass-fraction (f) of soot ranges from 0.01 to 0.06 ppmw (parts per million by weight), as observed in the Arctic snow/ice (Warren, 1982). Then, b_{ext} , ω and g of the mixture are obtained as follows:

$$\begin{aligned}
b_{\text{ext}}(R_g) &= \rho(R_g) [(1-f)K_{\text{ext}}(\text{ice}) + fK_{\text{ext}}(\text{soot})] \\
\omega(R_g) &= \frac{(1-f)K_{\text{sca}}(\text{ice}) + fK_{\text{sca}}(\text{soot})}{(1-f)K_{\text{ext}}(\text{ice}) + fK_{\text{ext}}(\text{soot})} \\
g(R_g) &= \frac{(1-f)K_{\text{sca}}(\text{ice})g(\text{ice}) + fK_{\text{sca}}(\text{soot})g(\text{soot})}{(1-f)K_{\text{sca}}(\text{ice}) + fK_{\text{sca}}(\text{soot})} \quad (3.21)
\end{aligned}$$

where K_{ext} and K_{sca} are the mass extinction and scattering cross-section for each component, respectively. $\rho(R_g)$ is the density of the mixture for grain radius (R_g). Because of the relatively small amounts of soot in snow/ice, $\rho(R_g)$ can be approximated by the density of snow/ice only. $K_{\text{ext}}(\text{soot})$ is obtained as $Q_{\text{ext}}(\text{soot})$ times $X_m(\text{soot})$, where $X_m = 0.75/(RE*\rho)$ denotes the cross-section area per unit mass ($\text{m}^2.\text{g}^{-1}$).

Data sets for Figures 3.21-23 were kindly provided by Dr. Warren (1985, personal communication) and can also be reproduced through Mie computations here.

CHAPTER 4. RESULTS AND DISCUSSION

The performance of model computations will be presented by means of comparisons with existing results of theoretical studies and measurements. Unfortunately, there is a paucity of tabulated or graphical results for intensity in the open literature. Some self-testing of the intensity computations have been made in Chapter Two. Therefore, in this chapter, comparisons of the flux and heating/cooling rate calculations are essential. For clear sky radiation, results will be compared mainly with those from the Line-By-Line methods. For cloudy and/or hazy sky radiation, results will be tested with the measurements obtained in the Arctic Stratus Clouds Experiment of 1980. Discussions follow the comparisons. By assuming the persistent characteristics of arctic stratus and haze, the radiative energy budgets for the atmosphere and the snow surface are computed daily under various conditions. A summary of this study is also given.

4.1 Clear Sky Radiation

For the purpose of clear sky comparisons, five profiles of McClatchey atmospheres are used as the basic input data - tropical, midlatitude summer and winter, subarctic summer

and winter atmospheres (McClatchey et al., 1972). Figures 4.1a to 4.1d show temperature, water vapor density, ozone density, and air density, respectively, as functions of pressure. Outstanding features of temperature profiles are the coldest tropopause of the tropical atmosphere at about 100mb (or 17Km) and a surface inversion layer for the subarctic winter atmosphere. Except for the tropical atmosphere, tropopauses for the remaining four are located at about 300mb (or 10Km). The water vapor densities in lower tropospheres differ by about one order of magnitude from the tropical to the subarctic winter atmospheres. The subarctic winter stratosphere (100mb) contains the maximum ozone concentration and as much as twice that in the tropical stratosphere (30mb). The density of uniformly mixed gases is proportional to the air density, which does not differ too much for the five model atmospheres. CO₂ concentration is assumed to be 330ppmv throughout this study.

Table 4.1 shows fluxes computed at the top and bottom of the tropical and subarctic winter atmospheres for water vapor absorption (0-580cm⁻¹ and 1220-2020cm⁻¹) and carbon dioxide absorption (540-800cm⁻¹) in the infrared regions. Values for the Line-By-Line method are obtained from Chou and Arking (1980) and Chou and Peng (1983) for H₂O and CO₂, respectively. Fluxes obtained from the Line-By-Line method are computed based upon the line parameters for the H₂O and

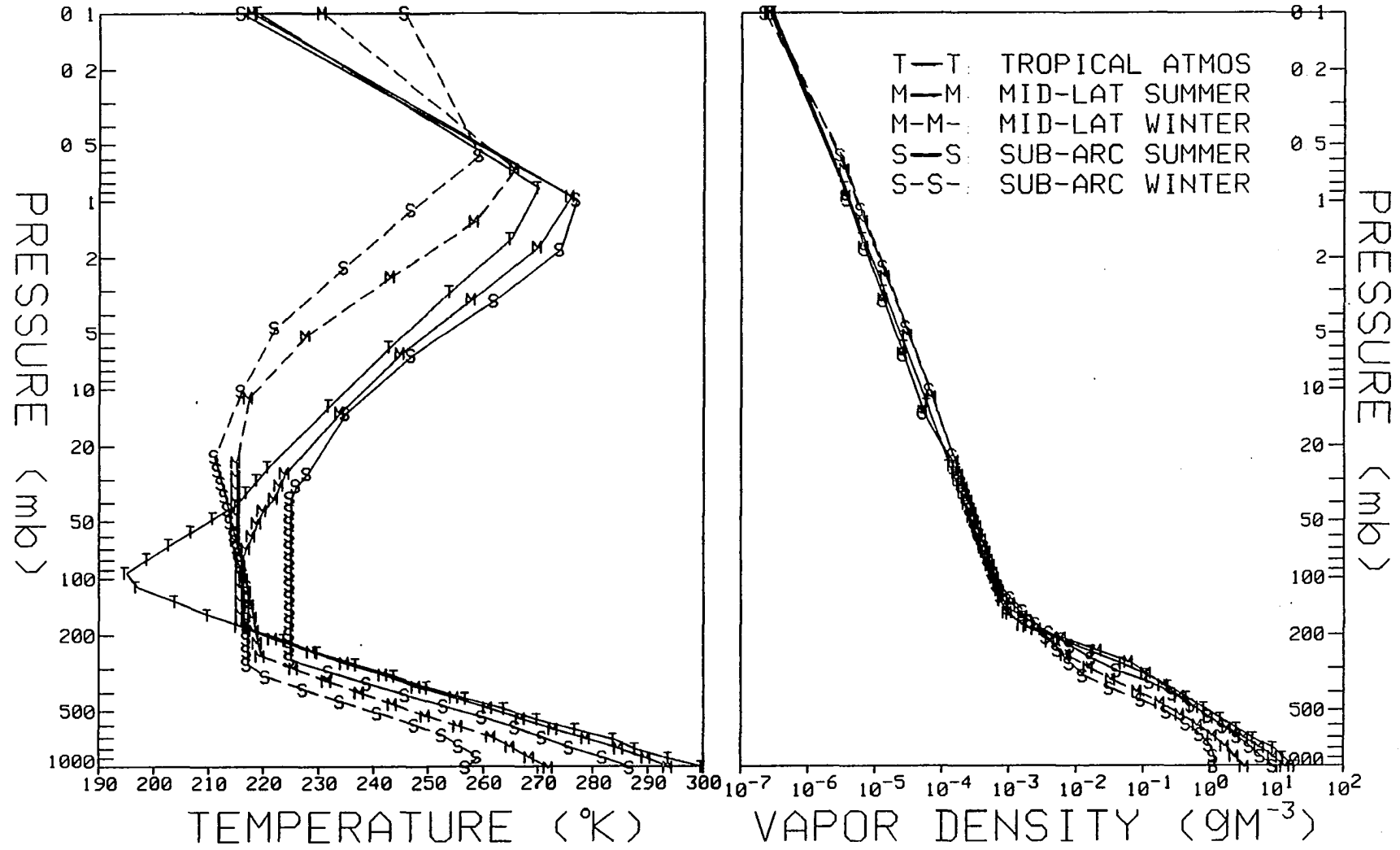


Figure 4.1 (a) Temperature, (b) water vapor density profiles as function of pressure for five McClatchey atmospheres

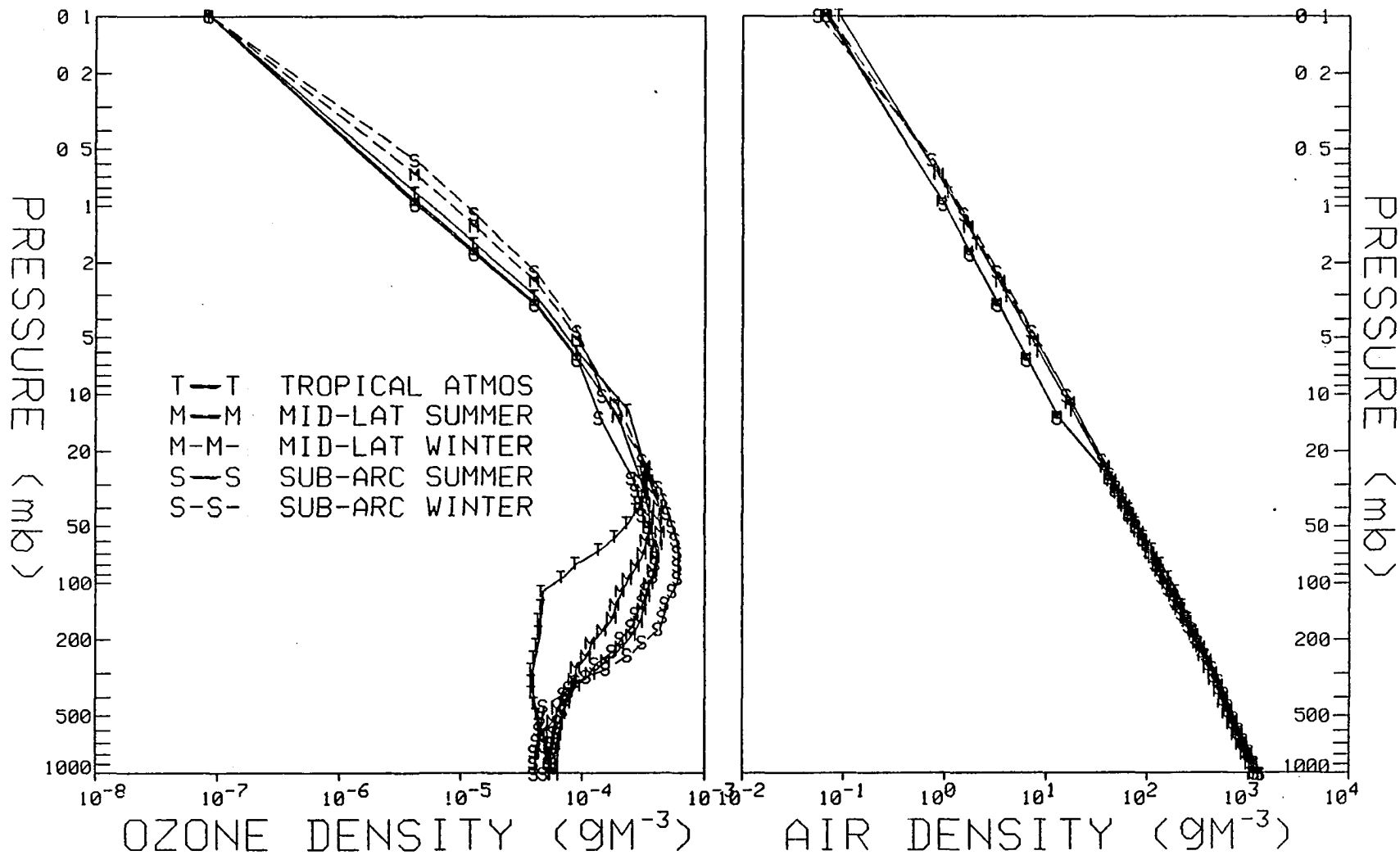


Figure 4.1 (c) Ozone density, (d) air density profiles as function of pressure for five McClatchey atmospheres

Table 4.1 Comparisons of flux computations for water vapor absorption ($0-580\text{cm}^{-1}$ and $1220-2020\text{cm}^{-1}$) and CO_2 absorption ($540-800\text{cm}^{-1}$) (values in parentheses are for double CO_2 amount) in tropical and subarctic winter atmospheres

| (a) Tropical Atmosphere | | | | | |
|-------------------------|----------------------|---------------|------------------|------------------|-------------------------|
| Method | Gas | $F^+(\tau_N)$ | $F^-(\tau_N)$ | $F^+(0)$ | ΔF_{atm} |
| Line-By-Line | H_2O | 221.29 | 211.88 | 133.40 | 123.99 |
| ESFT 20cm^{-1} | H_2O | 221.29 | 208.66 | 137.58 | 124.95 |
| Line-By-Line | CO_2 | 120.76 | 78.45 (84.98) | 75.11 (70.88) | 32.80 (35.10) |
| ESFT 20cm^{-1} | CO_2 | 120.76 | 77.29 (83.18) | 71.75 (68.16) | 28.28 (30.58) |

| (b) Subarctic Winter | | | | | |
|-------------------------|----------------------|---------------|------------------|------------------|-------------------------|
| Method | Gas | $F^+(\tau_N)$ | $F^-(\tau_N)$ | $F^+(0)$ | ΔF_{atm} |
| Line-By-Line | H_2O | 130.85 | 99.45 | 106.85 | 75.45 |
| ESFT 20cm^{-1} | H_2O | 130.85 | 106.19 | 108.22 | 83.56 |
| Line-By-Line | CO_2 | 69.63 | 41.75 (45.22) | 50.94 (49.16) | 23.06 (24.75) |
| ESFT 20cm^{-1} | CO_2 | 69.63 | 46.40 (49.69) | 49.30 (47.68) | 26.07 (27.74) |

Note: $F^+(\tau_N)$, upward flux at bottom; $F^-(\tau_N)$, downward flux at bottom; $F^+(0)$, upward flux at top; ΔF_{atm} , net flux loss of entire atmosphere (in dimension of W.m^{-2})

CO₂ molecules compiled by McClatchey et al. (1973) and serve as benchmarks. The line shape is assumed to be the Voigt profile (combination of molecular collision and movement), cutoff at 10cm^{-1} from the line center (Chou and Arking, 1980). Instead of having 33 layers, the McClatchey atmospheres were interpolated to have 55 layers. The temperature of each layer is constant. The top of the atmosphere is at 1mb and the surface assumed to be blackbody is at 1000mb.

Good agreement between Line-By-Line and present ESFT 20cm^{-1} is found in the tropical atmosphere for water vapor absorption. The difference in fluxes ranges from $3\text{W}\cdot\text{m}^{-2}$ in tropical (TRO) to $8\text{W}\cdot\text{m}^{-2}$ in subarctic winter (SAW) atmospheres, which is attributed to the large discrepancy in the downward fluxes at the surface. Two main reasons account for this. First, the water vapor is highly concentrated in the lower troposphere. Different interpolation schemes of the absorber amount will affect the H₂O absorption in the wing region. Second, the isothermal approximation used in the Line-By-Line method may be the major source of these differences. In the sensitivity study of Chapter Two, the superiority of the linear approximation was demonstrated. The surface inversion in SAW, in contrast to TRO, could be the major cause of the discrepancy in the downward flux.

The differences in CO₂ absorption are around $3-4\text{W}\cdot\text{m}^{-2}$, which is maximum in the upward flux for the TRO and in the

downward flux for the SAW. The changes in absorber amounts, even if double, do not alter discrepancies of the net flux loss for the entire atmosphere, but affect redistribution instead. Because CO_2 is assumed to be a uniformly mixed gas and also because the air densities do not change significantly from TRO to SAW, the possible cause of these differences could be the isothermal approximation. The Lorentz half-width of the absorption line is assumed to vary with the temperature (T) as $T^{-1/2}$ and might change appreciably across a layer.

Figure 4.2 shows the heating/cooling rate profiles of water vapor absorption for TRO and SAW. Results from the Line-By-Line and the present ESFT methods agree generally within 0.1-0.2°C per day, except for the large difference in the surface inversion for SAW. The inclusion of H_2O absorption (not continuum) in the $580\text{-}1220\text{cm}^{-1}$ region increases the cooling in the lower troposphere and is more pronounced in TRO than in SAW, because of the greater absorber amount available. Heating/cooling rates due to CO_2 absorption for TRO and SAW are shown in Figure 4.3. Very good agreement between two methods is found below the lower stratospheres of TRO and SAW. However, the large discrepancies (up to 2°C per day) of cooling rates above 40mb are partially due to the lower spatial resolution used. Three more sublayers between each original layer were introduced into the TRO atmo-

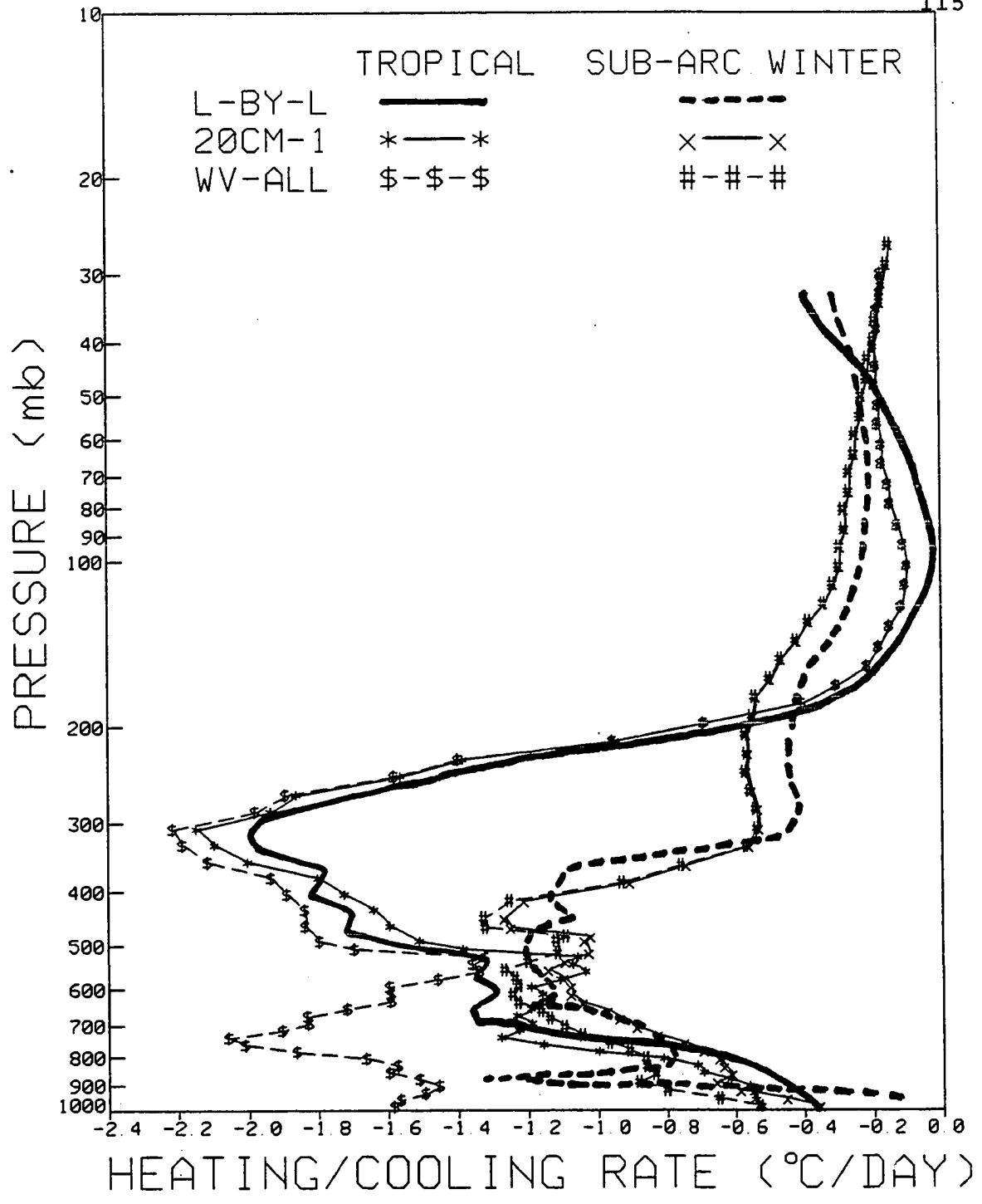


Figure 4.2 Heating/cooling rates of water vapor absorption for tropical and subarctic winter atmospheres

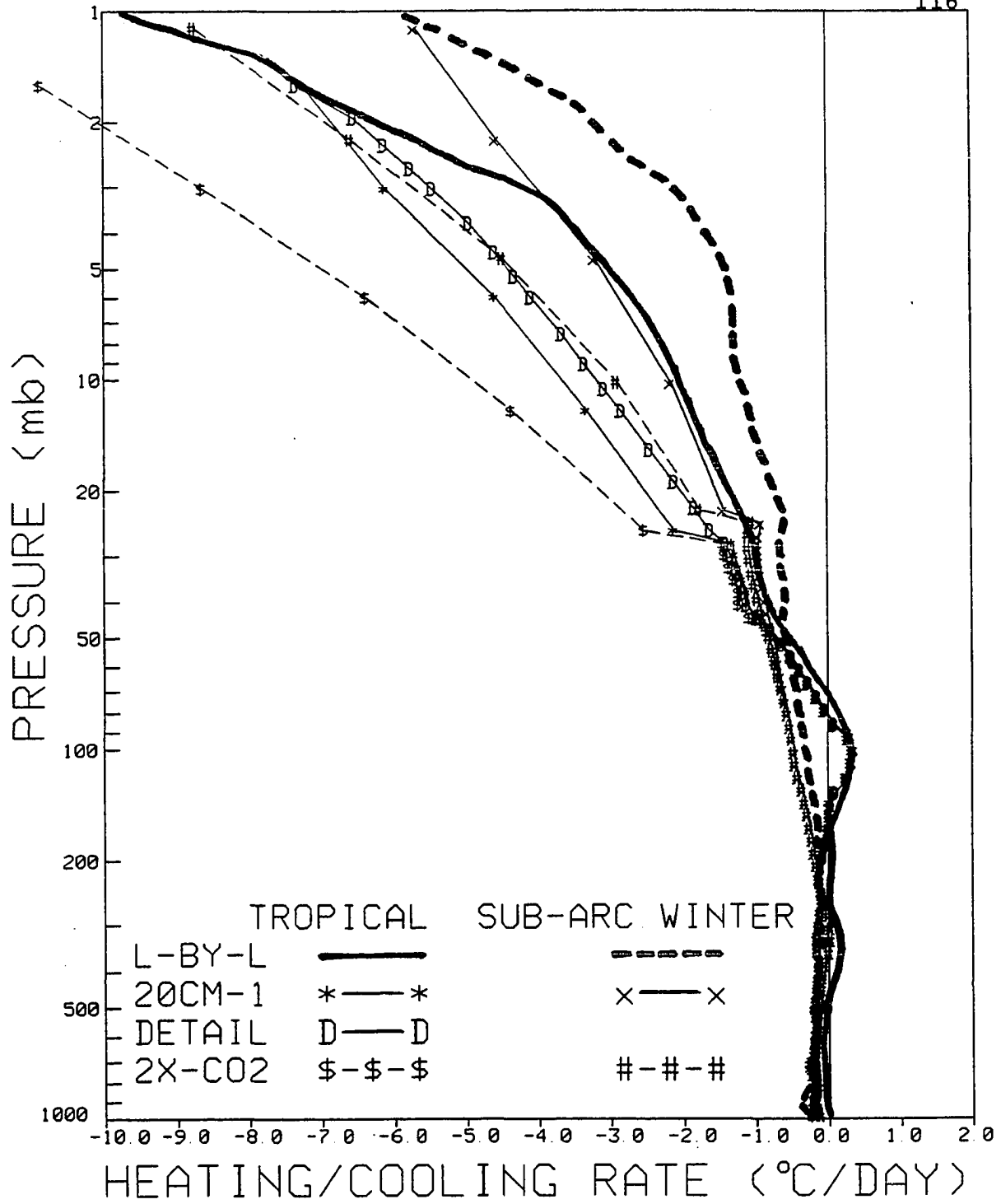


Figure 4.3 Heating/cooling rates of carbon dioxide absorption for tropical and subarctic winter atmospheres

sphere to improve the resolution. Better agreement is found (i.e., the heavy solid line and the solid line with "D"), while the discrepancy in the fluxes shown in Table 4.1 for TRO remains the same. This also suggests the main drawback of the isothermal approximation. Doubling the CO₂ absorber amount does not significantly change the heating/cooling rates below 40mb in either TRO or SAW. However, it increases the downward radiation at the surface by about 6W.m⁻² and 3W.m⁻² for TRO and SAW, respectively.

The other Line-By-Line methods reported in the ICRCCM (1984) are provided by four study groups: the Geophysical Fluid Dynamics Laboratory (GFDL), the Goddard Institute for Space Studies (GISS), the Goddard Laboratory for Atmospheric Studies (GLAS) and the Laboratoire de Meteorologie Dynamique (LMD). Table 4.2 compares fluxes as computed by the GFDL, the LMD and the present ESFT for various gaseous absorptions in the midlatitude summer atmosphere. Very good agreement is found for surface fluxes to within 2-3W.m⁻² for three major gaseous absorption (CO₂, O₃, and H₂O without continuum). The ozone absorption in the 580-1280cm⁻¹ region increases the surface downward flux by about 6 W.m⁻² and is relatively unimportant. The major difference in the upward flux at the top (within 5-6 W.m⁻²) is essentially due to CO₂.

The heating/cooling rate profiles for CO₂, O₃, and H₂O (with and without continuum) absorption are shown in Figure

4.4. The inclusion of continuum absorption is important when considering the lower troposphere because of the high-vapor partial pressure, especially near the surface. Generally, very good agreement is achieved between the present ESFT and the GFDL Line-By-Line methods to within 0.2°C per day below the 30mb level. However, even though the excellent agreement of fluxes between the GFDL and the LMD methods (as shown in Table 4.2) is to within $1 \text{ W}\cdot\text{m}^{-2}$, their cooling rates show a maximum discrepancy up to 0.3°C per day in the troposphere. This suggests that care should be taken in studies of atmospheric thermal stability in terms of bulk radiative quantities, due to their possible compensating errors.

For the purpose of discussion, the infrared region is roughly divided into three bands: the water vapor rotational band ($0\text{-}840\text{cm}^{-1}$), the window ($840\text{-}1400\text{cm}^{-1}$), and the water vapor vibrational band ($1400\text{-}2500\text{cm}^{-1}$). The heating/cooling rates for each and the total gaseous absorption in the sub-arctic summer atmosphere are shown in Figure 4.5. The water vapor vibrational band contributes very little to the total cooling due to the small amount of Planckian flux in this spectral region at earth temperature. Therefore, very small cooling is observed in the lower troposphere due to the major concentration of water vapor. Ozone absorption ($580\text{-}1280\text{cm}^{-1}$) partially overlaps with both the H_2O rotational band and the window band. The heating caused by O_3 between

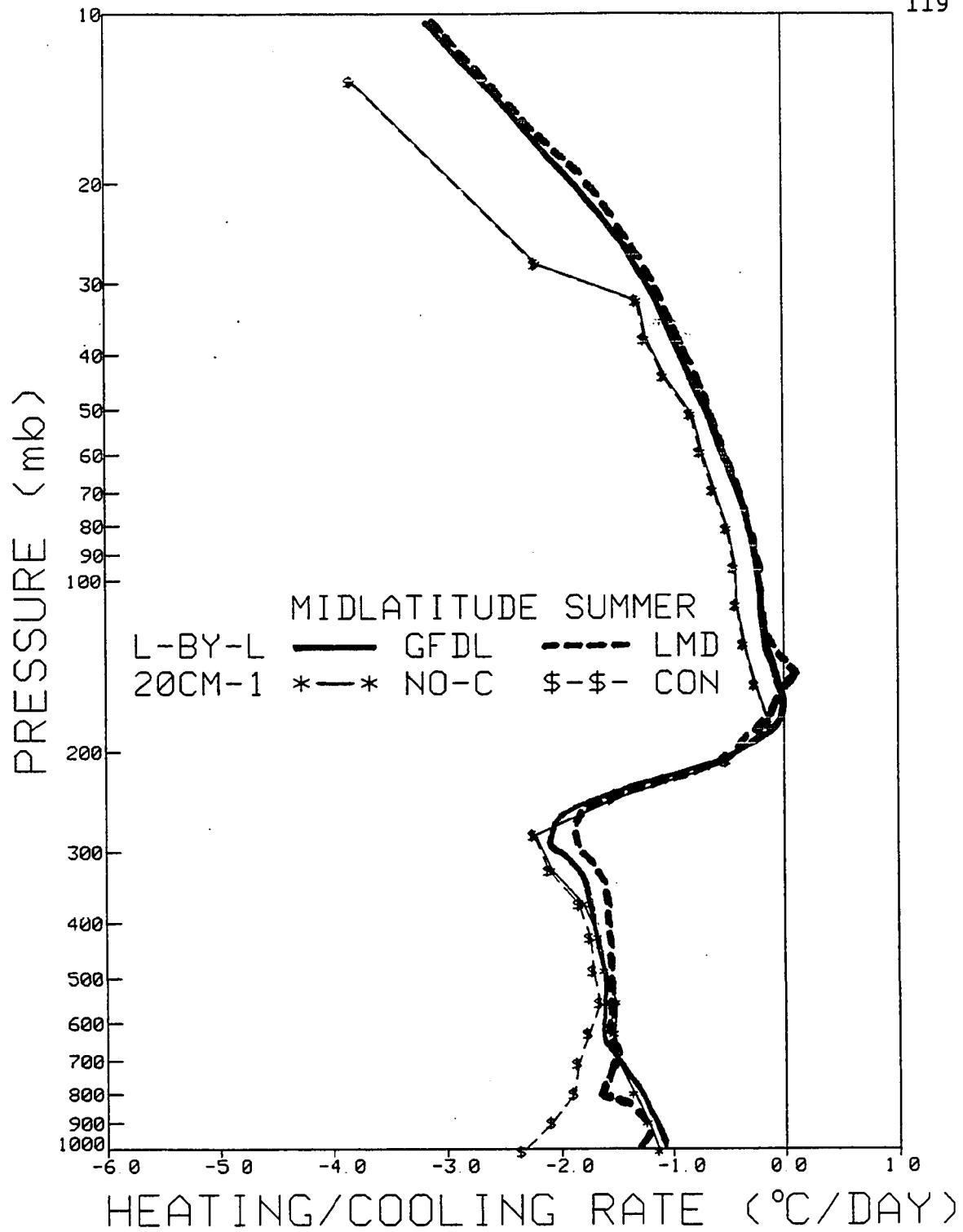


Figure 4.4 Heating/cooling rates of carbon dioxide, ozone, water vapor (with and without continuum) absorption for midlatitude summer atmosphere

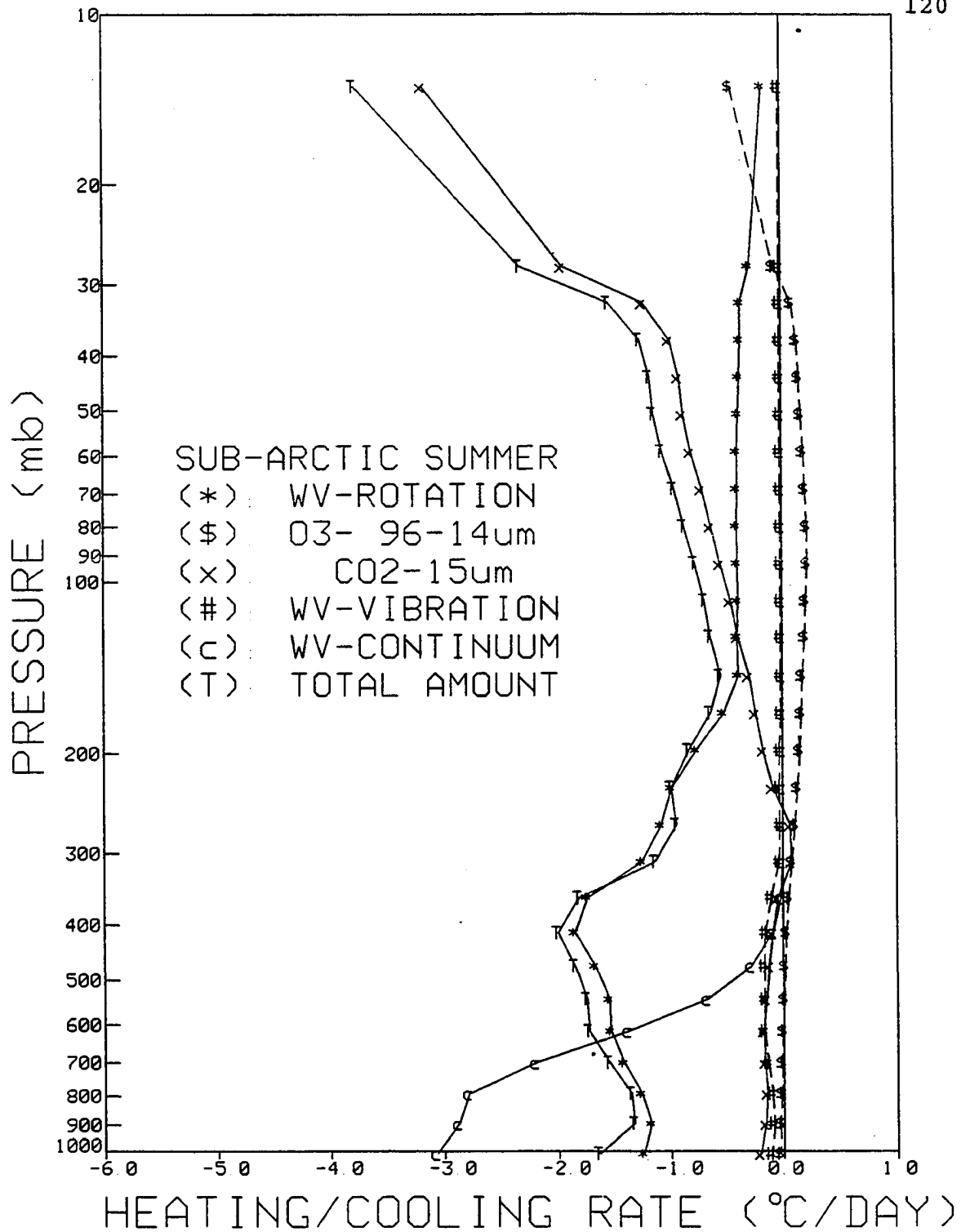


Figure 4.5 Heating/cooling rates of carbon dioxide, ozone, water vapor, continuum, and total absorption for subarctic summer atmosphere

the upper troposphere and the lower stratosphere, the region of maximum O_3 concentration (Figure 4.1c), is due mainly to radiation emitted from the warm surface. Above the lower stratosphere, cooling is caused by ozone radiating into colder space, whence there is very little return radiation.

Carbon dioxide absorption ($540-800\text{cm}^{-1}$) contributes largely to the major cooling above the lower stratosphere because CO_2 is an efficient emitter, assuming uniform mixing. The slight heating of CO_2 near the tropopause is caused by a warmer surface. The H_2O continuum absorption ($320-1400\text{cm}^{-1}$) overlaps with the H_2O rotational band partially and with the window entirely. The strong cooling by the H_2O continuum alone in the lower troposphere is due to high H_2O partial pressure; and 90% of the cooling comes from the $320-840\text{cm}^{-1}$ region. Finally, the water vapor rotational band contributes to the major cooling in the troposphere, due to the high concentration of H_2O molecules.

The heating/cooling rate of a layer is computed by the divergence of net fluxes at two boundaries. When the absorption spectra of gaseous species are not overlapping, the net heating/cooling rate is a simple summation of each individual heating/cooling rate. However, this breaks down when the overlapping of absorption occurs. In this case, the net fluxes at the boundaries are changed, depending upon the final optical properties of the mixed absorbing gases. For

example, in the strong absorption of the water vapor rotational band, absorption could become saturated easily by H_2O alone. Adding any absorbing gases would not alter the bulk radiative quantities of the layer. This is shown clearly by the heating/cooling profile of total gaseous absorption in Figure 4.5. Therefore, above the troposphere, cooling of the atmosphere is due mainly to CO_2 emission and some portion of the cooling is contributed to O_3 emission. In the troposphere, the H_2O rotational band accounts for the major cooling and the H_2O continuum contributes in some degree to the cooling in the boundary layer. However, the importance of including the H_2O continuum absorption is its additional downward radiation back to the surface of about $50W.m^{-2}$, which produces a lesser cooling of the surface.

Although the Line-By-Line methods can be very accurate, they are very time-consuming. The AFGL (Air Force Geophysics Laboratory) compilation contains over 159,000 lines from 0.3 to $17880cm^{-1}$ (Rothman, 1981). Therefore, when applying the Line-By-Line methods, the transfer equation (Eq. 2.2) has to be solved over 159,000 times. Practically, this is suitable for validating models only. The present ESFT method contains about 16,000 terms (i.e., $w_i \dots w_j$ of Eq. 3.6) from $20cm^{-1}$ to $40000cm^{-1}$ for H_2O , CO_2 and O_3 gaseous absorptions, in which 9800 terms are in the infrared region. If detailed overlapping gaseous absorption is not essential, only 2800 terms in

the infrared are needed since it is possible to eliminate unimportant overlapping without making any serious errors. Further reduction of the fitting terms might be sought. However, the significant digits of the VAX computer are not sufficient for this type of study.

In the solar spectrum, the intervals of the ESFT are in general larger than 20cm^{-1} and occur irregularly. However, the near-infrared region is still in the category of narrow band model (NBM), in which the spectral resolution is less than 100cm^{-1} (ICRCCM, 1984). On the other hand, broad band models (BBM) contain spectral widths larger than 100cm^{-1} (e.g., Slingo and Schrecker, 1982). The present ESFT-NBM treats the gaseous absorption of H_2O , CO_2 and O_3 ; and the BBM includes an additional absorbing gas of O_2 , which is an extension of the model of Slingo and Schrecker (1982).

Table 4.3 shows net fluxes gained and heating/cooling rates of the entire atmosphere for various methods dealing with water vapor absorption in the tropical and midlatitude winter atmospheres, where the zenith angle is 60° and the surface albedo is zero. Values for the Line-By-Line and Far-Wing scaling are obtained from Chou and Arking (1981). The Line-by-Line method is essentially the same as the one mentioned previously. The Far-Wing scaling method is based on the so-called k-distribution function (Arking and Grossman, 1972), where the spectral interval is set to be 40cm^{-1} . The

Table 4.2 Comparisons of flux computations for CO₂, O₃, and H₂O (without continuum) absorption (0-2600cm⁻¹) in midlatitude summer atmosphere

| Method | F ⁺ (τ _N) | F ⁻ (τ _N) | ΔF _{sfc} | F ⁺ (0) | ΔF _{atm} |
|-------------------------|----------------------------------|----------------------------------|-------------------|--------------------|-------------------|
| GFDL L-BY-L | 423.15 | 303.46 | 119.69 | 294.42 | 174.73 |
| LMD L-BY-L | 423.09 | 302.80 | 120.29 | 293.69 | 173.40 |
| ESFT 20cm ⁻¹ | 423.13 | 300.22 | 122.91 | 288.22 | 165.31 |

Table 4.3 Comparisons of flux and heating/cooling rate computations for water vapor absorption with 60° zenith angle and zero surface albedo in tropical and midlatitude winter atmospheres

| (a) Tropical Atmosphere | | | |
|-----------------------------|------------------|-------------------|-------|
| Spectral(cm ⁻¹) | Method | ΔF _{atm} | HCR |
| 2600-12040 | Line-By-Line | 105.60 | 0.892 |
| 2600-12040 | Far-Wing Scaling | 104.70 | 0.884 |
| 2600-12040 | ESFT Narrow-Band | 98.55 | 0.831 |
| 2500-12820 | ESFT Narrow-Band | 101.07 | 0.852 |
| 2500-12820 | ESFT Broad-Band | 102.00 | 0.860 |
| (b) Midlatitude Winter | | | |
| Spectral(cm ⁻¹) | Method | ΔF _{atm} | HCR |
| 2600-12040 | Line-By-Line | 71.20 | 0.601 |
| 2600-12040 | Far-Wing Scaling | 72.70 | 0.615 |
| 2600-12040 | ESFT Narrow-Band | 72.55 | 0.608 |
| 2500-12820 | ESFT Narrow-Band | 73.61 | 0.617 |
| 2500-12820 | ESFT Broad-Band | 74.52 | 0.626 |

Note: F⁺(τ_N), upward flux at bottom; F⁻(τ_N), downward flux at bottom; ΔF_{sfc}, net flux gain/loss from surface; F⁺(0), upward flux at top; ΔF_{atm}, net flux gain/loss of entire atmosphere (all in dimension of W.m⁻²); HCR, heating/cooling rate (°C/day)

k-distribution assumes that the transmission depends upon the fraction of existing coefficient k instead of its ordering of k in the spectral interval. Therefore, the distribution functions are weighted by the corresponding fluxes in that interval. Despite the different spectral ranges used, systematic discrepancies are observed. The Broad-Band values are consistently larger than those of the Narrow-Band ESFT by about 1W.m^{-2} for both atmospheric absorptions. However, values obtained by the Far-Wing scaling differ from those obtained by the Line-By-Line, with alternate sign of about 1W.m^{-2} even though their computational setup is identical. When the results of ESFT-NBM are performed in the same spectral region as the Line-By-Line, good agreement is achieved for the midlatitude winter but only fair for the tropical atmosphere. Therefore, the absorption by H_2O of the solar spectrum is quite sensitive to the computation of humidity profiles.

The heating/cooling rate profiles for the tropical and midlatitude winter atmospheres are shown in Figure 4.6. Very good agreement of heating profiles between the ESFT-NBM and the ESFT-BBM are achieved as expected from Table 4.3, except around the tropopause. The major difference of heating rates (maximum of 0.3°C per day) between the Line-By-Line and the ESFT for the tropical atmosphere is observed below 600 mb, the location of the major concentration of H_2O . The

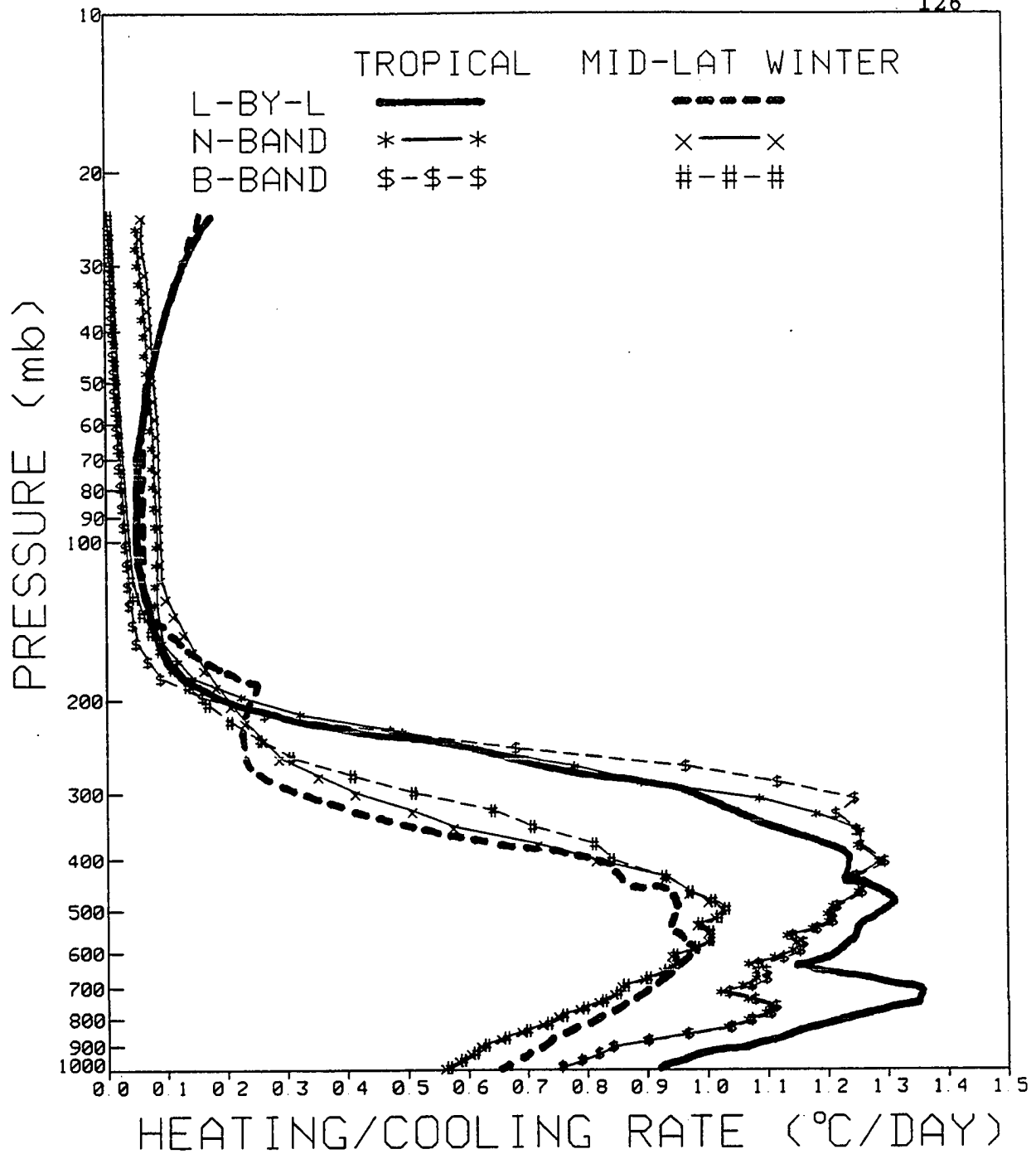


Figure 4.6 Solar heating rates of water vapor absorption for tropical and midlatitude summer atmospheres

sudden jump of the heating rate for the Line-By-Line method around the tropopause of the midlatitude winter atmosphere is quite strange, and could be caused by the interpolation of layering.

Because of the limited studies in the open literature, further comparisons between the ESFT and other Line-By-Line methods are difficult to make, such as the O_3 absorption. Therefore, the intercomparison of the ESFT is attempted for O_3 absorption and others. Table 4.4 shows the comparisons of fluxes for O_3 absorption with a 30° solar zenith angle and a 0 surface albedo in the subarctic summer atmosphere. Slingo and Schrecker (1982) argued against the empirical constant (0.4) of LOWTRAN scaling for ozone absorber amount (Eq.3.5), especially under the condition of multiple scattering. Therefore, tests are conducted with and without scaling.

The Narrow-Band-S (NBS) contains two weak O_3 absorption bands (3.3 and $3.6\mu\text{m}$) in the near-infrared region and strong absorption bands at wavelengths shorter than $0.7\mu\text{m}$. On the other hand, the Narrow-Band-V (NBV) eliminates the two weak absorption bands and so does the Broad-Band-V (BBV) but with wider spectral intervals. Additional absorptions by entire atmospheres due to the weak bands range from 0.2 to $0.5\text{W}\cdot\text{m}^{-2}$ for this case and take place above the tropopause. For most applications, the weak band absorption could be eliminated without making serious errors. The BBV systematically over-

Table 4.4 Comparisons of flux computations for O₃ absorption with 30° zenith angle and zero surface albedo in subarctic summer atmosphere

(a) O₃ absorber amount without scaling

| Method | $F^-(0)$ | $F^-(\tau_N)$ | ΔF_{atm} | ΔF_{tro} |
|---------------|----------|---------------|------------------|------------------|
| Narrow-Band-S | 645.11 | 616.42 | 28.69 | 27.31 |
| Narrow-Band-V | 534.47 | 506.31 | 28.16 | 26.83 |
| Broad-Band-V | 534.47 | 504.94 | 29.53 | 28.22 |

(b) O₃ absorber amount with scaling

| Method | $F^-(0)$ | $F^-(\tau_N)$ | ΔF_{atm} | ΔF_{tro} |
|---------------|----------|---------------|------------------|------------------|
| Narrow-Band-S | 645.11 | 626.30 | 18.81 | 17.09 |
| Narrow-Band-V | 534.47 | 515.86 | 18.61 | 16.94 |
| Broad-Band-V | 534.47 | 515.12 | 19.35 | 17.77 |

Note: $F^-(0)$, downward flux at top; $F^-(\tau_N)$, downward flux at bottom; ΔF_{atm} , net flux gain of entire atmosphere; ΔF_{tro} , net flux gain above tropopause (all in dimension of $W \cdot m^{-2}$); S, shortwave region $2500-40000cm^{-1}$; V, wavelengths shorter than visible region $14500-40000cm^{-1}$

estimates the ozone absorption by the entire atmosphere by about $1\text{W}\cdot\text{m}^{-2}$, which is consistent with the H_2O absorption in Table 4.3. This could be caused by the approximation of solar radiation being constant over the spectral intervals.

Pressure and temperature scaling decreases substantially the absorber amount in the upper atmosphere where the major absorption of ozone occurs. This causes absorption by the entire atmosphere to be reduced by about 40%. The reduction is due mainly to the weak absorption of ozone in the visible region because the strong ozone absorption in the ultraviolet becomes saturated easily whether scaling is used or not. However, the major heating for the scaled ozone profile shifts downward and becomes weak, because radiation penetrates deeply and diverges gradually due to the diluted effective absorber amount. Therefore, further studies are needed to assess the necessity and accuracy of this scaling.

The Rayleigh scattering is important in the shortwave region. Table 4.5 examines two different data sets of Rayleigh optical parameters for flux computations with various zenith angles and surface albedo in the subarctic summer atmosphere. Excellent agreements are found between results of using Penndorf's data (Eq. 3.12) and of using Nicolet's fit (Eq. 3.13) in $0.25\mu\text{m}$ to $1.0\mu\text{m}$, where the O_3 , O_2 and H_2O absorptions occur. Absorptions by entire atmospheres are almost identical and differences of the upward fluxes at top and the downward fluxes at bottom are within $0.5\text{W}\cdot\text{m}^{-2}$.

Table 4.5 Comparisons of flux computations for Rayleigh scattering with various zenith angles and surface albedo in subarctic summer atmosphere

| (a) Surface albedo (0.0) | | | | | | |
|--------------------------|---------------|----------|------------------|----------------|----------|------------------|
| Penndorf (1957) | | | | Nicolet (1984) | | |
| Zenith | $F^-(\tau_N)$ | $F^+(0)$ | ΔF_{atm} | $F^-(\tau_N)$ | $F^+(0)$ | ΔF_{atm} |
| 30 | 700.29 | 51.88 | 59.00 | 700.80 | 51.37 | 59.00 |
| 60 | 378.89 | 46.12 | 43.31 | 379.31 | 45.70 | 43.31 |
| 75 | 175.10 | 37.35 | 29.97 | 175.38 | 37.05 | 29.99 |

| (b) Surface albedo (0.8) | | | | | | |
|--------------------------|---------------|----------|------------------|----------------|----------|------------------|
| Penndorf (1957) | | | | Nicolet (1984) | | |
| Zenith | $F^-(\tau_N)$ | $F^+(0)$ | ΔF_{atm} | $F^-(\tau_N)$ | $F^+(0)$ | ΔF_{atm} |
| 30 | 762.52 | 576.67 | 81.99 | 762.53 | 576.66 | 81.99 |
| 60 | 410.96 | 331.80 | 54.34 | 411.13 | 331.75 | 54.34 |
| 75 | 188.97 | 170.23 | 34.40 | 189.15 | 170.17 | 34.42 |

Note: $F^-(\tau_N)$, downward flux at bottom; $F^+(0)$, upward flux at top; ΔF_{atm} , net flux gain of entire atmosphere (all in dimension of $W.m^{-2}$); $1342.338W.m^{-2}$ for solar constant

Absorptions of O_2 and CO_2 in the near-infrared region are also examined for the scattering atmosphere, as shown in Table 4.6. Because the CO_2 absorption is overlapping with the strong absorption of H_2O , the inclusion of CO_2 only increases atmospheric absorption by about 4.3 W.m^{-2} and cools the surface by about 3.3 W.m^{-2} . The effect of O_2 absorption has the same order of magnitude as does the CO_2 absorption.

Therefore, in the shortwave region, the broad-band ESFT is acceptable for some types of applications which allow errors in fluxes to within a few watts per square meter. Substantial amounts of computer time are saved due to the reduction of terms from 6,500 in the narrow-band to 410 in the broad-band ESFT method. When the absorption of O_2 and CO_2 can be neglected, the number of terms can be reduced to 141, as in the model of Slingo and Schrecker (1982).

4.2 Cloudy And/Or Hazy Sky Radiation

Recent measurements of solar and terrestrial radiation for the Arctic were reported by Herman and Curry (1984) and Curry and Herman (1985), respectively. Their papers contain essentially the measured fluxes under cloudy conditions. The physical properties of the arctic stratus, together with the associated meteorological conditions, were reported by Tsay and Jayaweera (1984). No arctic haze measurement has been

Table 4.6 Comparisons of flux computations for gaseous absorption with 30° zenith angle and 0.8 surface albedo in subarctic summer atmosphere

(a) Gases + Rayleigh scattering in $2500-12820\text{cm}^{-1}$

| Gases | $F^-(0)$ | $F^-(\tau_N)$ | ΔF_{atm} | ΔF_{tro} |
|------------------------------------|----------|---------------|-------------------------|-------------------------|
| $\text{H}_2\text{O} + \text{CO}_2$ | 528.09 | 386.72 | 165.18 | 7.63 |
| H_2O only | 528.09 | 390.03 | 160.89 | 5.64 |

(b) Gases + Rayleigh scattering in $12820-40000\text{cm}^{-1}$

| Gases | $F^-(0)$ | $F^-(\tau_N)$ | ΔF_{atm} | ΔF_{tro} |
|------------------------------------------------|----------|---------------|-------------------------|-------------------------|
| $\text{O}_3 + \text{H}_2\text{O} + \text{O}_2$ | 634.41 | 605.47 | 54.35 | 43.38 |
| $\text{O}_3 + \text{H}_2\text{O}$ | 634.41 | 609.54 | 49.21 | 41.85 |

Note: $F^-(0)$, downward flux at top; $F^-(\tau_N)$, downward flux at bottom; ΔF_{atm} , net flux gain of entire atmosphere; ΔF_{tro} , net flux gain above tropopause (all in dimension of $\text{W}\cdot\text{m}^{-2}$); $1342.338\text{W}\cdot\text{m}^{-2}$ for solar constant

made in the meantime. Figure 4.7 shows two atmospheric profiles for the low stratus clouds, which were recommended for detailed radiation studies by the above authors. Two-layer clouds are observed on June 28, associated with the surface and cloud top inversions. A single-layer cloud is measured on June 20, which extended to the surface and was capped by a strong inversion at the cloud top. None of these clouds are saturated, they show a relative humidity range from as low as about 80% on June 20. Very dry conditions aloft are also observed on June 20.

Radiative fluxes are computed by the broad-band method, which treats overlapping gaseous absorption (ESFT), Rayleigh scattering, and cloud absorption and scattering. The entire solar spectrum (0.28-4.0 μm), the near-infrared (NIR, 0.78 - 4.0 μm), and the visible (VIS, 0.28-0.78 μm) are defined corresponding to the sensitivity ranges of Eppley pyranometers. Boundary conditions are taken from the observed data, which are 53.8° (June 28) and 53.6° (June 20) for zenith angles; 1337.19W.m⁻² for the solar constant (0.28-4.0 μm); and 0.68 (VIS, June 28), 0.35 (NIR, June 28), 0.60 (VIS, June 20) and 0.43 (NIR, June 20) for surface albedos. Figures 4.8 and 4.9 show the computed and observed upward and downward fluxes on June 28 and June 20, respectively. The measured fluxes for the visible region are computed as the difference between the total and the near-infrared (Herman and Curry, 1984).

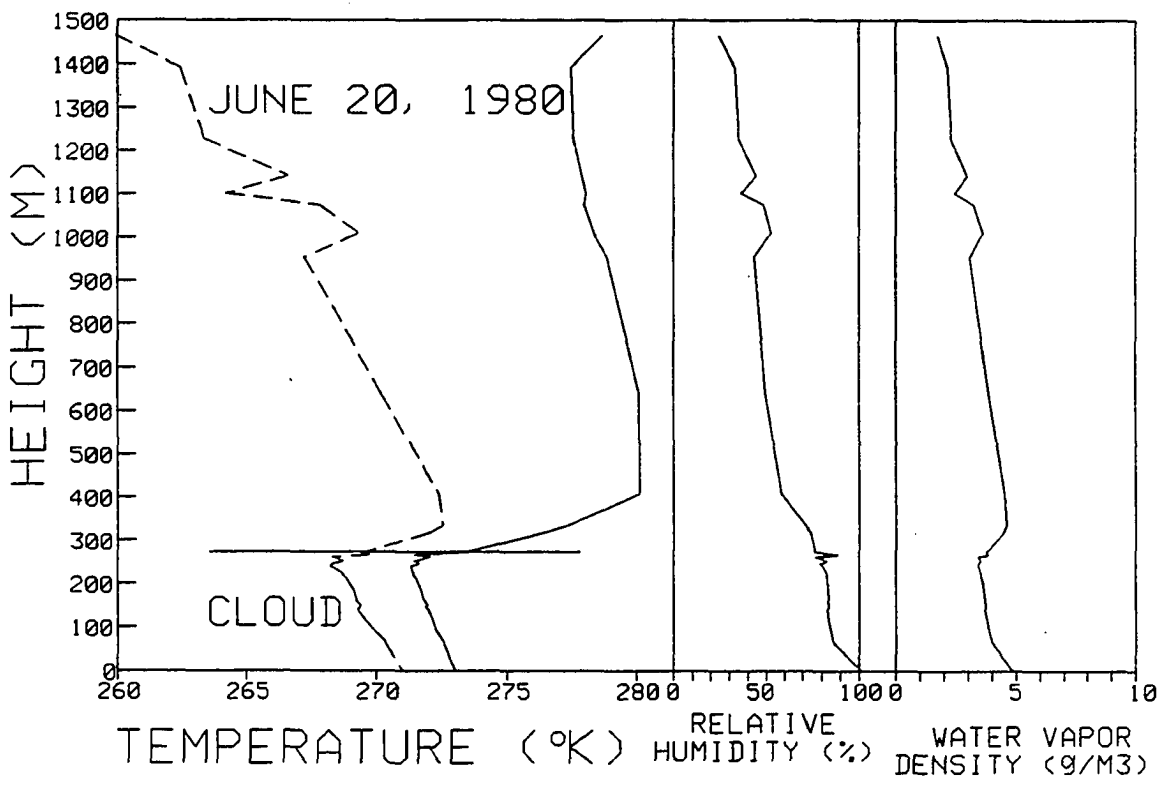
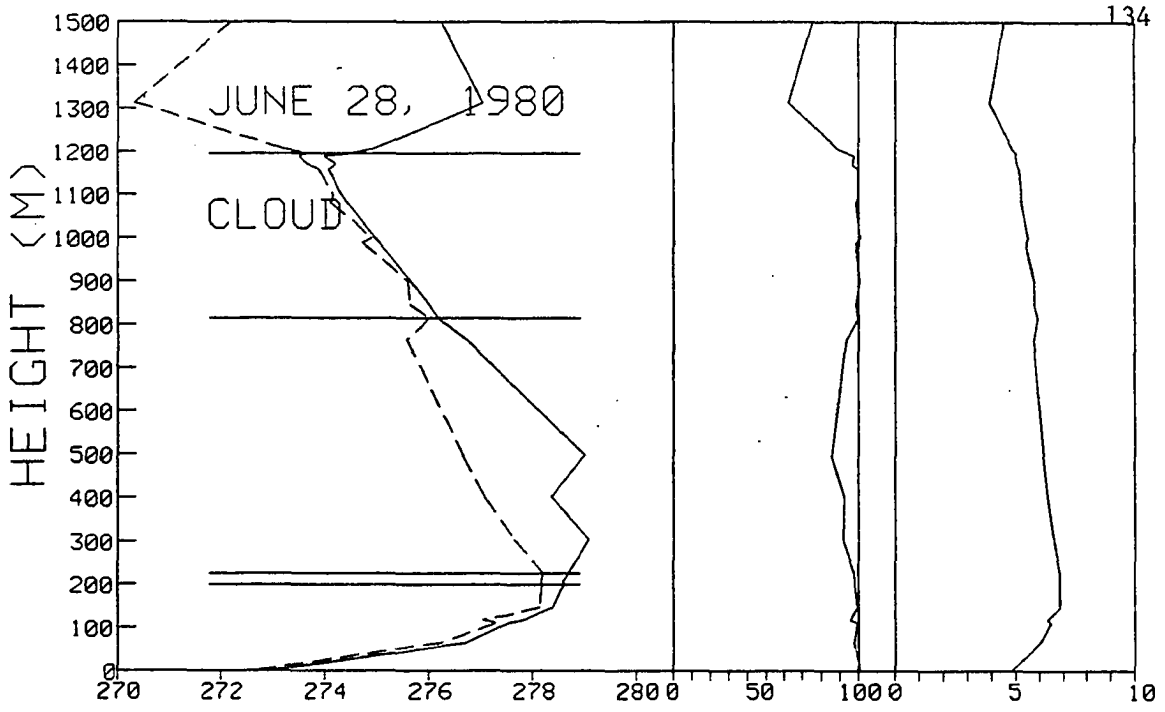


Figure 4.7 Atmospheric profiles for two observed arctic stratus clouds on June 20 and 28, 1980

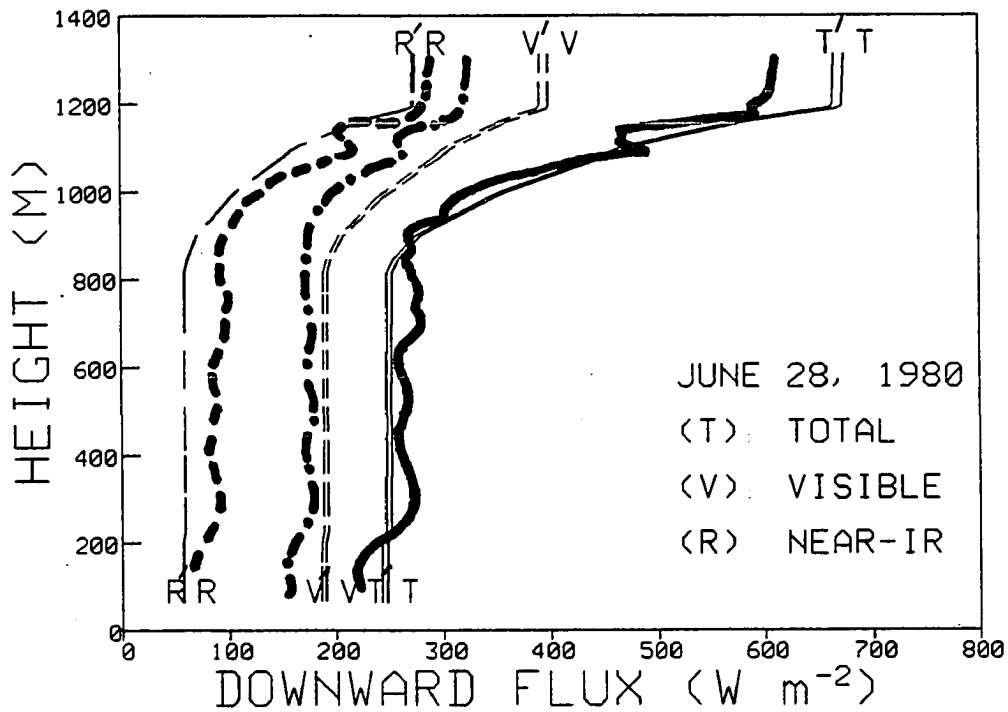
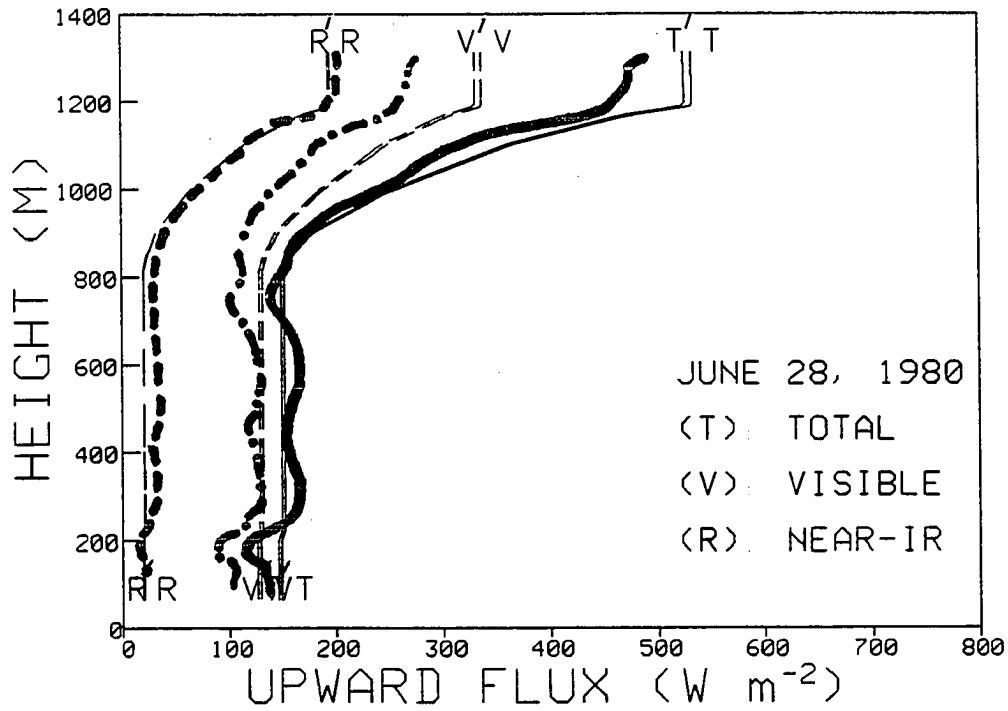


Figure 4.8 Comparison of observed (heavy lines) and computed fluxes for stratus clouds on June 28, 1980

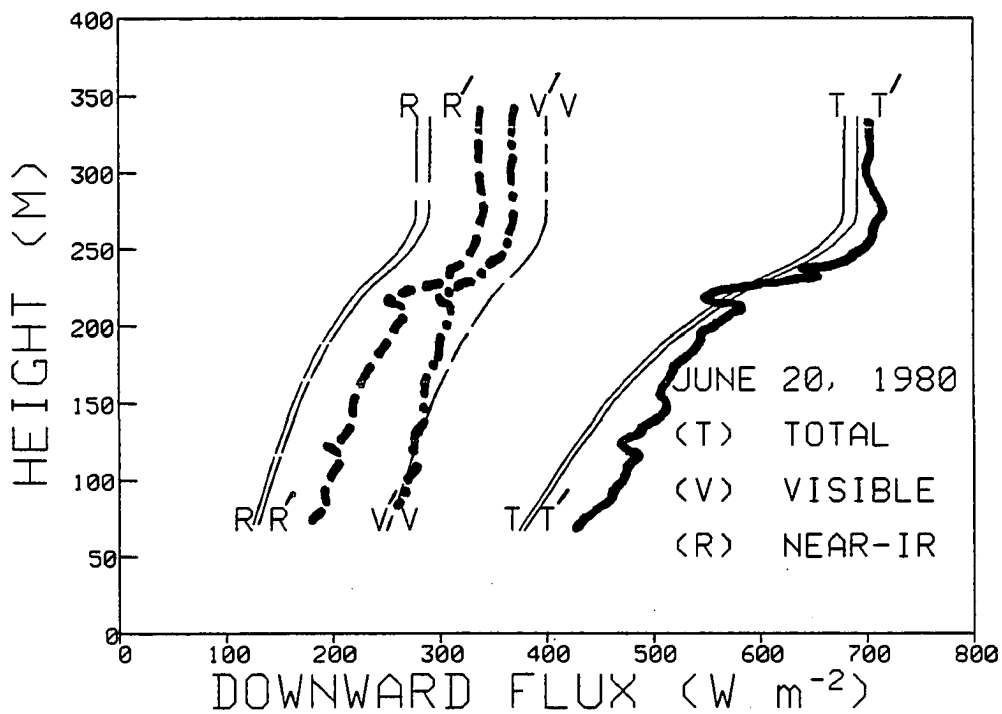
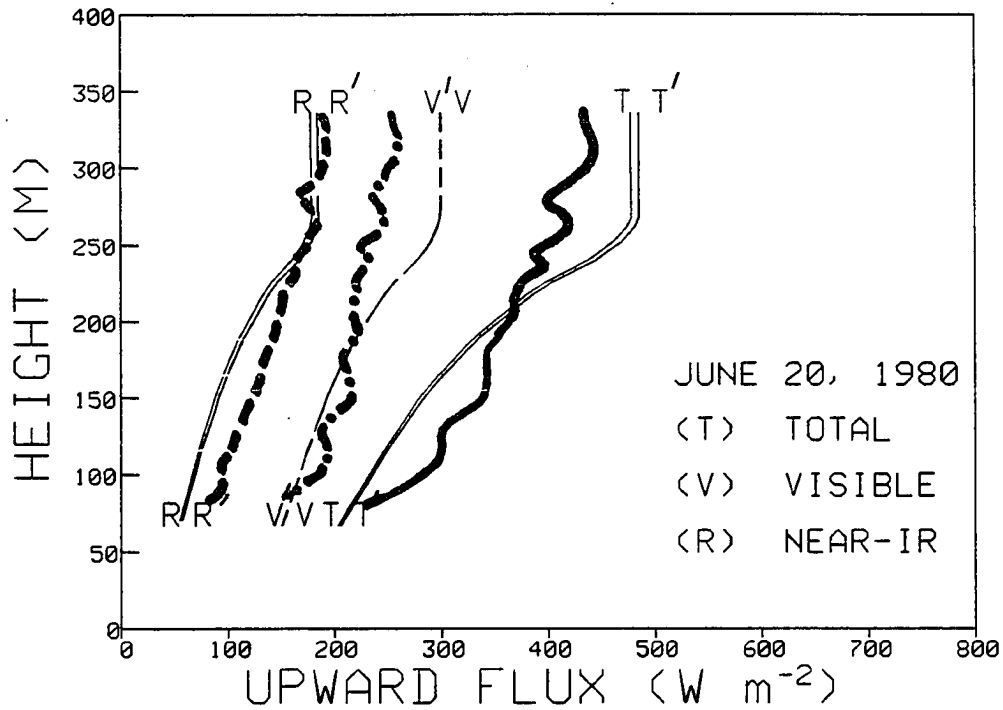


Figure 4.9 Comparison of observed (heavy lines) and computed fluxes for stratus cloud on June 20, 1980

Generally, the agreements between computed and observed fluxes are good if the deducing procedure of measurement and the difference between detectors are considered (pages 9, 14 and 15 of Herman and Curry, 1984). In addition to the uncertainty of measurements, three causes may be responsible for the discrepancies between observed and computed fluxes. They are the improper treatment of spectrally fixed surface albedo, the insufficient absorption of clouds in the visible region and the improperly determined cloud boundaries. The effects of spectrally dependent albedo are shown in Figure 4.10. The spectral snow albedo is obtained from Mie computations (Figures 3.21-3.23), while the fixed snow albedo is determined from the average albedo in the visible and near-infrared bands. The same albedos, being ratios, do not necessarily have the same upward and downward fluxes at the surface. The fixed albedo overestimates fluxes in $0.3-0.6\mu\text{m}$ region and underestimates fluxes in $0.7-1.0\mu\text{m}$ region, which are associated with the major solar energy and weak gaseous and droplet absorptions. These discrepancies coincide with those in Figures 4.8 and 4.9. Upward and downward fluxes depend sensitively on the surface albedo because of multiple scattering.

Since the early 1950's, the cloud absorptivity paradox has been noted (Fritz, 1951). The insufficient absorption of clouds predicted by theoretical calculations at 6%, is far

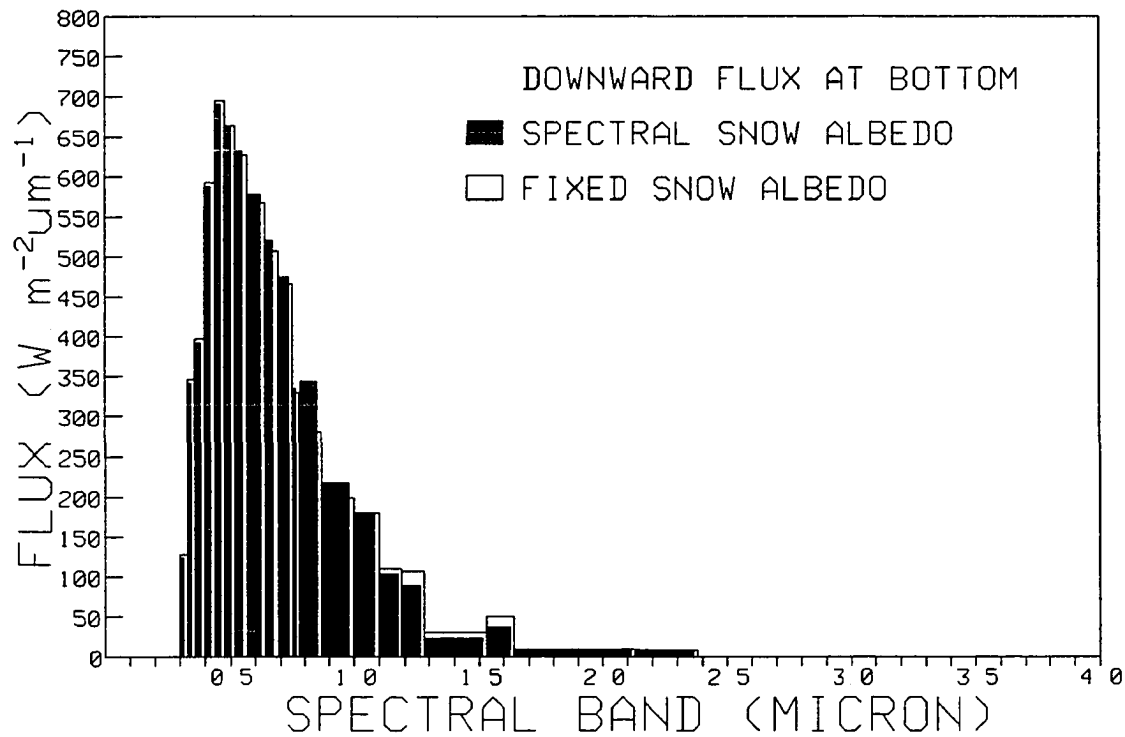
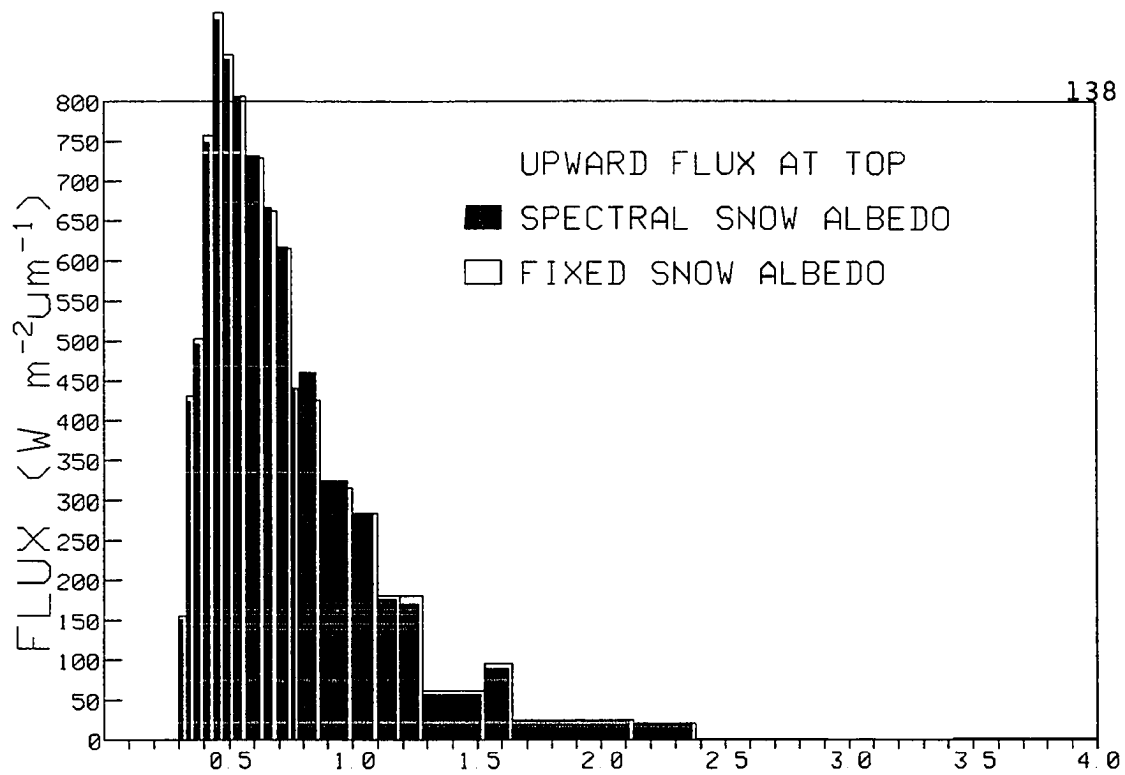


Figure 4.10 Comparison of spectral fluxes under different distributions of snow albedo

less than the actually measured values of about 20% absorption. Subsequent aircraft measurements (i.e., Reynolds et al., 1975) obtained even larger cloud absorption than before - about 20-40%. This discrepancy was recently attributed to the leakage of radiation through cloud sides (Welch et al., 1980), the effects of very large droplets (Wiscombe et al., 1984), and the effects of graphitic carbon (Chylek et al., 1984). However, the first two may not be applicable to the problem of arctic stratus. The leakage of radiation through cloud sides is important for the cube-shaped clouds but may be negligible for the extensive stratiform clouds. About 2% to 4% of cloud absorption is increased by very large drops of 40-50 μm in radius, which allow solar radiation to penetrate deeply into the clouds. But such large drops were not observed in the Arctic Stratus Clouds Experiment, in which drop radii of about 20-25 μm are the maximum.

Therefore, the impurities of clouds may play an important role in increasing cloud absorption. Indeed, there is plenty of soot in the arctic atmosphere. Curves marked with primes in Figure 4.8 are computed under the hazy sky condition, which corresponds to the optical depth about 0.06 at 0.5 μm wavelength in the arctic summer (Shaw, 1982). Some reductions of fluxes are achieved in the visible but not in the near-infrared regions. Instead of introducing haze, a 50% reduction of water vapor density is made for the entire

column in June 20. Better agreement is found in the near-infrared. However, 50% errors in H_2O density correspond to 10% (or $30^\circ K$) errors in dew-point temperature measurements. This seems not to account for the discrepancy of downward flux (NIR) on June 20. More detailed studies of various atmospheric conditions will be made later.

In the plane-parallel approximation, boundary layers of cloud-air interface are assumed to be homogeneous, and this assumption is certainly not applicable to the observed wavy cloud boundary (Tsay and Jayaweera, 1984). A different scattering pattern is expected for this wavy condition. The diffuse to total ratio in the downward radiation at the cloud top is about 20% in the visible and about 1% in the near-infrared. At the cloud base, radiation is essentially diffused. The assessment of this effect and the modification of the plane-parallel approximation are beyond the scope of the present study.

Unfortunately, corresponding measurements of infrared fluxes in the atmospheric profiles for June 20 and 28 were not reported in the paper of Curry and Herman (1985). Only four out of twelve profiles were documented and two of them were altostratus clouds. Therefore, the following studies in the infrared region are based on theoretical grounds.

To study the energy budget of both solar and terrestrial radiation, the surface condition has to be simulated

properly. In the arctic summer the surface conditions are very complicated, and may be composed of open leads, pack ice, melting ponds, refrozen ice, old snow, new snow, etc. However, from the flight notes and pictures, the surface of June 28 (at latitude of 77°N) is known to be essentially snow covered. Unfortunately, there are no detailed spectral measurements of snow albedo available. Broad-band albedos, such as total, visible and near-infrared are often measured. Even so, snow albedo measured from aircraft depends not only upon the grain size and density of snow but also upon the atmospheric conditions (e.g., solar zenith angle, cloud cover, etc.).

Figure 4.11 shows surface and system (atmosphere-snow) albedos for the solar spectrum under clear and cloudy skies, as functions of zenith angle. If the measurement is made right above the surface, the albedo is referred to as the surface albedo. Otherwise, it is referred to as the system albedo. Under a cloudy sky, snow albedo is almost independent of the zenith angle. This is because the diffuse radiation at the cloud base, after strong multiple scattering inside the cloud layer, tends to become isotropic. Also, cloud absorption is somewhat overlapping with snow absorption in the near-infrared. Radiation reaching the surface is relative non-absorptive in snow.

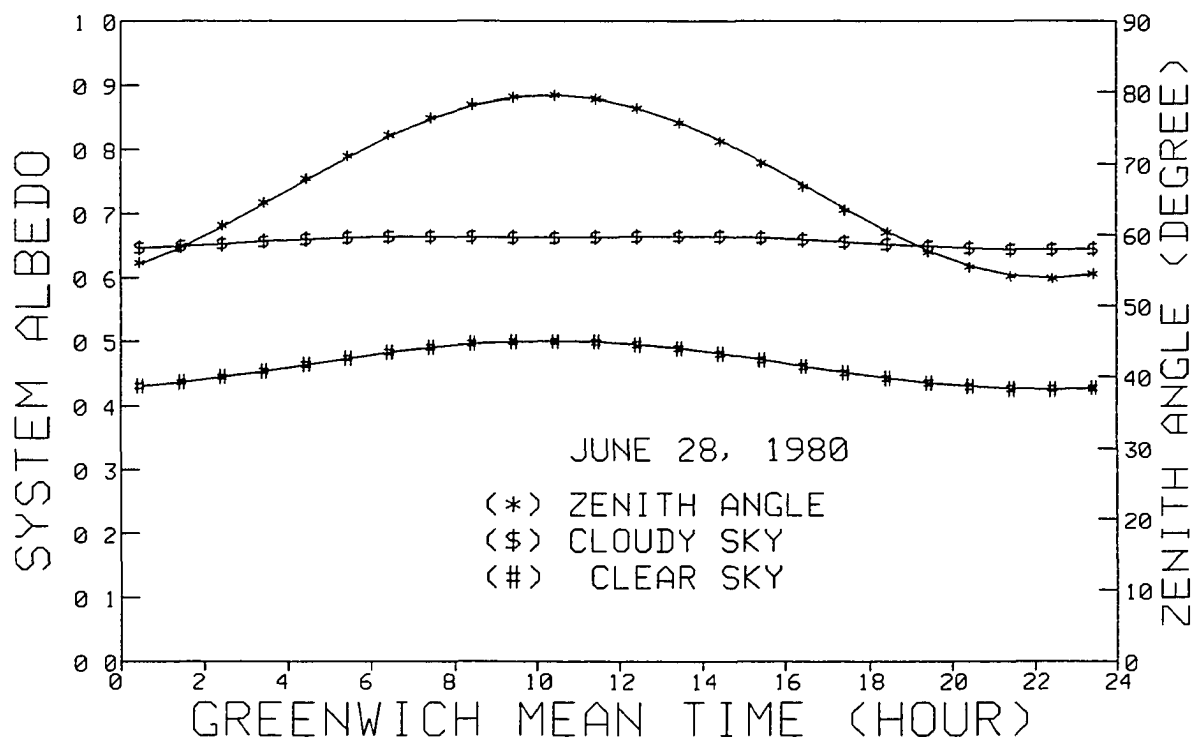
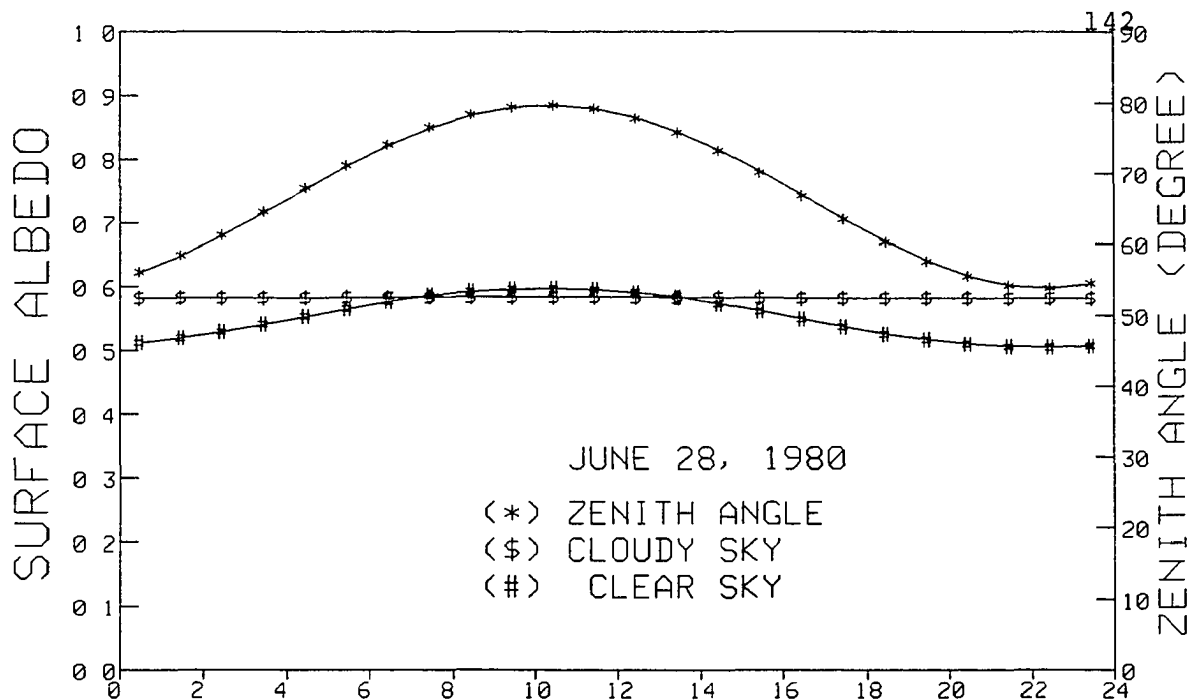


Figure 4.11 Surface and system albedos for the solar spectrum under clear and cloudy skies, as function of zenith angle

However, under a clear sky and at the same distance traveled in the snow layer, photons penetrate vertically deeper at a smaller zenith angle. Therefore, few photons can escape to the snow surface, and a lower albedo is measured. In most cases, snow albedo is higher under a cloudy sky than under a clear sky except for very large zenith angles. This indicates the extent to which the zenith angle dominates the change of radiation as redistributed by cloud absorption. For a clear sky, the system albedo has less dependence on zenith angle than does the surface albedo, due to the slight modification by Rayleigh scattering and gaseous absorption. Again, even with the same zenith angle and albedo, different upward and downward fluxes are found for cloudy and clear sky conditions.

The spectral albedo of snow is also computed as a function of grain radius, density, impurity and atmospheric conditions, as shown in Figures 4.12 and 4.13. New snow has a higher spectral albedo than old snow, except for 2.4-4.0 μm where the imaginary part of the ice refractive index is high. Large snow grains produce further absorption, due to the long traveling distance for photons. Generally, snow grains increase in size with depth. However, snow density is not related to grain size and ranges from about 0.15 to 0.50 g.cm^{-3} . In the Arctic, wind-packed snow has a small grain radius of about 100 μm but a high density of about 0.45

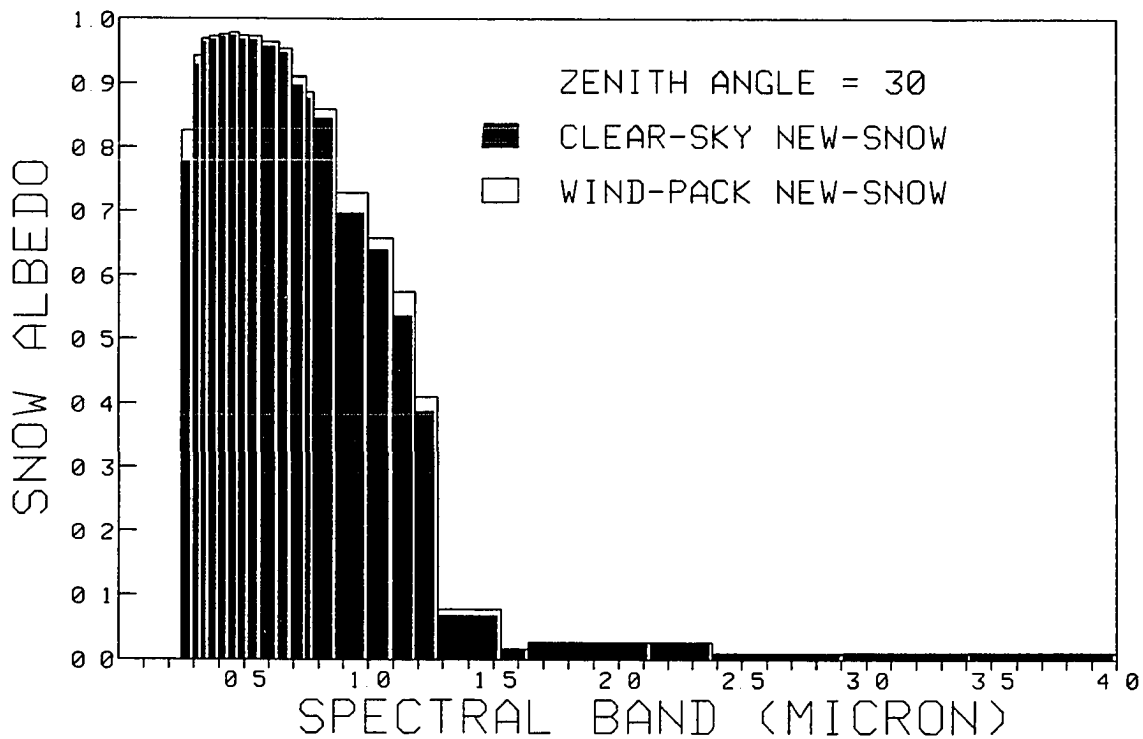
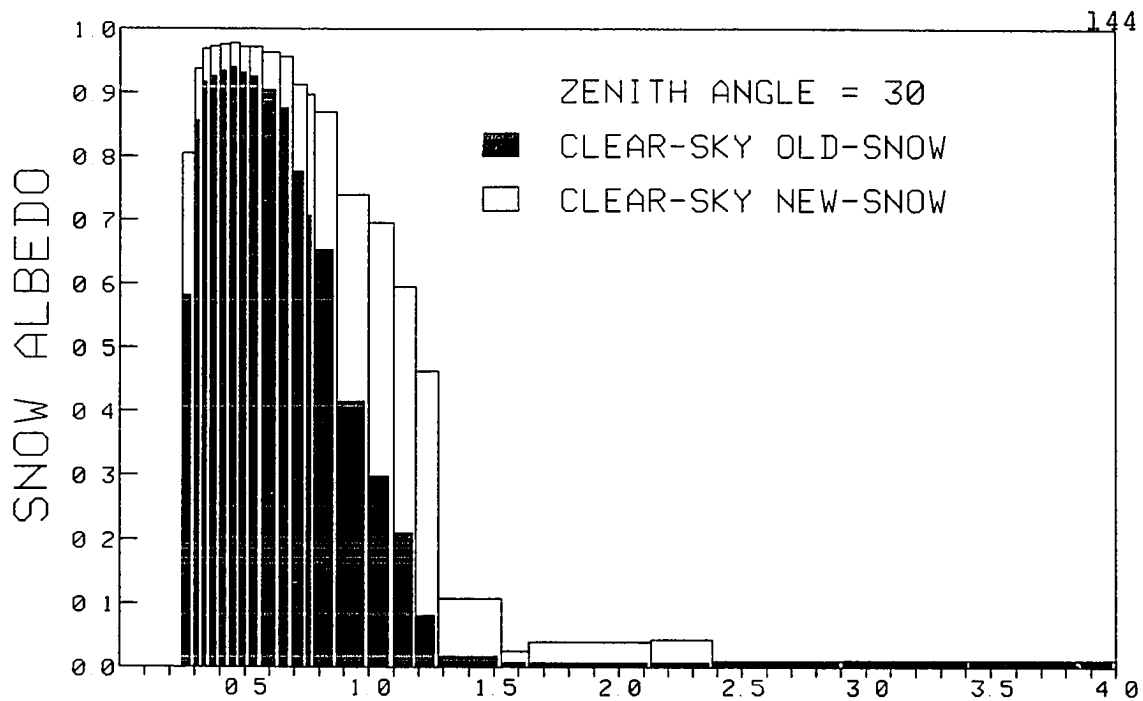


Figure 4.12 Spectral albedo of snow as function of grain size and density (old-snow and new-snow)

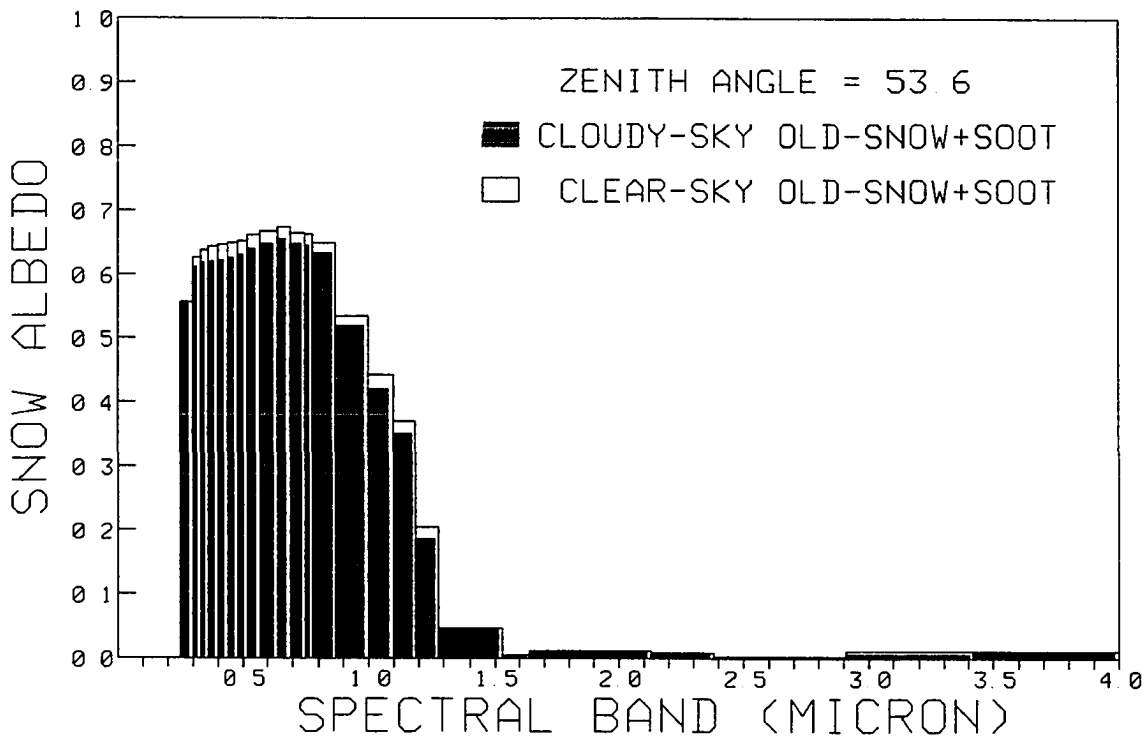
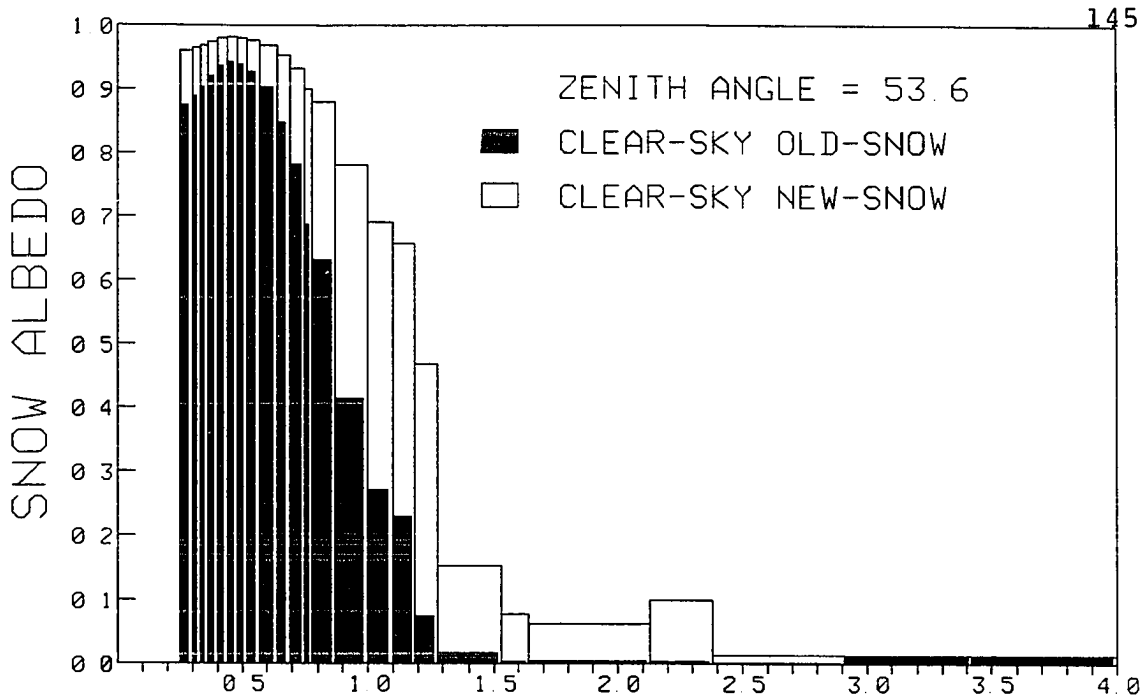


Figure 4.13 Spectral albedo of snow as function of grain size (old-snow and new-snow) and impurity (soot)

g.cm^{-3} (Benson, 1969). Therefore, wind-packed snow has an even higher spectral albedo than does usual new snow. Under such conditions, photons are highly back scattered in the upper layer and only a small portion will reach the large grains below for absorption. If the snowlayer underlying the wind-packed snow had the same grain radius, this high spectral albedo would not be observed.

The spectral albedo of snow also depends on the zenith angle in the clear sky as does the total albedo. However, pure snow displays a higher computed albedo than the usual measured value in the visible and the albedo is somewhat wavelength independent. To reduce this discrepancy, soot is introduced. The effect of soot impurity is essentially to increase the absorption of snow in the visible and to create zenith angle dependence as well. It is most interesting that the broad-band albedo behaves differently from the spectral albedo. Under a cloudy sky for soot contaminated snow, the broad-band albedos for total and near-infrared are larger than those under a clear sky. Therefore, care should be taken when applying broad-band properties of the snow albedo to studies of spectral dependence.

To simulate the surface condition of June 28, the grain radius is assumed to be $2000\mu\text{m}$, corresponding to snow near the melting point. The mass-fraction of soot in the snow is assumed to be 0.24 ppmw, which is somewhat larger than the

observed value. However, it leads to computed broad-band albedos matching closely the observed broad-band albedos of the total (0.57), visible (0.68) and near-infrared (0.35) regions. Therefore, the effects of various atmospheric conditions are studied. Figures 4.14 and 4.15 show the atmospheric heating profiles under various conditions. The base line is represented by "CLOUD" only. The exclusion of CO_2 and O_2 absorption is denoted by "CLOUD- CO_2 - O_2 ." "HAZE(A)" denotes the dry (RH = 50%) haze condition, located above the upper cloud. "HAZE(B)" is the wet (RH = 99%) haze condition, mixed with drops for the entire cloud. "HAZE(C)" denotes the intermediate (RH = 50%-99%) haze condition, extended between the upper and lower clouds. The optical depth of all hazes is weighted to have the value of 0.06 at $0.5\mu\text{m}$ wavelength.

Strong cloud heating takes place in the upper 100m and reaches 60°C per day (or $5^\circ\text{C}/\text{hrs}$). This heating profile corresponds to the local solar noon of maximum heating. Because of the relatively drier and colder air above in the Arctic than elsewhere, more radiation is available for cloud drop absorption. The same enhancement can be found when the absorption of CO_2 and O_2 is excluded, resulting in extra heating in the upper part of the cloud. The inclusion of haze conditions do not alter significantly the atmospheric heating, except for a $0.7^\circ\text{C}/\text{day}$ increase in HAZE(A) located from 1.2Km to 3.8Km height. Similar results are found when

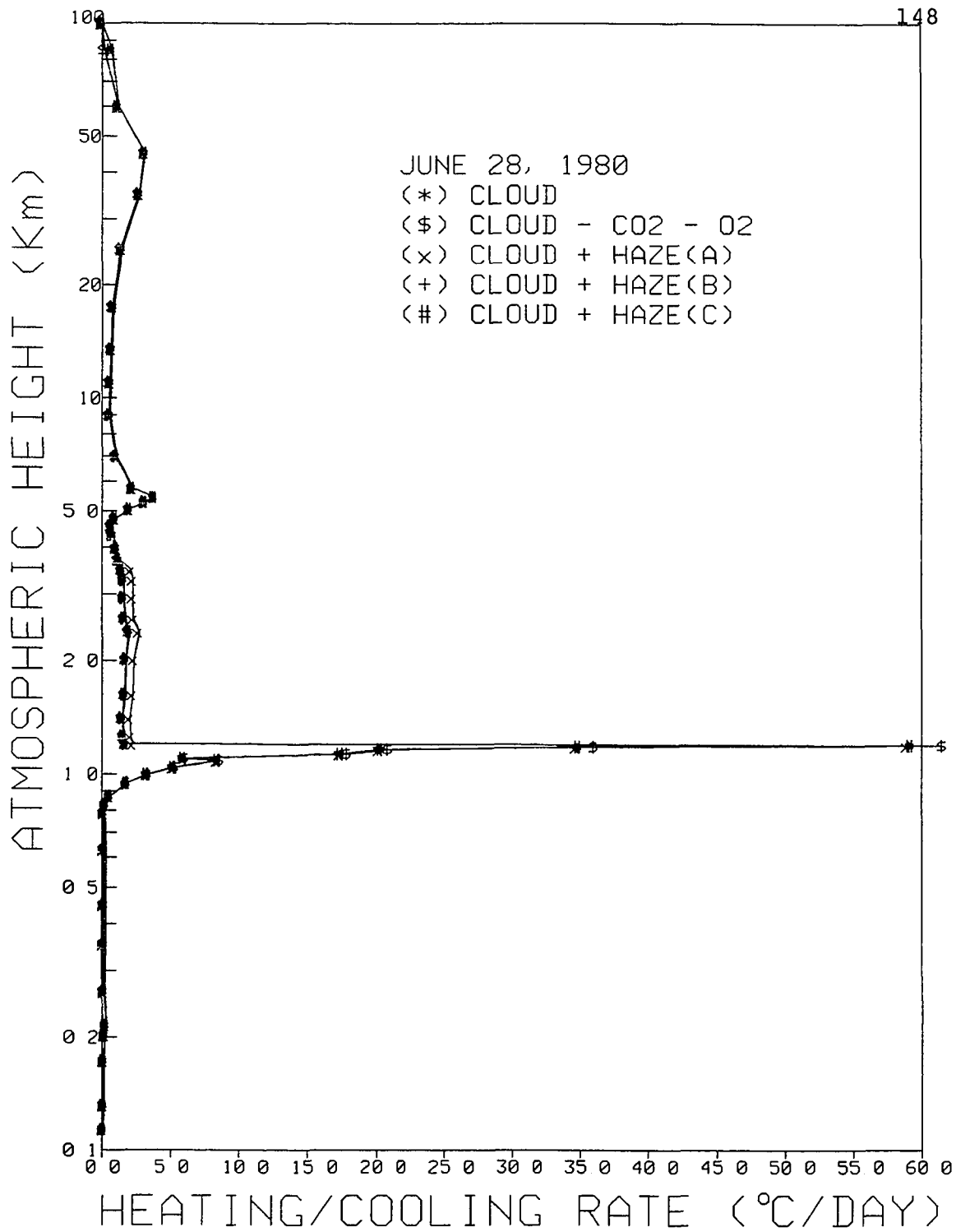


Figure 4.14 Atmospheric heating profiles for various conditions on June 28, 1980

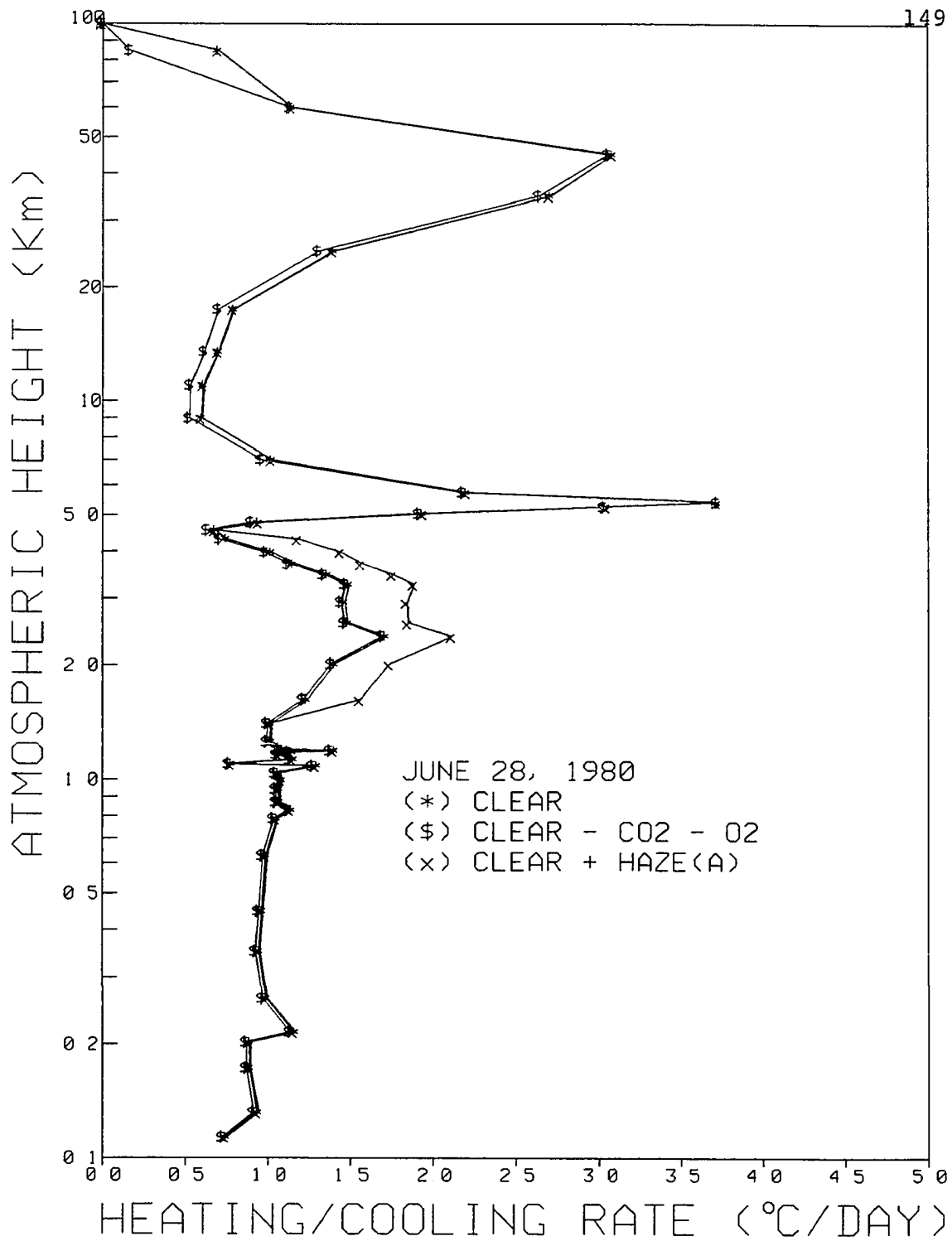


Figure 4.15 Atmospheric heating profiles for clear and hazy conditions on June 28, 1980

clouds are artificially removed to make the "CLEAR" case, as shown in Figure 4.15. The multiple scattering and surface reflections increase the heating of HAZE(A) slightly in this clear case.

Spectral absorption of clouds, together with the dry and wet haze conditions, are shown in Figures 4.16 and 4.17. The white areas between two curves of net fluxes at boundaries represent the flux absorbed. Dry haze particles have strong absorption in the visible wavelengths while drops do not. In the near-infrared, the opposite situation is found, except for the 0.9 and 1.3 μm bands. When haze particles are absorbing water vapor (wet), they start losing their identities and behaving like tiny droplets. Some small absorption around 1.0 μm is observed, due to their relatively important size parameters and refractive index. However, the absorption bands of wet haze are completely overlapping with cloud absorption. With the assumption of external mixing, in which haze particles occur in the interstitial areas between drops not inside the drops themselves, the absorption of wet haze particles is strongly diluted by cloud absorption. When haze exists in between clouds "HAZE(C)" with high relative humidity (90%, Figure 4.7), little radiation is absorbed. This is because the strong scattering in the visible and strong absorption in the near-infrared by the upper cloud leaves less radiation for the haze to interact with. The finding

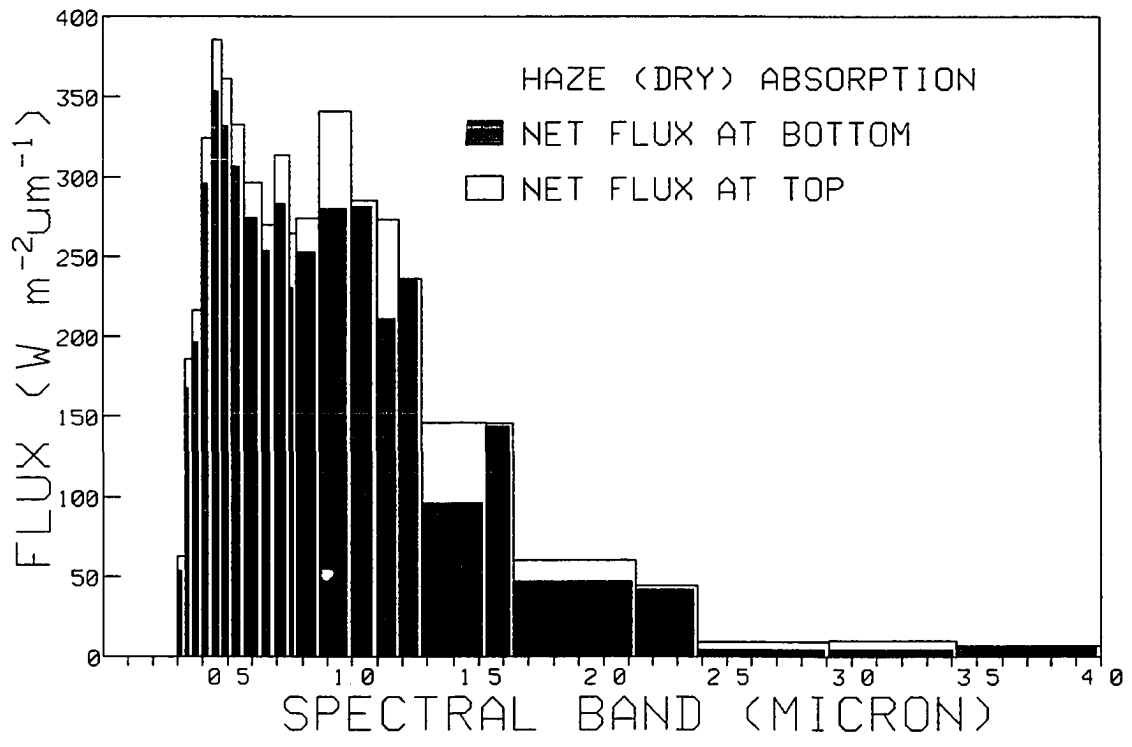
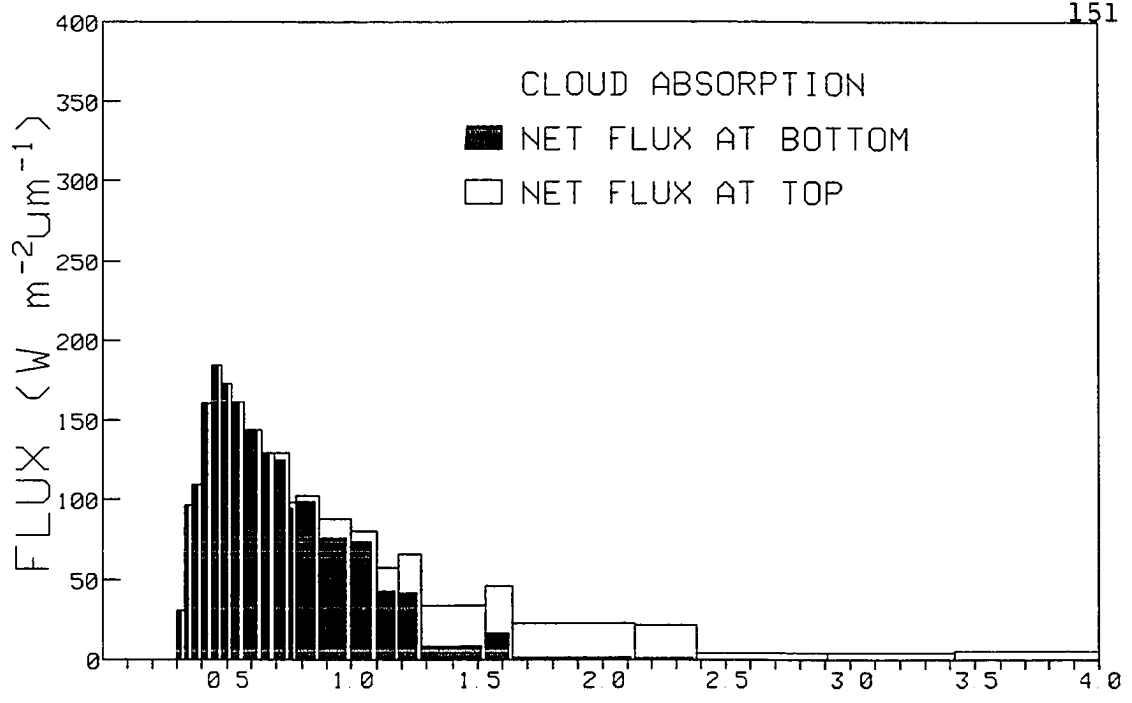


Figure 4.16 Spectral absorption of cloud and dry haze

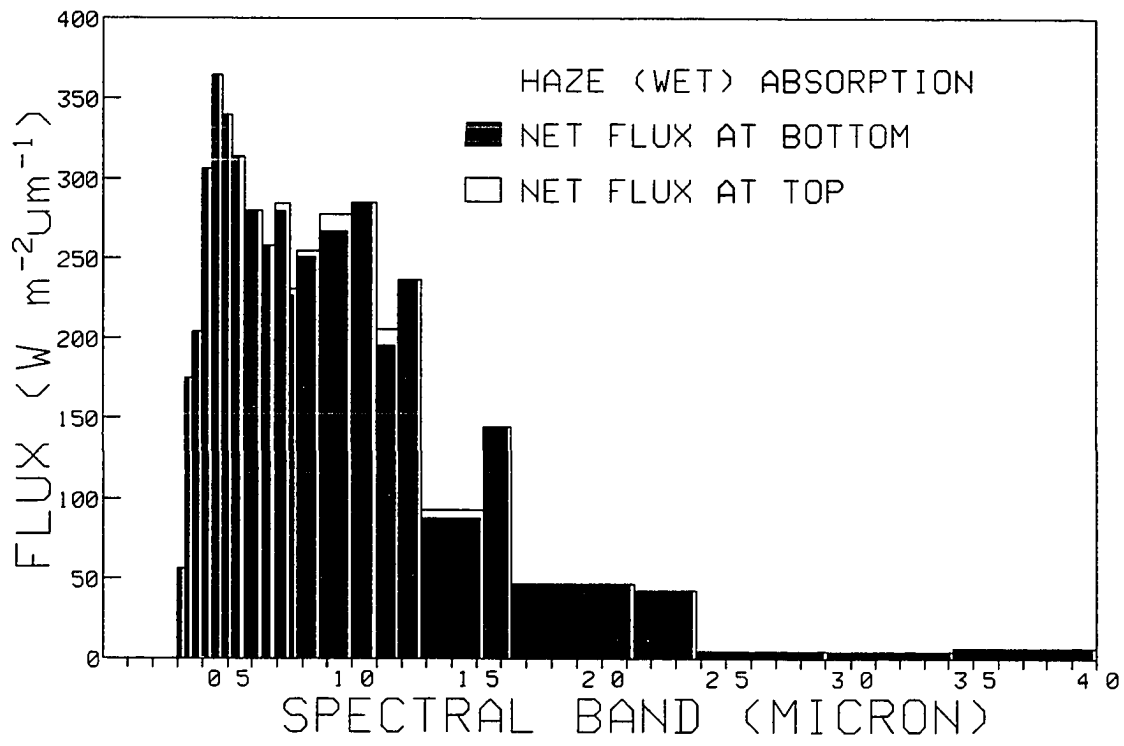
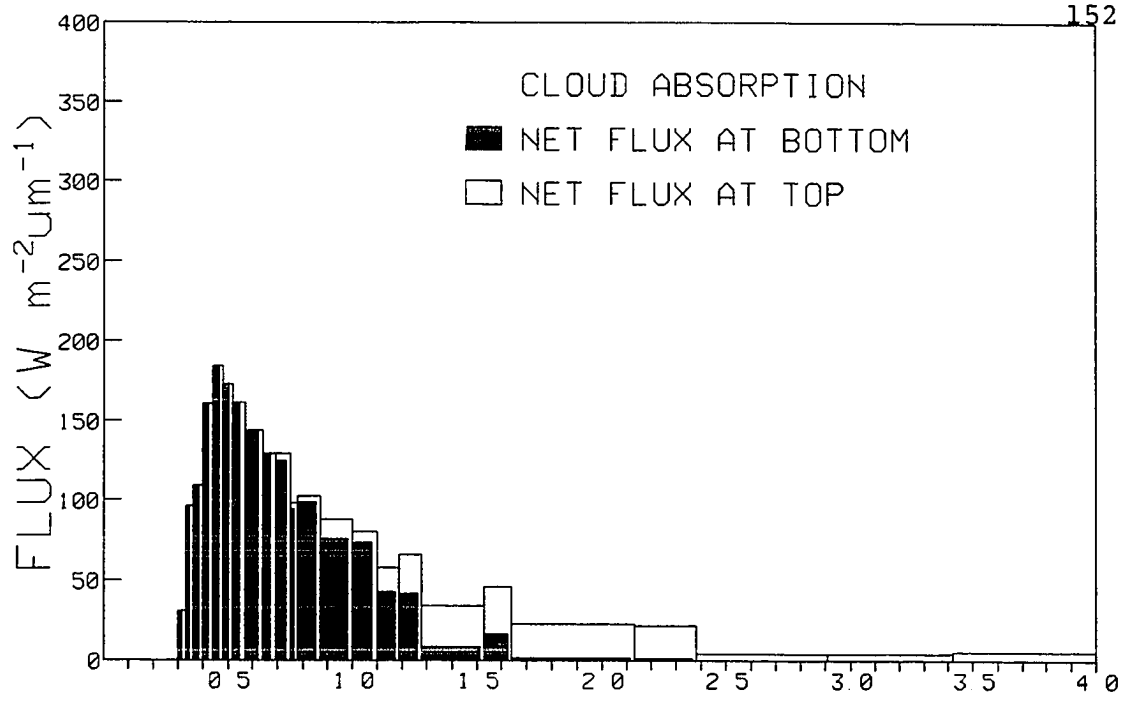


Figure 4.17 Spectral absorption of cloud and wet haze

of aerosols increasing absorption in clouds by about 1 to 5% by Herman and Curry (1984) is due to the neglect of the humidity effect in their adopted "haze" model of Shettle and Fenn (1976).

Tables 4.7 and 4.8 show fluxes computed for solar and near-infrared radiation with various atmospheric conditions on June 28 and 20, respectively. The exclusion of CO_2 and O_2 increases surface absorption by 0.7W.m^{-2} in the cloudy case and 3.8W.m^{-2} in the clear case. This increase is mainly caused by the extra absorption of radiation at $0.7\mu\text{m}$ band. Also, the entire atmosphere loses about 6W.m^{-2} and the extra heating in the cloud top (Figure 4.14) is caused by extra absorption of 1W.m^{-2} due to lack of CO_2 . The introduction of HAZE(A) decreases the surface absorption by about 2W.m^{-2} , because soot-contaminated snow has similar absorption bands in the visible region. This effect is enhanced in the clear condition, due to large amounts of radiation available. The absorption of the atmosphere ranges from 11W.m^{-2} to 16W.m^{-2} for clear and cloudy conditions with HAZE(A), respectively. 80% of this absorption comes from visible wavelengths, as expected. However, the absorption of HAZE(A) depletes the absorption of the underlying cloud to within 1W.m^{-2} . Indeed, a dry haze particle is a relatively efficient absorber, absorbing 30-40% of the flux absorbed by the cloud, despite its small optical depth. Multiple scattering enhances the

Table 4.7 Model computations of fluxes for solar and near-infrared (in parentheses) radiation with various components in the atmospheric profile of June 28, 1980

| Components | $F^+(0)$ | $F^-(\tau_N)$ | ΔF_{sfc} | ΔF_{atm} | ΔF_{lyr} |
|---------------------------------------------|--------------------|--------------------|--------------------|--------------------|------------------|
| Cloud | 517.00 (187.82) | 242.77 (57.79) | 101.20 (37.74) | 171.56 (134.64) | 38.47 (38.02) |
| Cloud - CO ₂ - O ₂ | 521.86 (189.58) | 244.39 (57.94) | 101.91 (37.88) | 165.98 (132.74) | 39.55 (39.23) |
| Cloud + Haze(A) | 503.37 (184.73) | 237.33 (57.14) | 99.16 (37.34) | 187.23 (138.14) | 16.31 (3.73) |
| Cloud + Haze(B) | 517.00 (187.82) | 242.77 (57.79) | 101.20 (37.74) | 171.56 (134.64) | 0.00 (0.00) |
| Cloud + Haze(C) | 516.72 (187.81) | 241.03 (57.61) | 100.59 (37.64) | 172.45 (134.76) | 0.90 (0.12) |
| Clear | 333.10 (65.21) | 647.07 (259.45) | 319.18 (192.91) | 137.47 (102.09) | - - |
| Clear - CO ₂ - O ₂ | 335.60 (65.23) | 652.93 (262.16) | 322.99 (195.59) | 131.16 (99.38) | - - |
| Clear + Haze(A) | 326.62 (64.71) | 635.93 (257.13) | 314.40 (191.20) | 148.74 (104.29) | 11.65 (2.33) |

Note: $F^+(0)$, upward flux at top; $F^-(\tau_N)$, downward flux at bottom; ΔF_{sfc} , net flux gain at surface; ΔF_{atm} , net flux gain of entire atmosphere; ΔF_{lyr} , net flux gain at layer (all in dimension of $W.m^{-2}$)
input solar flux at top: $789.76 W.m^{-2}$; near-infrared flux at top: $360.20 W.m^{-2}$ for 53.8° zenith angle

Table 4.8 Model computations of fluxes for solar and near-infrared (in parentheses) radiation with various components in the atmospheric profile of June 20, 1980

| Components | $F^+(0)$ | $F^-(\tau_N)$ | ΔF_{sfc} | ΔF_{atm} | ΔF_{lyr} |
|---------------------------------------------|--------------------|--------------------|--------------------|--------------------|------------------|
| Cloud | 492.77 (176.86) | 353.88 (109.92) | 151.31 (62.91) | 149.44 (122.15) | 31.23 (30.90) |
| Cloud - CO ₂ - O ₂ | 497.64 (178.67) | 356.31 (110.40) | 154.45 (63.39) | 143.43 (119.85) | 32.19 (31.94) |
| Cloud + Haze(A) | 480.22 (174.00) | 346.05 (108.67) | 148.27 (62.28) | 165.03 (125.64) | 13.01 (2.98) |
| Cloud + Haze(A&B) | 491.00 (176.46) | 352.78 (109.75) | 150.88 (62.83) | 151.64 (122.63) | 2.06 (0.45) |
| Clear | 364.33 (93.77) | 669.02 (275.04) | 313.80 (178.92) | 115.39 (89.23) | - - |
| Clear + Haze(A) | 357.41 (92.62) | 657.82 (272.87) | 309.08 (177.54) | 127.03 (91.76) | 11.86 (2.57) |

Note: $F^+(0)$, upward flux at top; $F^-(\tau_N)$, downward flux at bottom; ΔF_{sfc} , net flux gain at surface; ΔF_{atm} , net flux gain of entire atmosphere; ΔF_{lyr} , net flux gain at layer (all in dimension of $W.m^{-2}$)
input solar flux at top: $793.52 W.m^{-2}$; near-infrared flux at top: $361.92 W.m^{-2}$ for 53.6° zenith angle

absorption of dry particles to about $2-5\text{W.m}^{-2}$, depending on the height of the cloud.

The solar heating of the earth-atmosphere system has to be balanced by the infrared cooling. In the infrared region, pure snow and soot-contaminated snow demonstrate very simple characteristics. The emissivity of snow is quite insensitive to the snowpack parameters (i.e., grain size, density) and can be approximated to be 0.99 as measured by Griggs (1968). Even a thin layer of snow behaves like a black-body, due to the large imaginary part of the ice refractive index throughout the infrared region.

Figures 4.18 and 4.19 show the atmospheric cooling rate of various conditions for June 28 and 20, respectively. In the clear sky condition, the cooling rate is similar to that in Figure 4.5, but for a larger cooling profile. This is because a warmer temperature profile is used and a larger H_2O density is made artificially. (The clouds have been removed but the H_2O still remains near saturated.) The temperature inversion near the surface on June 28 results in a slight heating to the underlying surface. A similar result is also found at the 1.2Km inversion layer. This is much enhanced on June 20, when the inversion is stronger than on June 28.

When clouds are formed, intensive coolings are found in the upper 100m. Because clouds are very efficient emitters, such a layer produces quasi-black body behavior. Therefore,

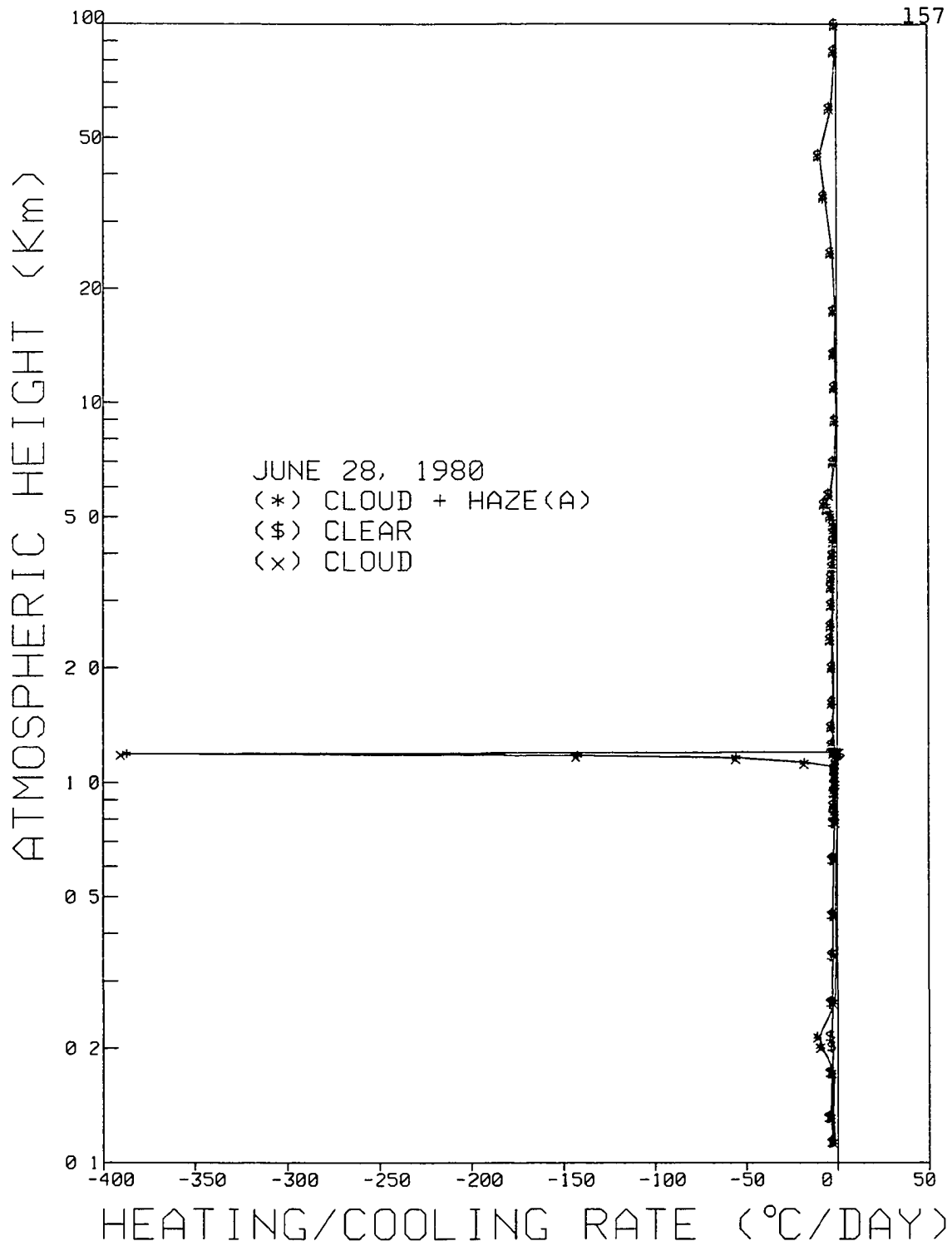


Figure 4.18 Infrared cooling profiles for clear, cloudy and hazy conditions on June 28, 1980

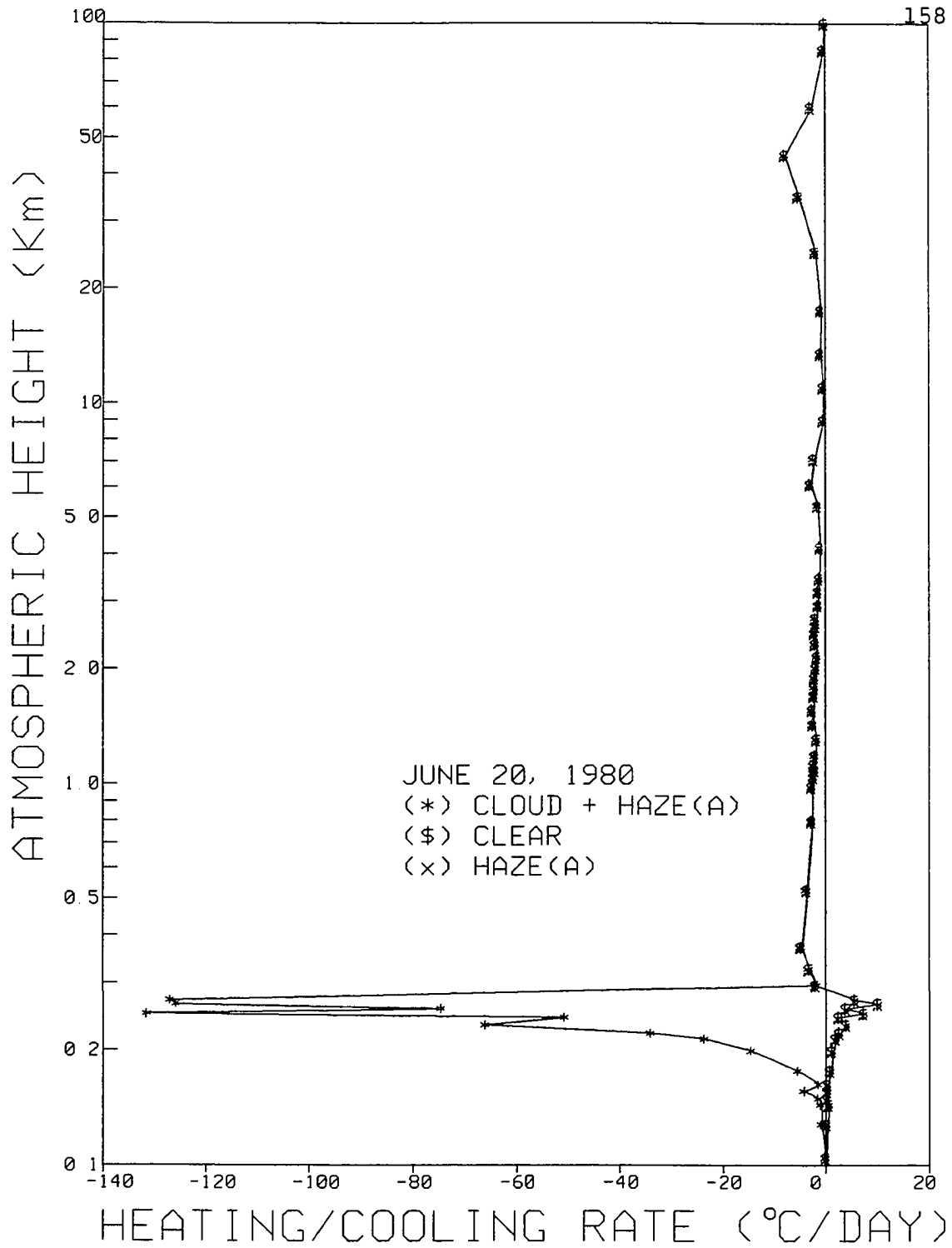


Figure 4.19 Infrared cooling profiles for clear, cloudy and hazy conditions on June 20, 1980

the cooling occurs in this layer which radiates to the cold layer above with little return radiation. The upper cloud on June 28 is much denser than on June 20; therefore, stronger cooling is expected. The low-level cloud on June 28 is very thin and underlying a dense cloud, which prevents its further cooling. The introduction of HAZE(A) does not alter the cooling profile significantly for either cloudy or clear conditions.

Table 4.9 shows infrared fluxes computed for June 20 and 28, under various atmospheric conditions. The effects of HAZE(A) in the thermal radiation are less than $1\text{W}\cdot\text{m}^{-2}$ under both cloudy and clear conditions. In the clear condition, the downward flux at the surface for June 28 is $25\text{W}\cdot\text{m}^{-2}$ larger than that of June 20. The surface inversion on June 28 is responsible for this, and also the water vapor density is very high, which makes absorption saturate easily. This results in a net warming at the surface for June 28. In the clear condition, the net loss from the surface is produced by the window region. However, when clouds are present, the return radiation from cloud to surface offsets the cooling greatly.

After examining the solar and terrestrial radiative components in the Arctic, it would be interesting to see the net effects. Doing this involves tremendous computations, assumptions and uncertainties. For instance, the radiation

Table 4.9 Model computations of fluxes for infrared radiation with various components in atmospheric profiles of June 20 and 28, 1980

(a) June 20, 1980 (single-layer cloud)

| Components | $F^+(\tau_N)$ | $F^-(\tau_N)$ | ΔF_{sfc} | $F^+(0)$ | ΔF_{atm} |
|--------------------|---------------|---------------|------------------|----------|------------------|
| Clear | 313.83 | 232.28 | -81.55 | 253.60 | -172.05 |
| Haze(A) | 313.84 | 232.78 | -81.06 | 253.61 | -172.55 |
| Cloud + Haze(A) | 314.65 | 313.72 | -0.93 | 249.46 | -248.53 |

(b) June 28, 1980 (multi-layer clouds)

| Components | $F^+(\tau_N)$ | $F^-(\tau_N)$ | ΔF_{sfc} | $F^+(0)$ | ΔF_{atm} |
|--------------------|---------------|---------------|------------------|----------|------------------|
| Clear | 314.09 | 257.65 | -56.44 | 247.99 | -191.55 |
| Cloud | 314.78 | 327.53 | +12.75 | 246.16 | -258.91 |
| Cloud + Haze(A) | 314.78 | 327.53 | +12.75 | 246.19 | -258.94 |

Note: $F^+(\tau_N)$, upward flux at bottom; $F^-(\tau_N)$, downward flux at bottom; ΔF_{sfc} , net flux gain/loss at surface; $F^+(0)$, upward flux at top; ΔF_{atm} , net flux loss of entire atmosphere (all in dimension of $W.m^{-2}$)

field is strongly dependent on the atmospheric compositions, such as clouds, haze particles, etc. The changes of radiation forcing will lead to dynamical mixing internally. Subsequently, the changes of atmospheric compositions feed back to the radiation field. This process is made under the assumed absence of external forcings, such as advection. All these processes may happen simultaneously and remain poorly understood. However, it is still worthwhile to isolate some processes and get a basic understanding of the others.

The persistent characteristics of arctic stratus clouds and haze particles suggest that their mean conditions may not change dramatically with time. Therefore, the integration of radiation field over a short period of time may have its representiveness. Solar radiation is highly dependent on zenith angle. However, under the assumption of a static state of atmospheric compositions, the infrared radiation remains time independent. Figures 4.20 and 4.21 show the 24 hours integration of solar heating and infrared cooling, together with the net effects, for the cloudy conditions of June 28 and 20. Very intense net cooling is achieved near the cloud top on June 28. The solar heating for 24 hours integration is reduced by about 20% (Figure 4.14) of that in the local solar noon. Intense mixing between cloud layer and entrained air will be expected. However, the low-level cloud undergoes a net cooling, which indicates that the dis-

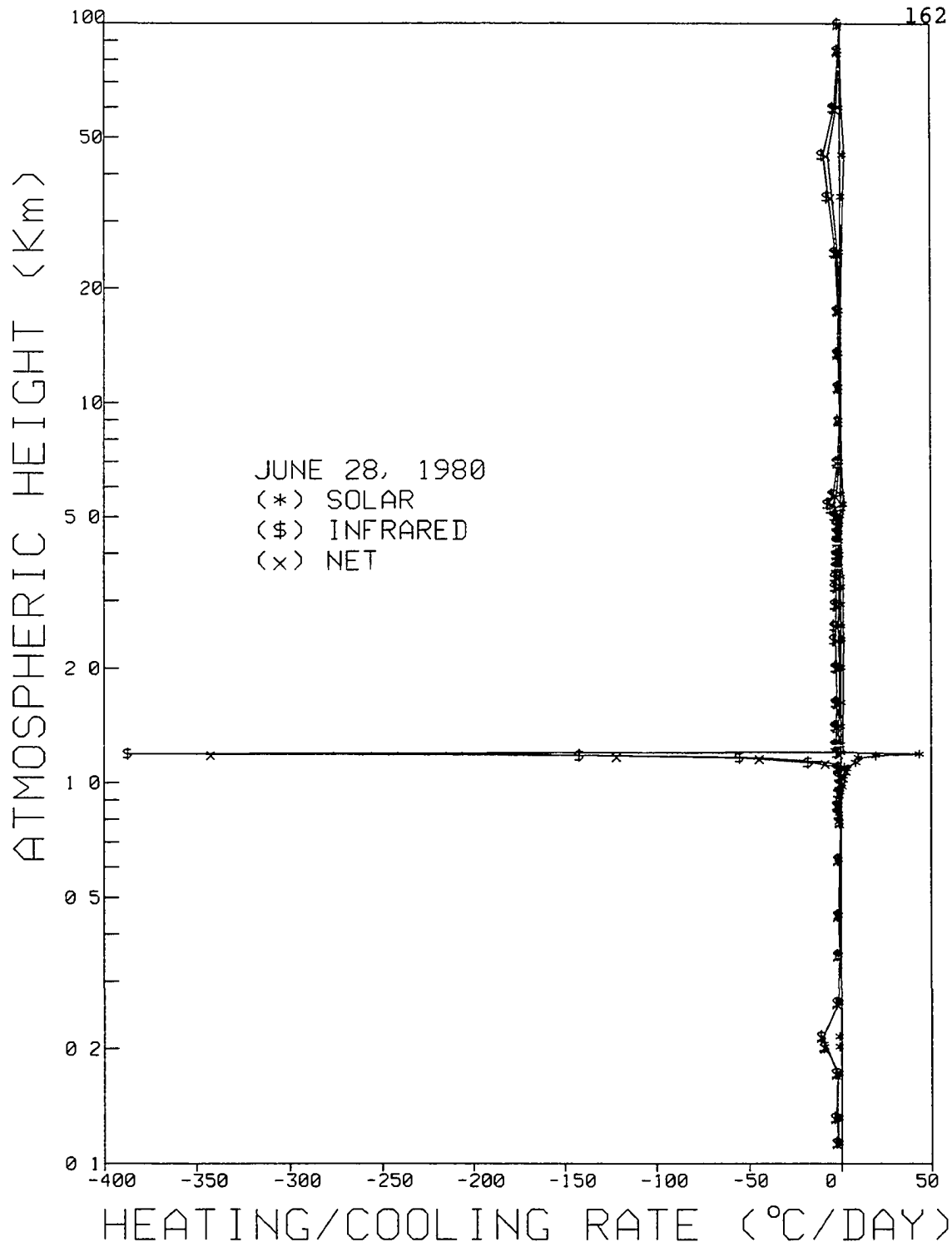


Figure 4.20 Daily solar heating and infrared cooling profiles for cloudy condition on June 28, 1980

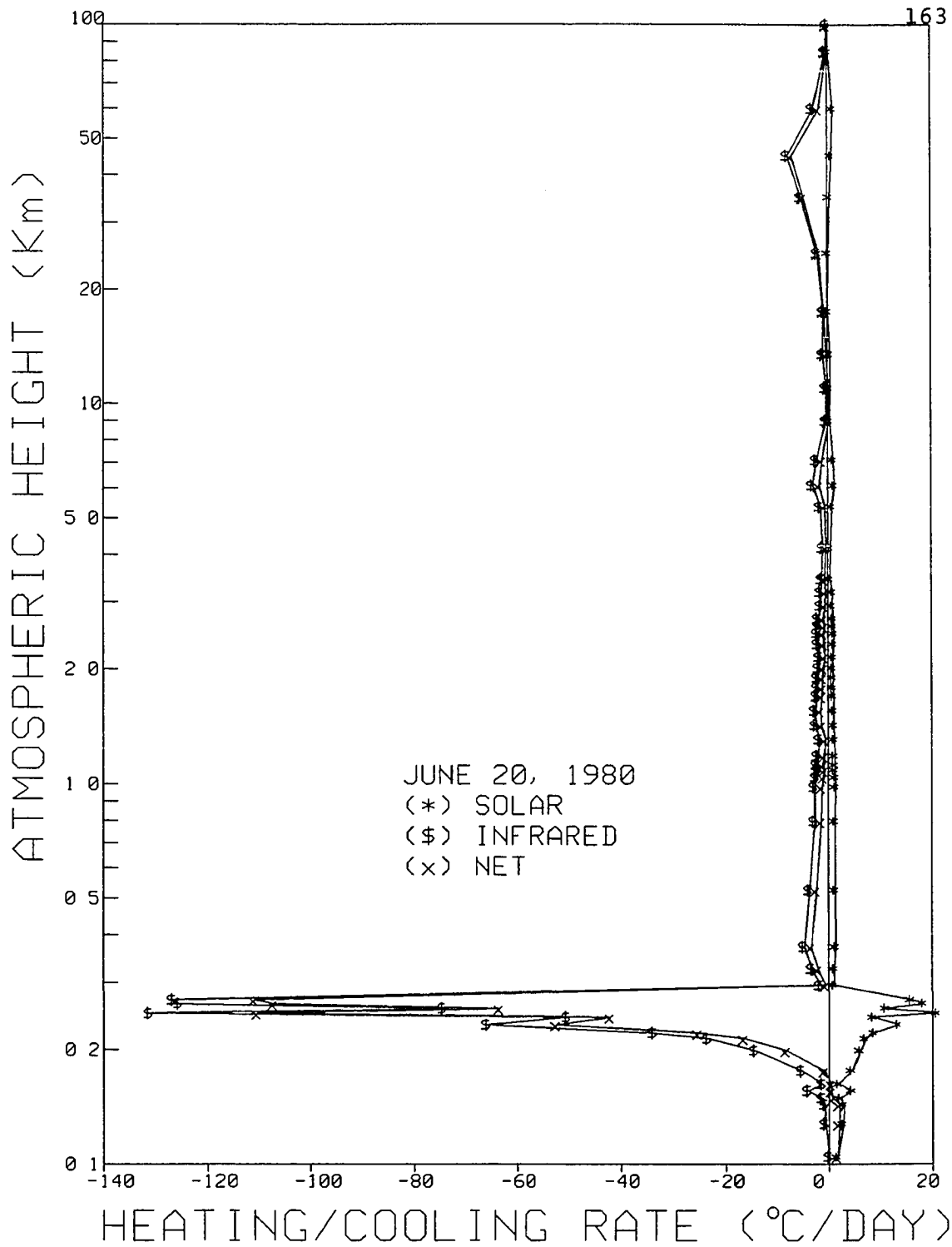


Figure 4.21 Daily solar heating and infrared cooling profiles for cloudy condition on June 20, 1980

sipation mechanism does not arise from radiation itself. However, on June 20, a slightly different picture is found. The net cooling at the cloud top is only about one-third of that on June 28. A slight heating is also found at about 100m below the cloud top. For this less dense and low-level cloud, the solar radiation may penetrate into the cloud layer but the infrared cooling is not enough to offset it, resulting in a net heating. This effect has been used to explain the layering of arctic stratus cloud by Herman and Goody (1976).

Figure 4.22 shows the net heating/cooling rates of June 20, under clear and HAZE(A) conditions. The effect of haze in 24 hours integration becomes less pronounced in the role of the atmospheric energy budget. Table 4.10 shows the fluxes computed for 24 hours period with various atmospheric conditions on June 20 and 28. In the clear condition on June 20, the HAZE(A) reduces the net downward flux by about 12 W.m^{-2} , which is about 16 times less efficient than the cloud does. However, it is still efficient enough to offset the warming effect of doubling the CO_2 amount, which increases from about 4 to 7 W.m^{-2} to the surface. Multiple scattering enhances the absorption of HAZE(A) in the layer, but the location of haze layer is more important. On June 28, a net absorption of 14 W.m^{-2} is found in the haze layer but it is only 4 W.m^{-2} for June 20, due to much competition with other gaseous absorption.

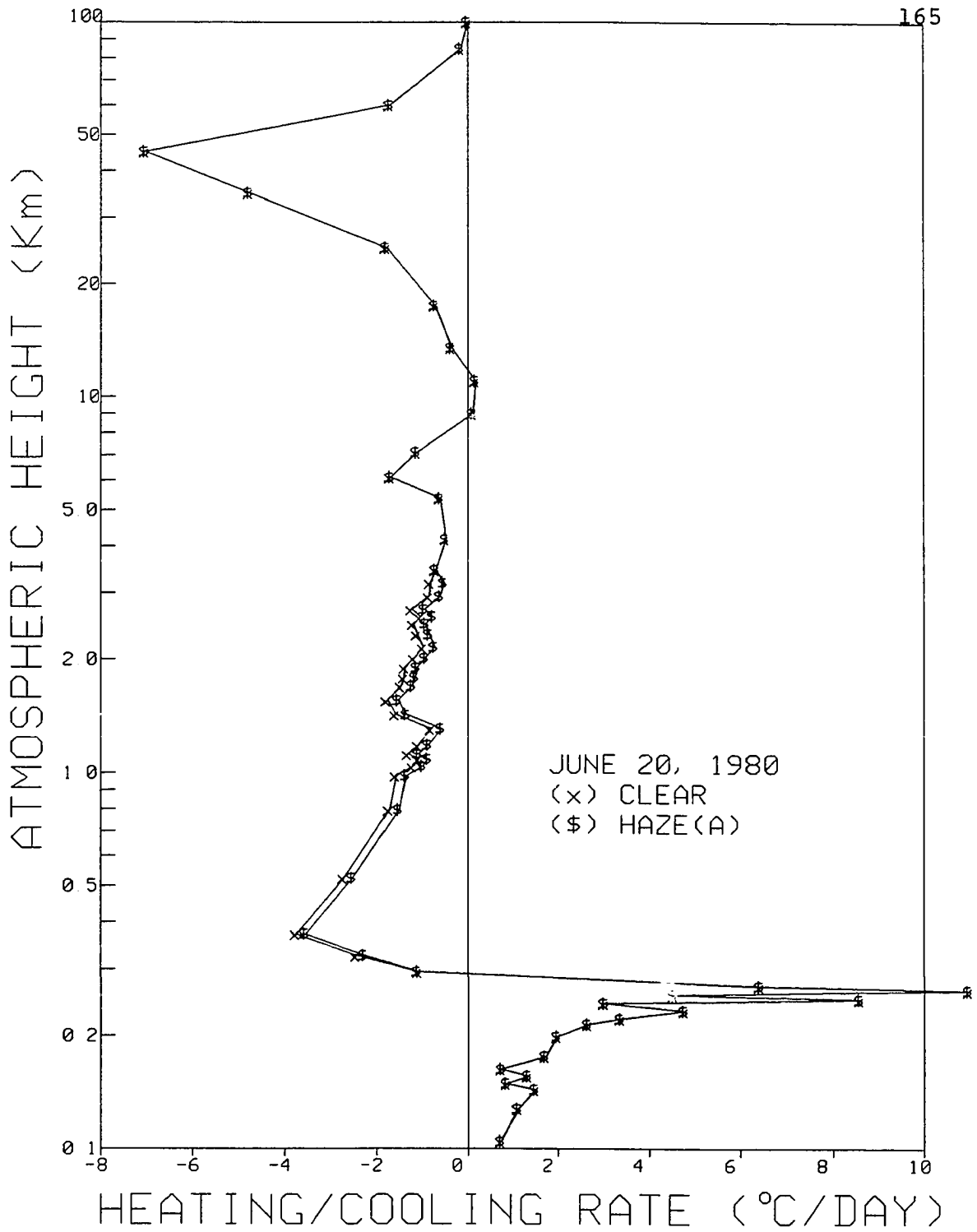


Figure 4.22 Daily nte heating/cooling profiles clear and hazy conditions on June 20, 1980

Table 4.10 Model computations of fluxes in daily radiation with various components in atmospheric profiles of June 20 and 28, 1980

(a) June 20, 1980 (single-layer cloud)

| Components | $F^-(\tau_N)$ | ΔF_{sfc} | $F^+(0)$ | ΔF_{atm} | ΔF_{lyr} |
|-----------------------|---------------|------------------|----------|------------------|------------------|
| Clear(S) | 418.18 | +185.12 | 249.73 | 75.97 | - |
| Clear(I) | 232.28 | -81.55 | 253.60 | -172.05 | - |
| Haze-A(S) | 406.20 | +181.75 | 244.30 | 84.77 | +8.97 |
| Haze-A(I) | 232.78 | -81.06 | 253.61 | -172.55 | -0.53 |
| Cloud (S) + Haze-A | 197.15 | +84.30 | 321.87 | 104.65 | +9.94 +5.52 |
| Cloud (I) + Haze-A | 313.72 | -0.93 | 249.46 | -248.53 | -74.24 -1.76 |

(b) June 28, 1980 (multi-layer clouds)

| Components | $F^-(\tau_N)$ | ΔF_{sfc} | $F^+(0)$ | ΔF_{atm} | ΔF_{lyr} |
|-----------------------|---------------|------------------|----------|------------------|------------------|
| Clear (S) | 407.06 | +188.24 | 232.94 | +93.94 | - |
| Clear (I) | 257.65 | -56.44 | 247.99 | -191.55 | - |
| Cloud (S) | 136.04 | +56.65 | 346.94 | +111.53 | +18.15 |
| Cloud (I) | 327.53 | +12.75 | 246.16 | -258.91 | -79.50 |
| Cloud (S) + Haze-A | 132.45 | +55.30 | 336.57 | +123.24 | +17.98 +16.48 |
| Cloud (I) + Haze-A | 327.53 | +12.75 | 246.19 | -258.94 | -77.54 -2.62 |

Note: $F^-(\tau_N)$, downward flux at bottom; ΔF_{sfc} , net flux gain/loss at surface; $F^+(0)$, upward flux at top; ΔF_{atm} , net flux loss of entire atmosphere; ΔF_{lyr} , net flux gain/loss at layer (all in dimension of $W.m^{-2}$); S, solar radiation; I, infrared radiation

The absorption of the snow surface is larger under a clear sky than a cloudy sky in late June. In the case of June 20, a total amount of 104 W.m^{-2} is absorbed under a clear sky, but 84 W.m^{-2} under a cloudy sky. On June 28, this difference is even further enhanced to 132 W.m^{-2} under a clear sky and 70 W.m^{-2} under a cloudy sky. These results support the early finding of Vowinckel and Orvig (1964a), as shown in Figure 1.3c. The absorption of 1 W.m^{-2} corresponds to a melting rate of ice at about 0.84 cm per month, or 2.36 cm per month for snow. As can be expected, if the snow/ice starts melting this process will be accelerated, due to the increase of grain size (or decreasing albedo).

4.3 Summary

In this thesis, a high-order discrete-ordinate method is implemented and utilized to solve the radiative transfer equation throughout the entire solar and terrestrial spectra. The solutions have been compared with other methods and found to be reliable and efficient. It has been found that computations of bulk radiative properties (e.g. fluxes and heating/cooling rates, etc.) do not differ significantly by using 2-, 4- or 8-stream approximations. However, for the angular distribution of intensity, a 16-stream approximation is generally required.

These solutions have been used to construct a complete and comprehensive radiation model, which treats Rayleigh scattering, gaseous absorption/emission, scattering and absorption/emission by cloud droplets and haze particles. Snow conditions of the arctic region are simulated by snow grains and soot contamination in the surface layers. For gaseous absorption/emission, the exponential-sum fitting of transmission is adopted. Mie scattering properties for drops are parameterized as functions of the second and third moments of drop size distributions throughout the entire spectrum. For arctic haze and snow conditions, optical properties computed by Blanchet and List (1983) and Warren and Wiscombe (1980) are adopted, respectively. Thus, a unified treatment of shortwave and longwave radiative transfer is achieved.

For clear sky comparisons, the McClatchey atmospheres are used. Data from the Arctic Stratus Clouds Experiment collected in 1980 are used for comparisons of cloudy and/or hazy skies. Results are compared with other models having different spectral resolution (Δs). Specifically, we compare broad-band ($\Delta s > 100 \text{cm}^{-1}$), narrow-band ($\Delta s < 100 \text{cm}^{-1}$) and line-by-line (restricted to gases) computations and find that at the expense of accuracy by a few watts.m^{-2} for flux or a few tenths $^{\circ}\text{C/day}$ for heating/cooling rate computations, the broad-band models are very fast and suitable for certain types of climate modelling.

The line-by-line model calls for the multiple scattering scheme by about 159,000 times; the narrow-band model, 16,300 times; and the broad-band model, 3,200 times. The accuracy loss for flux computations, from line-by-line to narrow-band models, ranges from 1 to 5W.m^{-2} for the solar radiation and 1 to 7W.m^{-2} for the infrared radiation. This discrepancy is attributed mainly to the scaling of gaseous absorber amounts used in the narrow-band model. This indicates the need of further study for proper treatment of gaseous absorption. In addition, different temperature scaling is also found in the infrared radiation for both models. Simple isothermal approximation is used in the line-by-line model and linear approximation has been found to be better for the narrow-band model. The accuracy loss for flux computations, from narrow-band to broad-band models, is found to be less than 1W.m^{-2} for the solar radiation. In the infrared radiation, the elimination of unimportant overlapping for gaseous absorption generates an accuracy loss ranging from 1 to 3W.m^{-2} .

During the arctic summer, stratus clouds are a persistent feature and decrease the downward flux at the surface by about $130\text{-}200\text{W.m}^{-2}$. This is made by artificially removing the stratus clouds from two observed profiles. Arctic haze in the summertime is important if it is above the cloud layer or in air with low relative humidity, and it also decreases

the downward flux at the surface by about $10-12\text{W.m}^{-2}$. The greenhouse effect of doubling the CO_2 amount increases the downward flux at the surface by about $4-7\text{W.m}^{-2}$ in the clear McClatchey atmospheres and can be offset by the haze condition or by an increase in cloudiness of about 4%.

Assuming steady microstructures of stratus clouds in late June, we find that a clear sky condition results in more available downward flux ($100-130\text{W.m}^{-2}$) for snow melt (9.3cm/day) than does a cloudy sky condition ($70-80\text{W.m}^{-2}$ or 6cm/day). This is because the increase of infrared radiation diffused back to surface by the cloud can not compensate for the reduction of solar radiation. When the snow starts to melt, the decreasing snow albedo further accelerates the melting process.

Appendix A: Principal Symbols

| | |
|------------------|----------------------------------------------------------------------------------------------------------------------|
| Abs | absorptivity of medium (dimensionless) |
| B | monochromatic black body radiance (or the Planck function, in $\text{W.m}^{-2}.\text{sr}^{-1}.\mu\text{m}^{-1}$) |
| C_{ij} | elements of coefficient matrix in Eq. 2.28 |
| C_p | specific heat at constant pressure ($\text{J}.\text{°K}^{-1}.\text{Kg}^{-1}$) |
| CON | total number concentration (cm^{-3}) |
| D_{jp} | components of scaling scheme in Eq. 2.44 |
| E _{mt} | emissivity of medium (dimensionless) |
| F | monochromatic flux density (or irradiance, in $\text{W.m}^{-2}.\mu\text{m}^{-1}$) |
| GMT | Greenwich Mean Time (in hours) |
| I | monochromatic intensity (or radiance, in $\text{W.m}^{-2}.\text{sr}^{-1}.\mu\text{m}^{-1}$) |
| J | internal source function (in $\text{W.m}^{-2}.\text{sr}^{-1}.\mu\text{m}^{-1}$) |
| K_{abs} | mass-absorption coefficient (in $\text{m}^2.\text{Kg}^{-1}$) |
| K_{ext} | mass-extinction coefficient (in $\text{m}^2.\text{Kg}^{-1}$) |
| K_{sca} | mass-scattering coefficient (in $\text{m}^2.\text{Kg}^{-1}$) |
| L_j | constants of integration in Eq. 2.36 |
| LWC | liquid water content (g.m^{-3}) |
| M | true solar noon in Eq. 3.3 (in hours) |
| P | phase function (dimensionless) |
| P_l^m | associated Legendre polynomials of degree m |
| Q | internal source term |

| | |
|------------------|------------------------------------------------------------------------------|
| Q_{ext} | extinction efficiency factors |
| Q_{sca} | scattering efficiency factors |
| RE | equivalent radius (μm) |
| Ref | reflectivity of medium (dimensionless) |
| R_g | mean grain radius of snow/ice (μm) |
| T | temperature (in degrees Kelvin) |
| Trn | transmissivity of medium (dimensionless) |
| X | component of thermal emission source in Eq.2.38 |
| X_m | cross-section area per unit mass (in $\text{m}^2 \cdot \text{Kg}^{-1}$) |
| Z | component of particular solution for intensity |
| a_j | quadrature weights and $a_{-j} = a_j$ |
| a_n | Mie coefficients (complex values) |
| b_n | Mie coefficients (complex values) |
| b_{ext} | volume extinction coefficient (m^{-1}) |
| b_i | equivalent absorption coefficient in ESFT method |
| b_R | Rayleigh volume extinction coefficient (m^{-1}) |
| c | speed of light, $3 \times 10^8 \text{ m} \cdot \text{sec}^{-1}$ |
| g | asymmetry factor or the first moment of phase function |
| g^\pm | eigenvectors of coefficient matrix in Eq. 2.30 |
| g_a | gravitational acceleration ($\approx 9.8 \text{ m} \cdot \text{sec}^{-2}$) |
| g_l^m | moments of phase function with respect to the Legendre polynomials |
| h | the Planck constant, $6.6262 \times 10^{-34} \text{ J} \cdot \text{sec}$ |
| k | eigenvalues of coefficient matrix in Eq. 2.30 |
| n_a | refractive index of air |
| n_c | complex refractive index ($n_c = n_r - in_i$) |

| | |
|------------------------|---------------------------------------------------------------------|
| p | atmospheric pressure (in kPa = 10 mb) |
| s | actual path-length (in meters) |
| u | effective absorber amount in ESFT method |
| w_i | weight in Exponential-Sum of Fitting Transmission |
| $\delta_{0,m}$ | = 1 for $m = 0$ (= 0, otherwise) |
| Δt | period of time (in hours) |
| Δz | thickness of medium (in meters) |
| $\alpha_{i,j}$ | elements of coefficient matrix in Eq. 2.29 |
| $\beta_{i,j}$ | elements of coefficient matrix in Eq. 2.29 |
| χ | size parameter ($2\pi r/\lambda$) |
| ϕ | azimuthal angle (in degrees) |
| η | solar declination (in degrees) |
| Ξ | angle between incident and scattered rays |
| θ | polar angle (in degrees) |
| κ | the Boltzmann constant, $1.3806 \times 10^{-23} \text{ J.deg}^{-1}$ |
| λ | monochromatic wavelength of radiation (in μm) |
| ν | wavenumber (in cm^{-1}) |
| ψ | latitude (in degrees) |
| ρ | density of medium (in Kg.m^{-3}) |
| σ_R | Rayleigh scattering cross-section (cm^2) |
| τ | normal optical depth (or thickness, dimensionless) |
| ξ | solar elevation (in degrees) |
| ζ | solar hour angle (in degrees) |
| μ | cosine of the polar angle |
| μ_0 | cosine of the solar zenith angle |
| $\mu_0 I^{\text{inc}}$ | incident solar flux |

μ_j quadrature points and $\mu_{-j} = -\mu_j$
 ω single-scattering albedo (dimensionless)

Appendix B: Derivation of the Multiple Scattering Term in
Eq.2.26

The diffuse intensity (I), expanded as a Fourier cosine series of $2n-1$ terms, is given by Eq. 2.22:

$$I(\tau, \mu, \phi) = \sum_{m=0}^{2n-1} I^m(\tau, \mu) \cos m(\phi_0 - \phi) \quad (A1)$$

The phase function (P) expanded in a series of $2n-1$ Legendre polynomials by using the addition theorem for spherical harmonics is given by Eq. 2.24:

$$P(\mu, \phi; \mu', \phi') = \sum_{m=0}^{2n-1} (2-\delta_{0,m}) \sum_{l=m}^{2n-1} (2l+1) g_l^m P_l^m(\mu) P_l^m(\mu') \cos m(\phi' - \phi) \quad (A2)$$

Substitution of Eqs. A1 and A2 yields

$$\begin{aligned} & \frac{\omega}{4\pi} \int_0^{2\pi} \int_{-1}^1 P(\mu, \phi; \mu', \phi') I(\tau, \mu', \phi') d\mu' d\phi' = \\ & \frac{\omega}{4\pi} \int_0^{2\pi} \int_{-1}^1 \left\{ \sum_{m=0}^{2n-1} (2-\delta_{0,m}) \sum_{l=m}^{2n-1} (2l+1) g_l^m P_l^m(\mu) P_l^m(\mu') \cos m(\phi' - \phi) \right\} \times \\ & \quad \left\{ \sum_{r=0}^{2n-1} I^r(\tau, \mu') \cos r(\phi_0 - \phi') \right\} d\mu' d\phi' \end{aligned}$$

Concentrating on the integration of:

$$\sum_{m=0}^{2n-1} \int_0^{2\pi} (2-\delta_{0,m}) \sum_{r=0}^{2n-1} I^r(\tau, \mu') \cos m(\phi' - \phi) \cos r(\phi_0 - \phi') d\phi'$$

$$\text{for } m=0: \quad \sum_{r=0}^{2n-1} I^r(\tau, \mu') \int_0^{2\pi} \cos r(\phi_0 - \phi') d\phi' = 2\pi I^0(\tau, \mu')$$

$$\text{for } m=1: \quad 2 \sum_{r=0}^{2n-1} I^r(\tau, \mu') \int_0^{2\pi} \cos m(\phi' - \phi) \cos r(\phi_0 - \phi') d\phi' = \\ 2\pi I^1(\tau, \mu') \cos(\phi_0 - \phi)$$

for all m's, only r=m term exists for r=0 to 2n-1. Then,

$$\sum_{m=0}^{2n-1} \int_0^{2\pi} (2-\delta_{0,m}) \sum_{r=0}^{2n-1} I^r(\tau, \mu') \cos m(\phi' - \phi) \cos r(\phi_0 - \phi') d\phi' = \\ 2\pi \sum_{m=0}^{2n-1} I^m(\tau, \mu') \cos m(\phi_0 - \phi)$$

Or:

$$\frac{\omega}{4\pi} \int_0^{2\pi} \int_{-1}^1 P(\mu, \phi; \mu', \phi') I(\tau, \mu', \phi') d\mu' d\phi' = \\ \sum_{m=0}^{2n-1} \frac{\omega}{2} \sum_{l=m}^{2n-1} (2l+1) g_l^m P_l^m(\mu) \cos m(\phi_0 - \phi) \int_{-1}^1 P_l^m(\mu') I(\tau, \mu') d\mu'$$

Appendix C: Derivation of the Analytic Interpolation Scheme
for Intensity at Arbitrary Angles (Eq.2.49)

The source function (J) given by Eq. 2.48 for the azimuth-independent case (m=0) is repeated as follows:

$$J(\tau, \mu) = \sum_{i=-n}^n (1+k_i \mu) L_i g_i(\mu) e^{-k_i \tau} + (1 + \frac{\mu}{\mu_0}) Z(\mu) e^{-\tau/\mu_0} + Z_0(\mu) + (\tau - \mu) Z_1 \quad (B1)$$

Also, from Eqs. 2.28, 2.37, and 2.39, the source function can be rewritten as follows:

$$J(\tau, \mu) = \frac{\omega}{2} \sum_{l=0}^{2n-1} (2l+1) g_l P_l(\mu) \sum_{j=-n}^n a_j P_l(\mu_j) I(\tau, \mu_j) + \frac{\omega I_{inc}}{4\pi} \sum_{l=0}^{2n-1} (-1)^l (2l+1) g_l P_l(\mu) P_l(\mu_0) e^{-\tau/\mu_0} + (1-\omega)(X_0 + X_1 \tau) \quad (B2)$$

with $X_1 = [B(T_N) - B(T_0)] / (\tau_N - \tau_0)$ and $X_0 = B(T_0) - X_1 \tau_0$.

Substitution of the complete solution of intensity at the quadrature angles (Eq. 2.42)

$$I(\tau, \mu_j) = \sum_{i=-n}^n L_i g_i(\mu_j) e^{-k_i \tau} + Z(\mu_j) e^{-\tau/\mu_0} + Z_0(\mu_j) + Z_1 \tau$$

into Eq. B2 yields

$$J(\tau, \mu) = \frac{\omega}{2} \sum_{l=0}^{2n-1} (2l+1) g_l P_l(\mu) \sum_{j=-n}^n a_j P_l(\mu_j) \sum_{i=-n}^n L_i g_i(\mu_j) e^{-k_i \tau} + \frac{\omega}{2} \sum_{l=0}^{2n-1} (2l+1) g_l P_l(\mu) \sum_{j=-n}^n a_j P_l(\mu_j) Z(\mu_j) e^{-\tau/\mu_0} +$$

$$\begin{aligned} & \frac{\omega I \text{ inc}}{4\pi} \sum_{l=0}^{2n-1} (-1)^l (2l+1) g_l P_l(\mu) P_l(\mu_0) e^{-\tau/\mu_0} + \\ & \frac{\omega}{2} \sum_{l=0}^{2n-1} (2l+1) g_l P_l(\mu) \sum_{j=-n}^n a_j P_l(\mu_j) [Z_0(\mu_j) + Z_1 \tau] + \\ & (1-\omega)(X_0 + X_1 \tau) \end{aligned}$$

Equating these two identical source functions, the analytic interpolation scheme is obtained in three parts:

(a) Multiple scattering part:

$$\begin{aligned} & \sum_{i=-n}^n (1+k_i \mu) L_i g_i(\mu) e^{-k_i \tau} = \\ & \frac{\omega}{2} \sum_{l=0}^{2n-1} (2l+1) g_l P_l(\mu) \sum_{j=-n}^n a_j P_l(\mu_j) \sum_{i=-n}^n L_i g_i(\mu_j) e^{-k_i \tau} \end{aligned}$$

Or:

$$g_i(\mu) = \frac{\omega}{1+k_i \mu} \sum_{l=0}^{2n-1} (2l+1) g_l P_l(\mu) \left(\frac{1}{2} \sum_{j=-n}^n a_j P_l(\mu_j) g_i(\mu_j) \right)$$

(b) Solar radiation part:

$$\begin{aligned} & \left(1 + \frac{\mu}{\mu_0} \right) Z(\mu) e^{-\tau/\mu_0} = \\ & \frac{\omega}{2} \sum_{l=0}^{2n-1} (2l+1) g_l P_l(\mu) \sum_{j=-n}^n a_j P_l(\mu_j) Z(\mu_j) e^{-\tau/\mu_0} + \\ & \frac{\omega I \text{ inc}}{4\pi} \sum_{l=0}^{2n-1} (-1)^l (2l+1) g_l P_l(\mu) P_l(\mu_0) e^{-\tau/\mu_0} \end{aligned}$$

Or:

$$\begin{aligned} Z(\mu) = & \frac{\omega}{1+\mu/\mu_0} \sum_{l=0}^{2n-1} (2l+1) g_l P_l(\mu) \left(\frac{1}{2} \sum_{j=-n}^n a_j P_l(\mu_j) Z(\mu_j) + \right. \\ & \left. \frac{I \text{ inc}}{4\pi} (-1)^l P_l(\mu_0) \right) \end{aligned}$$

(c) Thermal emission part:

$$z_0(\mu) + (\tau - \mu)z_1 = (1 - \omega)(x_0 + x_1\tau) + \frac{\omega}{2} \sum_{l=0}^{2n-1} (2l+1)g_l P_l(\mu) \sum_{j=-n}^n a_j P_l(\mu_j) [z_0(\mu_j) + z_1\tau]$$

(Note: $\frac{\omega}{2} \sum_{l=0}^{2n-1} \sum_{j=-n}^n a_j (2l+1)g_l P_l(\mu) P_l(\mu_j) = 1$ and $x_1 = z_1$)

Or:

$$z_0(\mu) = \mu z_1 + (1-\omega)x_0 + \frac{\omega}{2} \sum_{l=0}^{2n-1} (2l+1)g_l P_l(\mu) \sum_{j=-n}^n a_j P_l(\mu_j) z_0(\mu_j)$$

Appendix D: Delta-M Transformation

The azimuthal average of Eq. 2.20 is

$$\mu \frac{dI(\tau, \mu)}{d\tau} = I(\tau, \mu) - \frac{\omega}{2} \int_{-1}^1 P(\mu, \mu') I(\tau, \mu') d\mu' - Q(\tau, \mu). \quad (D1)$$

The Delta-M transformation of the phase function is given by Wiscombe (1977), as follows:

$$P(\mu, \mu') = 2f\delta(\mu - \mu') + (1-f)P_{\delta-M}(\mu, \mu') \quad (D2)$$

where f denotes the truncated fraction and $P_{\delta-M}$ represents the Delta-M phase function. Substituting Eq. D2 into Eq. D1 yields

$$\begin{aligned} \mu \frac{dI(\tau, \mu)}{d\tau} &= (1-\omega f)I(\tau, \mu) - \frac{\omega(1-f)}{2} \int_{-1}^1 P_{\delta-M}(\mu, \mu') I(\tau, \mu') d\mu' \\ &\quad - Q(\tau, \mu) \end{aligned} \quad (D3)$$

If τ and ω are replaced by the following scalings

$$d\tau' = (1-\omega f)d\tau$$

$$\text{and } \omega' = \omega(1-f)/(1-\omega f),$$

Eq. D3 becomes

$$\begin{aligned} \mu \frac{dI(\tau', \mu)}{d\tau'} &= I(\tau', \mu) - \frac{\omega'}{2} \int_{-1}^1 P_{\delta-M}(\mu, \mu') I(\tau', \mu') d\mu' \\ &\quad - Q(\tau, \mu)/(1-\omega f) \end{aligned} \quad (D4)$$

Substituting the azimuthal average of internal source term (Eq. 2.21) into Eq. D4 yields the scaled source term:

$$\begin{aligned}
Q(\tau', \mu) &= \frac{Q(\tau, \mu)}{1-\omega f} = \frac{\omega(1-f)I^{\text{inc}}}{2(1-\omega f)} P_{\delta-M}(\mu, -\mu_0) e^{-\tau/\mu_0} \\
&\quad + \frac{(1-\omega)}{1-\omega f} B(T) \\
&= \frac{\omega' I^{\text{inc}}}{2} P_{\delta-M}(\mu, -\mu_0) e^{-\tau/\mu_0} + (1-\omega') B(T)
\end{aligned}$$

Or Eq. D1 becomes

$$\begin{aligned}
\mu \frac{dI(\tau', \mu)}{d\tau'} &= I(\tau', \mu) - \frac{\omega'}{2} \int_{-1}^1 P_{\delta-M}(\mu, \mu') I(\tau', \mu') d\mu' \\
&\quad - Q(\tau', \mu)
\end{aligned}$$

Therefore, the Delta-M transformation of the phase function does not change the form of the radiative transfer equation.

Appendix E: Derivation of the Expansions of Legendre

Polynomials for Rayleigh and Henyey-Greenstein
Phase Functions

(A) The Rayleigh phase function is given as follows:

$$P_R(\cos\Xi) = 0.75 (1 + \cos^2\Xi)$$

Expanding $P_R(\cos\Xi)$ in a series of Legendre polynomials of order N yields

$$P_R(\cos\Xi) = \sum_{n=0}^N (2n+1) Y_n P_n(\cos\Xi)$$

and the coefficients (Y_n) are the moments of phase function (P_R) with respect to the Legendre polynomials (P_n)

$$Y_n = \frac{1}{2} \int_0^\pi P_R(\cos\Xi) P_n(\cos\Xi) \sin\Xi d\Xi = \frac{1}{2} \int_{-1}^1 P_R(\mu) P_n(\mu) d\mu$$

Noting the orthogonality of the Legendre polynomials:

$$\int_{-1}^1 P_m(\mu) P_n(\mu) d\mu = \begin{cases} 0, & m \neq n \\ \frac{2}{2n+1}, & m=n \end{cases}$$

and $\int_{-1}^1 \mu^m P_n(\mu) d\mu = 0$ for $m < n$; $P_0(\mu)=1$, $P_1(\mu)=\mu$, and $P_2(\mu)=0.5(3\mu^2-1)$, the coefficients (Y_n) of Rayleigh phase function are obtained as follows:

$$Y_n = \frac{1}{2} \int_{-1}^1 \frac{3}{4} (1+\mu^2) P_n(\mu) d\mu = \frac{3}{8} \int_{-1}^1 [P_0(\mu) + \mu^2] P_n(\mu) d\mu \quad (E1)$$

Obviously for $n > 2$ $\int_{-1}^1 \mu^2 P_n(\mu) d\mu = 0$ and $\int_{-1}^1 P_0(\mu) P_n(\mu) d\mu = 0$,

therefore, only three terms (Ψ_0, Ψ_1, Ψ_2) need be considered. Substituting the first three terms of $P_n(\mu)$ into Eq. E1 and performing the simple integration yields $\Psi_0 = 1, \Psi_1 = 0,$ and $\Psi_2 = 0.1,$ or

$$P_R(\cos \Xi) = \sum_{n=0}^N (2n+1) \Psi_n P_n(\cos \Xi) = P_0(\cos \Xi) + \frac{1}{2} P_2(\cos \Xi)$$

(B) The expansion of the Henyey-Greenstein phase function in a series of Legendre polynomials of order N can be done with the same method as above. However, another method starts from the generating function of Legendre polynomials:

$$\frac{1}{\sqrt{1 - 2tx + t^2}} = \sum_{n=0}^N P_n(x) t^n \quad (\text{E2})$$

(E2) + $2 \frac{\partial(\text{E2})}{\partial t}$:

$$\frac{1 - t^2}{[1 - 2tx + t^2]^{3/2}} = \sum_{n=0}^N (2n+1) t^n P_n(x)$$

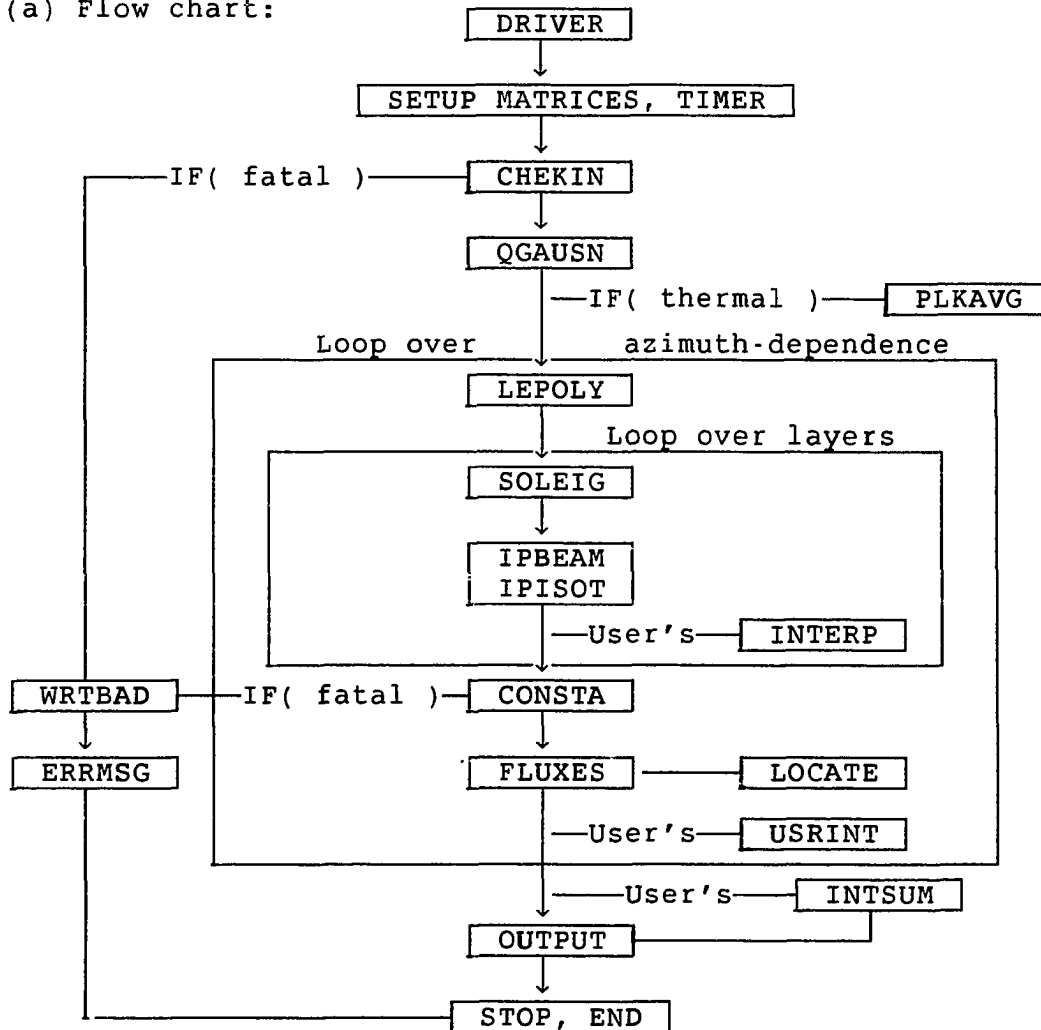
Setting $1 \geq t = g \geq -1$ and $x = \cos \Xi$, the expansion of the Henyey-Greenstein phase function is obtained as follows:

$$P_{HG}(\cos \Xi) = \frac{1 - g^2}{[1 + g^2 - 2g \cos \Xi]^{3/2}} = \sum_{n=0}^N (2n+1) g^n P_n(\cos \Xi)$$

where g is the asymmetry factor and the coefficients of the expansion are simply the power of g .

Appendix F: Computing Code of the Discrete Ordinate Method

(a) Flow chart:



NOTE:

- CHEKIN: checks input dimensions and variables.
- CONSTA: calculates constants of integration.
- ERRMSG: prints out error message and kills run if fatal.
- FLUXES: computes upward and downward fluxes.
- INTERP: interpolates eigenvectors etc. for user's intensity.
- INTSUM: sums up the Fourier expansion of intensity.
- IPBEAM: finds particular solution of solar radiation.
- IPISOT: finds particular solution of thermal radiation.
- LEPOLY: evaluates the associated Legendre polynomials.
- LOCATE: finds locations for output optical depth.
- PLKAVG: computes the Planck function over $\Delta\lambda$.
- QGAUSN: computes the Gaussian quadrature points and weights.
- SOLEIG: solves eigenfunction problems.
- USRINT: computes user's intensity components.
- WRTBAD: writes out names of erroneous input variables.

```

C      (b) PROGRAM DRIVER                ! TEST DISCRETE ORDINATE CODE
C+-----+
C!      *** INPUT VARIABLE SPECIFICATIONS ***      !
C+-----+
PARAMETER ( NLYRI   = 51 )   ! MAX NO. OF COMPUTATIONAL LEVELS
PARAMETER ( NPFMOM  = 33 )   ! MAX NO. OF PHASE FCN MOMENTS
PARAMETER ( NPHII   = 4  )   ! MAX NO. OF AZIMUTHAL OUTPUT ANGLES
PARAMETER ( NTAUI   = 51 )   ! MAX NO. OF OUTPUT LEVELS
PARAMETER ( NTHETAI = 32 )   ! MAX NO. OF POLAR OUTPUT ANGLES
PARAMETER ( PI      = 3.1415926535898 )

C
CHARACTER*80  HEADER
LOGICAL  DELTAM, NOPLK, ONLYFL, PRNT( 5 ), USRANG, USRTAU
INTEGER  IBCND, IPHAS( NLYRI ), NSTR, NTHETA, NLYR, NPHI, NTAU
REAL    AG, COSTH( NTHETAI ), FBEAM, FISO, GEMI, GTEMP,
$       GG( NLYRI ), GL( NPFMOM,NLYRI ), OPDEP( NLYRI ),
$       PHI( NPHII ), SSALB( NLYRI ), TAU( NTAUI ),
$       TEMPER( 0:NLYRI ), TEMI, TTEMP, WVNML0, WVMNHI, X0
C+-----+
C!      *** OUTPUT VARIABLE SPECIFICATIONS ***      !
C+-----+
REAL    FLDIR( NTAUI ), FLDN( NTAUI ), FLUP( NTAUI ),
$       RINTT( NTAUI,NTHETAI,NPHII )
C*****
C*      THIS IS A TEST PROBLEM SUGGESTED BY DALE      *
C*****
DELTAM = .FALSE.
NOPLK  = .TRUE.
ONLYFL = .FALSE.
USRANG = .FALSE.
USRTAU = .FALSE.
NSTR   = 16
NLYR   = 1
OPDEP(1) = 1.0
SSALB(1) = 0.5
IPHAS(1) = 1
IBCND  = 0
FBEAM  = 1.0
FISO   = 0.0
WVNML0 = 0.
WVMNHI = 50000.
X0     = 1.0
AG     = 0.0
GTEMP  = 0.0
GEMI   = 1.0
TTEMP  = 0.0
TEMI   = 1.0
DO 1 I = 0,NLYR
      TEMPER(I) = 250.0
1      CONTINUE
DO 2 I = 1,5

```

```

      PRNT(I) = .TRUE.
2  CONTINUE
  HEADER = 'TEST CASE NO. 0, REF. 2, P. 19, TABLE 4a-4c
  NTAU   = 7
  TAU(1) = 0.0
  TAU(2) = 0.05
  TAU(3) = 0.1
  TAU(4) = 0.2
  TAU(5) = 0.5
  TAU(6) = 0.75
  TAU(7) = 1.0
  NTHETA = 10
  DO 3  I = 1,5
      COSTH(10-I+1) = 1.0 - 0.2*(I-1)
      COSTH(I)      = 0.2*(I-1) - 1.0
3  CONTINUE
  NPFI   = 3
  PHI(1) = 0.0
  PHI(2) = 90.0
  PHI(3) = 180.0
  CALL DISORT( AG, COSTH, DELTAM, FBEAM, FISO, GEMI, GG, GL, GTEMP,
$             HEADER, IBCND, IPHAS, NLYR, NOPLK, NPFMOM, NPFI,
$             NSTR, NTAU, NTHETA, ONLYFL, OPDEP, PRNT, PHI, SSALB,
$             TAU, TEMI, TEMPER, TTEMP, USRANG, USRTAU, WVMNHI,
$             WVMNLO, X0, FLDIR, FLDN, FLUP, RINTT )
C
  STOP
  END
C***** END OF DRIVER *****
C*****

```

```

C*****
C*   DISORT: DIScrete Ordinates Radiative Transfer PROGRAM   *
C*****
SUBROUTINE DISORT( AG, COSTH, DELTAM, FBEAM, FISO, GEMI, GG, GL,
$           GTEMP, HEADER, IBCND, IPHAS, NLYR, NOPLK,
$           NPFMOM, NPFI, NSTR, NTAU, NTHETA, ONLYFL,
$           OPDEP, PRNT, PHI, SSALB, TAU, TEMI, TEMPER,
$           TTEMP, USRANG, USRTAU, WVMNHI, WVMNLO, X0,
$           FLDIR, FLDN, FLUP, RINTT )
C*****
C*   AUTHORS :
C*           Knut Stamnes and Collaborators*
C*           Auroral Observatory
C*           University Of Tromso
C*           P.O. Box 953, N-9001
C*           Tromso, NORWAY
C*
C*   *Collaborators: cf. REFERENCES
C*
C*   MODIFIED EXTENSIVELY BY:
C*           Warren Wiscombe
C*           NASA Goddard Space Flight Center
C*           Greenbelt, MD 20771
C*
C*   DOCUMENTED FINALLY BY:
C*           Si-Chee Tsay
C*           Geophysical Institute
C*           University Of Aalska
C*           Fairbanks, AK 99775-0800
C*
C*   REFERENCES :
C*
C*           SS: Stamnes, K. and R. Swanson, 1981: A New Look at
C*               the Discrete Ordinate Method for Radiative Transfer
C*               Calculations in Anisotropically Scattering
C*               Atmospheres, J. Atmos. Sci. 38, 387-399
C*
C*           SD: Stamnes, K. and H. Dale, 1981: A New Look at the
C*               Discrete Ordinate Method for Radiative Transfer
C*               Calculations in Anisotropically Scattering
C*               Atmospheres. II: Intensity Computations,
C*               J. Atmos. Sci. 38, 2696-2706
C*
C*           S1: Stamnes, K., 1982: On the Computatioiv of Angular
C*               Distributions of Radiation in Planetary
C*               Atmospheres, J.Q.S.R.T. 28, 47-51
C*
C*           S2: Stamnes, K., 1982: Reflection and Transmission by
C*               a Vertically Inhomogeneous Planetary Atmosphere,
C*               Planet. Space Sci. 30, 727-732
C*

```

```

C*          SC: Stamnes, K. and P. Conklin, 1984: A New Multi-Layer      *
C*          Discrete Ordinate Approach to Radiative Transfer          *
C*          in Vertically Inhomogeneous Atmospheres,                  *
C*          J.Q.S.R.T. 31, 273-282                                     *
C*          *
C*****
C*          EXTERNAL SUBROUTINES REQUIRED :                               *
C*          FROM LINPACK :  SGBCO, SGBSL, AND OTHERS (IN LINPACK)      *
C*          CALLED BY THESE TWO SUBROUTINES                            *
C*          FROM IMSL      :  LEQTLF, EIGRF, AND OTHERS (IN IMSL)      *
C*          CALLED BY THESE TWO SUBROUTINES                            *
C*          *
C*          INTERNAL SUBROUTINES REQUIRED : (ATTACHED)                  *
C*          CHEKIN: CHECKS INPUT DIMENSIONS AND VARIABLES              *
C*          CONSTA: CALCULATES CONSTANTS OF INTEGRATION IN EQ. SS(13) *
C*          ERRMSG: PRINTS OUT ERROR MESSAGE AND KILLS RUN IF FATAL   *
C*          FLUXES: COMPUTES UPWARD AND DOWNWARD FLUXES                *
C*          INTERP: INTERPOLATES EIGENVECTORS IN EQS. SD(8-9)         *
C*          INTSUM: SUMS UP FOURIER EXPAN. FOR INTENSITY IN EQ. SD(2) *
C*          IPBEAM: FINDS PARTICULAR SOLUTION IN EQ. SS(18)           *
C*          IPISOT: FINDS PARTICULAR SOLUTION IN EQ. SS(15)           *
C*          LEPLOY: EVALUATES ASSOCIATED LEGENDRE POLYNOMIALS          *
C*          LOCATE: FINDS LOCATIONS FOR OUTPUT OPTICAL DEPTH           *
C*          PLKAVG: COMPUTES PLANCK FUNCTION OVER DELTA-LUMDA          *
C*          QGAUSN: COMPUTES GAUSSIAN QUAD. POINTS AND WEIGHTS         *
C*          SOLEIG: SOLVES EIGENFUNCTION PROBLEMS IN EQS. SS(6-12)    *
C*          USRINT: COMPUTES USER INTENSITIES IN EQ. SS(27-29)        *
C*          WRBAD: WRITES OUT NAMES OF ERRONEOUS INPUT VARIABLES       *
C*          ZEROAL: CALLS *ZEROIT* TO ZERO ALL GIVEN MATRICES         *
C*          ZEROIT: ZEROS A GIVEN MATRIX                               *
C*          *
C*****
C+-----+
C!
C!          INDEX CONVENTIONS ( FOR ALL VARIABLES DESCRIBED BELOW ) : !
C!
C!          IU   :  FOR USER POLAR ANGLES (WHERE INTENSITIES ARE COMPUTED) !
C!          IQ   :  FOR COMPUTATIONAL POLAR ANGLES ('QUADRATURE ANGLES') !
C!          J    :  FOR USER AZIMUTHAL ANGLES                             !
C!          K    :  FOR PHASE FUNCTION LEGENDRE EXPANSION COEFFICIENTS    !
C!          LU   :  FOR USER LAYERS (WHERE FLUXES AND INTENSITIES        !
C!                  ARE COMPUTED)                                         !
C!          LC   :  FOR COMPUTATIONAL LAYERS (EACH HAVING A DIFFERENT     !
C!                  SINGLE-SCATTER ALBEDO AND/OR PHASE FUNCTION)         !
C!          M    :  FOR AZIMUTHAL COMPONENTS IN FOURIER COSINE EXPANSION !
C!                  OF INTENSITY AND PHASE FUNCTION                       !
C!
C+-----+
C!          I N P U T   V A R I A B L E S                               !
C+-----+
C!          ** CONTROL FLAGS **                                         !

```

```

C! DELTAM = TRUE, USE DELTA-M METHOD TO SCALE OPTICAL DEPTHS, ETC. !
C! = FALSE, DON'T USE DELTA-M METHOD !
C! NOPLK = TRUE, IGNORE PLANCK FUNCTION THERMAL EMISSION !
C! FALSE, INCLUDE THERMAL EMISSION !
C! ONLYFL = TRUE, CALCULATE FLUXES ONLY !
C! = FALSE, CALCULATE FLUXES AND INTENSITIES !
C! USRANG = TRUE, USE USER-SPECIFIED POLAR ANGLE COSINES (-COSTH-)!
C! = FALSE, USE THE -NSTR- QUADRATURE ANGLES; IGNORE -COSTH-!
C! USRTAU = TRUE, FLUXES AND/OR INTENSITIES ARE TO BE EVALUATED !
C! AT USER-SPECIFIED OPTICAL DEPTHS -TAU- ; !
C! = FALSE, AT BOUNDARY OF EVERY COMPUTATIONAL LAYER. !
C! !
C! ** OPTICAL PARAMETERS ** !
C! NSTR : NUMBER OF POLAR QUADRATURE ANGLES TO BE USED !
C! (= NUMBER OF 'STREAMS') ( SHOULD BE EVEN ) !
C! NLYR : NUMBER OF LAYERS !
C! OPDEP(LC): LC=1 TO NLYR, !
C! OPTICAL DEPTHS OF COMPUTATIONAL LEVELS !
C! SSALB(LC): LC=1 TO NLYR, !
C! SINGLE-SCATTER ALBEDOS OF COMPUTATIONAL LAYERS !
C! IPHAS(LC): LC=1 TO NLYR, !
C! PHASE FUNCTION OPTIONS FOR COMPUTATIONAL LAYERS !
C! 0 : USE USER-SPECIFIED PHASE FUNCTION MOMENTS -GL- !
C! 1 : ISOTROPIC SCATTERING !
C! 2 : RAYLEIGH SCATTERING !
C! 3 : HENYEY-GREENSTEIN PHASE FUNCTION WITH !
C! ASYMMETRY FACTOR -GG(L)- !
C! 4 : HAZE L PHASE FUNCTION AS SPECIFIED BY LENOBLE IN !
C! 'STANDARD PROCEDURES ..... ' !
C! GG(LC) : ASYMMETRY FACTOR FOR LAYER WITH IPHAS(LC)=3 !
C! GL(K,LC) : K=1 TO N+1, !
C! PHASE FUNCTION MOMENTS FOR LAYERS WITH IPHAS(LC) = 0. !
C! GL(1,LC)=1, GL(2,LC) = ASYMMETRY FACTOR, ETC. !
C! !
C! ** BOUNDARY CONDITIONS ** !
C! IBCND = 0 : PARALLEL BEAM ILLUMINATION FROM THE TOP OF !
C! INTENSITY -FBEAM- AND/OR DIFFUSE ILLUMINATION FROM !
C! THE TOP OF INTENSITY -FISO- AND/OR THERMAL EMISSION !
C! FROM THE TOP ( SEE -TEMI,TTEMP- ) AND/OR INTERNAL !
C! THERMAL EMISSION SOURCES ( IF ANY ) !
C! = 1 : ISOTROPIC ILLUMINATION FROM TOP AND BOTTOM !
C! ( IN ORDER TO GET ALBEDO AND TRANSMISSIVITY OF THE !
C! ENTIRE SLAB AT ANY SUN ANGLE; SEE S2 FOR DETAILS ) !
C! FBEAM : INTENSITY OF INCIDENT BEAM (IBCND=0 ONLY) !
C! FISO : INTENSITY OF ISOTROPIC ILLUMINATION (IBCND=0 OR 1) !
C! WVNML0 & : WAVENUMBERS (INV CM) OF SPECTRAL INTERVAL !
C! WVNMMHI ( USED ONLY FOR CALCULATING PLANCK FUNCTION ) !
C! X0 : POLAR ANGLE COSINE OF INCIDENT BEAM (IBCND=0 ONLY) !
C! AG : SURFACE ALBEDO !
C! GTEMP : TEMPERATURE OF GROUND (K) !
C! GEMI : EMISSIVITY OF GROUND !

```



```

C!      TTEMP      : TEMPERATURE OF TOP BOUNDARY (K)           !
C!      TEMI       : EMISSIVITY OF TOP BOUNDARY               !
C!      TEMPER(LC) : LC=0 TO NLYR, TEMPERATURES (K) OF LEVELS !
C!
C!      ** OUTPUT CONTROL FLAGS AND PARAMETERS **             !
C!      PRNT(1)    = TRUE, PRINT INPUT VARIABLES              !
C!      PRNT(2)    = TRUE, PRINT FLUXES                      !
C!      PRNT(3)    = TRUE, PRINT AZIMUTHALLY-AVERAGED INTENSITIES (WHICH !
C!                  ARE EQUAL TO INTENSITIES IF PROBLEM IS AZIMUTHALLY !
C!                  SYMMETRIC) AT USER LEVELS AND QUADRATURE POLAR ANGLES !
C!      PRNT(4)    = TRUE, PRINT INTENSITIES AT USER LEVELS AND ANGLES !
C!      HEADER     : AN 80- (OR LESS) CHARACTER HEADER FOR PRINTS !
C!      NTAU       : NUMBER OF OPTICAL DEPTHS AT WHICH FLUXES AND/OR !
C!                  INTENSITIES ARE TO BE CALCULATED         !
C!      TAU(LU)    : LU=1 TO NTAU, THE OPTICAL DEPTHS        !
C!                  (DO NOT HAVE TO BE IDENTICAL TO COMPUTATIONAL LEVELS) !
C!      NTHETA     : NO. OF POLAR ANGLES AT WHICH TO CALCULATE INTENSITIES !
C!      COSTH(IU) : IU=1 TO NTHETA, COSINES OF POLAR OUTPUT ANGLES IN !
C!                  INCREASING ORDER (STARTING WITH NEGATIVE VALUES, IF !
C!                  ANY, AND GOING UPWARDS THROUGH POSITIVE VALUES); !
C!                  *** MUST NOT HAVE ANY ZERO VALUES ***    !
C!      NPHI      : NUMBER OF AZIMUTHAL ANGLES AT WHICH TO CALCULATE !
C!                  INTENSITIES                               !
C!      PHI(J)     : J=1 TO NPHI, AZIMUTHAL OUTPUT ANGLES (IN DEGREES) !
C!
C+-----+
C!                  O U T P U T   V A R I A B L E S           !
C+-----+
C!      FLDIR(LU)  : DIRECT-BEAM FLUX                        !
C!      FLDN(LU)   : DIFFUSE DOWN-FLUX                      !
C!      FLUP(LU)   : DIFFUSE UP-FLUX                       !
C!      RINTT(LU,IU,J): INTENSITY                            !
C!
C+-----+
C!                  I N T E R N A L   V A R I A B L E S       !
C+-----+
C!      AMB(IQ,IQ) (ALFA-BETA), ONE OF THE MATRICES IN THE REDUCED !
C!                  EIGENVALUE PROBLEM EQ. SS(12)           !
C!      APB(IQ,IQ) (ALFA+BETA) IN EQ. SS(12)               !
C!      ARRAY(IQ,IQ) MATRIX FOR *INTERP*, *IPBEAM*, *IPISOT*, AND !
C!                  *SOLEIG* (SEE EACH SUBROUTINE FOR DEFINITION) !
C!      B( )       RIGHT-HAND SIDE VECTOR OF EQ. SC(5) GOING INTO !
C!                  *CONSTA*; RETURNS FROM *CONSTA* AS SOLUTION !
C!                  VECTOR CAPITAL-L-SUB-JP, THE CONSTANTS OF !
C!                  INTEGRATION                             !
C!      CBAND( )   MATRIX OF LEFT-HAND SIDE OF THE LINEAR SYSTEM !
C!                  EQ. SC(5), SCALED BY EQ. SC(12); IN BANDED !
C!                  FORM REQUIRED BY LINPACK SOLUTION ROUTINES !
C!      CIJ(IQ,IQ) CAPITAL-C-SUB-IJ IN EQ. SS(5)           !
C!      COSTHP(IU) STORAGE FOR POSITIVE USER-SELECTED ANGLES !
C!                  (EITHER INPUT VALUES OR THE QUADRATURE ANGLES) !

```

```

C!   COSTHW(IU)          STORAGE FOR USER-SELECTED ANGLES (EITHER INPUT !
C!                       VALUES OR THE QUADRATURE ANGLES) !
C!   CP(IQ,IQ)          (ALFA-BETA)*(ALFA+BETA) IN EQ. SS(12) !
C!   DELOMP             = 1, FOR AZIMUTHAL INDEPENDENCE; = 0, OTHERWISE !
C!   FLYR(LC)          TRUNCATED FRACTION IN WISCOMBE DELTA-M METHOD !
C!   GAUPIN(LU,IQ)     AZIMUTHALLY-AVERAGED INTENSITY, I-SUPER-ZERO !
C!                       IN EQ. SD(2) !
C!   GLYRIJ(LC,IQ,IQ)  EIGENVECTORS AT POLAR QUADRATURE ANGLES, !
C!                       LITTLE-G IN EQ. SC(1) !
C!   GLYRMUJ(LC,IU,IQ) EIGENVECTORS INTERPOLATED TO USER POLAR ANGLES !
C!                       ( LITTLE-G IN EQS. SC(3) AND S1(8-9), I.E. !
C!                       CAPITAL-G WITHOUT THE CAPITAL-L FACTOR ) !
C!   GMU(IQ)           ABSCISSAE FOR GAUSS QUADRATURE OVER ANGLE COSINE !
C!   GWT(IQ)           WEIGHTS FOR GAUSS QUADRATURE OVER ANGLE COSINE !
C!   GPLANK            INTEGRATED PLANCK FUNCTION FOR EMISSION FROM !
C!                       BOTTOM BOUNDARY !
C!   IPVT()           INTEGER VECTOR OF PIVOT INDICES FOR LINPACK !
C!   LJLYR(IQ,LC)     CONSTANTS OF INTEGRATION CAPITAL-L IN EQ. SC(1), !
C!                       OBTAINED BY SOLVING SCALED VERSION OF EQ. SC(5) !
C!   NAZ              NUMBER OF AZIMUTHAL COMPONENTS CONSIDERED !
C!   NHOM            DIRECTION OF ILLUMINATION FROM TOP OR BOTTOM !
C!   PKAG(LC)        INTEGRATED PLANCK FUNCTION FOR INTERNAL EMISSION !
C!   PLM0(IQ)        ASSOCIATED LEGENDRE POLYNOMIAL P-SUB-L-SUPER-M !
C!                       AT THE BEAM ANGLE MU-SUB-ZERO IN EQ. SD(9) !
C!   POL(IQ,IQ)       ASSOCIATED LEGENDRE POLYNOMIAL P-SUB-L-SUPER-M !
C!                       AT THE QUADRATURE ANGLES MU-SUB-J IN EQ. SD(8) !
C!   POLM(IQ,IU) &    ASSOCIATED LEGENDRE POLYNOMIALS P-SUB-L-SUPER-M !
C!   POLP(IQ,IU)       AT THE USER ANGLES MU IN EQS. SD(8-9) !
C!   PSI(IQ)          SUM JUST AFTER SQUARE BRACKET IN EQ. SD(9) !
C!   RINTS(M,IU,LU)   FOURIER COMPONENTS OF THE INTENSITY I-SUPER-M !
C!                       IN EQ. SD(2) !
C!   ROOLYRJ(LC,IQ)  EIGENVALUES OF COEFF. MATRIX IN EQ. SS(7) !
C!   ROOT(IQ)        TEMPORARY STORAGE FOR EIGENVALUES OF EQ. SS(12) !
C!                       ON RETURN FROM *EIGRF*, THEN STORED PERMANENTLY !
C!                       IN -ROOLYRJ- !
C!   TAULYR(LC)      CUMULATIVE OPTICAL DEPTH (UN-DELTA-M-SCALED) !
C!   TPLANK          INTEGRATED PLANCK FUNCTION FOR EMISSION FROM !
C!                       TOP BOUNDARY !
C!   TPRLYR(LC)      CUMULATIVE OPTICAL DEPTH (DELTA-M-SCALED) !
C!   WJI(IQ,IQ)      FIRST: EIGENVECTORS [(G+) + (G-)] OF SYSTEM !
C!                       SS(12) ON RETURN FROM *EIGRF*; AUGMENTED BY !
C!                       (G+) & (G-) DERIVED FROM EQS. SS(10-11). !
C!                       THEN, COMPLETE EIGENVECTORS SS(7) ON RETURN !
C!                       FROM *SOLEIG* AND STORED PERMANENTLY IN -GLYRIJ- !
C!   WK(IQ)          SCRATCH ARRAY REQUIRED BY *LEQTLF* !
C!   WKX()          SCRATCH ARRAY REQUIRED BY *EIGRF* !
C!   WX(IQ)          COMPLEX EIGENVALUES OF SYSTEM SS(12) (SEE -ZX-) !
C!   XR0(LC)        X-SUB-ZERO IN EXPANSION OF THERMAL SOURCE FUNC- !
C!                       TION PRECEDING EQ. SS(14) (HAS NO MU-DEPENDENCE) !
C!   XR1(LC)        X-SUB-ONE IN EXPANSION OF THERMAL SOURCE FUNC- !
C!                       TION; SEE EQS. SS(14-16) !

```

```

C!      Z( )          SCRATCH ARRAY USED IN *CONSTA* TO SOLVE A      !
C!      LINEAR SYSTEM FOR THE CONSTANTS OF INTEGRATION      !
C!      Z0(IQ)        SOLUTION VECTORS Z-SUB-ZERO OF EQ. SS(16)    !
C!      Z0MUJ(LC,IU)  Z-SUB-ZERO IN EQ. SS(16) INTERPOLATED TO USER !
C!      ANGLES FROM AN EQUATION DERIVED FROM SS(16)        !
C!      Z1(IQ)        SOLUTION VECTORS Z-SUB-ONE OF EQ. SS(16)    !
C!      Z1MUJ(LC,IU)  Z-SUB-ONE IN EQ. SS(16) INTERPOLATED TO USER !
C!      ANGLES FROM AN EQUATION DERIVED FROM SS(16)        !
C!      ZJ(IQ)        RIGHT-HAND SIDE VECTOR CAPITAL-X-SUB-ZERO IN !
C!      EQ. SS(19), ALSO THE SOLUTION VECTOR CAPITAL        !
C!      -Z-SUB-ZERO AFTER SOLVING THAT SYSTEM              !
C!      ZLYRI(LC,IQ)  PERMANENT STORAGE FOR THE BEAM SOURCE VECTORS !
C!      -ZJ-                                                !
C!      ZLYRI0(LC,IQ) PERMANENT STORAGE FOR THE THERMAL SOURCE    !
C!      VECTORS -Z0- OBTAINED BY SOLVING EQ. SS(16)        !
C!      ZLYRI1(LC,IQ) PERMANENT STORAGE FOR THE THERMAL SOURCE    !
C!      VECTORS -Z1- OBTAINED BY SOLVING EQ. SS(16)        !
C!      ZX(IQ,IQ)     COMPLEX EIGENVECTORS OF SYSTEM SS(12) (THEY ARE !
C!      ACTUALLY REAL BUT *EIGRF* REQUIRES A COMPLEX      !
C!      ARRAY TO RETURN THE EIGENVECTORS SINCE THEY      !
C!      ARE COMPLEX IN THE GENERAL CASE)                   !
C!

```

```

C+-----+
C!      *** DISORT INPUT VARIABLE SPECIFICATIONS ***      !
C+-----+

```

```

CHARACTER*80  HEADER

```

```

LOGICAL DELTAM, NOPLK, ONLYFL, PRNT( 5 ), USRANG, USRTAU
INTEGER IBCND, IPHAS( 1 ), NSTR, NTHETA, NLYR, NPHI, NTAU
REAL      AG, COSTH( 1 ), FBEAM, FISO, GEMI, GTEMP, GG( 1 ),
$      GL( NPFMOM,1 ), OPDEP( 1 ), PHI( 1 ), SSALB( 1 ),
$      TAU( 1 ), TEMPER( 0:1 ), TEMI, TTEMP, WVNML0, WVNMMHI, X0

```

```

C+-----+
C!      *** DISORT INTERNAL VARIABLE SPECIFICATIONS ***    !
C+-----+

```

```

PARAMETER ( NI      = 32 ) ! MAX NO. OF POLAR QUADRATURE ANGLES
PARAMETER ( NLYRI   = 51 ) ! MAX NO. OF COMPUTATIONAL LEVELS
PARAMETER ( NTAUI   = 51 ) ! MAX NO. OF OUTPUT LEVELS
PARAMETER ( NTHETAI = 32 ) ! MAX NO. OF POLAR OUTPUT ANGLES
PARAMETER ( NPHII   = 4  ) ! MAX NO. OF AZIMUTHAL OUTPUT ANGLE
PARAMETER ( NAZZI   = NI-2 ) ! MAX NO. OF TERMS IN FOURIER
PARAMETER ( NINLYRI = NI*NLYRI ) ! EXPANSION OF INTENSITY
PARAMETER ( MI = NI/2, MI9M2 = 9*MI - 2, MI2MI = MI*( 2+MI ) )
PARAMETER ( PI      = 3.1415926535898 )

```

```

C

```

```

INTEGER IPVT( NINLYRI )
COMPLEX WX( MI ), ZX( MI,MI )
REAL      AMB( MI,MI ), APB( MI,MI ), ARRAY( NI,NI ), B( NINLYRI ),
$      CBAND( MI9M2,NINLYRI ), CIJ( NI,NI ), COSTHP( NTHETAI ),
$      COSTHW( NTHETAI ), CP( MI,MI ), FLYR( NLYRI ),
$      GAUPIN( NTAUI,-MI:MI ), GLYRIJ( NLYRI,-MI:MI,-MI:MI ),
$      GLYRMUJ( NLYRI,NTHETAI,-MI:MI ), GMU( NI ), GWT( NI ),

```

```

$      LJLYR( -MI:MI,NLYRI ), PKAG( 0:NLYRI ), PLM0( NI ),
$      POL( NI,NI ), POLM( NI,NTHETA ), POLP( NI,NTHETA ),
$      PSI( NI ), RINTS( NAZZI,NTHETA,NTAU ),
$      ROOLYRJ( NLYRI,-MI:MI ), ROOT( NI ),
$      TAULYR( 0:NLYRI ), TPRLYR( 0:NLYRI ), WJI( NI,NI ),
$      WK( NI ), WKX( MI2MI ), XR0( NLYRI ), XR1( NLYRI ),
$      Z( NINLYRI ), Z0( NI ), ZOMUJ( NLYRI,NTHETA ), Z1( NI ),
$      Z1MUJ( NLYRI,NTHETA ), ZJ( NI ), ZLYRI( NLYRI,-MI:MI ),
$      ZLYRI0( NLYRI,-MI:MI ), ZLYRI1( NLYRI,-MI:MI )
C+-----+
C!      *** DISORT OUTPUT VARIABLE SPECIFICATIONS ***      !
C+-----+
      REAL      FLDIR( NTAUI ), FLDN( NTAUI ), FLUP( NTAUI ),
$      RINTT( NTAUI,NTHETA,NPHI )
C
      LOGICAL      INPERR
      CHARACTER*3  LABPHAS( 5 )
      REAL      HAZLMOM( 49 )
      DATA LABPHAS / 'USR', 'ISO', 'RAY', 'HGR', 'HZL' /
      DATA HAZLMOM / 1.0, 0.804190, 0.646057, 0.481903, 0.358989,
$      0.262966, 0.191905, 0.140808, 0.102725, 0.076044, 0.055940,
$      0.041904, 0.031179, 0.023632, 0.017807, 0.013620, 0.010405,
$      7.9968E-3, 6.2022E-3, 4.7666E-3, 3.7587E-3, 2.8749E-3,
$      2.3077E-3, 1.7493E-3, 1.4303E-3, 1.0708E-3, 8.9191E-4,
$      6.5772E-4, 5.5773E-4, 4.0425E-4, 3.4870E-4, 2.4799E-4,
$      2.1735E-4, 1.5129E-4, 1.3464E-4, 9.1495E-5, 8.2514E-5,
$      5.4396E-5, 4.9488E-5, 3.1083E-5, 2.8321E-5, 1.6194E-5,
$      1.4708E-5, 6.9497E-6, 6.7011E-6, 2.4188E-6, 2.9653E-6,
$      7.8238E-7, 1.3756E-6/
C
      T1 = CPUSECNS(0.0)      ! SET TIMER
C
C+-----+
C!      ZEROAL: CALLS *ZEROIT* TO ZERO ALL GIVEN MATRICES      !
C+-----+
      CALL ZEROAL( AMB, APB, ARRAY, B, CBAND, CIJ, COSTHP, COSTHW,
$      CP, FLYR, GAUPIN, GLYRIJ, GLYRMUJ, GMU, GWT, LJLYR,
$      PKAG, PLM0, POL, POLM, POLP, PSI, RINTS, ROOLYRJ,
$      ROOT, TAULYR, TPRLYR, WJI, WK, WKX, WX, XR0, XR1,
$      Z, Z0, Z1, ZJ, ZLYRI, ZLYRI0, ZLYRI1, ZOMUJ,
$      Z1MUJ, ZX, MI, MI2MI, MI9M2, NAZZI, NI, NINLYRI,
$      NLYRI, NTAUI, NTHETA )
C
      FBEAM = FBEAM / PI      ! CHANGE TO INTENSITY UNIT
      M      = NSTR / 2
      NHOM  = 1      ! FROM TOP (SEE DO-500)
      IF ( IBCND.EQ.1 ) THEN
          NHOM = 2      ! FROM TOP AND BOTTOM (SEE DO-500)
          X0  = 1.0      ! PREVENT OVERFLOW IN DIVIDES BY -X0-
      END IF
C

```

```

TAULYR( 0 ) = 0.
DO 10  LYR = 1, NLYR
    TAULYR(LYR) = TAULYR(LYR-1) + OPDEP(LYR)
10 CONTINUE
C
IF ( .NOT.USRTAU ) THEN      !  CALCULATE FLUXES etc. AT EACH -LC-
    NTAU = NLYR + 1
    DO 20  LC = 0, NTAU-1
        TAU(LC+1) = TAULYR(LC)
20 CONTINUE
    END IF
C
C+-----+
C!      DOUBLE GAUSSIAN QUADRATURE POINTS AND WEIGHTS ARE CONSTRUCTED !
C!      FROM THE ORDINARY GAUSSIAN QUADRATURE RULE FOR INTERVAL (0,1)..!
C!      NEGATIVE POINTS AND ASSOCIATED WEIGHTS ARE STORED IN I > M.    !
C+-----+
CALL  QGAUSN( GWT, GMU, M )
DO 30  I = 1, M
    GMU(I+M) = - GMU(I)
    GWT(I+M) =  GWT(I)
30 CONTINUE
C
IF ( USRANG ) THEN          !  SPECIFY POLAR OUTPUT ANGLES
    DO 40  I = 1, NTHETA
        COSTHW(I) = COSTH(I)
        COSTHP(I) = ABS( COSTHW(I) )
40 CONTINUE
    ELSE                      !  SET QUADRATURE OUTPUT ANGLES
        NTHETA = NSTR
        DO 50  I = 1, NSTR
            IF ( I.LE.M ) COSTHW(I) = GMU(NSTR-I+1)
            IF ( I.GT.M ) COSTHW(I) = GMU(I-M)
            COSTHP(I) = ABS( COSTHW(I) )
50 CONTINUE
        END IF
C
IF ( .NOT.NOPLK ) THEN      !  CALCULATE PLANCK FUNCTIONS
    DO 60  LEV = 0, NLYR
        PKAG( LEV ) = PLKAVG( WVNML0, WVNMHI, TEMPER(LEV) )
60 CONTINUE
        GPLANK = GEMI * PLKAVG( WVNML0, WVNMHI, GTEMP )
        TPLANK = TEMI * PLKAVG( WVNML0, WVNMHI, TTEMP )
    END IF
C
C+-----+
C!      CHEKIN: CHECKS INPUT DIMENSIONS AND VARIABLES                      !
C+-----+
CALL  CHEKIN( AG, COSTH, FBEAM, FISO, GEMI, GG, GTEMP,
$      IBCND, INPERR, IPHAS, NI, NLYRI, NLYR, NOPLK,
$      NPFMOM, NPHI, NPHII, NSTR, NTAU, NTAUI, NTHETA,

```

```

$           NTHETA, OPDEP, PHI, SSALB, TAU, TAULYR, TEMI,
$           TEMPER, TTEMP, USRANG, USRTAU, WVMNHI, WVMNLO, X0 )
C
IF ( PRNT(1) ) THEN      ! PRINT OUT INPUT INFORMATION
      WRITE( 6,1001 )  HEADER
      WRITE( 6,1002 )  NSTR, NLYR
      IF ( USRTAU ) WRITE( 6,1003 ) NTAU, ( TAU(LU), LU = 1, NTAU )
      IF ( USRANG ) WRITE( 6,1004 ) NTHETA, (COSTH(IU), IU = 1, NTHETA)
      IF ( NPHI.GT.0 ) WRITE( 6,1005 ) NPHI, ( PHI(J), J = 1, NPHI)
      IF ( IBCND.EQ.0 ) WRITE( 6,1006 ) FBEAM, X0, FISO
      IF ( IBCND.EQ.1 ) WRITE( 6,1007 ) FISO
      WRITE( 6,1010 )  AG, GEMI, TEMI
      IF ( DELTAM ) WRITE( 6,1012 )
      IF ( .NOT.DELTAM ) WRITE( 6,1013 )
      IF ( ONLYFL ) WRITE( 6,1015 )
      IF ( .NOT.ONLYFL ) WRITE( 6,1016 )
      IF ( .NOT.NOPLK ) WRITE( 6,1018 ) WVMNLO, WVMNHI, GTEMP, TTEMP
      WRITE ( 6,1030 ) ' QUAD. PTS. ', ( GMU(I), I = 1, NSTR )
      WRITE ( 6,1030 ) ' QUAD. WTS. ', ( GWT(I), I = 1, NSTR )
END IF
C
C+-----+
C!           DO-600 LOOP OVER AZIMUTHAL COMPONENT 'M' (NAZ)           !
C+-----+
      NAZ = MAX0( 1, NSTR-2 ) ! SET MAX. NUMBER OF INTEGRATION
      IF ( FBEAM.EQ.0.0 .OR. ONLYFL .OR.
$           IBCND.EQ.1 .OR. 1.-X0.LT.1.E-5 ) THEN
      NAZ = 1 ! AZIMUTH-INDEPENDENT CASE
      NPHI = 1
      PHI(1) = 0.0
      END IF
C
      DO 600 LAZI = 1, NAZ
      MAZ = LAZI - 1
      MP = LAZI
C
C+-----+
C!           LEPLY: EVALUATES ASSOCIATED LEGENDRE POLYNOMIALS           !
C+-----+
      CALL LEPOLY( POL, GMU, M, MAZ, NI, NSTR ) ! FOR QUADRATURE
      SGN0 = (-1)**(MP+MAZ)
      SGN = SGN0
      DO 80 L = MP, NSTR
      SGN = - SGN
      DO 80 K = 1, M
      POL(L,K+M) = SGN * POL(L,K)
80 CONTINUE
C
      CALL LEPOLY( PLM0, X0, 1, MAZ, NI, NSTR ) ! FOR INCIDENT BEAM
      SGN = SGN0
      DO 90 L = MP, NSTR

```

```

      SGN = - SGN
      PLM0(L) = SGN*PLM0(L)
90    CONTINUE
C
      IF ( .NOT.ONLYFL ) THEN                ! FOR USER INTENSITY
      CALL LEPOLY( POLP, COSTHP, NTHETA, MAZ, NI, NSTR )
      SGN = SGN0
      DO 100 L = MP, NSTR
      SGN = - SGN
      DO 100 K = 1, NTHETA
      POLM(L,K) = SGN * POLP(L,K)
100   CONTINUE
      END IF
C
C+-----+
C!           DO-400 LOOP OVER COMPUTATIONAL LAYERS           !
C+-----+
      TPRLYR(0) = 0.
      IF ( MAZ.EQ.0 .AND. PRNT(1) ) WRITE ( 6,1050 )
C
      DO 400 LYR = 1,NLYR
      OMEGA = SSALB(LYR)
      TSTAR = TAULYR(LYR)-TAULYR(LYR-1)
C
      GL(1,LYR) = 1.0                        ! ZERO MOMENT OF PHASE FUNC.
      IF ( IPHAS(LYR).GT.0 ) THEN           ! START FROM ISOTROPIC
      DO 110 K = 2, NSTR+1
      GL(K,LYR) = 0.0
110   CONTINUE
      END IF
C
      IF ( IPHAS(LYR).EQ.2 ) THEN           ! RAYLEIGH
      GL(3,LYR) = 0.1
      ELSE IF ( IPHAS(LYR).EQ.3 ) THEN     ! HENYEY-GREENSTEIN
      DO 120 K = 2, NSTR+1
      GL(K,LYR) = GG(LYR)**(K-1)
120   CONTINUE
      ELSE IF ( IPHAS(LYR).EQ.4 ) THEN     ! HAZE-L
      DO 130 K = 2, MIN0(49,NSTR+1)
      GL(K,LYR) = HAZLMOM(K)
130   CONTINUE
      END IF
C
      ASYMM = GL( 2,LYR )
C
C+-----+
C!           DO DELTA-M TRANSFORMATION IF( DELTAM )           !
C!           cf. Wiscombe, W.J., 1977, J. Atmos. Sci., 34, 4108-1422.   !
C+-----+
      F = 0.0
      IF ( DELTAM ) F = GL( NSTR+1,LYR )

```

```

OPRIM = OMEGA * ( 1.-F ) / ( 1.-F*OMEGA )
FLYR(LYR) = F
TSTPR = ( 1.-OMEGA*FLYR(LYR) ) * TSTAR
TPRLYR(LYR) = TPRLYR(LYR-1) + TSTPR
DO 140 K = 1, NSTR
    GL(K,LYR) = ( 2*K-1 ) * OPRIM * ( GL(K,LYR)-F ) / ( 1.-F )
140 CONTINUE
C
IF ( MAZ.EQ.0 .AND. PRNT(1) ) THEN
    WRITE ( 6,1060 ) LYR, TSTAR, TAULYR(LYR), OMEGA, F, TSTPR,
$         TPRLYR(LYR), OPRIM, LABPHAS( IPHAS(LYR)+1 ),
$         ASYMM, TEMPER(LYR-1)
END IF
C
C+-----+
C!          SOLEIG: SOLVES EIGENFUNCTION PROBLEMS IN EQS. SS(6-12)          !
C+-----+
CALL SOLEIG( AMB, APB, ARRAY, CIJ, CP, GL(1,LYR), GMU, GWT, MI,
$           MP, NI, NSTR, POL, ROOT, WJI, WKX, WX, ZX )
C
C+-----+
C!          SAVE ROOTS FOR EACH LAYER IN -ROOLYRJ- PERMANENTLY.          !
C!          SAVE EIGENVECTORS FOR EACH AZIMUTH COMPONENT -MP- IN          !
C!          -GLYRIJ- PERMANENTLY FOR LATER USE (i.e., IN *CONSTA*,          !
C!          *FLUXES*, AND *USRINT*), AND KEEP PRESENT SET IN -WJI-          !
C!          FOR USE IN EQ. SD(8) IF ( .NOT.ONLYFL ).                      !
C+-----+
DO 150 I = 1, NSTR
    IF ( I.LE.M ) THEN
        ROOLYRJ(LYR, I) = ROOT(I)
    ELSE
        ROOLYRJ(LYR, -I+M) = ROOT(I)
    END IF
150 CONTINUE
C
DO 160 I = 1, M
    DO 160 J = 1, M
        GLYRIJ(LYR, I, J) = WJI(I, J)
        GLYRIJ(LYR, -I, J) = WJI(I+M, J)
        GLYRIJ(LYR, I, -J) = WJI(I, J+M)
        GLYRIJ(LYR, -I, -J) = WJI(I+M, J+M)
160 CONTINUE
C
C+-----+
C!          IPBEAM & IPISOT CALCULATE THE PARTICULAR SOLUTIONS OF          !
C!          EQ. SS(18) & SS(15), RESPECTIVELY.                            !
C+-----+
IF( IBCND.EQ.0 ) THEN          ! GENERAL ILLUMINATION FROM TOP
C
CALL IPBEAM( ARRAY, CIJ, FBEAM, GL(1,LYR), GMU, MP,
$           NI, NSTR, PLM0, POL, WK, X0, ZJ )

```



```

DO 170 I = 1, NSTR
  IF( I.LE.M ) THEN
    ZLYRI(LYR, I) = ZJ(I)
  ELSE
    ZLYRI(LYR, -I+M) = ZJ(I)
  END IF
170 CONTINUE
C
IF ( .NOT.NOPLK ) THEN
  XR1(LYR) = ( PKAG(LYR) - PKAG(LYR-1) ) / TSTPR
  XR0(LYR) = PKAG(LYR-1) - XR1(LYR)*TPRLYR(LYR-1)
C
CALL IPISOT( ARRAY, CIJ, GMU, NI, NSTR, OPRIM, WK,
$           XR0(LYR), XR1(LYR), Z0, Z1 )
DO 180 I = 1, NSTR
  IF( I.LE.M ) THEN
    ZLYRIO(LYR,I) = Z0(I)
    ZLYRII(LYR,I) = Z1(I)
  ELSE
    ZLYRIO(LYR, -I+M) = Z0(I)
    ZLYRII(LYR, -I+M) = Z1(I)
  END IF
180 CONTINUE
END IF
C
ELSE IF ( IBCND.EQ.1 ) THEN      ! ISOTROPIC ILLUMINATION (IF ANY)
  DO 190 J = - M, M
    ZLYRI(LYR,J) = 0.0
190 CONTINUE
END IF
C
IF ( .NOT.ONLYFL ) THEN      ! FOR USER INTENSITY COMPUTATION
C+-----+
C!          INTERP: INTERPOLATES EIGENVECTORS IN EQS. SD(8-9)      !
C!          AND FIRST COMPONENT OF THERMAL SOURCE SS(16)          !
C+-----+
CALL INTERP( ARRAY, COSTHW, FBEAM, GL(1,LYR), GWT, IBCND,
$           MP, NI, NOPLK, NSTR, NTHETA, OPRIM, PLM0, POL,
$           POLM, POLP, PSI, ROOT, USRANG, WJI, X0, XR0,
$           XR1, Z0, ZJ)
C
C+-----+
C!          STORE EIGENVECTORS OF EQ. SD(8) IN -GLYRMUJ- PERMANENTLY.  !
C!          THE INHOMOGENEOUS BEAM SOURCE TERMS OF EQ. SD(9) STORE IN  !
C!          GLYRMUJ(LYR,J,0) AND THERMAL SOURCE TERMS OF EQ. SS(16) IN  !
C!          Z0MUJ(LYR,K) & Z1MUJ(LYR,K).                               !
C+-----+
DO 300 I =1, NTHETA
  DO 300 J=1, M
    GLYRMUJ(LYR,I,-J) = WJI(I,J )
    GLYRMUJ(LYR,I,+J) = WJI(I,J+M)

```

```

300      CONTINUE
        IF ( IBCND.EQ.0 ) THEN          ! GENERAL ILLUMINATION FROM TOP
          DO 310 K = 1, NTHETA
            GLYRMUJ(LYR,K,0) = ARRAY(1,K)
310      CONTINUE
          IF ( (.NOT. NOPLK) .AND. (MP.EQ.1) ) THEN ! THERMAL SOURCE
            DO 320 K = 1, NTHETA
              Z1MUJ(LYR,K) = ZLYR11(LYR,1)
              Z0MUJ(LYR,K) = ARRAY(2,K)
320      CONTINUE
            END IF
          ELSE IF ( IBCND.EQ.1 ) THEN ! ISOTROPIC ILLUMINATION (IF ANY)
            DO 330 K = 1, NTHETA
              GLYRMUJ(LYR,K,0) = 0.0
330      CONTINUE
            END IF
          END IF
        END IF
400      CONTINUE          ! END OF LOOP OVER LAYERS
C
      IF ( MAZ.EQ.0 .AND. PRNT(1) ) WRITE( 6,1080 ) TEMPER(NLYR)
C
C+-----+
C!      DO-500 LOOP OVER DIRECTIONS OF ILLUMINATION          !
C+-----+
      DO 500 IHOM = 1, NHOM
C
C+-----+
C!      CONSTA: CALCULATES CONSTANTS OF INTEGRATION i.e.,SS(13) !
C+-----+
      CALL CONSTA( AG, B, CBAND, FBEAM, FISO, GLYRIJ, GMU, GPLANK,
$              GWT, IBCND, IHOM, IPVT, M, MI, MI9M2, NLYR,
$              NLYRI, NSTR, ROOLYRJ, TPLANK, TPRLYR, X0, Z,
$              ZLYRI, ZLYRI0, ZLYRI1 )
C
      DO 420 K = 1, NLYR
        IPNT = K*NSTR - M
        DO 420 J = 1, M
          LJLYR(-J,K) = B(IPNT+1-J)
          LJLYR( J,K) = B(IPNT+J)
420      CONTINUE
C
C+-----+
C!      FLUXES: COMPUTES UPWARD AND DOWNWARD FLUXES          !
C+-----+
      IF ( MAZ.EQ.0 ) THEN
        CALL FLUXES( FBEAM, FLYR, GLYRIJ, GMU, GWT, IBCND, LJLYR,
$              M, MI, NLYR, NLYRI, NTAU, PRNT, ROOLYRJ,
$              SSALB, TAU, TAULYR, TPRLYR, X0, XR0, XR1,
$              ZLYRI, ZLYRI0, ZLYRI1,
$              GAUPIN, FLDIR, FLDN, FLUP )
      END IF

```

```

C
      IF ( ONLYFL ) GO TO 600
C+-----+
C!          USRINT: COMPUTES USER INTENSITIES IN EQS. SS(27-29)      !
C+-----+
      CALL USRINT( AG, COSTHW, FBEAM, FLYR, GLYRIJ, GLYRMUJ, GMU,
$           GPLANK, GWT, IBCND, LJLYR, M, MI, MP, NAZZI,
$           NLYR, NLYRI, NTAU, NTAUI, NTHETA, NTHETAI,
$           RINTS, ROOLYRJ, SSALB, TAU, TAULYR, TPRLYR, X0,
$           Z0MUJ, Z1MUJ, ZLYRI, ZLYRIO, ZLYRIL )
C
      IF ( NHOM.EQ.2 ) THEN
          DO 440 IOL = 1, NTAU, NTAU-1
          DO 440 IOM = 1, NTHETA
              WRITE (6,1100) TAU(IOL), COSTHW(IOM), RINTS(1,IOM,IOL)
440      CONTINUE
          END IF
500 CONTINUE
600 CONTINUE          ! END LOOP ON AZIMUTHAL COMPONENTS
C
C+-----+
C!          INTSUM: CALCULATES INTENSITY BY SUMMING FOURIER COSINE  !
C!          SERIES OVER ALL AZIMUTHAL COMPONENTS IN EQ. SD(2)!
C+-----+
      IF ( .NOT.( IBCND.EQ.1 .OR. ONLYFL ) )
$ CALL INTSUM( COSTHW, NAZ, NAZZI, NPHI, NTAU, NTAUI, NTHETA,
$           NTHETAI, PHI, PRNT, RINTS, TAU, RINTT )
C
      ET = CPUSECND(T1)          ! FIND END TIME
      WRITE (6,1110) ET
C
1001 FORMAT ( ///, ' ++++++ VERSION 7/85: DISCRETE ORDINATE ',
$ ' RADIATIVE TRANSFER PROGRAM ++++++', //, 1X, A )
1002 FORMAT( /, ' NO. STREAMS =', I4, ' NO. COMPUTATIONAL LAYERS =',
$ I4 )
1003 FORMAT( I4, ' USER LEVELS AT OPTICAL DEPTHS :', /, (10X,10F10.4) )
1004 FORMAT( I4, ' USER POLAR ANGLES WITH COSINES :', /, (10X,10F10.4) )
1005 FORMAT( I4, ' USER AZIMUTHAL ANGLES :', 10F8.2, /, (29X,10F8.2) )
1006 FORMAT( ' INCIDENT BEAM WITH INTENSITY =', 1PE11.3, ' AND ',
$ ' POLAR ANGLE COSINE =', 0PF8.4, ' PLUS ISOTROPIC INCIDENT',
$ ' INTENSITY =', 1PE11.3 )
1007 FORMAT( ' ISOTROPIC ILLUMINATION FROM TOP AND BOTTOM OF',
$ ' INTENSITY =', 1PE11.3 )
1010 FORMAT( /, ' SURFACE ALBEDO =', 0PF8.4, ' SURFACE EMISSIVITY =',
$ F8.4, ' TOP EMISSIVITY =', F8.4 )
1012 FORMAT( ' USES DELTA-M METHOD' )
1013 FORMAT( ' DOES NOT USE DELTA-M METHOD' )
1015 FORMAT( ' CALCULATE FLUXES ONLY' )
1016 FORMAT( ' CALCULATE FLUXES AND INTENSITIES' )
1018 FORMAT( ' THERMAL EMISSION IN WAVENUMBER INTERVAL :', 2F11.3,
$ ' SURFACE TEMPERATURE =', F8.2, ' TOP TEMPERATURE =',

```

```

$ F8.2 )
1030 FORMAT (A13,10F7.3/(13X,10F7.3))
1050 FORMAT( /, 37X, '<----- DELTA-M ----->', /,
$ 19X, 'TOTAL SINGLE', 27X, 'TOTAL SINGLE PHASE', /,
$ 7X, 'OPTICAL OPTICAL SCATTER TRUNCATED OPTICAL ',
$ 'OPTICAL SCATTER FUNCTION ASYMM', /,
$ 9X, 'DEPTH DEPTH ALBEDO FRACTION DEPTH ',
$ 'DEPTH ALBEDO TYPE FACTOR TEMPERATURE', / )
1060 FORMAT( I4, 2F10.4, F10.5, F12.5, 2F10.4, F10.5, A11, F9.4,F14.3 )
1080 FORMAT( 96X, F14.3 )
1100 FORMAT( 20X, 'INTEN(' , F5.3, ', ', F6.3, ') =', 1PE12.3 )
1110 FORMAT ( //, ' DISORT EXECUTION TIME =', F8.3, ' SECONDS' )
C
RETURN
END
C***** END OF DISORT *****
C*****

```

```

SUBROUTINE CHEKIN( AG, COSTH, FBEAM, FISO, GEMI, GG, GTEMP,
$ IBCND, INPERR, IPHAS, NI, NLYRI, NLYR, NOPLK,
$ NPFMOM, NPFI, NPFI, NSTR, NTAU, NTAUI,
$ NTHETA, NTHETA, OPDEP, PHI, SSALB, TAU,
$ TAULYR, TEMI, TEMPER, TTEMP, USRANG, USRTAU,
$ WVMHI, WVMLO, X0 )
C+-----+
C!          CHECKS THE INPUT DIMENSIONS AND VARIABLES          !
C+-----+
LOGICAL  INPERR, NOPLK, USRANG, USRTAU
INTEGER  IPHAS( 1 )
REAL     COSTH( 1 ), GG( 1 ), OPDEP( 1 ), PHI( 1 ), SSALB( 1 ),
$        TAU( 1 ), TAULYR( 0:1 ), TEMPER( 0:1 )
C
IF ( NSTR.LT.2 .OR. NSTR.GT.NI .OR. MOD(NSTR,2).NE.0 )
$   CALL WRTBAD( 6, 'NSTR      ', INPERR )
IF ( NPFMOM.LT.NSTR+1 )
$   CALL WRTBAD( 6, ' NPFMOM  ', INPERR )
IF ( NLYR.LT.1 .OR. NLYR.GT.NLYRI )
$   CALL WRTBAD( 6, 'NLYR      ', INPERR )
C
IF ( USRANG ) THEN
IF ( NTHETA.LT.0 .OR. NTHETA.GT.NTHETA )
$   CALL WRTBAD( 6, 'NTHETA  ', INPERR )
DO 10 IU = 1, NTHETA
IF ( COSTH(IU).LT.-1.0 .OR. COSTH(IU).GT.1.0
$   .OR. COSTH(IU).EQ.0.0 )
$   CALL WRTBAD( 6, 'COSTH    ', INPERR )
IF ( IU.GT.1 .AND. ( COSTH(IU).LT.COSTH(IU-1) ) )
$   CALL WRTBAD( 6, 'COSTH    ', INPERR )
10 CONTINUE
END IF
C
IF ( NPFI.LT.0 .OR. NPFI.GT.NPFI )
$   CALL WRTBAD( 6, 'NPFI      ', INPERR )
IF ( NPFI.GT.0 ) THEN
DO 20 J = 1, NPFI
IF ( PHI(J).LT.0.0 .OR. PHI(J).GT.360.0 )
$   CALL WRTBAD( 6, 'PHI      ', INPERR )
20 CONTINUE
END IF
C
IF ( USRTAU ) THEN
IF ( NTAU.LT.1 .OR. NTAU.GT.NTAUI )
$   CALL WRTBAD( 6, 'NTAU      ', INPERR )
DO 30 LU = 1, NTAU
IF ( TAU(LU).LT.0.0 .OR. TAU(LU).GT.TAULYR(NLYR) )
$   CALL WRTBAD( 6, 'TAU      ', INPERR )
30 CONTINUE
END IF
C

```

```

IF ( IBCND.LT.0 .OR. IBCND.GT.1 )
$   CALL WRTBAD( 6, 'IBCND  ', INPERR )
IF ( IBCND.EQ.0 ) THEN
  IF ( X0.LE.0.0 .OR. X0.GT.1.0 )
$   CALL WRTBAD( 6, 'X0      ', INPERR )
  IF ( FBEAM.LT.0.0 ) CALL WRTBAD( 6, 'FBEAM ', INPERR )
END IF
IF ( AG.LT.0.0 .OR. AG.GT.1.0 )
$   CALL WRTBAD( 6, 'AG      ', INPERR )
IF ( FISO.LT.0.0 )   CALL WRTBAD( 6, 'FISO   ', INPERR )
C
IF ( .NOT.NOPLK ) THEN
  IF ( WVNML0.LT.0.0 .OR. WVNML1.LE.WVNML0 )
$   CALL WRTBAD( 6, 'WVNML,H ', INPERR )
  IF ( GEMI.LT.0.0 .OR. GEMI.GT.1.0 )
$   CALL WRTBAD( 6, 'GEMI    ', INPERR )
  IF ( TEMI.LT.0.0 .OR. TEMI.GT.1.0 )
$   CALL WRTBAD( 6, 'TEMI    ', INPERR )
  IF ( GTEMP.LT.0.0 ) CALL WRTBAD( 6, 'GTEMP   ', INPERR )
  IF ( TTEMP.LT.0.0 ) CALL WRTBAD( 6, 'TTEMP   ', INPERR )
END IF
C
DO 40 LC = 1, NLYR
  IF ( OPDEP(LC).LE.0.0 )
$   CALL WRTBAD( 6, 'OPDEP  ', INPERR )
  IF ( SSALB(LC).LT.0.0 .OR. SSALB(LC).GT.1.0 )
$   CALL WRTBAD( 6, 'SSALB  ', INPERR )
  IF ( .NOT.NOPLK .AND. ( TEMPER(LC).LT.0.0 ) )
$   CALL WRTBAD( 6, 'TEMPER ', INPERR )
  IF ( IPHAS(LC).LT.0 .OR. IPHAS(LC).GT.4 )
$   CALL WRTBAD( 6, 'IPHAS  ', INPERR )
  IF ( IPHAS(LC).EQ.3 .AND. ( GG(LC).LT.-1.0 .OR.
$   GG(LC).GT.1.0 ) )
$   CALL WRTBAD( 6, 'GG      ', INPERR )
40 CONTINUE
C
IF ( INPERR ) CALL ERRMSG( 'DISORT--INPUT ERRORS      ', .TRUE. )
C
RETURN
END
C***** END OF CHEKIN *****
C*****

```

```

SUBROUTINE CONSTA( AG, B, CBAND, FBEAM, FISO, GLYRIJ, GMU,
$                GPLANK, GWT, IBCND, IHOM, IPVT, M, MI, MI9M2,
$                NLYR, NLYRI, NSTR, ROOLYRJ, TPLANK, TPRLYR,
$                X0, Z, ZLYRI, ZLYRI0, ZLYRI1 )

```

```

C+-----+
C!          CALCULATES THE CONSTANTS OF INTEGRATION IN EQ. SC(12)          !
C+-----+
C!          I N P U T                V A R I A B L E S:                !
C+-----+
C!          AG          :  SURFACE ALBEDO                                !
C!          CBAND       :  LEFT-HAND SIDE MATRIX OF LINEAR SYSTEM EQ. SC(5), !
C!                    :  SCALED BY EQ. SC(12); IN BANDED FORM REQUIRED      !
C!                    :  BY LINPACK SOLUTION ROUTINES                    !
C!          FBEAM       :  INTENSITY OF INCIDENT BEAM (IBCND=0 ONLY)      !
C!          FISO        :  INTENSITY OF ISOTROPIC ILLUMINATION (IBCND=0 OR 1)!
C!          GLYRIJ      :  EIGENVECTORS AT POLAR QUADRATURE ANGLES, SC(1)  !
C!          GMU         :  ABSCISSAE FOR GAUSS QUADRATURE OVER ANGLE COSINE !
C!          GPLANK      :  INTEGRATED PLANCK FUNCTION FOR EMISSION FROM    !
C!                    :  BOTTOM BOUNDARY                                  !
C!          GWT        :  WEIGHTS FOR GAUSS QUADRATURE OVER ANGLE COSINE   !
C!          IBCND       :  BOUNDARY CONDITIONS (0, PARALLEL BEAM FROM TOP;  !
C!                    :  1, ISOTROPIC ILLUMINATION FROM TOP AND BOTTOM)    !
C!          IHOM       :  DIRECTION OF ILLUMINATION FROM TOP OR BOTTOM     !
C!          M          :  ORDER OF DOUBLE-GAUSS QUADRATURE (NSTR/2)       !
C!          MI         :  INITIAL DIMENSION (i.e., -GLYRIJ- )             !
C!          MI9M2      :  INITIAL DIMENSION (i.e., -CBAND-, -Z- )         !
C!          NLYR       :  TOTAL NUMBER OF COMPUTATIONAL LAYERS            !
C!          NLYRI      :  INITIAL DIMENSION OF COMPUTATIONAL LAYERS       !
C!          NSTR       :  NUMBER OF POLAR QUADRATURE ANGLES                !
C!          ROOLYRJ    :  EIGENVALUES OF COEFF. MATRIX IN EQ. SS(7)       !
C!          TPLANK     :  INTEGRATED PLANCK FUNCTION FOR EMISSION FROM    !
C!                    :  TOP BOUNDARY                                     !
C!          TPRLYR     :  CUMULATIVE OPTICAL DEPTH (DELTA-M-SCALED)       !
C!          X0         :  POLAR ANGLE COSINE OF INCIDENT BEAM (IBCND=0 ONLY)!
C!          ZLYRI      :  BEAM SOURCE VECTORS IN EQ. SS(19)               !
C!          ZLYRI0     :  THERMAL SOURCE VECTORS -Z0-, BY SOLVING EQ. SS(16)!
C!          ZLYRI1     :  THERMAL SOURCE VECTORS -Z1-, BY SOLVING EQ. SS(16)!
C+-----+
C!          O U T P U T                V A R I A B L E S:                !
C+-----+
C!          B          :  RIGHT-HAND SIDE VECTOR OF EQ. SC(5) GOING INTO   !
C!                    :  *SGBSL*; RETURNS AS SOLUTION VECTOR OF EQ. SC(12), !
C!                    :  CONSTANTS OF INTEGRATION WITHOUT EXPONENTIAL TERM !
C+-----+
C!          I N T E R N A L            V A R I A B L E S:                !
C+-----+
C!          IPVT       :  INTEGER VECTOR OF PIVOT INDICES                  !
C!          IROW       :  POINTS TO ROW IN -CBAND-                        !
C!          IT         :  POINTER FOR -B- POSITION                          !
C!          JCOL       :  POINTS TO POSITION IN LAYER BLOCK                 !
C!          NCD        :  NUMBER OF CODIAGONALS                            !

```

```

C!      NCOL      :   COUNTS OF COLUMNS IN -CBAND-           !
C!      LDA       :   ROW DIMENSION OF -CBAND-               !
C!      NSHIFT    :   FOR POSITIONING NUMBER OF ROWS IN BAND STORAGE !
C!      RCOND     :   INDICATOR OF SINGULARITY FOR -CBAND-   !
C!      Z         :   SCRATCH ARRAY REQUIRED BY *SGBCO*       !
C+-----+
      INTEGER IPVT(1)
      REAL      B( 1 ), CBAND( MI9M2,1 ), GLYRIJ( NLYRI,-MI:MI,-MI:MI ),
$             GMU( 1 ), GWT( 1 ), ROOLYRJ( NLYRI,-MI:MI ),
$             TPRLYR( 0:NLYRI ), Z( 1 ), ZLYRI( NLYRI,-MI:MI ),
$             ZLYRI0( NLYRI,-MI:MI ), ZLYRI1( NLYRI,-MI:MI )
C
      IF ( IHOM.EQ.2 ) GO TO 100
C
      NCD = 3*M - 1
      LDA = 3*NCD + 1
      NSHIFT = LDA - 2*NSTR + 1
      NCOL = 0
C
C+-----+
C!      FIRST: USES CONTINUITY CONDITIONS OF EQS. SC(4b & 5b) AND !
C!      SCALING SCHEME OF EQ. SC(12) TO FORM COEFFICIENT !
C!      MATRIX, i.e. SC(7), AND STORE IN BAND FORM IN -CBAND- !
C+-----+
      DO 30 K = 1, NLYR
      DTAU = TPRLYR(K) - TPRLYR(K-1)
      JCOL = 0
      DO 20 J = - M, M
      IF ( J.EQ.0 ) GO TO 20
      NCOL = NCOL+1
      EXPA = EXP( - ABS( ROOLYRJ(K,J) * DTAU ) )
      IROW = NSHIFT-JCOL
      DO 10 I = - M, M
      IF ( I.EQ.0 ) GO TO 10
      IF ( J.GT.0 ) THEN
      CBAND(IROW+NSTR,NCOL) = GLYRIJ(K,I,J)*EXPA
      CBAND(IROW,          NCOL) = - GLYRIJ(K,I,J)
      ELSE
      CBAND(IROW+NSTR,NCOL) = GLYRIJ(K,I,J)
      CBAND(IROW,          NCOL) = - GLYRIJ(K,I,J)*EXPA
      END IF
      IROW = IROW + 1
10      CONTINUE
      JCOL = JCOL + 1
20      CONTINUE
30      CONTINUE
C
C+-----+
C!      SECOND: USE TOP BOUNDARY CONDITIONS OF EQS. SC(4a & 5a) !
C!      FOR LAYER 1 WITH PROPER COEFFICIENTS Gij'S !
C+-----+

```



```

JCOL = 0
DO 50 J = - M, M
  IF ( J.EQ.0 ) GO TO 50
  IF ( J.LT.0 ) EX = EXP( ROOLYRJ(1,J) * TPRLYR(1) )
  IROW = NSHIFT-JCOL+M
  DO 40 I = 1, M
    IF ( J.GT.0 ) THEN
      CBAND(IROW,JCOL+1) = GLYRIJ(1,-I,J)
    ELSE
      CBAND(IROW,JCOL+1) = GLYRIJ(1,-I,J) * EX
    END IF
    IROW = IROW+1
40  CONTINUE
    JCOL = JCOL+1
50  CONTINUE
C
C+-----+
C!      THIRD: USE BOTTOM CONDITIONS OF EQS. SC(4c & 5c), INCLUDING !
C!      SURFACE REFLECTION IN LAST LAYER !
C+-----+
NNCOL = NCOL - NSTR
JCOL = 0
DO 80 J = - M, M
  IF ( J.EQ.0 ) GO TO 80
  NNCOL = NNCOL + 1
  IF ( J.GT.0 ) EX = EXP(- ROOLYRJ(NLYR,J) * DTAU )
  SUM = 0.0
  DO 60 K = 1, M
    SUM = SUM + GWT(K) * GMU(K) * GLYRIJ(NLYR,-K,J)
60  CONTINUE
    SUM = 2.0 * AG * SUM
    IROW = NSHIFT - JCOL + NSTR
    DO 70 I = 1, M
      IF ( J.GT.0 ) THEN
        CBAND(IROW,NNCOL) = ( GLYRIJ(NLYR,I,J) - SUM ) * EX
      ELSE
        CBAND(IROW,NNCOL) = ( GLYRIJ(NLYR,I,J) - SUM )
      END IF
      IROW = IROW + 1
70  CONTINUE
    JCOL = JCOL + 1
80  CONTINUE
C
C+-----+
C!      SPECTICAL CASE: !
C!      CONSTRUCT RIGHT-HAND SIDE VECTOR -B- FOR ISOTROPIC INCIDENCE !
C!      AND CALL LINPACK ROUTINES *SGBCO* & *SGBSL* (SEE BELOW) !
C+-----+
C
100 CONTINUE
    CALL ZEROIT( B, NCOL )

```

```

C
  IF ( IBCND.EQ.1 ) THEN
    IF ( IHOM.EQ.2 ) THEN
      CALL ZEROIT( B, M )
      DO 110 I = 1, M
        B(NCOL-M+I) = FISO
110      CONTINUE
    ELSE IF ( IHOM.EQ.1 ) THEN
      CALL ZEROIT( B(NCOL-M+1), M )
      DO 120 I = 1, M
        B(I) = FISO
120      CONTINUE
      RCOND = 0.0
      CALL SGBCO( CBAND, MI9M2, NCOL, NCD, NCD, IPVT, RCOND, Z )
      IF ( 1.0+RCOND .EQ. 1.0 ) CALL ERRMSG
$      ( 'CONSTA--SGBCO SAYS MATRIX NEAR SINGULAR', .FALSE. )
    END IF
    CALL SGBSL( CBAND, MI9M2, NCOL, NCD, NCD, IPVT, B, 0 )
C
  RETURN
C
END IF
C
C+-----+
C!      NORMAL CASE:                                     !
C!      CONSTRUCT RIGHT-HAND SIDE VECTOR -B- FOR PARALLEL BEAM + !
C!      ISOTROPIC ILLUMINATION + THERMAL EMISSION AT TOP      !
C+-----+
      DO 200 I = 1, M
        B(I) = - ZLYRI(1,-I) - ZLYRI0(1,-I) + FISO + TPLANK
200      CONTINUE
C
C+-----+
C!      PARALLEL BEAM + SURFACE REFLECTION + THERMAL EMISSION AT BOTTOM !
C+-----+
      EXB = EXP( - TPRLYR(NLYR) / X0 )
      S1 = 0.
      DO 210 L = 1, M
        S1 = S1 + GWT(L) * GMU(L) * ( ZLYRI(NLYR,-L)*EXB
$          + ZLYRI0(NLYR,-L) + ZLYRI1(NLYR,-L)*TPRLYR(NLYR) )
210      CONTINUE
C
      DO 220 I = 1, M
        B(NCOL-M+I) = AG * ( 2.*S1 + X0*FBEAM*EXB ) + GPLANK
$          - ZLYRI(NLYR,I)*EXB -
$          ( ZLYRI0(NLYR,I) + ZLYRI1(NLYR,I)*TPRLYR(NLYR) )
220      CONTINUE
C
C+-----+
C!      CONTINUITY CONDITIONS FOR LAYER INTERFACES          !
C+-----+

```

```

IT = M
DO 240 K = 1, NLYR-1
  DO 230 I = - M, M
    IF ( I.NE.0 ) THEN
      IT = IT + 1
      B(IT) = ( ZLYRI(K+1,I) - ZLYRI(K,I))*EXP(-TPRLYR(K)/X0)
$          + ZLYRIO(K+1,I) - ZLYRIO(K,I)
$          + ( ZLYRII(K+1,I) - ZLYRII(K,I)) * TPRLYR(K)
      END IF
230    CONTINUE
240  CONTINUE

```

```

C
C+-----+
C! SUBROUTINE *SGBCO* OF LINPACK ROUTINE FACTORS BAND MATRIX !
C! -CBAND- INTO UPPER/LOWER DECOMPOSITION AND ESTIMATES THE !
C! CONDITION OF THE MATRIX (SINGULARITY) !
C! !
C! ON ENTRY : !
C! CBAND = MATRIX IN BAND STORAGE !
C! MI9M2 = LEADING DIMENSION OF -CBAND-, .GE. 3*NCD+1 !
C! NCOL = ORDER OF -CBAND- !
C! NCD = NUMBER OF DIAGONALS BELOW THE MAIN DIAGONAL !
C! NCD = NUMBER OF DIAGONALS ABOVE THE MAIN DIAGONAL !
C! !
C! ON RETURN: !
C! CBAND = UPPER TRIANGULAR MATRIX IN BAND STORAGE !
C! IPVT = INTEGER VECTOR OF PIVOT INDICES !
C! RCOND = INDICATOR OF SINGULARITY FOR -CBAND- IN WORKING !
C! PRECISION IF ( 1.0+RCOND .EQ. 1.0 ) !
C! Z = A WORK VECTOR !
C+-----+
RCOND = 0.0
CALL SGBCO( CBAND, MI9M2, NCOL, NCD, NCD, IPVT, RCOND, Z )
IF ( 1.0+RCOND .EQ. 1.0 ) CALL ERRMSG
$ ( 'CONSTA--SGBCO SAYS MATRIX NEAR SINGULAR',.FALSE.)

```

```

C
C+-----+
C! SUBROUTINE *SGBSL* OF LINPACK ROUTINE SOLVES BAND SYSTEM !
C! A * X = B OR TRANS(A) * X = B AFTER *SGBCO* !
C! !
C! ON ENTRY : !
C! CBAND = MATRIX IN BAND STORAGE !
C! MI9M2 = LEADING DIMENSION OF -CBAND-, .GE. 3*NCD+1 !
C! NCOL = ORDER OF -CBAND- !
C! NCD = NUMBER OF DIAGONALS BELOW THE MAIN DIAGONAL !
C! NCD = NUMBER OF DIAGONALS ABOVE THE MAIN DIAGONAL !
C! IPVT = INTEGER VECTOR OF PIVOT INDICES !
C! B = RIGHT-HAND SIDE VECTOR !
C! JOB = 0; TO SOLVE A * X = B !
C! NONZERO; TO SOLVE TRANSPOSE(A) * X = B !
C! !

```

```
C!      ON RETURN:                                     !
C!          B = THE SOLUTION VECTOR X                 !
C!                                                    !
C!      ERROR CONDITION:  A DIVISION BY ZERO WILL OCCUR IF THE INPUT !
C!                        FACTOR CONTAINS A ZERO ON THE DIAGONAL.    !
C!                        THIS INDICATES SINGULARITY.                !
C+-----+
C
      CALL  SGBSL( CBAND, MI9M2, NCOL, NCD, NCD, IPVT, B, 0 )
C
      RETURN
      END
C*****          END OF CONSTA          *****
C*****
```

```

SUBROUTINE ERRMSG( MESSAGE, FATAL )
C+-----+
C!      PRINTS OUT AN ERROR MESSAGE AND KILLS RUN IF ( FATAL )      !
C+-----+
C!      I N P U T                V A R I A B L E S:                !
C+-----+
C!      FATAL   :    TRUE, WRITES OUT ERROR MESSAGE AND KILLS RUN  !
C+-----+
C!      O U T P U T            V A R I A B L E S:                !
C+-----+
C!      MESSAGE:    ERROR MESSAGE DETECTED                        !
C+-----+
C!      I N T E R N A L        V A R I A B L E S:                !
C+-----+
C!      NUMMSG  :    NUMBER OF ERRORS OCCURRED (START FROM 0)      !
C!      MAXMSG  :    MAX. NUMBER OF ERRORS OCCURRED (200) BEFORE  !
C!                ABORTING THE JOB, IF (.NOT. FATAL)              !
C+-----+
      CHARACTER*40 MESSAGE
      LOGICAL      FATAL
      INTEGER      MAXMSG, NUMMSG
      DATA        NUMMSG / 0 /, MAXMSG / 200 /
C
      WRITE( 6,100 ) MESSAGE
      NUMMSG = NUMMSG + 1
      IF ( FATAL ) THEN
        STOP
      ELSE IF ( NUMMSG.EQ.MAXMSG ) THEN
        WRITE( 6,200 )
        STOP
      ELSE
        RETURN
      END IF
100  FORMAT( ///, ' ----->>> ERROR : ', A, /// )
200  FORMAT( ///, 15('*'), 'TOO MANY ERRORS. ABORTING....' )
C
      END
C***** END OF ERRMSG *****
C*****

```

```

SUBROUTINE FLUXES( FBEAM, FLYR, GLYRIJ, GMU, GWT, IBCND, LJLYR,
$              M, MI, NLYR, NLYRI, NTAU, PRNT, ROOLYRJ,
$              SSALB, TAU, TAULYR, TPRLYR, X0, XR0, XR1,
$              ZLYRI, ZLYRI0, ZLYRI1,
$              GAUPIN, FLDIR, FLDN, FLUP )
C+-----+
C!      CALCULATES THE RADIATIVE FLUXES FROM THE M=0 INTENSITY      !
C!      COMPONENTS (THE AZIMUTHALLY-AVERAGED INTENSITY)             !
C+-----+
C!      I N P U T                V A R I A B L E S:                  !
C+-----+
C!      FBEAM      :  INTENSITY OF INCIDENT BEAM (IBCND=0 ONLY)      !
C!      FLYR       :  TRUNCATED FRACTION IN WISCOMBE DELTA-M METHOD   !
C!      GLYRIJ     :  EIGENVECTORS AT POLAR QUADRATURE ANGLES, SC(1)  !
C!      GMU        :  ABSCISSAE FOR GAUSS QUADRATURE OVER ANGLE COSINE !
C!      GWT        :  WEIGHTS FOR GAUSS QUADRATURE OVER ANGLE COSINE  !
C!      IBCND      :  BOUNDARY CONDITIONS (0, PARALLEL BEAM FROM TOP;  !
C!                  1, ISOTROPIC ILLUMINATION FROM TOP AND BOTTOM)    !
C!      LJLYR     :  CONSTANTS OF INTEGRATION IN EQ. SC(1), OBTAINED  !
C!                  BY SOLVING SCALED VERSION OF EQ. SC(5);           !
C!                  EXPONENTIAL TERM OF EQ. SC(12) NOT INCLUDED      !
C!      M          :  ORDER OF DOUBLE-GAUSS QUADRATURE (NSTR/2)      !
C!      MI         :  INITIAL DIMENSION                               !
C!      NLYR       :  TOTAL NUMBER OF COMPUTATIONAL LAYERS           !
C!      NLYRI      :  INITIAL DIMENSION OF COMPUTATIONAL LAYERS      !
C!      NTAU       :  TOTAL NUMBER OF OUTPUT LAYERS                  !
C!      PRNT       :  OUTPUT CONTROL FLAGS                            !
C!      ROOLYRJ    :  EIGENVALUES OF COEFF. MATRIX IN EQ. SS(7)      !
C!      SSALB      :  SINGLE-SCATTER ALBEDOS OF COMPUTATIONAL LAYERS !
C!      TAU        :  USER OUTPUT OPTICAL DEPTHS                     !
C!      TAULYR     :  CUMULATIVE OPTICAL DEPTH (UN-DELTA-M-SCALED)   !
C!      TPRLYR     :  CUMULATIVE OPTICAL DEPTH (DELTA-M-SCALED)      !
C!      X0         :  POLAR ANGLE COSINE OF INCIDENT BEAM (IBCND=0 ONLY)!
C!      XR0        :  EXPANSION OF THERMAL SOURCE FUNCTION IN EQ. SS(14)!
C!      XR1        :  EXPANSION OF THERMAL SOURCE FUNCTION EQS. SS(16) !
C!      ZLYRI      :  BEAM SOURCE VECTORS IN EQ. SS(19)              !
C!      ZLYRI0     :  THERMAL SOURCE VECTORS -Z0-, BY SOLVING EQ. SS(16)!
C!      ZLYRI1     :  THERMAL SOURCE VECTORS -Z1-, BY SOLVING EQ. SS(16)!
C+-----+
C!      O U T P U T            V A R I A B L E S:                    !
C+-----+
C!      ALB        :  ALBEDO                                          !
C!      DFDTAU     :  FLUX DIVERGENCE IN LAYER OF OPTICAL THICK TAU   !
C!      FDNTOT     :  TOTAL DOWNWARD FLUX (DIRECT + DIFFUSE)         !
C!      FLDIR      :  DIRECT-BEAM FLUX                                 !
C!      FLDN       :  DIFFUSE DOWN-FLUX                               !
C!      FLUP       :  DIFFUSE UP-FLUX                                 !
C!      FNET       :  NET FLUX (TOTAL-DOWN - DIFFUSE-UP)             !
C!      GAUPIN     :  AZIMUTHALLY-AVERAGED INTENSITY, IN EQ. SD(2)   !
C!      PLSORC     :  PLANCK SOURCE FUNCTION (THERMAL)                !
C!      TRANS      :  TRANSMISSIVITY                                  !

```

```

C+-----+
C!          I N T E R N A L          V A R I A B L E S:          !
C+-----+
C!          AVGINT      :  MEAN INTENSITY SUMMATION              !
C!          DIRINT      :  DIRECT INTENSITY ATTENUATED           !
C!          FLX          :  FLUXES CALCULATED FIRST DOWNWARD,   !
C!          FACT         :  EXP( -TAUPR / X0 )                   !
C!          LAYER        :  LAYER NUMBER OF USER OUTPUT (TAU)   !
C!          TAUDIF       :  DELTA TAU BETWEEN TAUPR AND SCALING  !
C!          TAUPR        :  CUMULATIVE OPTICAL DEPTH OF TAU      !
C!          ZINT         :  INTENSITY OF m = 0 CASE, IN EQ. SC(1) !
C+-----+
          LOGICAL PRNT( 1 )
          REAL  FLDIR( 1 ), FLDN( 1 ), FLUP( 1 ), GAUPIN( NLYRI,-MI:MI )
          REAL  FLYR( 1 ), GLYRIJ( NLYRI,-MI:MI,-MI:MI ), GMU( 1 ),
$           GWT( 1 ), LJLYR( -MI:MI,1 ), ROOLYRJ( NLYRI,-MI:MI ),
$           SSALB( 1 ), TAU( 1 ), TAULYR( 0:1 ), TPRLYR( 0:1 ),
$           XR0( 1 ), XR1( 1 ), ZLYRI( NLYRI,-MI:MI ),
$           ZLYRI0( NLYRI,-MI:MI ), ZLYRI1( NLYRI,-MI:MI )
          DATA  PI / 3.1415926535898 /
C
          IF ( PRNT(2) ) WRITE( 6,100 )
C
          DO 30  ITAU = 1, NTAU
          CALL  LOCATE( FLYR, LAYER, NLYR, SSALB, TAU(ITAU), TAULYR,
$           TAUPR, TPRLYR )
          FLX      = 0.
          AVGINT  = 0.
          IF( X0.GT.0.0 ) FACT = EXP( -TAUPR / X0 )
C
          DO 20  I = - M, M
          IF( I.EQ.0 ) THEN
          FLDN(ITAU) = (2.0*PI) * FLX
          FLX = 0.
          GOTO 20
          END IF
C
C+-----+
C!          DOWN: TAUDIF.LE.0 .AND. ROOLYRJ.LE.0 => EXP(-ABS(X)) CONVERGE !
C!          UP: TAUDIF.GE.0 .AND. ROOLYRJ.GE.0 => EXP(-ABS(X)) CONVERGE !
C+-----+
          ZINT = 0.0
          DO 10  J = - M, M
          IF( J.LT.0 ) TAUDIF = TAUPR - TPRLYR(LAYER)
          IF( J.GT.0 ) TAUDIF = TAUPR - TPRLYR(LAYER-1)
          IF( J.NE.0 )
$           ZINT = ZINT + GLYRIJ(LAYER,I,J) * LJLYR(J,LAYER) *
$           EXP( - ROOLYRJ(LAYER,J)*TAUDIF )
10          CONTINUE
C
          JABS = ABS(I)

```

```

          GAUPIN(ITAU,I) = ZINT + ZLYRI(LAYER,I)*FACT +
$          ZLYRIO(LAYER,I) + ZLYRIL(LAYER,I)*TAUPR
          FLX      = FLX + GMU(JABS) * GWT(JABS) * GAUPIN(ITAU,I)
          AVGINT = AVGINT + GWT(JABS) * GAUPIN(ITAU,I)
20      CONTINUE
C
          FLUP(ITAU) = (2.0*PI) * FLX
          IF ( IBCND.EQ.1 ) THEN
              FLDIR(ITAU) = 0.0
              DIRINT      = 0.0
          ELSE
              FLDIR(ITAU) = PI* X0 * FBEAM * FACT
              DIRINT      = PI * FBEAM * FACT
          END IF
          FDNTOT = FLDN(ITAU) + FLDIR(ITAU)
          FNET   = FDNTOT - FLUP(ITAU)
          AVGINT = (2.0*PI) * AVGINT + DIRINT
          PLSORC = 4.*PI * ( XR0(LAYER) + XR1(LAYER)*TAUPR )
          DFDTAU = ( 1.0 - SSALB(LAYER) ) * ( AVGINT - PLSORC )
          IF ( PRNT(2) ) WRITE( 6,200 ) TAU(ITAU), LAYER, FLDIR(ITAU),
$          FLDN(ITAU), FDNTOT, FLUP(ITAU),
$          FNET, AVGINT, PLSORC, DFDTAU
30      CONTINUE
C
          IF( FBEAM.NE.0.0 .AND. PRNT(2) ) THEN
              ALB = FLUP(1) / ( FLDN(1) + FLDIR(1) )
              TRANS = ( FLDN(NTAU) + FLDIR(NTAU) ) / ( FLDN(1) + FLDIR(1) )
              IF ( NTAU.EQ.1 ) WRITE( 6,300 ) ALB
              IF ( NTAU.GT.1 ) WRITE( 6,300 ) ALB, TRANS
          END IF
C
          IF ( PRNT(3) ) THEN
              WRITE ( 6,400 )
              DO 40 I = 1, NTAU
                  WRITE( 6,500 ) TAU(I)
                  DO 40 J = 1, M
                      WRITE( 6,600 ) GMU(M+J), GAUPIN(I,-J), GMU(M-J+1),
$                      GAUPIN(I,M-J+1)
40      CONTINUE
          END IF
C
100     FORMAT( //, 22X, '<----- FLUXES ----->',
$         '----->', /, ' OPTICAL DOWNWARD ',
$         'DOWNWARD DOWNWARD UPWARD', 20X, 'MEAN PLANCK',
$         ' D(NET FLUX)', /, ' DEPTH LAYER DIRECT ',
$         'DIFFUSE TOTAL DIFFUSE NET INTENSITY',
$         ' SOURCE /D(OP DEP)', / )
200     FORMAT( 0PF11.4, I7, 1P7E12.3, E14.3 )
300     FORMAT( /, ' ALBEDO =', 1PE12.5, :, ' TRANSMISSIVITY =', E12.5 )
400     FORMAT( //, ' ***** AZIMUTHALLY AVERAGED INTENSITIES',
$         ' *****' )

```



```
500  FORMAT( //, ' OPTICAL DEPTH =', F10.4,  
$      //, 8X, 'COS(ANGLE)      INTENSITY', 9X,  
$      'COS(ANGLE)      INTENSITY' )  
600  FORMAT( 4X, 0PF14.5, 1PE14.4, 5X, 0PF14.5, 1PE14.4 )  
C  
      RETURN  
      END  
C***** END OF FLUXES *****  
C*****
```

```

SUBROUTINE INTERP( ARRAY, COSTHW, FBEAM, GL, GWT, IBCND, MP, NI,
$                NOPLK, NSTR, NTHETA, OPRIM, PLM0, POL, POLM,
$                POLP, PSI, ROOT, USRANG, WJI, X0, XR0, XR1,
$                Z0, ZJ)

```

```

C+-----+
C!      INTERPOLATES EIGENVECTORS OF EQS. SD(8-9) AND FIRST      !
C!      COMPONENT OF THERMAL SOURCE SS(16) FOR LINEAR APPROXIMATION !
C+-----+
C!      I N P U T                V A R I A B L E S:                !
C+-----+
C!      COSTHW : STORAGE FOR USER-SELECTED ANGLES                !
C!      FBEAM  : INTENSITY OF INCIDENT BEAM (IBCND=0 ONLY)       !
C!      GL     : i.e.,  $w*(2k+1)*g_k$ ,  $k=0$  to  $2k-1$  IN EQ. SS(5)    !
C!      GWT    : WEIGHTS FOR GAUSS QUADRATURE OVER ANGLE COSINE    !
C!      IBCND  : BOUNDARY CONDITIONS (0, PARALLEL BEAM FROM TOP;  !
C!              1, ISOTROPIC ILLUMINATION FROM TOP AND BOTTOM)    !
C!      MP     : ORDER OF AZIMUTHAL COMPONENT                    !
C!      NI     : INITIAL DIMENSION                                !
C!      NOPLK  : TRUE, IGNORE PLANCK FUNCTION THERMAL EMISSION    !
C!              FALSE, INCLUDE THERMAL EMISSION                  !
C!      NSTR   : NUMBER OF POLAR QUADRATURE ANGLES                !
C!      NTHETA : NUMBER OF USER POLAR ANGLES                    !
C!      OPRIM  : SINGLE SCATTERING ALBEDO                        !
C!      PLM0   : ASSOCIATED LEGENDRE POLYNOMIAL P-SUB-L-SUPER-M   !
C!              AT THE BEAM ANGLE MU-SUB-ZERO IN EQ. SD(9)       !
C!      POL    : ASSOCIATED LEGENDRE POLYNOMIAL P-SUB-L-SUPER-M   !
C!              AT THE QUADRATURE ANGLES MU-SUB-J IN EQ. SD(8)   !
C!      POLM & : ASSOCIATED LEGENDRE POLYNOMIALS P-SUB-L-SUPER-M  !
C!      POLP   : AT THE USER ANGLES MU IN EQS. SD(8-9)          !
C!      PSI    : SUM JUST AFTER SQUARE BRACKET IN EQ. SD(9)     !
C!      ROOT   : EIGENVALUES OF EQ. SS(7)                        !
C!      USRANG : TRUE, USE USER-SPECIFIED POLAR ANGLE COSINES    !
C!              FALSE, USE THE -NSTR- QUADRATURE ANGLES          !
C!      X0     : POLAR ANGLE COSINE OF INCIDENT BEAM (IBCND=0 ONLY) !
C!      XR0    : EXPANSION OF THERMAL SOURCE FUNCTION              !
C!      XR1    : EXPANSION OF THERMAL SOURCE FUNCTION EQS.SS(14-16) !
C!      Z0     : SOLUTION VECTORS Z-SUB-ZERO OF EQ. SS(16)      !
C!      ZJ     : SOLUTION VECTOR CAPITAL -Z-SUB-ZERO AFTER SOLVING !
C!              EQ. SS(19)                                       !
C+-----+
C!      O U T P U T                V A R I A B L E S:                !
C+-----+
C!      WJI    : FIRST, STORAGE OF EIGENVECTORS AT QUADRATURE    !
C!              POINTS. THEN, ON RETURN OF INTERPOLATED EIGENVECTORS!
C!      ARRAY  : FIRST, STORAGE OF PSI-FUNCTION. THEN, ARRAY(1,K) !
C!              FOR INHOMOGENEOUS BEAM SOURCE; ARRAY(2,K) FOR    !
C!              COMPONENT OF LINEAR-DEPENDENT THERMAL SOURCE     !
C+-----+
C!      I N T E R N A L                V A R I A B L E S:                !
C+-----+
C!      DELOMP : = 1, FOR AZIMUTHAL INDEPENDENCE; = 0, OTHERWISE !

```

```

C!      M      : ORDER OF DOUBLE-GAUSS QUADRATURE (NSTR/2)      !
C!      PSI    : SUM JUST AFTER SQUARE BRACKET IN EQ. SD(9)    !
C+-----+
      LOGICAL  NOPLK, USRANG
      REAL     COSTHW( 1 ), GL( 1 ), GWT( 1 ), PLM0( 1 ), POL( NI,1 ),
$          POLM( NI,1 ), POLP( NI,1 ), PSI( 1 ), ROOT( 1 ),
$          Z0( 1 ), ZJ( 1 )
      REAL     ARRAY( NI,1 ), WJI( NI,1 )

C
      M = NSTR/2
      SGN = (-1)**MP
C+-----+
C!      COMPUTE PSI-FUNCTION AND STORE IN -ARRAY- (LAST PART OF      !
C!      EQ. SD(8)), THEN COMPUTE EIGENVECTORS AND STORE IN -WJI-.    !
C!      FOR THE CASES OF 1 + MU*ROOT = 0.0, THEY WILL BE TREATED      !
C!      BY USING L'HOSPITAL'S RULE IN "USRINT."                        !
C+-----+
      DO 20  IS = MP, NSTR
          SGN = - SGN
          DO 20  JS = 1, M
              SUM = 0.0
              DO 10  LS = 1, NSTR
                  SUM = SUM + GWT(LS) * POL(IS,LS) * WJI(LS,JS)
10          CONTINUE
              ARRAY(IS, JS) = 0.5 * GL(IS) * SUM
              ARRAY(IS,JS+M) = SGN * ARRAY(IS,JS)
20      CONTINUE
C
      IST = NTHETA / 2 + 1
      IF( .NOT.USRANG ) IST = M + 1
      DO 40  I = IST, NTHETA
          DO 40  J = 1, M
              GPLU = 0.
              GMIN = 0.
              DO 30  L = MP, NSTR
                  GPLU = GPLU + ARRAY(L,J)*POLP(L,I)
                  GMIN = GMIN + ARRAY(L,J)*POLM(L,I)
30          CONTINUE
              WJI(I,J+M) = GPLU / ( 1.+ABS(COSTHW(I))*ROOT(J) )
              IF ( ABS( 1. - ABS(COSTHW(I))*ROOT(J) ).LT.0.0001 ) THEN
                  WJI(I,J) = GMIN
              ELSE
                  WJI(I,J) = GMIN/( 1.-ABS(COSTHW(I))*ROOT(J) )
              END IF
40      CONTINUE
C
      NEND = NTHETA / 2
      IF( .NOT.USRANG ) NEND = M
      DO 50  I = 1, NEND
          DO 50  J = 1, M
              WJI(I,J) = WJI( NTHETA+1-I,J+M )

```

```

WJI(I,J+M) = WJI( NTHETA+1-I,J )
50 CONTINUE
C
C+-----+
C! THE INHOMOGENEOUS BEAM SOURCE TERMS OF EQ. SD(9) STORE IN !
C! ARRAY(1,K). FOR THE CASES OF  $1 + \mu/x_0 = 0.0$ , THEY WILL BE !
C! TREATED BY USING L'HOSPITAL'S RULE IN "USRINT." !
C! LINEAR APPROXIMATION OF THERMAL SOURCE TERMS OF EQ. SS(16) !
C! STORE IN ARRAY(2,K). !
C+-----+
IF ( IBCND.EQ.0 ) THEN
DO 70 L = MP, NSTR
PSUM = 0.
DO 60 J = 1, NSTR
PSUM = PSUM + GWT(J) * POL(L,J) * ZJ(J)
60 CONTINUE
PSI(L) = 0.5 * GL(L) * PSUM
70 CONTINUE
C
DELOMP = 0.0
IF( MP.EQ.1 ) DELOMP = 1.0
FACT = ( 2. - DELOMP ) * FBEAM / 4.0
DO 90 J = 1, NTHETA
SUM = 0.
DO 80 L = MP, NSTR
IF ( COSTHW(J).LT.0. ) THEN
SUM = SUM + POLM(L,J)*(PSI(L)+FACT*GL(L)*PLM0(L))
ELSE
SUM = SUM + POLP(L,J)*(PSI(L)+FACT*GL(L)*PLM0(L))
END IF
80 CONTINUE
IF ( ABS(1.+COSTHW(J)/X0) .LT. 0.0001 ) THEN
ARRAY(1,J) = SUM
ELSE
ARRAY(1,J) = SUM / ( 1. + COSTHW(J)/ X0 )
END IF
90 CONTINUE
C
IF ( (.NOT.NOPLK) .AND. (MP.EQ.1) ) THEN ! THERMAL
DO 110 L = MP, NSTR
PSUM = 0.0
DO 100 J = 1, NSTR
PSUM = PSUM + GWT(J)*POL(L,J)*Z0(J)
100 CONTINUE
PSI(L) = 0.5 * GL(L) * PSUM
110 CONTINUE
C
DO 140 K = 1, NTHETA
SUM = 0.0
IF ( COSTHW(K).LT.0.0 ) THEN
DO 120 L = MP, NSTR

```

```

          SUM = SUM + POLM(L,K)*PSI(L)
120      CONTINUE
      ELSE
          DO 130 L = MP, NSTR
              SUM = SUM + POLP(L,K)*PSI(L)
130          CONTINUE
          END IF
          ARRAY(2,K) = SUM + (1.-OPRIM)*XR0 + COSTHW(K)*XR1
140      CONTINUE
      END IF
  END IF
C
  RETURN
  END
C***** END OF INTERP *****
C*****
```

```

SUBROUTINE INTSUM( COSTHW, NAZ, NAZZI, NPHI, NTAU, NTAUI, NTHETA,
$                NTHETA1, PHI, PRNT, RINTS, TAU, RINTT )
C+-----+
C!      SUMS UP THE FOURIER COSINE SERIES FOR THE INTENSITY      !
C+-----+
C!      I N P U T                V A R I A B L E S:                !
C+-----+
C!      COSTHW :   STORAGE FOR USER-SELECTED ANGLES              !
C!      RINTS  :   FOURIER COMPONENTS OF THE INTENSITY IN EQ. SD.2 !
C!      TAU    :   STORAGE FOR USER-SELECTED OUTPUT OPTICAL DEPTH !
C+-----+
C!      O U T P U T            V A R I A B L E S:                !
C+-----+
C!      RINTT  :   USER OUTPUT INTENSITIES                        !
C+-----+
LOGICAL  PRNT( 1 )
REAL     COSTHW( 1 ), PHI( 1 ), RINTS( NAZZI,NTHETA1,1 ),
$        RINTT( NTAUI,NTHETA1,1 ), TAU( 1 )
DATA    PI/ 3.141592654 /
RPD =   PI/180.
C
DO 30 NT = 1, NTAU
  DO 30 L = 1, NTHETA
    DO 20 IP = 1, NPHI
      SUM = RINTS( 1,L,NT )
      DO 10 MP = 2, NAZ
        SUM = SUM + RINTS(MP,L,NT) * COS( (MP-1)*RPD*PHI(IP) )
10      CONTINUE
      RINTT( NT,L,IP ) = SUM
20      CONTINUE
30      CONTINUE
C
IF ( PRNT(4) ) THEN
  IF ( NPHI.GT.10 ) THEN
    CALL ERRMSG( 'INTSUM--TOO MANY AZIM. ANGLES FOR PRINT',
$              .FALSE. )
    LIMPHI = 10
  ELSE
    LIMPHI = NPHI
  END IF
C
WRITE( 6,100 ) ( PHI(IP), IP = 1, LIMPHI )
DO 40 NT = 1, NTAU
  WRITE( 6,200 )
  DO 40 L = 1, NTHETA
    WRITE( 6,300 ) TAU(NT), COSTHW(L),
$              ( RINTT( NT,L,IP ), IP = 1, LIMPHI )
40      CONTINUE
END IF
100  FORMAT( //, ' ***** INTENSITIES *****', //, 10X,
$         'ZENITH AZIMUTHAL ANGLES (DEGREES)', //,

```

```
          $      ' OPTICAL ANGLE', /, ' DEPTH COSINE', 10F11.1 )
200  FORMAT( )
300  FORMAT( 0PF8.3, F7.3, 1P10E11.3 )
C
      RETURN
      END
C***** END OF INTSUM *****
C*****
```

```

SUBROUTINE IPBEAM( ARRAY, CIJ, FBEAM, GL, GMU, MP, NI, NSTR,
$               PLM0, POL, WK, X0, ZJ )

```

```

C+-----+
C!       FINDS THE PARTICULAR SOLUTION OF SOLAR RADIATION OF SS(18)   !
C+-----+
C!       I N P U T           V A R I A B L E S:                       !
C+-----+
C!       CIJ   : CAPITAL-C-SUB-IJ IN EQ. SS(5)                       !
C!       FBEAM : INTENSITY OF INCIDENT BEAM (IBCND=0 ONLY)          !
C!       GL    : i.e., w*(2k+1)*gk, k=0 to 2k-1 IN EQ. SS(5)        !
C!       GMU   : ABSCISSAE FOR GAUSS QUADRATURE OVER ANGLE COSINE    !
C!       MP    : ORDER OF AZIMUTHAL COMPONENT                       !
C!       NI    : INITIAL DIMENSION                                  !
C!       NSTR  : NUMBER OF POLAR QUADRATURE ANGLES                  !
C!       POL   : ASSOCIATED LEGENDRE POLYNOMIAL P-SUB-L-SUPER-M     !
C!              AT THE QUADRATURE ANGLES MU-SUB-J IN EQ. SD(8)      !
C!       PLM0  : ASSOCIATED LEGENDRE POLYNOMIAL P-SUB-L-SUPER-M     !
C!              AT THE BEAM ANGLE MU-SUB-ZERO IN EQ. SD(9)          !
C!       X0    : POLAR ANGLE COSINE OF INCIDENT BEAM (IBCND=0 ONLY) !
C+-----+
C!       O U T P U T       V A R I A B L E S:                       !
C+-----+
C!       ZJ    : RIGHT-HAND SIDE VECTOR CAPITAL-X-SUB-ZERO IN      !
C!              EQ. SS(19), ALSO THE SOLUTION VECTOR CAPITAL-Z-    !
C!              SUB-ZERO AFTER SOLVING THAT SYSTEM                 !
C+-----+
C!       I N T E R N A L   V A R I A B L E S:                       !
C+-----+
C!       ARRAY : COEFFICIENT MATRIX IN LEFT-HAND SIDE OF EQ. SS(19) !
C!       DELOMP: = 1, FOR AZIMUTHAL INDENPENDCE; = 0, OTHERWISE    !
C!       WK    : SCRATCH ARRAY REQUIRED BY *LEQT1F*                 !
C+-----+
      REAL   ARRAY( NI,1 ), CIJ( NI,1 ), GL( 1 ), GMU( 1 ),
$          PLM0( 1 ), POL( NI,1 ), WK( 1 ), ZJ( 1 )
C
      DO 20 I = 1, NSTR
        DO 10 J = 1, NSTR
          ARRAY(I,J) = - CIJ(I,J)
10      CONTINUE
        ARRAY(I,I) = 1. + GMU(I) / X0 + ARRAY(I,I)
20      CONTINUE
C
      DO 40 I = 1, NSTR
        SUM = 0.
        DO 30 L = MP, NSTR
          SUM = SUM + POL(L,I)*PLM0(L)*GL(L)
30      CONTINUE
        DELOMP = 0.0
        IF( MP.EQ.1 ) DELOMP = 1.0
        ZJ(I) = ( 2. - DELOMP ) * FBEAM * SUM / 4.0
40      CONTINUE

```



```

C
C+-----+
C!      SUBROUTINE *LEQTLF* OF IMSL RETURNS THE SOLUTION OF LINEAR      !
C!      EQUATION:  AX = B                                             !
C!                                                                    !
C!      ARRAY = COEFFICIENT MATRIX OF EQUATION (LEFT-HAND SIDE)      !
C!      1 = NUMBER OF RIGHT-HAND SIDES                                !
C!      NSTR = ORDER OF -ARRAY- (NSTR BY NSTR) AND NUMBER OF         !
C!      ROWS IN -ZJ-                                                 !
C!      NI = INITIAL DIMENSION OF -ARRAY- AND -ZJ-                   !
C!      ZJ = INPUT MATRIX (NSTR BY 1) OF RIGHT-HAND SIDES           !
C!      OF THE EQUATION; ON OUTPUT, -ZJ- IS THE SOLUTION             !
C!      5 = -ARRAY- AND -ZJ- ARE ASSUMED TO BE CORRECT TO           !
C!      5 DECIMAL DIGITS AND THE ROUTINE PERFORMS AN                 !
C!      ACCURACY TEST                                                !
C!      WK = WORK AREA OF DIMENSION .GE. NSTR                        !
C!      IER = OUTPUT ERROR PARAMETER                                  !
C!      0 : SUCCESSFUL                                               !
C!      34 : ACCURACY TEST FAILED                                     !
C!      129 : MATRIX -ARRAY- ALGORITHMICALLY SINGULAR               !
C+-----+
      CALL LEQTLF( ARRAY, 1, NSTR, NI, ZJ, 5, WK, IER )
C
      RETURN
      END
C*****      END OF IPBEAM      *****
C*****

```

```

SUBROUTINE IPISOT( ARRAY, CIJ, GMU, NI, NSTR, OPRIM, WK,
$                XR0, XR1, Z0, Z1 )
C+-----+
C!       FINDS THE PARTICULAR SOLUTION OF THERMAL RADIATION OF SS(15) !
C+-----+
C!       I N P U T           V A R I A B L E S:           !
C+-----+
C!       CIJ   :   CAPITAL-C-SUB-IJ IN EQ. SS(5)         !
C!       GMU   :   ABSCISSAE FOR GAUSS QUADRATURE OVER ANGLE COSINE !
C!       NI    :   INITIAL DIMENSION                     !
C!       NSTR  :   NUMBER OF POLAR QUADRATURE ANGLES      !
C!       OPRIM :   SINGLE SCATTERING ALBEDO              !
C!       XR0   :   EXPANSION OF THERMAL SOURCE FUNCTION  !
C!       XR1   :   EXPANSION OF THERMAL SOURCE FUNCTION EQS. SS(14-16) !
C+-----+
C!       O U T P U T       V A R I A B L E S:           !
C+-----+
C!       Z0    :   SOLUTION VECTORS Z-SUB-ZERO OF EQ. SS(16) !
C!       Z1    :   SOLUTION VECTORS Z-SUB-ONE OF EQ. SS(16) !
C+-----+
C!       I N T E R N A L   V A R I A B L E S:           !
C+-----+
C!       ARRAY :   COEFFICIENT MATRIX IN LEFT-HAND SIDE OF EQ. SS(16) !
C!       WK    :   SCRATCH ARRAY REQUIRED BY *LEQTLF*       !
C+-----+
REAL ARRAY( NI,1 ), CIJ( NI,1 ), GMU( 1 ), WK( 1 ),
$    Z0( 1 ), Z1( 1 )
C
DO 10 I = 1, NSTR
    Z1(I) = XR1
10 CONTINUE
C
DO 30 I = 1, NSTR
    DO 20 J = 1, NSTR
        ARRAY(I,J) = - CIJ(I,J)
20 CONTINUE
    ARRAY(I,I) = 1.0 + ARRAY(I,I)
30 CONTINUE
C
DO 40 I = 1, NSTR
    Z0(I) = (1. - OPRIM)*XR0 + GMU(I)*Z1(I)
40 CONTINUE
C+-----+
C!       *LEQTLF*: SAME AS IN *IPBEAM*, EXCEPT -ZJ- REPLACED BY -Z0- !
C+-----+
CALL LEQTLF( ARRAY, 1, NSTR, NI, Z0, 5, WK, IER )
C
RETURN
END
C***** END OF IPISOT *****
C*****

```

```

SUBROUTINE LEPOLY( YLM, U, M, MAZ, NI, NSTR )
C+-----+
C!      COMPUTES THE ASSOCIATED LEGENDRE POLYNOMIAL OF DEGREE -MAZ- !
C!      AND ALL ORDERS INCLUDING NSTR (L,MP,NSTR CORRESPOND TO !
C!      1 (LITTLE-L), m, (2*n - 1), i.e., IN EQ. SD(8) !
C+-----+
C!      I N P U T          V A R I A B L E S: !
C+-----+
C!      MAZ      :  DEGREE OF ASSOCIATED LEGENDRE POLYNOMIAL !
C!      M        :  NUMBER OF HEMISPHERIC POLAR-QUADRATURE ANGLES !
C!      NI       :  INITIAL DIMENSION !
C!      NSTR     :  NUMBER OF POLAR QUADRATURE ANGLES !
C!      U        :  COSINE OF POLAR ANGLES !
C+-----+
C!      O U T P U T      V A R I A B L E S: !
C+-----+
C!      YLM      :  ASSOCIATED LEGENDRE POLYNOMIAL EVALUATED AT THE !
C!                  COSINE OF POLAR ANGLES U !
C+-----+
REAL U( 1 ), YLM( NI,1 )
IF ( MAZ.EQ.0 ) THEN ! UPWARD RECURRENCE FOR ORDINARY LEGENDRE
DO 10 I = 1, M
  YLM(1,I) = 1.
  YLM(2,I) = U(I)
DO 10 L = 2, NSTR-1
  YLM(L+1,I) = ( (2*L-1)*U(I)*YLM(L,I)
$              - (L-1)*YLM(L-1,I) ) / L
10  CONTINUE
ELSE
DO 40 I = 1, M
  IF ( ABS( U(I)**2-1.0 ) .LT. 1.E-5 ) THEN
DO 20 L = MAZ+1, NSTR
  YLM( L,I ) = 0.0
20  CONTINUE
ELSE
  YLM(MAZ+1,I) = SQRT( 0.5*(2*MAZ-1)
$              * ( 1. - U(I)**2 ) / MAZ ) * YLM(MAZ,I)
  YLM(MAZ+2,I) = SQRT(2*MAZ+1.0) * U(I) * YLM(MAZ+1,I)
DO 30 L = MAZ+2, NSTR-1
  TMP1 = (L-MAZ)*(L+MAZ)
  TMP2 = (L-MAZ-1)*(L+MAZ-1)
  YLM(L+1,I) = ( (2*L-1) * U(I) * YLM(L,I) - SQRT(TMP2)
$              * YLM(L-1,I) ) / SQRT( TMP1 )
30  CONTINUE
  END IF
40  CONTINUE
  END IF
RETURN
END
C***** END OF LEPOLY *****
C*****

```

```

SUBROUTINE LOCATE( FLYR, LAYER, NLYR, SSALB, TAU, TAULYR,
$                TAUPR, TPRLYR )
C+-----+
C!       FINDS THE OUTPUT LAYER AND OPTICAL DEPTH           !
C+-----+
C!       I N P U T                V A R I A B L E S:         !
C+-----+
C!       FLYR      :  TRUNCATED FRACTION IN WISCOMBE DELTA-M METHOD  !
C!       NLYR     :  TOTAL NUMBER OF COMPUTATIONAL LAYERS          !
C!       SSALB    :  SINGLE-SCATTER ALBEDOS OF COMPUTATIONAL LAYERS !
C!       TAU      :  USER OUTPUT OPTICAL DEPTHS                   !
C!       TAULYR   :  CUMULATIVE OPTICAL DEPTH (UN-DELTA-M-SCALED)  !
C!       TPRLYR   :  CUMULATIVE OPTICAL DEPTH (DELTA-M-SCALED)    !
C+-----+
C!       O U T P U T            V A R I A B L E S:           !
C+-----+
C!       LAYER     :  LAYER NUMBER OF USER OUTPUT (TAU)           !
C!       TAUPR     :  CUMULATIVE OPTICAL DEPTH OF TAU (DELTA-M-SCALED) !
C+-----+
C!       I N T E R N A L        V A R I A B L E S:           !
C+-----+
C!       DTAU     :  DELTA TAU BETWEEN TAULYR(LAYER) AND TAU      !
C!       DTPR     :  DTAU OF DELTA-M-SCALED                       !
C+-----+
      REAL FLYR( 1 ), SSALB( 1 ), TAULYR( 0:1 ), TPRLYR( 0:1 )
C
      IF ( TAU.LT.TAULYR(0) .OR. TAU.GT.TAULYR(NLYR) )
$      CALL ERRMSG( 'LOCATE--TAU OUT OF RANGE OF ATMOS.', .TRUE. )
      DO 10 L = 1, NLYR
          IF ( TAU.GE.TAULYR(L-1) .AND. TAU.LE.TAULYR(L) ) GOTO 20
10      CONTINUE
C
20      LAYER = L
          DTAU = TAULYR(LAYER) - TAU
          DTPR = ( 1. - SSALB(LAYER)*FLYR(LAYER) ) * DTAU
          TAUPR = TPRLYR(LAYER) - DTPR
C
      RETURN
      END
C***** END OF LOCATE *****
C*****

```

FUNCTION PLKAVG(WVNML0, WVNMI, TEMP)

```

C+-----+
C!      COMPUTES PLANCK FUNCTION INTEGRATED BETWEEN TWO WAVENUMBERS  !
C!      !
C!      REFERENCES: 1. HOUGHTON, PHYSICS OF ATMOSPHERES, APPENDIX 7  !
C!                  2. SPECIFICATIONS OF THE PHYSICAL WORLD:      !
C!                  NEW VALUE OF THE FUNDAMENTAL CONSTANTS,      !
C!                  DIMENSIONS/N.B.S. JAN. 1974                    !
C!      ACCURACY: 6 SIGNIFICANT DIGITS                               !
C!      METHOD: HOUGHTON'S EXPONENTIAL SERIES IS USED FOR V.GT.VCUT  !
C!            ( 'V' IS HOUGHTON'S NOTATION ) AND HIS POWER SERIES  !
C!            IN V FOR V.LE.VCUT. MORE TERMS ARE TAKEN IN THE     !
C!            EXPONENTIAL SERIES, THE LARGER V IS. ( NOTE THAT    !
C!            HOUGHTON'S ASSESSMENT THAT THE POWER SERIES IS USEFUL !
C!            FOR V.LT.2*PI IS INCORRECT--VCUT MUST BE LESS THAN  !
C!            2 JUST IN ORDER TO GET 4-5 SIGNIFICANT DIGITS. )    !
C+-----+
C!      DATA                V A R I A B L E S:                      !
C+-----+
C!      C2      :  SECOND RADIATION CONSTANT                        !
C!      CONA    :  15 / PI**4 / 13305600                          !
C!      CONB    :  440 / 9                                         !
C!      F15DPI4 :  15 / PI**4                                       !
C!      SIGDPI  :  STEFAN-BOLTZMANN CONSTANT DIVIDED BY PI        !
C!      VCUT    :  POWER-SERIES CUTOFF POINT                       !
C!      VCP     :  EXPONENTIAL SERIES CUTOFF POINTS                !
C+-----+
C!      I N P U T          V A R I A B L E S:                      !
C+-----+
C!      WVNML0  :  LOWER WAVENUMBER ( INV CM ) OF SPECTRAL INTERVAL !
C!      WVNMI   :  UPPER WAVENUMBER                                !
C!      TEMP    :  TEMPERATURE ( K )                               !
C+-----+
C!      O U T P U T      V A R I A B L E S:                      !
C+-----+
C!      PLKAVG  :  INTEGRATED PLANCK FUNCTION ( WATTS/SQ M )      !
C+-----+
C!      I N T E R N A L  V A R I A B L E S:                      !
C+-----+
C!      D      :  INTEGRAL OF NORMALIZED PLANCK FUNCTION          !
C!              FROM 0 TO CURRENT WAVENUMBER                      !
C!      EX     :  EXP( - V ) .                                     !
C!      MMAX   :  NO. OF TERMS TO TAKE IN EXPONENTIAL SERIES     !
C!      MV     :  MULTIPLES OF *V*                                !
C!      V      :  H*C*NU / (K*T), WHERE H=PLANCKS CONSTANT, C=SPEED !
C!              OF LIGHT, K=BOLTZMANN CONSTANT, NU=WAVENUMBER    !
C+-----+
REAL      TEMP, WVNML0, WVNMI
REAL      C2, CONA, CONB, D( 2 ), EX, F15DPI4, MV, SIGDPI,
$         V, VCUT, VCP( 7 ), VSQ
DATA     C2      / 1.438786      /,  CONA      / 0.11573303E-7 /,

```

```

$          CONB / 48.888889 //, F15DPI4 / 0.15398973 //,
$          SIGDPI / 1.804919E-8 //, VCUT / 1.5 //,
$          VCP / 10.25, 5.7, 3.9, 2.9, 2.3, 1.9, 0.0 /
C
IF( TEMP.LT.0.0 .OR. WVMHI.LT.WVMLO .OR. WVMLO.LT.0.0 )
$ CALL ERRMSG('PLKAVG--TEMPERATURE OR WAVENOS. WRONG ',.TRUE.)
IF ( TEMP.LT.1.E-4 ) THEN
    PLKAVG = 0.0
    RETURN
END IF
C
DO 40 I = 1, 2
    IF( I.EQ.1 ) V = ( C2 / TEMP ) * WVMLO
    IF( I.EQ.2 ) V = ( C2 / TEMP ) * WVMHI
C+-----+
C!      IF V.LT.VCUT:
C!      HOUGHTON'S POWER SERIES (FACTORED USING HORNER'S RULE)
C!      ELSE
C!      HOUGHTON'S EXPONENTIAL SERIES AND SET SET UPPER LIMIT OF
C!      SERIES DEPENDING ON VALUE OF V
C+-----+
    IF ( V.LT.VCUT ) THEN
        VSQ = V**2
        D(I) = 1.0 - CONA *VSQ * V * ( 4435200. + V * ( -1663200.
$          + V * ( 221760. + VSQ * ( -2640. + VSQ * ( CONB
$          - VSQ ) ) ) ) )
    ELSE
        MMAX = 0
        MMAX = MMAX + 1
20      IF ( V.LT.VCP( MMAX ) ) GO TO 20
        EX = EXP( -V )
        D(I) = EX * ( 6. + V * ( 6. + V * ( 3. + V ) ) )
        DO 30 M = 2, MMAX
            MV = M * V
            D(I) = D(I) + EX**M * ( 6. + MV * ( 6. + MV *
$          ( 3. + MV ) ) ) / M**4
30      CONTINUE
        D(I) = F15DPI4 * D(I)
    END IF
40      CONTINUE
C
    PLKAVG = SIGDPI * TEMP**4 * ( D(1) - D(2) )
C
    RETURN
END
C***** END OF PLKAVG *****
C*****

```

SUBROUTINE QGAUSN(GWT, GMU, M)

```

C+-----+
C!      COMPUTE WEIGHTS AND ABSCISSAE FOR ORDINARY GAUSSIAN QUADRATURE!
C!      (NO WEIGHT FUNCTION INSIDE INTEGRAL) ON THE INTERVAL (0,1)      !
C!                                                                           !
C!      REFERENCE:  DAVIS,P.J. AND P. RABINOWITZ, METHODS OF NUMERICAL!
C!                  INTEGRATION,ACADEMIC PRESS, NEW YORK, 1975, PP. 87!
C!                                                                           !
C!      METHOD:     COMPUTE THE ABSCISSAE AS ROOTS OF THE LEGENDRE      !
C!                  POLYNOMIAL P-SUB-N USING A CUBICALLY CONVERGENT    !
C!                  REFINEMENT OF NEWTON'S METHOD.  COMPUTE THE        !
C!                  WEIGHTS FROM EQ. 2.7.3.8 OF DAVIS/RABINOWITZ.      !
C!                                                                           !
C!      ACCURACY:  AT LEAST 13 SIGNIFICANT DIGITS                       !
C+-----+
C!      DATA          V A R I A B L E S:                               !
C+-----+
C!      TOL            :  1.0D-21                                       !
C!                    CRAY OR CDC DOUBLE PRECISION (24 SIG. DIGITS)    !
C!                    IBM-LIKE DOUBLE PRECISION (14 SIG. DIGITS)       !
C+-----+
C!      INPUT          V A R I A B L E S:                               !
C+-----+
C!      M              :  ORDER OF QUADRATURE RULE                       !
C+-----+
C!      OUTPUT        V A R I A B L E S:                               !
C+-----+
C!      GMU(I)        :  I = 1 TO M,   ARRAY OF ABSCISSAE              !
C!      GWT(I)        :  I = 1 TO M,   ARRAY OF WEIGHTS                !
C+-----+
C!      INTERNAL      V A R I A B L E S:                               !
C+-----+
C!      PM2,PM1,P    :  3 SUCCESSIVE LEGENDRE POLYNOMIALS              !
C!      PPR          :  DERIVATIVE OF LEGENDRE POLYNOMIAL              !
C!      P2PRI        :  2ND DERIVATIVE OF LEGENDRE POLYNOMIAL          !
C!      TOL          :  CONVERGENCE CRITERION                          !
C!      X,XI         :  SUCCESSIVE ITERATES IN CUBICALLY-              !
C!                    CONVERGENT VERSION OF NEWTON'S METHOD            !
C!                    ( SEEKING ROOTS OF LEGENDRE POLYNOMIAL )        !
C+-----+
REAL      CONA, GMU( 1 ), GWT( 1 ), PI, T
INTEGER   LIM, M, NP1
DOUBLE   PRECISION  EN, NNP1, P, PM1, PM2, PPR, P2PRI, PROD,
$        TMP, TOL, X, XI
DATA     TOL / 1.0D-13 /
DATA     PI  / 3.1415926535898 /
C
IF ( M.LE.1 ) THEN
M = 1
GMU( 1 ) = 0.5
GWT( 1 ) = 1.0

```

```

      RETURN
      END IF
C
      EN   = M
      NP1  = M + 1
      NNp1 = M * NP1
      CONA = FLOAT( M-1 ) / ( 8 * M**3 )
C+-----+
C!          INITIAL GUESS FOR K-TH ROOT OF LEGENDRE POLYNOMIAL,      !
C!          FROM DAVIS/RABINOWITZ  EQ. (2.7.3.3A)                    !
C+-----+
      LIM = M / 2
      DO 30 K = 1, LIM
          T = ( 4*K - 1 ) * PI / ( 4*M + 2 )
          X = COS ( T + CONA / TAN( T ) )
C
C 10      PM2 = 1.D0          ! INITIALIZE LEGENDRE POLYNOMIALS
          PM1 = X            ! P-SUB-0 AND P-SUB-1
C          *** RECURSION RELATION FOR LEGENDRE POLYNOMIALS
          DO 20 NN = 2, M
              P = ( ( 2*NN - 1 ) * X * PM1 - ( NN-1 ) * PM2 ) / NN
              PM2 = PM1
              PM1 = P
C 20      CONTINUE
C
          TMP = 1.D0 / ( 1.D0 - X**2 )
          PPR = EN * ( PM2 - X * P ) * TMP
          P2PRI = ( 2.D0 * X * PPR - NNp1 * P ) * TMP
          XI = X - ( P / PPR ) * ( 1.D0 +
$              ( P / PPR ) * P2PRI / ( 2.D0 * PPR ) )
C
          IF ( DABS(XI-X) .GT. TOL ) THEN      ! CHECK FOR CONVERGENCE
              X = XI
              GO TO 10
          END IF
C
C          ** ITERATION FINISHED--CALC. WEIGHTS, ABSCISSAE FOR (-1,1)
          GMU( K ) = - X
          GWT( K ) = 2.D0 / ( TMP * ( EN * PM2 )**2 )
          GMU( NP1 - K ) = - GMU( K )
          GWT( NP1 - K ) = GWT( K )
C 30      CONTINUE
C
          IF ( MOD( M,2 ) .NE. 0 ) THEN      ! SET MIDDLE ABSCISSA AND
              GMU( LIM + 1 ) = 0.0          ! WEIGHT FOR RULES OF ODD ORDER
              PROD = 1.D0
              DO 40 K = 3, M, 2
                  PROD = PROD * K / ( K-1 )
C 40      CONTINUE
          GWT( LIM + 1 ) = 2.D0 / PROD**2
      END IF

```



```
C
DO 50 K = 1, M ! CONVERT FROM (-1,1) TO (0,1)
    GMU( K ) = 0.5 * GMU( K ) + 0.5
    GWT( K ) = 0.5 * GWT( K )
50 CONTINUE
C
    RETURN
    END
C***** END OF QGAUSN *****
C*****
```

```

SUBROUTINE SOLEIG( AMB, APB, ARRAY, CIJ, CP, GL, GMU, GWT, MI,
$ MP, NI, NSTR, POL, ROOT, WJI, WKX, WX, ZX )

```

```

C+-----+
C!      *SOLEIG* SOLVES EIGENFUNCTION PROBLEMS IN EQS. SS(6-12)      !
C!      FIRST,  USES EQS. SS(5-6) TO FORM          ( -ALFA -BETA ) !
C!      COEFF. MATRIX OF EQ. SS(7):   ARRAY= (  BETA  ALFA ) !
C!      SECOND, FINDS THE COEFFICIENT MATRIX IN EQ. SS(12)        !
C!      [ CP = ( ALFA - BETA )*( ALFA + BETA ) ]                !
C!      THIRD,  SOLVES EIGENVALUE AND EIGENVECTOR PROBLEMS BY USING !
C!      IMSL *EIGRF* ROUTINE.                                     !
C!      FORTH,  FROM SYMMETRY CONSIDERATION DETERMINES COMPLETE SET !
C!      OF EIGENVALUES AND EIGENVECTORS.                         !

```

```

C+-----+
C!      I N P U T          V A R I A B L E S:                      !

```

```

C+-----+
C!      GL      :  i.e., w*(2k+1)*gk, k=0 to 2k-1 IN EQ. SS(5)    !
C!      GMU     :  ABSCISSAE FOR GAUSS QUADRATURE OVER ANGLE COSINE !
C!      GWT     :  WEIGHTS FOR GAUSS QUADRATURE OVER ANGLE COSINE  !
C!      MI      :  INITIAL DIMENSION                               !
C!      MP      :  ORDER OF AZIMUTHAL COMPONENT                   !
C!      NI      :  INITIAL DIMENSION                               !
C!      NSTR    :  NUMBER OF POLAR QUADRATURE ANGLES              !
C!      POL     :  ASSOCIATED LEGENDRE POLYNOMIAL P-SUB-L-SUPER-M !
C!              AT THE QUADRATURE ANGLES MU-SUB-J IN EQ. SD(8)    !

```

```

C+-----+
C!      O U T P U T      V A R I A B L E S:                      !

```

```

C+-----+
C!      CIJ     :  CAPITAL-C-SUB-IJ IN EQ. SS(5) (NEEDED IN SS(15&18)) !
C!      ROOT    :  EIGENVALUES OF EQ. SS(7)                       !
C!      WJI     :  EIGENVECTORS OF EQ. SS(7)                     !

```

```

C+-----+
C!      I N T E R N A L  V A R I A B L E S:                      !

```

```

C+-----+
C!      AMB     :  MATRIX IN REDUCED EIGENVALUE PROBLEM OF EQ. SS(10) !
C!      APB     :  MATRIX IN REDUCED EIGENVALUE PROBLEM OF EQ. SS(11) !
C!      ARRAY   :  MATRIX ON LEFT-HAND SIDE OF EQ. SS(7)           !
C!      CP      :  (ALFA-BETA)*(ALFA+BETA) IN EQ. SS(12)          !
C!      WKX     :  SCRATCH ARRAY REQUIRED BY *EIGRF*                !
C!      WX      :  COMPLEX EIGENVALUES OF SYSTEM SS(12) (SEE -ZX-) !
C!      ZX      :  COMPLEX EIGENVECTORS OF SYSTEM SS(12) (THEY ARE !
C!                ACTUALLY REAL BUT *EIGRF* REQUIRES A COMPLEX    !
C!                ARRAY TO RETURN THE EIGENVECTORS SINCE THEY    !
C!                ARE COMPLEX IN THE GENERAL CASE)                !

```

```

C+-----+
      COMPLEX WX( 1 ), ZX( MI,1 )
      REAL   AMB( MI,1 ), APB( MI,1 ), ARRAY( NI,1 ), CP( MI,1 ),
$          GL( 1 ), GMU( 1 ), GWT( 1 ), POL( NI,1 ), WKX( 1 )
      REAL   CIJ( NI,1 ), ROOT( 1 ), WJI( NI,1 )

```

```

C
      M = NSTR / 2
      DO 20 I = 1, M

```

```

DO 20 J = 1, NSTR
  SUM = 0.
  DO 10 L = MP, NSTR
    SUM = SUM + GL(L)*POL(L,I)*POL(L,J)
10  CONTINUE
  CIJ(I,J) = 0.5*SUM*GWT(J)
C
  IF ( I.EQ.J ) THEN
    ARRAY(I,J) = ( CIJ(I,J) - 1.0 ) / GMU(I)
  ELSE
    ARRAY(I,J) = CIJ(I,J) / GMU(I)
  END IF
C
  IF ( J.LE.M ) THEN
    CIJ(I+M,J+M) = CIJ(I,J)
  ELSE
    CIJ(I+M,J-M) = CIJ(I,J)
    ARRAY(I,J) = - ARRAY(I,J)
  END IF
20 CONTINUE
C
DO 30 I = 1, M
  DO 30 J = 1, M
    ARRAY(I+M,J) = - ARRAY(I,J+M)
    ARRAY(I+M,J+M) = - ARRAY(I,J)
30 CONTINUE
C
DO 40 I = 1, M
  DO 40 J = 1, M
    AMB(I,J) = ARRAY(I,J) - ARRAY(I,J+M)
    APB(I,J) = ARRAY(I,J) + ARRAY(I,J+M)
40 CONTINUE
C
DO 50 I = 1, M
  DO 50 J = 1, M
    CP(I,J) = 0.
    DO 50 L = 1, M
      CP(I,J) = CP(I,J) + AMB(I,L)*APB(L,J)
50 CONTINUE
C
C+-----+
C!      SUBROUTINE *EIGRF* OF IMSL RETURNS EIGENVALUES AND      !
C!      CORRESPONDING EIGENVECTORS OF MATRIX -CP-.           !
C!                                                           !
C!      CP = GENERAL REAL MATRIX, M X M                       !
C!      M = ORDER OF -CP-                                     !
C!      MI = FIRST DIMENSION OF -CP-                          !
C!      IJOB = 0, EIGENVALUES ONLY                             !
C!      1, EIGENVALUES + EIGENVECTORS                         !
C!      (BOTH THESE DESTROY -CP-)                             !
C!      2, EIGENVALUES + EIGENVECTORS + PERFORMANCE INDEX    !

```

```

C!      WX = VECTOR OF M EIGENVALUES (COMPLEX)           !
C!      ZX = MATRIX OF M EIGENVECTORS (COMPLEX); COLUMN J !
C!      CORRESPONDS TO -WX(J)-                          !
C!      MI = FIRST DIMENSION OF -ZX-                    !
C!      WKX = SCRATCH ARRAY OF LENGTH                   !
C!      M, IF IJOB=0; 2M, IF IJOB=1                     !
C!      M(2+M) IF IJOB=2                                !
C!      **ALSO** WKX(1) IS PERFORMANCE INDEX FOR IJOB=2 CASE. !
C!      WKX(1).LT.1 ==> WELL                            !
C!      1.LT.WKX(1).LT.100 ==> SATISFACTORY             !
C!      WKX(1).GT.100 ==> POOR                         !
C!      IER = 0 IF SUCCESSFUL                            !
C!      128+J IF EIGENVALUES 1,...,J NOT FOUND SUCCESSFULLY !
C+-----+
      IJOB = 2
      CALL EIGRF( CP, M, MI, IJOB, WX, ZX, MI, WKX, IER )
      IF ( IER.EQ.66 .OR. IER.EQ.67 )
$      CALL ERRMSG( 'EIGRF--IJOB VALUE IN ERROR ',.TRUE. )
      IF ( IER.GT.128 )
$      CALL ERRMSG( 'EIGRF--FAILED TO CONVERGE ',.TRUE. )
      IF ( WKX(1).GT.100. )
$      CALL ERRMSG( 'EIGRF--POOR PERFORMANCE ON EIGENVALS',.FALSE. )
C
C+-----+
C!      SAVE EIGENVALUES (OCCUR IN PAIRS +k, -k) IN -ROOT- AND !
C!      EIGENVECTORS OF [ (g+) + (g-) ] IN -WJI-          !
C+-----+
      DO 100 J = 1, M
      ROOT(J) = SQRT( ABS( REAL( WX(J) ) ) )
      ROOT(J+M) = - ROOT(J)
      DO 100 I = 1, M
      WJI(I,J) = REAL( ZX(I,J) )
100  CONTINUE
C
C+-----+
C!      FIND EIGENVECTORS OF [ (g+) - (g-) ] FROM EQ. SS(11) !
C+-----+
      DO 130 K = 1, M
      DO 130 I = 1, M
      SUM = 0.
      DO 120 J = 1, M
      SUM = SUM + APB(I,J)*WJI(J,K)
120  CONTINUE
      WJI(I+M,K) = SUM / ROOT(K)
130  CONTINUE
C
C+-----+
C!      FIND EIGENVECTORS g+ AND g- FROM THE REDUCED SYSTEM. !
C!      FROM SYMMETRY CONSIDERATIONS DETERMINE COMPLETE SET OF !
C!      EIGENVECTORS (ONE FOR EACH EIGENVALUE) OF ORIGINAL SYSTEM !
C!      IN EQ. SS(7) AND STACK THEM INTO A SINGLE MATRIX -WJI-. !

```

```
C+-----+
  DO 140 K = 1, M
    DO 140 J = 1, M
      ARRAY(J, K) = WJI(J, K) + WJI(J+M,K)
      ARRAY(J+M,K) = WJI(J+M,K) - WJI(J, K)
140 CONTINUE
C
  DO 150 K = 1, M
    DO 150 J = 1, M
      WJI(J, K) = ARRAY(J, K)
      WJI(J+M, K) = ARRAY(J+M,K)
      WJI(J, K+M) = ARRAY(J+M,K)
      WJI(J+M,K+M) = ARRAY(J, K)
150 CONTINUE
C
  RETURN
  END
C***** END OF SOLEIG *****
C*****
```

```

SUBROUTINE USRINT( AG, COSTHW, FBEAM, FLYR, GLYRIJ, GLYRMUJ, GMU,
$              GPLANK, GWT, IBCND, LJLYR, M, MI, MP, NAZZI,
$              NLYR, NLYRI, NTAU, NTAUI, NTHETA, NTHETAI,
$              RINTS, ROOLYRJ, SSALB, TAU, TAULYR, TPRLYR,
$              X0, Z0MUJ, Z1MUJ, ZLYRI, ZLYRIO, ZLYRI1 )
C+-----+
C!      COMPUTES INTENSITY COMPONENTS AT OUTPUT ANGLES (COSTHW)      !
C!      FOR AZIMUTHAL EXPANSION TERMS (MP) IN EQ. SD(2)              !
C+-----+
C!      AG      : SURFACE ALBEDO                                     !
C!      COSTHW  : STORAGE FOR USER-SELECTED ANGLES                 !
C!      FBEAM   : INTENSITY OF INCIDENT BEAM (IBCND=0 ONLY)        !
C!      FLYR    : TRUNCATED FRACTION IN WISCOMBE DELTA-M METHOD      !
C!      GLYRIJ  : EIGENVECTORS AT POLAR QUADRATURE ANGLES, SC(1)    !
C!      GLYRMUJ : EIGENVECTORS INTERPOLATED TO USER POLAR ANGLES    !
C!              (i.e., g IN EQ. SC(1))                              !
C!      GMU     : ABSCISSAE FOR GAUSS QUADRATURE OVER ANGLE COSINE   !
C!      GPLANK  : INTEGRATED PLANCK FUNCTION FOR EMISSION FROM      !
C!              BOTTOM BOUNDARY                                     !
C!      GWT     : WEIGHTS FOR GAUSS QUADRATURE OVER ANGLE COSINE     !
C!      IBCND   : BOUNDARY CONDITIONS (0, PARALLEL BEAM FROM TOP;   !
C!              1, ISOTROPIC ILLUMINATION FROM TOP AND BOTTOM)      !
C!      LJLYR   : CONSTANTS OF INTEGRATION IN EQ. SC(1), OBTAINED   !
C!              BY SOLVING SCALED VERSION OF EQ. SC(5);            !
C!              EXPONENTIAL TERM OF EQ. SC(12) NOT INCLUDED        !
C!      M       : ORDER OF DOUBLE-GAUSS QUADRATURE (NSTR/2)        !
C!      MI      : INITIAL DIMENSION (i.e., -GLYRIJ- )              !
C!      MP      : ORDER OF AZIMUTHAL COMPONENT                      !
C!      NAZZI   : INITIAL DIMENSION OF FOURIER EXPANSION            !
C!      NLYR    : TOTAL NUMBER OF COMPUTATIONAL LAYERS              !
C!      NLYRI   : INITIAL DIMENSION OF COMPUTATIONAL LAYERS        !
C!      NTAU    : TOTAL NUMBER OF OUTPUT LAYERS                    !
C!      NTAUI   : INITIAL DIMENSION OF OUTPUT LAYERS               !
C!      NTHETA  : NUMBER OF USER POLAR ANGLES                      !
C!      NTHETAI : INITIAL DIMENSION OF USER POLAR ANGLES           !
C!      ROOLYRJ : EIGENVALUES OF COEFF. MATRIX IN EQ. SS(7)        !
C!      SSALB   : SINGLE-SCATTER ALBEDOS OF COMPUTATIONAL LAYERS   !
C!      TAU     : USER OUTPUT OPTICAL DEPTHS                       !
C!      TAULYR  : CUMULATIVE OPTICAL DEPTH (UN-DELTA-M-SCALED)     !
C!      TPRLYR  : CUMULATIVE OPTICAL DEPTH (DELTA-M-SCALED)        !
C!      X0      : POLAR ANGLE COSINE OF INCIDENT BEAM (IBCND=0 ONLY)!
C!      Z0MUJ   : Z-SUB-ZERO IN EQ. SS(16) INTERPOLATED TO USER    !
C!              ANGLES FROM AN EQUATION DERIVED FROM SS(16)       !
C!      Z1MUJ   : Z-SUB-ONE IN EQ. SS(16) INTERPOLATED TO USER    !
C!              ANGLES FROM AN EQUATION DERIVED FROM SS(16)       !
C!      ZLYRI   : BEAM SOURCE VECTORS IN EQ. SS(19)                !
C!      ZLYRIO  : THERMAL SOURCE VECTORS -Z0-, BY SOLVING EQ. SS(16)!
C!      ZLYRI1  : THERMAL SOURCE VECTORS -Z1-, BY SOLVING EQ. SS(16)!
C+-----+
C!      O U T P U T      V A R I A B L E S:                          !
C+-----+

```

```

C!      RINTS      :   FOURIER COMPONENTS OF THE INTENSITY IN EQ. SD(2)   !
C+-----+
C!      I N T E R N A L      V A R I A B L E S:                               !
C+-----+
C!      BOTINT     :   INTENSITY REFLECTED ISOTROPICALLY (i.e., SS(22))   !
C!      DTAU      :   DELTA TAU BETWEEN COMPUTATIONAL LAYERS              !
C!      FACT      :   EXP( -TAUPR / X0 )                                  !
C!      FLIP      :   CONTROL FLAG FOR CHANGING DIRECTION OF INTEGRATION!
C!      FLXBOT    :   DIFFUSE FLUX DOWN AT THE BOTTOM                      !
C!      FLXDIR    :   DIRECT FLUX DOWN AT THE BOTTOM                      !
C!      LYREND    :   END LAYER OF INTEGRATION                          !
C!      LYRSTART  :   START LAYER OF INTEGRATION                        !
C!      PALINT    :   INTENSITY COMPONENT FROM PARALLEL BEAM             !
C!      PLKINT    :   INTENSITY COMPONENT FROM PLANCK SOURCE             !
C!      PTAU      :   DELTA TAU BETWEEN OUTPUT LAYER AND LAST            !
C!                INTEGRATION LAYER IN EQ. S1(8-9)                      !
C!      SFCINT    :   INTENSITY COMPONENT FROM SURFACE (REFL. + EMIS.)   !
C!      TAUDIF    :   DELTA TAU BETWEEN TAUPR AND SCALING FACTOR SC(12) !
C!      TAUPR     :   CUMULATIVE OPTICAL DEPTH OF TAU (DELTA-M-SCALED)  !
C!      ZINT      :   INTENSITY OF m = 0 CASE, IN EQ. SC(1)              !
C+-----+
      LOGICAL  FLIP
      REAL    COSTHW( 1 ), FLYR( 1 ), GLYRIJ( NLYRI, -MI:MI, -MI:MI ),
$           GLYRMUJ( NLYRI, NTHETA, -MI:MI ), GMU( 1 ), GWT( 1 ),
$           LJLYR( -MI:MI, 1 ), ROOLYRJ( NLYRI, -MI:MI ),
$           RINTS( NAZZI, NTHETA, 1 ), SSALB( 1 ), TAU( 1 ),
$           TAULYR( 0:1 ), TPRLYR( 0:1 ), ZOMUJ( NLYRI, 1 ),
$           Z1MUJ( NLYRI, 1 ), ZLYRI( NLYRI, -MI:MI ),
$           ZLYRIO( NLYRI, -MI:MI ), ZLYRII( NLYRI, -MI:MI )

C
      PI = 3.1415926535898
      DO 10 LYR = 1, NLYR
        DO 10 MU = 1, NTHETA
          DO 10 J = - M, M
            IF ( J.NE.0 )
$           GLYRMUJ( LYR, MU, J ) = GLYRMUJ( LYR, MU, J ) * LJLYR( J, LYR )
10      CONTINUE
C
C+-----+
C!      DO-200 LOOPS OVER LAYERS AT WHICH INTENSITIES ARE DESIRED,      !
C!      CALL *LOCATE* TO FIND OUTPUT LOCATION "LAYER"                    !
C+-----+
      DO 200 NT = 1, NTAU
$     CALL LOCATE( FLYR, LAYER, NLYR, SSALB, TAU(NT), TAULYR,
$           TAUPR, TPRLYR )

C
      LYRSTART = 1
      LYREND = LAYER - 1
      FLIP = .FALSE.
C+-----+
C!      DO-100 CALCULATES INTENSITIES: FOR DOWNWARD, INTEGRATE FROM    !

```

```

C!      TOP TO 'LAYER-1' IN EQ. S1(8); FOR UPWARD, INTEGRATE FROM      !
C!      BOTTOM TO 'LAYER+1' IN EQ. S1(9). THIS IS DONE IN DO-30 LOOP. !
C!      THE CONTRIBUTION FROM 'OUTPUT LAYER' TO LAST INTEGRATION     !
C!      LAYER OF EACH DIRECTION IS CALCULATED IN DO-40 LOOP.        !
C!      ALL THE EXPONENTIAL FACTORS (i.e., EXP1, EXPN,... etc.)      !
C!      COME FROM THE SUBSTITUTION OF CONSTANTS OF INTEGRATION IN   !
C!      EQ. SC(12) INTO EQS. S1(8-9).                                !
C+-----+
      DO 100  MU = 1, NTHETA
          IF( .NOT.FLIP .AND. COSTHW(MU).GT.0.0 ) THEN
              FLIP = .TRUE.
              LYRSTART = LAYER + 1
              LYREND = NLYR
          END IF
          PALINT = 0.0
          PLKINT = 0.0
          SFCINT = 0.0
          ROOLYRJ( LAYER,0 ) = ( 1.0 / X0 )
C
          IF ( LYRSTART .LE. LYREND ) THEN
              DO 30  LYR = LYRSTART, LYREND
                  DTAU = TPRLYR(LYR) - TPRLYR(LYR-1)
                  EXP1 = EXP( (TAUPR-TPRLYR(LYR-1))/COSTHW(MU) )
                  EXP2 = EXP( (TAUPR-TPRLYR( LYR ))/COSTHW(MU) )
C
                  DO 20  J = - M, M
C
                      IF ( ABS(1.0+COSTHW(MU)*ROOLYRJ(LYR,J)).LT.0.0001 )
                          $ THEN
C+-----+
C!      APPLY L'HOSPITAL'S RULE TO CASE WHERE OUTPUT ANGLE EQUAL TO !
C!      SUN ANGLE OR INVERSE OF ROOT SINCE AT THAT POINT SOURCE TERM !
C!      Z0 (J=0 TERM IN SUM) AND EIGENVECTOR GLYRIJ(+J,-MU),        !
C!      GLYRIJ(-J,+MU) ARE NOT DEFINED.                              !
C+-----+
                      IF ( J.LT.0 ) EXPN = -ROOLYRJ(LYR,J)*DTAU *
                          $ EXP( ROOLYRJ(LYR,J)*(TPRLYR( LYR )-TAUPR) )
                      IF ( J.EQ.0 ) EXPN = (DTAU/X0) * EXP( -TAUPR/X0 )
                      IF ( J.GT.0 ) EXPN = ROOLYRJ(LYR,J)*DTAU *
                          $ EXP( -ROOLYRJ(LYR,J)*(TAUPR-TPRLYR(LYR-1)) )
                      ELSE
C
                          *** NORMAL CASE ***
                          IF( J.EQ.0 ) THEN
                              EXPN1 = EXP1*EXP( -TPRLYR(LYR-1)/X0 )
                              EXPN2 = EXP2*EXP( -TPRLYR( LYR )/X0 )
                          ELSE IF( J.LT.0 ) THEN
                              EXPN1 = EXP1*EXP( ROOLYRJ(LYR,J)*DTAU )
                              EXPN2 = EXP2
                          ELSE
                              EXPN1 = EXP1
                              EXPN2 = EXP2*EXP( -ROOLYRJ(LYR,J)*DTAU )

```



```

                END IF
                EXPN = ( EXPN1-EXPN2 ) * SIGN( 1.0, COSTHW(MU) )
                END IF
C
                PALINT = PALINT + GLYRMUJ(LYR,MU,J)*EXPN
20 CONTINUE
C
                PLKINT = PLKINT + ( ZOMUJ(LYR,MU)*(EXP1-EXP2) +
$                 Z1MUJ(LYR,MU) * ( TPRLYR(LYR-1)*EXP1 -
$                 TPRLYR(LYR)*EXP2) ) * SIGN( 1.0, COSTHW(MU) )
30 CONTINUE
                END IF
C
                PTAU = TPRLYR(LAYER) - TPRLYR(LAYER-1)
                DO 40 J = - M, M
C
                IF ( ABS(1.0+COSTHW(MU)*ROOLYRJ(LAYER,J)).LT.0.0001 ) THEN
                IF ( J.LT.0 )
$                 EXPN = -ROOLYRJ(LAYER,J)*(TPRLYR( LAYER )-TAUPR) *
$                 EXP( ROOLYRJ(LAYER,J)*(TPRLYR( LAYER )-TAUPR) )
                IF ( J.EQ.0 ) EXPN = EXP( - TAUPR/X0 ) *
$                 ( ( TAUPR-TPRLYR(LAYER-1))/X0 )
                IF ( J.GT.0 )
$                 EXPN = ROOLYRJ(LAYER,J)*(TAUPR-TPRLYR(LAYER-1)) *
$                 EXP( -ROOLYRJ(LAYER,J)*(TAUPR-TPRLYR(LAYER-1)) )
                ELSE
                IF( J.EQ.0 ) THEN
                EXPN1 = EXP( -TAUPR/X0 )
                IF ( COSTHW(MU).LT.0.0 ) EXPN2 = EXP( -TPRLYR(LAYER-1)
$                 /X0 + (TAUPR-TPRLYR(LAYER-1))/COSTHW(MU) )
                IF ( COSTHW(MU).GT.0.0 ) EXPN2 = EXP( -TPRLYR( LAYER )
$                 /X0 + (TAUPR-TPRLYR( LAYER ))/COSTHW(MU) )
                ELSE IF( J.LT.0 ) THEN
                EXPN1 = EXP( ROOLYRJ(LAYER,J)*(TPRLYR(LAYER)-TAUPR) )
                IF ( COSTHW(MU).LT.0.0 )
$                 EXPN2 = EXP( ROOLYRJ(LAYER,J)*PTAU ) *
$                 EXP( (TAUPR-TPRLYR(LAYER-1))/COSTHW(MU) )
                IF ( COSTHW(MU).GT.0.0 )
$                 EXPN2 = EXP( (TAUPR-TPRLYR( LAYER ))/COSTHW(MU) )
                ELSE
                EXPN1 = EXP(-ROOLYRJ(LAYER,J)*(TAUPR-TPRLYR(LAYER-1)))
                IF ( COSTHW(MU).LT.0.0 )
$                 EXPN2 = EXP( (TAUPR-TPRLYR(LAYER-1))/COSTHW(MU) )
                IF ( COSTHW(MU).GT.0.0 )
$                 EXPN2 = EXP( -ROOLYRJ(LAYER,J)*PTAU ) *
$                 EXP( (TAUPR-TPRLYR( LAYER ))/COSTHW(MU) )
                END IF
                EXPN = EXPN1 - EXPN2
                END IF
C
                PALINT = PALINT + GLYRMUJ(LAYER,MU,J)*EXPN

```

```

40      CONTINUE
C
      IF ( COSTHW(MU).LT.0.0 ) THEN
          EXPN = EXP( (TAUPR-TPRLYR(LAYER-1))/COSTHW(MU) )
          FACT = TPRLYR(LAYER-1)
      ELSE
          EXPN = EXP( (TAUPR-TPRLYR( LAYER ))/COSTHW(MU) )
          FACT = TPRLYR( LAYER )
      END IF
      PLKINT = PLKINT + ZOMUJ(LAYER,MU)*( 1.-EXPN ) +
$          Z1MUJ(LAYER,MU)*( TAUPR-FACT*EXPN )
C
C+-----+
C!      CALCULATE INTENSITY COMPONENT FROM SURFACE REFLECTION AND      !
C!      EMISSION.  COMPUTATION OF MEAN INTENSITY DOWN AT BOTTOM IS    !
C!      THE SAME AS IN *FLUXES*                                       !
C+-----+
      IF ( COSTHW(MU).GT.0.0 ) THEN
          FLXBOT = 0.
          IF ( AG.NE.0.0 ) THEN
              IF ( X0.GT.0. ) FACT = EXP( -TPRLYR(NLYR) / X0 )
              DO 60 I = -M, -1
                  ZINT = 0.0
                  DO 50 J = -M, M
                      IF ( J.LT.0 ) TAUDIF = 0.0
                      IF ( J.GT.0 ) TAUDIF = TPRLYR(NLYR) -
$                          TPRLYR(NLYR-1)
                      IF ( J.NE.0 ) ZINT = ZINT + GLYRIJ(NLYR,I,J) *
$                          LJLYR(J,NLYR)*EXP( -ROOLYRJ(NLYR,J)*TAUDIF )
50                      CONTINUE
                      JABS = ABS(I)
                      FLXBOT = FLXBOT + GMU(JABS)*GWT(JABS)*( ZINT +
$                          ZLYRI(NLYR,I)*FACT + ZLYRI0(NLYR,I) +
$                          ZLYRI1(NLYR,I)*TPRLYR(NLYR) )
60                      CONTINUE
                      FLXDIR = PI * FBEAM * FACT
                      IF ( IBCND.EQ.1 ) FLXDIR = 0.0
                  END IF
                  BOTINT = 2.0*PI*FLXBOT + FLXDIR
                  SFCINT = ( GPLANK + AG*BOTINT/PI ) *
$                      EXP( (TAUPR-TPRLYR(NLYR))/COSTHW(MU) )
              END IF
C
              RINTS(MP,MU,NT) = PALINT + PLKINT + SFCINT
100      CONTINUE
200      CONTINUE
C
      RETURN
      END
C***** END OF USRINT *****
C*****

```

```

SUBROUTINE WRTBAD( LUNIT, VARNAM, ERRFLG )
C+-----+
C!      WRITES OUT NAMES OF ERRONEOUS INPUT VARIABLES      !
C+-----+
C!      I N P U T              V A R I A B L E S:          !
C+-----+
C!      LUNIT   :      LOGICAL UNIT ON WHICH TO WRITE      !
C!      VARNAM  :      NAME OF ERRONEOUS VARIABLE ( CHARACTER*8 ) !
C+-----+
C!      O U T P U T          V A R I A B L E S:          !
C+-----+
C!      ERRFLG  :      FLAG WHICH IS SET 'TRUE' BY THIS ROUTINE !
C+-----+
C!      I N T E R N A L      V A R I A B L E S:          !
C+-----+
C!      NUMMSG  :      NUMBER OF ERRORS OCCURRED (START FROM 0) !
C!      MAXMSG  :      MAX. NUMBER OF ERRORS OCCURRED (200) BEFORE !
C!      ABORTING THE JOB                                     !
C+-----+
CHARACTER*8  VARNAM
LOGICAL      ERRFLG
INTEGER      LUNIT, MAXMSG, NUMMSG
DATA         NUMMSG / 0 /, MAXMSG / 200 /

C
NUMMSG = NUMMSG + 1
WRITE ( LUNIT,100 ) VARNAM
ERRFLG = .TRUE.
IF ( NUMMSG.EQ.MAXMSG )
$   CALL ERRMSG('TOO MANY INPUT ERRORS. ABORTING....',.TRUE.)
100  FORMAT( ' ***** ERROR IN INPUT VARIABLE : ', A )
C
RETURN
END
C***** END OF WRTBAD *****
C*****

```

```

SUBROUTINE ZEROAL( AMB, APB, ARRAY, B, CBAND, CIJ, COSTHP, COSTHW,
$                CP, FLYR, GAUPIN, GLYRIJ, GLYRMUJ, GMU, GWT,
$                LJLYR, PKAG, PLM0, POL, POLM, POLP, PSI, RINTS,
$                ROOLYRJ, ROOT, TAULYR, TPRLYR, WJI, WK, WKX,
$                WX, XR0, XR1, Z, Z0, Z1, ZJ, ZLYRI, ZLYRI0,
$                ZLYRI1, ZOMUJ, Z1MUJ, ZX, MI, MI2MI, MI9M2,
$                NAZZI, NI, NINLYRI, NLYRI, NTAUI, NTHETA1 )

```

```

C+-----+
C!          CALL *ZEROIT* TO ZERO AN ARRAY -A- OF -LENGTH- ELEMENTS      !
C+-----+
C

```

```

COMPLEX WX( 1 ), ZX( MI,1 )
REAL      AMB( MI,1 ), APB( MI,1 ), ARRAY( NI,1 ),
$         B( 1 ), CBAND( MI9M2,1 ), CIJ( NI,1 ),
$         COSTHP( 1 ), COSTHW( 1 ), CP( MI,1 ), FLYR( 1 ),
$         GAUPIN( NTAUI,-MI:MI ), GLYRIJ( NLYRI,-MI:MI,-MI:MI ),
$         GLYRMUJ( NLYRI,NTHETA1,-MI:MI ), GMU( 1 ), GWT( 1 ),
$         LJLYR( -MI:MI,1 ), PKAG( 0:1 ), PLM0( 1 ), POL( NI,1 ),
$         POLM( NI,1 ), POLP( NI,1 ), PSI( 1 ),
$         RINTS( NAZZI,NTHETA1,1 ), ROOLYRJ( NLYRI,-MI:MI ),
$         ROOT( 1 ), TAULYR( 0:1 ), TPRLYR( 0:1 ),
$         WJI( NI,1 ), WK( 1 ), WKX( 1 ), XR0( 1 ), XR1( 1 ),
$         Z( 1 ), Z0( 1 ), ZOMUJ( NLYRI,1 ), Z1( 1 ),
$         Z1MUJ( NLYRI,1 ), ZJ( 1 ), ZLYRI( NLYRI,-MI:MI ),
$         ZLYRI0( NLYRI,-MI:MI ), ZLYRI1( NLYRI,-MI:MI )

```

```

C
CALL ZEROIT( AMB, MI*MI )
CALL ZEROIT( APB, MI*MI )
CALL ZEROIT( ARRAY, NI*NI )
CALL ZEROIT( B, NINLYRI )
CALL ZEROIT( CBAND, MI9M2*NINLYRI )
CALL ZEROIT( CIJ, NI*NI )
CALL ZEROIT( COSTHP, NTHETA1 )
CALL ZEROIT( COSTHW, NTHETA1 )
CALL ZEROIT( CP, MI*MI )
CALL ZEROIT( FLYR, NLYRI )
CALL ZEROIT( GAUPIN, NTAUI*(2*MI+1) )
CALL ZEROIT( GLYRIJ, NLYRI*(2*MI+1)*(2*MI+1) )
CALL ZEROIT( GLYRMUJ, NLYRI*NTHETA1*(2*MI+1) )
CALL ZEROIT( GMU, NI )
CALL ZEROIT( GWT, NI )
CALL ZEROIT( LJLYR, (2*MI+1)*NLYRI )
CALL ZEROIT( PKAG, NLYRI+1 )
CALL ZEROIT( PLM0, NI )
CALL ZEROIT( POL, NI*NI )
CALL ZEROIT( POLM, NI*NTHETA1 )
CALL ZEROIT( POLP, NI*NTHETA1 )
CALL ZEROIT( PSI, NI )
CALL ZEROIT( RINTS, NAZZI*NTHETA1*NTAUI )
CALL ZEROIT( ROOLYRJ, NLYRI*(2*MI+1) )
CALL ZEROIT( ROOT, NI )

```

```

CALL ZEROIT( TAULYR, NLYRI+1 )
CALL ZEROIT( TPRLYR, NLYRI+1 )
CALL ZEROIT( WJI, NI*NI )
CALL ZEROIT( WK, NI )
CALL ZEROIT( WKX, MI2MI )
CALL ZEROIT( WX, 2*MI )
CALL ZEROIT( XR0, NLYRI )
CALL ZEROIT( XR1, NLYRI )
CALL ZEROIT( Z, NINLYRI )
CALL ZEROIT( Z0, NI )
CALL ZEROIT( Z0MUJ, NLYRI*NTHETA )
CALL ZEROIT( Z1, NI )
CALL ZEROIT( Z1MUJ, NLYRI*NTHETA )
CALL ZEROIT( ZJ, NI )
CALL ZEROIT( ZLYRI, NLYRI*(2*MI+1) )
CALL ZEROIT( ZLYRI0, NLYRI*(2*MI+1) )
CALL ZEROIT( ZLYRI1, NLYRI*(2*MI+1) )
CALL ZEROIT( ZX, 2*MI*MI )

```

C

```

RETURN
END

```

```

C***** END OF ZEROAL *****
C*****

```

```

SUBROUTINE ZEROIT( A, LENGTH )

```

```

C+-----+
C!       ZEROS AN ARRAY -A- OF -LENGTH- ELEMENTS      !
C+-----+

```

```

REAL A( 1 )

```

C

```

DO 10 L = 1, LENGTH
  A( L ) = 0.0

```

```

10 CONTINUE

```

C

```

RETURN
END

```

```

C***** END OF ZEROIT *****
C*****

```

REFERENCES

- Asano, S., 1975, On the Discrete Ordinates Method for the Radiative Transfer, J. Meteor. Soc. Japan, 53, 92-95.
- Bakan, S. and H. Quenzel, 1976, Path Length Distributions of Photons Scattered in Turbid Atmospheres, Beitr. Phys. Atmo., 49, 272-284.
- , P. Koepke, and H. Quenzel, 1978, Radiation Calculations in Absorption Bands: Comparison of Exponential Series- and Path Length Distribution-Method, Beitr. Phys. Atmo., 51, 28-30.
- Benson, C.S., 1969, The Seasonal Snow Cover of Arctic Alaska, Tech. Report, ONR-403-1, the Arctic Institute of North America, 47pp.
- Blanchet, J. and R. List, 1983, Estimation of Optical Properties of arctic Haze Using a Numerical Model, Atmosphere-Ocean, 21, 444-465.
- Carlson, H., 1981, Infrared Water Vapor Continuum Absorption: Equilibrium of Ions and Natural Water Clusters, Appl. Opt., 20, 1316-1322.
- Carlson, T.N., 1981, Speculations on the Movement of Polluted Air to the Arctic, Atmos. Environ., 17, 1473-1477.
- Carrier, L.W., G.A. Cato, and K.J. von Essen, 1967, The Backscattering and Extinction of Visible and Infrared Radiation by Selected Major Cloud Models, App. Opt., 6, 1209-1216.
- Chou, M.D. and A. Arking, 1980, Computation of Infrared Cooling Rates in the Water Vapor Bands, J. Atmos. Sci., 37, 855-867.
- , and -----, 1981, An Efficient Method for Computing the Absorption of Solar Radiation by Water Vapor, J. Atmos. Sci., 38, 798-807.
- , and L. Peng, 1983, A Parameterization of the Absorption in the 15-microm CO₂ Spectral Region with Application to Climate Sensitivity Studies, J. Atmos. Sci., 40, 2183-2192.

- Chylek, P. and V. Ramaswamy, 1982, Lower and Upper Bounds on Extinction Cross Sections of Arbitrarily Shaped Strongly Absorbing or Strongly Reflecting Nonspherical Particles, Appl. Opt., 21, 4339-4344.
- , V. Ramaswamy and R.J. Cheng, 1984, Effect of Graphitic Carbon on the Albedo of Clouds, J. Atmos. Sci., 41, 3076-3084.
- Curry, J.A. and G.F. Herman, 1985, Infrared Radiative Properties of Summertime Arctic Stratus Clouds, J. Climate Appl. Meteor., 24, 525-538.
- Deepak, A., T.D. Wilkerson, and L.H. Ruhnke, 1980, Atmospheric Water Vapor, Academic Press, 695pp.
- Deirmendjian, D., 1969, Electromagnetic Scattering on Spherical Polydispersions, American Elsevier, 290pp.
- Doronin, Y.P., 1963, On the Heat Balance of the Central Arctic, Trudy AANI, 253, 178-184 (in Russian).
- Downing, H.D. and D. Williams, 1975, Optical Constants of Water in the Infrared, J. Geophys. Res., 80, 1656-1661.
- Feigel'son, E.M., 1964, Radiation Processes in Stratified Clouds, Academy of Sciences, Moscow, U.S.S.R.
- Feynman, R.P., R.B. Leighton, and M. Sands, 1977, The Feynman Lectures on Physics, vol. 2.
- Fricke, C.L., 1979, The Phase-Integral Method for Radiative Transfer Problems with Highly-Peaked Phase Functions, J. Quant. Spectrosc. Radiat. Transfer, 20, 429-445.
- Fritz, S., 1951, Solar Radiant Energy, Compendium of Meteorology, T.F. Malone, Ed., Wiley, 14-29.
- Goody, R., 1964, Atmospheric Radiation, Oxford University Press, 436pp.
- , R., 1980, Polar Process and World Climate (A Brief Overview), Mon. Wea. Rev., 108, 1935-1942.
- Griggs, M., 1968, Emissivities of Natural Surfaces in the 8- to 14-micron Spectral Region, J. Geophys. Res., 73, 7545-7551.
- Hale, G.M. and M.R. Querry, 1973, Optical Constants of Water in the 200-nm to 200- μ m Wavelength Region, Appl. Opt., 12, 555-563.

- Hansen, J.E. and J.B. Travis, 1974, Light Scattering in Planetary Atmospheres, Space Sci. Rev., 16, 527-610.
- Haurwitz, B., 1985, Meteorology in the 20th Century: A Participant's View, Part I-IV, Bull. Amer. Met. Soc., 66, March-June.
- Heintzenberg, J., 1980, Particle Size Distribution and Optical Properties of Arctic Haze, Tellus, 31, 251-260.
- Henye, L.G. and J.L. Greenstein, 1941, Diffuse Radiation in the Galaxy, Astrophys. J., 93, 70-83.
- Herman, G.F., 1977, Solar Radiation in Summertime Arctic Stratus Clouds, J. Atmos. Sci., 34, 1423-1432.
- , 1980, Thermal Radiation in Arctic Stratus Clouds, Quart. J. R. Met. Soc., 106, 771-780.
- , and R. Goody, 1976, Formation and Persistence of Summertime Arctic Stratus Clouds, J. Atmos. Sci., 33, 1537-1553.
- , and J.A. Curry, 1984, Observational and Theoretical Studies of Solar Radiation in Arctic Stratus Clouds, J. Climate Appl. Meteor., 23, 5-24.
- Hunt, G.E., and I.P. Grant, 1969, Discrete Space Theory of Radiative Transfer and its Application to Problems in Planetary Atmospheres, J. Atmo. Sci., 26, 963-972.
- Huschke, R.E., 1969, Arctic Cloud Statistics from Air Calibrated Surface Weather Observations, Mem. RM-6173-PR, Rand Corp., Santa Monica, CA, 79pp.
- ICRCCM, 1984, Longwave Clear-Sky Calculations, Report of a meeting in Frascati, Italy, 15-18 August 1984, the International Radiation Commission of IAMAP, pp. 37.
- IMSL Library, 1975, Library 3, Edition 5 Reference Manual (IMSL LIB3-005), available from: Sixth Floor, GNB Bldg. 7500 Bellaire Blvd., Houston, TX 77036.
- Iqbal, M., 1983, An Introduction to Solar Radiation, Academic press, 390pp.
- Irvine, W.M., 1964, The Formation of Absorption Bands and the Distribution of Photon Optical Paths in a Scattering Atmosphere, Bull. Astr. Inst. Netherlands., 17, 266-279.

- Jayaweera, K. and T. Ohtake, 1973, Concentration of Ice Crystals in Arctic Stratus Clouds, J. Rech. Atmos., 7, 199-207.
- Karp, A.H., 1981, Computing the Angular Dependence of the Radiation of a Planetary Atmosphere, J. Quant. Spectrosc. Radiat Transfer, 25, 403-412.
- Kellogg, W.W., 1975, Climatic Feedback Mechanisms Involving the Polar Regions, in 'Climate of the Arctic' (Eds., G. Weller and S. Bowling).
- Kneizys, F.X., E.P. Shettle, W.O. Gallery, J.H. Chetwynd, Jr., L.W. Abreu, J.E.A. Selby, R.W. Fenn, and R.A. McClatchey, 1980, Atmospheric Transmittance/Radiance: Computer Code LOWTRAN 5, Report No. AFGL-TR-80-0067, Air Force Geophysics Lab, Hanscom AFB, MA.
- Leavitt, E., M. Albright, and F. Carsey, 1978, Report on the AIDJEX Meteorological Experiment, AIDJEX Bull., 39, 121-148.
- LINPACK Library, 1979, available from: National Energy Software Center, Argonne National Laboratory, 9700 South Cass Ave., Argonne, IL 60439
- List, R.J., 1968, Smithsonian Meteorological Tables, Washington, D.C., Smithsonian Institution, pp527.
- Liou, K.N., 1973, A Numerical Experiment on Chandrasekhar's Discrete Ordinate Method for Radiative Transfer: Applications to Cloudy and Hazy atmospheres, J. Atmo. Sci., 30, 1303-1326.
- , 1975, Applications of the Discrete-Ordinate Method for Radiative Transfer to Inhomogeneous Aerosol Atmospheres, J. Geophys. Res., 80, 3434-3440.
- , 1980, An Introduction to Atmospheric Radiation, Academic Press, pp392.
- Maykut, G.A., 1983, Surface Heat and Mass Balance, in 'Air-Sea-Ice Interaction', (Eds., Untersteiner et al.).
- , and N. Untersteiner, 1971, Some Results from a Time-Dependent Thermodynamic Model of Sea Ice, J. Geophys. Res., 76, 1550-1575.
- McPhee, M.G. and N. Untersteiner, 1982, Using Sea Ice to Measure Vertical Heat Flux in the Ocean, J. Geophys. Res., 87, 2071-2074.

- McClatchey, R.A., R.W. Fenn, J.E.A. Selby, F.E. Volz, and J. S. Garing, 1972, Optical Properties of the Atmosphere, Air Force Cambridge Research Laboratories, AFCRL-72-0497, 108pp.
- , W.S. Benedict, S.A. Clough, D.E. Burch, R.F. Calfee, K. Fox, L.S. Rothman and J.S. Garing, 1973, AFCRL Atmospheric Absorption Line Parameters Compilation, Air Force Cambridge Research Laboratories, AFCRL-TR-73-0096, 78pp.
- Mie, G., 1908, Beigrade zur Optik trüber Medien, speziell kolloidaler Metallösungen, Ann. Physik., 25, 377-445.
- Mitchell, M., Jr., 1956, Visual Range in the Polar Regions with Particular Reference to the Alaskan Arctic, J. Atmos. Terr. Phys., supplement, 195-211.
- Mugnai, A. and W.J. Wiscombe, 1980, Scattering of Radiation by Moderately Nonspherical Particles, J. Atmos. Sci., 37, 1291-1307.
- Nicolet, M., 1984, On the Molecular Scattering in the Terrestrial Atmosphere: An Empirical Formula for its Calculation in the Homosphere, Planet. Space Sci., 32, 1467-1468.
- Oort, A.H., 1975, Year-to-Year Variations in the Energy Balance of the Arctic Atmosphere, in 'Climate of the Arctic' (Eds., G. Weller and S. Bowling, 68-75).
- Palmer, K.F. and D. Williams, 1974, Optical properties of Water in the Near Infrared, J. Opt. Soc. Am., 64, 1107-1110.
- Patterson, E.M., B.T. Marshall, and K.A. Rahn, 1982, Radiative Properties of the Arctic Aerosol, Atmos. Environ., 16, 2967-2977.
- Penndorf, R., 1957, Tables of the Refractive Index for Standard Air and the Rayleigh Scattering Coefficient for the Spectral Region between 0.2 and 20 μ m and Their Application to Atmospheric Optics, J. Opt. Soc. Am., 47, 176-182.
- Polar Group, 1980, Polar Atmosphere-Ice-Ocean Processes: A Review of Polar Problems, Rev. Geophy. and Space Phy., 18, 525-543.
- Radiation Commission, 1977, Standard Procedures to Compute Atmospheric Radiative Transfer in a Scattering Atmosphere, (Ed. J. Lenoble, IAMAP report ppl25).

- , 1980, Standard Procedures to Compute Atmospheric Radiative Transfer in a Scattering Atmosphere, (Eds., Y. Fouquart, W.M. Irvine and J. Lenoble, IAMAP report pp98).
- Rahn, K.A., 1978, Chemical and Optical Properties of the Barrow Aerosol, Geophysical Monitoring for Climatic Change, NTIS no. PB80-165962, 97-99.
- , 1981, Relative Importance of North America and Eurasia as Sources of Arctic Aerosol, Atmos. Environ., 15, 1447-1455.
- , R. Borys, and G.E. Shaw, 1977, The Asian Source of arctic Haze Bands, Nature, 268, 713.
- , and R.J. McCaffrey, 1980, On the Origin and Transport of the Winter Arctic Aerosol, Ann. N. Y. Acad. Sci., 338, 486-503.
- Reynolds, D., T. Vonder Haar and S. Cox, 1975, The Effect of Solar Radiation Absorption in the Tropical Atmosphere, J. Appl. Meteor., 14, 433-444.
- Rothman, L., 1981, AFGL Atmospheric Absorption Line Parameters Compilation: 1980 Version, Appl. Opt., 20, 791-795.
- Schwarzschild, K., 1906, in 'Selected Papers on the Transfer of Radiation' (Ed. D. Menzel).
- Semtner, A.J., 1976, A Model for the Thermodynamic Growth of Sea Ice in Numerical Investigations of Climate, J. Phys. Oceanogr., 6, 379-389.
- Shaw, G., 1975, The Vertical Distribution of Atmospheric Aerosols at Barrow, Alaska, Tellus, 27, 39-50.
- , 1982, Atmospheric Turbidity in the Polar Regions, J. Appl. Meteor., 21, 1080-1088.
- , 1985, On the Climatic Relevancy of Arctic Haze: Static Energy Balance Considerations, Tellus, 37, 50-52.
- , and G. Wendler, 1972, Atmospheric Turbidity Measurements at McCall Glacier in Northern Alaska, in proceedings of the Atmospheric Radiation Conference, Ft. Collins, CO., 181-187.

- , and K. Stamnes, 1980, Arctic Haze: Perturbation of the Polar Radiation Budget, Ann. N. Y. Acad. Sci., 338, 533-539.
- Shettle, E.P. and A.E.S. Green, 1974, Multiple Scattering Calculation of the Middle Ultraviolet Reaching the Ground, Appl. Opt., 13, 1567-1581.
- , and R.W. Fenn, 1976, Models for the Atmospheric Aerosol and their Optical Properties, Proc. AGARD Conf. (183) Optical Propagation in the Atmosphere, Lyngby, Denmark, 1975, 245pp.
- , and -----, 1979, Models for the Aerosols of the Lower Atmosphere and the Effects of Humidity Variations on Their Optical Properties, report no. AFGL-TR-0214, Hanscom AFB, MA., 94pp.
- Shine, K.P. and A. Henderson-Sellers, 1985, The Sensitivity of a Thermodynamic Sea Ice Model to Changes in Surface Albedo Parameterization, J. Geophys. Res., 90, 2243-2250.
- Slingo, A. and H.M. Schrecker, 1982, On the Shortwave Radiative Properties of Stratiform Water Clouds, Quart. J. R. Met. Soc., 108, 407-426.
- Stamnes, K., 1982, On the Computation of Angular Distributions of Radiation in Planetary Atmospheres, J. Quant. Spectrosc Radiat Transfer, 28, 47-51.
- , and R.A. Swanson, 1981, A New Look at the Discrete Ordinate Method for Radiative Transfer Calculations in Anisotropically Scattering Atmospheres, J. Atmos. Sci., 38, 387-399.
- , and H. Dale, 1981, A New Look at the Discrete Ordinate Method for Radiative Transfer Calculations in Anisotropically Scattering Atmospheres. II: Intensity Computations, J. Atmos. Sci., 38, 2696-2706.
- , and P. Conklin, 1984, A New Multi-Layer Discrete Ordinate Approach to Radiative Transfer in Vertically Inhomogeneous Atmospheres, J. Quant. Spectrosc. Radiat. Transfer, 31, 273-282.
- Stephens, G.L., 1978, Radiation Profiles in Extended Water Clouds. I: Theory, J. Atmos. Sci., 35, 2111-2122.
- , 1979, Optical Properties of Eight Water Cloud Types, CSIRO Aust. Div. Atmos. Phys. Tech. Pap. No. 36, 35pp.

- Tsay, S.C. and K. Jayaweera, 1984, Physical Characteristics of Arctic Stratus Clouds, J. Climate Appl. Meteor., 23, 584-596.
- , and -----, and K. Stamnes, 1983, Dependence of Radiative Properties of Arctic Stratus Clouds on Cloud Microstructure, Geophys. Res. Lett., 10, 1188-1191.
- Twitty, J.T. and J.A. Weinman, 1971, Radiative Properties of Carbonaceous Aerosols, J. Appl. Meteo., 10, 725-731.
- Twomey, S. and C.F. Bohren, 1980, Simple Approximations for Calculations of Absorption in Clouds, J. Atmos. Sci., 37, 2086-2094.
- U.S. Naval Observatory, 1945, Tables of Sunrise, Sunset, and Twilight, (Supplement to the American Ephemeris, 1946), Washington, D.C., Government Printing Office.
- Valero, F.R.J., T.P. Ackerman, and W.J.Y. Gore, 1983, Radiative Effects of the Arctic Haze, Geophys. Res. Lett., 10, 1184-1187.
- Van de Hulst, 1957, Light Scattering by Small Particles, Wiley, Now York, 470pp.
- Vowinckel, E. and S. Orvig, 1964a, Energy Balance of the Arctic, II Longwave Radiation and Total Radiation Blance at the Surface in the Arctic, Arch. Met. Geoph. Biokl., B., 13, 451-479.
- , and -----, 1964b, Energy Balance of the Arctic, III Radiation Balance of the Troposphere and of the Earth-Atmosphere System in the Arctic, Arch. Met. Geoph. Biokl., B., 13, 480-502.
- , and -----, 1970, The Climate of the North Polar Basin, World Survey of Climatology, vol. 14, Climates of the Polar Regions, S. Orvig, Ed., Elsevier, 129-252.
- Warren, S.G., 1982, Ice and Climate Modeling: An Editorial Essay, Climatic Change, 4, 329-340.
- , 1982, Optical Properties of Snow, Rev. Geophys. Space Phys., 20, 67-89.
- , 1984, Optical Constants of Ice from the Ultraviolet to the Microwave, App. Opt., 23, 1206-1225.
- , and W.J. Wiscombe, 1980, A Model for the Spectral Albedo of Snow. II: Snow Containing Atmospheric Aerosols, J. Atmos. Sci., 37, 2734-2745.

- Welch, R.M., S.K. Cox and J.M. Davis, 1980, Solar Radiation and Clouds, Meteor. Monogr., 39, 96pp.
- Wiscombe, W.J., 1975, Solar Radiation Calculations for Arctic Summer Stratus Conditions, in 'Climate of the Arctic' (Eds. G. Weller and S. Bowling).
- , 1976, On Initialization, Error and Flux Conservation in the Doubling Method, J. Quant. Spectrosc. Radiat. Transfer, 16, 637-658.
- , 1977, The Delta-M Method: Rapid Yet Accurate Radiative Flux Calculations for Strongly Asymmetric Phase Functions, J. Atmos. Sci., 34, 1408-1422.
- , and J.W. Evans, 1977, Exponential-Sum Fitting of Radiative Transmission Functions, J. Comp. Phys., 24, 416-444.
- , and S.G. Warren, 1980, A Model for the Spectral Albedo of Snow. I: Pure Snow, J. Atmos. Sci., 37, 2712-2733.
- , 1983, Atmospheric Radiation: 1975-1983, Rev. Geophys. Space Phys., 21, 997-1021.
- , R.M. Welch, and W.D. Hall, 1984, The Effects of Very Large Drops on Cloud Absorption. Part I: Parcel Models, J. Atmos. Sci., 41, 1336-1355.
- , and V. Ramanathan, 1985, The Role of Radiation and Other Renascent Sub-Fields in Atmospheric Science, Bull. Amer. Met. Soc., 66, 1278-1287.
- Woolf, H.M., 1968, On the Computation of Solar Elevation Angles and the Determination of Sunrise and Sunset Times, NASA technical report, [NASA TM X-1646] pp23.
- Yamamoto, G., M. Tanaka, and S. Asano, 1971, Radiative Heat Transfer in Water Clouds by Infrared Radiation, J. Quant. Spectrosc. Radiat. Transfer, 11, 697-708.